Process Intensification in the Synthesis of the Green Chemical Dimethyl Carbonate

Dissertation presented to the Faculdade de Engenharia da Universidade do Porto for the degree of Doctor in Chemical and Biological Engineering

by

Bruno André Vilela dos Santos

Supervised by Professor Alírio Egídio Rodrigues
and co-supervised by Professor José Miguel Loureiro

Laboratory of Separation and Reaction Engineering, Associate Laboratory LSRE/LCM
Department of Chemical Engineering, Faculty of Engineering, University of Porto, Portugal

November 2014

This Thesis was financially supported by *Fundação para a Ciência e a Tecnologia* (Portugal) through the Ph.D. grant SFRH/BD/68470/2010, under the Programme POPH/FSE.

Laboratory of Separation and Reaction Engineering

University of Porto - Faculty of Engineering

Rua Dr. Roberto Frias s/n, 4200-465 Porto

Portugal

Agradecimentos (*Acknowledgements*)

Ao longo dos últimos quatro anos de dedicação ao meu douramento vivi experiências extremamente enriquecedoras, tanto de caráter pessoal como profissional, e ultrapassei diversas barreiras, o que só foi possível graças ao apoio de certas pessoas, às quais gostaria de deixar aqui o meu profundo agradecimento.

Em primeiro lugar gostaria de agradecer ao meu orientador, Professor Alírio Egídio Rodrigues, por todo o conhecimento que me transmitiu, pelos "sermões" que me foi dando, e pelo rigor e exigência por trabalho de qualidade, que me fizeram desenvolver como pessoa e profissional. De seguida, quero expressar o meu profundo agradecimento ao meu coorientador, Professor José Miguel Loureiro, que sempre teve uma palavra amiga em alturas menos boas. Foi (e é) um verdadeiro mentor que me ajudou imenso nestes anos e com o qual também aprendi aspetos importantes, quer de âmbito técnico quer humano, que tenho a certeza que me vão ser úteis de futuro.

Quero também deixar o meu sincero Obrigado para a Viviana Silva, que foi inicialmente a minha supervisora e que tanto me ajudou no início do doutoramento; para a Carla Pereira, que além da grande amizade também contribuiu para esta tese; para o Professor Domingos Barbosa, pela sua preciosa ajuda com a termodinâmica; e para os meus colegas de laboratório, Rui Faria e Dânia Constantino, que aturaram os meus bons e maus humores, por eles guardo no meu coração uma enorme amizade.

Gostaria também de agradecer a todos os colegas e professores do LSRE por me acolherem tão bem ao ponto de me fazerem sentir em casa, em especial aos companheiros do gabinete E406. Um excelente grupo de investigação do qual me sinto orgulhoso de fazer parte.

Finalmente, queria agradecer à minha mulher, Joana Carvalho, por todo o seu apoio incondicional, paciência e amor.

Resumo

O constante aumento do consumo energético em todo o mundo tem consequências graves na sociedade atual e irá ter nas próximas gerações. Um dos problemas mais mediáticos é o aumento da concentração de dióxido de carbono na atmosfera, um dos principais compostos responsáveis pelo efeito de estufa e o consequente aquecimento global.

Estima-se que a população em 2050 atinja cerca de 9 mil milhões de habitantes o que se traduz num acréscimo de cerca de 30% face aos 7 mil milhões de habitantes atuais. Um dos maiores desafios que as próximas gerações vão enfrentar, é o contínuo aumento de emissões de dióxido de carbono. A fome, a escassez de energia e água potável e a poluição são outros pilares importantes que estão relacionados com este aumento de população.

Entre as formas de mitigar o problema da elevada emissão de dióxido de carbono pode-se destacar a redução de emissões por via de tecnologias energéticas mais eficientes, o sequestro do dióxido de carbono, e a utilização/valorização do dióxido de carbono para produção de outros químicos. O presente trabalho aborda a utilização de dióxido de carbono para a síntese de carbonato de dimetilo (DMC), um composto químico com inúmeras aplicações, nomeadamente como solvente, eletrólito para baterias de lítio, aditivo para gasolinas, ou como matéria-prima para reações de metilação e carbonilação.

Em particular, é estudada a síntese direta de carbonato de dimetilo a partir de dióxido de carbono e de metanol ($CO_2 + 2CH_3OH \rightleftharpoons DMC + H_2O$). Devido à elevada estabilidade da molécula de dióxido de carbono, a reação é muito limitada pela termodinâmica. Sendo assim, nesta tese é proposto um reator de leito móvel simulado para altas pressões (acima de 20 MPa), que conjuga a reação e separação da água formada por adsorção, de forma a deslocar o equilíbrio, melhorando assim o rendimento da reação.

Em resumo, ao longo desta tese são abordados o equilíbrio químico e físico da mistura reacional, a reação catalisada por óxido de cério (realizada num reator fechado), a adsorção de água e de DMC sobre a superfície do zeólito 3A (através de experiências num cromatógrafo supercrítico), e o dimensionamento do reator de leito móvel simulado (baseado em simulações numéricas).

Com este trabalho pretende-se também fomentar a utilização deste "resíduo" barato e abundante (dióxido de carbono), para produção de outros compostos do nosso quotidiano.

Abstract

The worldwide constant increase of energy demand has serious consequences in today's society and will have on future generations. One of the most well-known problems is the increase of carbon dioxide concentration in the atmosphere, which is one of the main compounds responsible for the greenhouse effect and the resulting global warming.

It is estimated that in 2050 the worldwide population will reach around 9 thousand million inhabitants, which translates into an increase of about 30% when compared with the current 7 thousand million inhabitants. The major challenge that the next generation will face, is the continuous increasing of carbon dioxide emissions. Food shortage, lack of energy and drinking water, and pollution are other important pillars that are related to this increase in population.

Among the ways to mitigate these high carbon dioxide emissions, it can be highlighted the emissions reduction through more efficient energy technologies, carbon dioxide sequestration, and utilisation/valorisation of carbon dioxide for the production of other chemicals. This work discusses the use of carbon dioxide for the synthesis of dimethyl carbonate (DMC), a chemical compound with countless applications, such as solvent electrolyte for lithium batteries, gasoline additive, or as raw material for methylation reactions and carbonylation.

In particular, it is studied the direct synthesis of dimethyl carbonate from carbon dioxide and methanol ($CO_2 + 2CH_3OH \rightleftharpoons DMC + H_2O$). Due to the high stability of the carbon dioxide molecule, the reaction is highly limited by the thermodynamics. Therefore, in this thesis it is proposed a simulated moving bed reactor at high pressure (over 20 MPa), which combines reaction with separation of the water produced by adsorption, in order to shift the equilibrium, thereby improving the yield of the reaction.

In summary, throughout this thesis are covered the chemical and physical equilibria of the reacting mixture, the reaction catalyzed by cerium oxide (performed in a batch reactor), the adsorption of water and DMC over the zeolite 3A surface (through experiments conducted in a supercritical fluid chromatograph), and the design of the simulated moving bed reactor (based on numerical simulations).

With this work it is also aimed to promote the use of this cheap and abundant "waste" (carbon dioxide) to produce other compounds of our daily lives.

Table of Contents

Chapter 1. Introduction **1**

1.1. Relevance and Motivation 2

1.2. Objectives and Outline 3

References 5

Chapter 2. State-of-the-Art **7**

2.1. Chemistry of Carbon Dioxide 8

2.1.1. Carbon dioxide as solvent 9

2.1.2. Carbon dioxide as building block 9

2.2. Organic Carbonates 11

2.2.1. Organic carbonates – properties 11

2.2.2. Organic carbonates as solvents 12

2.2.3. Organic carbonates as building blocks 13

2.3. Dimethyl Carbonate 13

2.3.1. Solvent and fuel additive 13

2.3.2. Building block 14

2.4. DMC Production 15

2.4.1. Conventional process 15

2.4.2. New alternative processes 17

2.5. Direct Synthesis of DMC from Carbonation of Methanol 26

2.5.1. Thermodynamic and kinetic limitations 26

2.5.2. Homogenous catalysis 27

2.5.3. Heterogeneous catalysis 29

2.5.4. Dehydrating agents 33

2.5.5. Side reactions 35

2.6. Conclusions 38

Nomenclature 39

References 39

Chapter 3. Vapour-Liquid Equilibrium for the Direct Synthesis of DMC 51

3.1. Introduction 52

3.1.1. Cubic equation of state for pure compounds 52

3.1.2. Mixing rules for cubic equations of state 53

3.2. Modelling Phase Equilibrium 55

3.2.1. Thermodynamic model 55

3.2.2. Experimental data collected 58

3.3. Results 58

3.3.1. Model optimization 58

3.3.2. Ternary validation 62

3.3.3. Simulation of binary equilibrium 63

3.4. Simulation of Pressure-Temperature Diagram 67

3.5. Conclusions 68

Nomenclature 68

References 70

Chapter 4. Direct Synthesis of DMC over CeO_2 at High Pressure Conditions 75

4.1. Introduction 76

4.2. Experimental 76

4.2.1. Materials and analytical method 76

4.2.2. Experimental set-up 77

4.2.3. Experimental procedure 77

4.3. Experimental Results 79

4.3.1. Catalyst characterization 79

4.3.2. Reproducibility and external resistance to mass transfer 80

4.3.3. Chemical equilibrium 82

4.4. Kinetic Models 84
4.5. Parameters Optimization 85
4.6. Simulation 87
4.7. Conclusions 89
4.8. Nomenclature 90
4.9. References 91

Chapter 5. Adsorption of Water and DMC over Zeolite 3A in Fixed Bed Column at High Pressure Conditions....95

5.1. Introduction 96
5.2. Experimental Procedure 97
5.2.1. Chemicals....97
5.2.2. Set-up 97
5.2.3. Methodology 101
5.2.4. Adsorbent characterization....103
5.3. Modelling 106
5.3.1. Mathematical model....106
5.3.2. MatLab® resolution 107
5.4. Results and Discussion....109
5.4.1. Tracer experiments....109
5.4.2. DMC and water pulses....112
5.5. Prediction of Mass Transfer 112
5.6. Conclusions 124
Nomenclature 125
Acknowledgements 127
References 128

Chapter 6. Process Intensification for the Direct Synthesis of DMC 133

6.1. Introduction 134

6.2. Methodology and Numerical Approach 138

6.3. Scenario 1: Batch Reaction with Adsorption 139

6.4. Scenario 2: Batch Reaction with External Adsorption in Fixed Bed Column 142

6.4.1. Single column without regeneration 145

6.4.2. Two parallel columns with regeneration 146

6.4.3. Scenario 2 overview 149

6.5. Scenario 3: Series of Alternating Reaction and Adsorption Columns 150

6.6. Design of a SMBR 154

6.6.1. Model 155

6.6.2. First guess design 157

6.6.3. Second guess design 161

6.7. Conclusions 179

Nomenclature 180

References 182

Chapter 7. Conclusion and Suggestions for Future Work 189

7.1. Main Conclusions 190

7.2. Suggestions for Future Work 192

Annex A. Analytical Method 195

A.1. Operating Conditions 195

A.2. Calibration 196

Annex B. Reactor Set-Up 197

Annex C. TMBR Concentration Profiles 201

To my lovely wife...

Chapter 1. Introduction

"Devemos julgar um homem mais pelas suas perguntas que pelas respostas."

Voltaire

1.1. Relevance and Motivation

Since the industrial revolution the global population has been continuously increasing, which led to an exponential rise of energy demand. Furthermore, most of this energy is still dependent on fossil fuel sources, such as coal, natural gas, and oil. In Figure 1.1 is depicted the world consumption of primary energy (1987-2012) from different sources, where it can be seen that the fossil sources are much higher than other energy sources. In fact, in 2012 the totality of non fossil sources (renewables, hydroelectricity, and nuclear energy) did not exceed 15% of the global consumption.

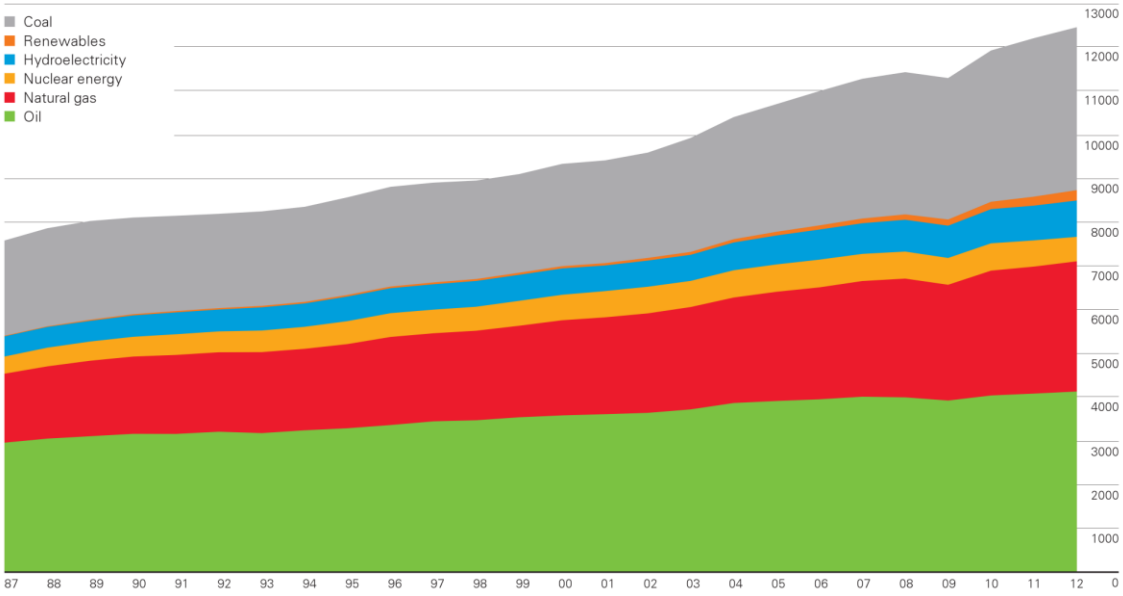

Figure 1.1: World consumption of primary energy until 2012, oil equivalent million tons (BP Statistical Review of World Energy June 2013) [1].

This high dependence of fossil sources has as consequence large emissions of greenhouse gases (especially carbon dioxide), responsible for one of the major problem that mankind has been fighting in the last decades: global warming. Therefore, it is urgent and mandatory to reduce the emissions of carbon dioxide (and others greenhouse gases). Although there is no miraculous solution for this challenging goal, there are two main pillars that can help us to manage this endless issue:

❖ Reduction: The fast advance of technology led to an excessive consumption of energy, therefore it is important to establish new standards of life compatible with the renewable resources. Besides, new technological improvements are essential to improve the efficiency of converting natural sources into daily commodities.

❖ Recovery: Other pathway (not solution) is the recovery / reutilization of residues: waste to energy. For instance, carbon dioxide can be used as either as solvent or feedstock for organic and inorganic synthesis [2, 3].

One example of a potential use of carbon dioxide is the synthesis of dimethyl carbonate (DMC). Dimethyl carbonate (DMC) is an important alkyl carbonate with large applications for novel green chemical processes. Its high versatility (as solvent [4], reactant [5] or fuel additive [6]) coupled with its low toxicity turns DMC into valuable chemical for industrial chemical engineering. For instance, DMC is able to replace the hazardous phosgene and dimethyl sulphate in carbonylation and methylation reactions [7, 8].

Nowadays, DMC is mainly produced by oxy-carbonylation [9] of methanol or methyl nitrile [10], using hazardous chemicals (O_2, CO, HCl), which demands a novel large scale process. Several processes were proposed as alternative for DMC synthesis [11]: transesterification of ethylene carbonate, transesterification of methyl carbamate, and carbonylation of methanol. The last alternative, carbonylation of methanol, also called the direct synthesis ($CO_2 + 2MeOH \rightleftharpoons DMC + H_2O$), is pointed to be one of the most promising alternatives since it uses cheap and low toxic chemicals and promotes the consumption of carbon dioxide. However, due to the high stability of carbon dioxide and its thermodynamic properties, the DMC yield are very low, even at high pressure conditions.

Usually, in this situation, an excessive use of one reactant is used to promote the conversion of the limiting species. In addition, another possibility to overcome this major drawback is the use of hybrid systems coupling reaction and product separation [12] (reactive distillation, reactive membranes, reactive extraction, or reactive chromatography), which have already been successfully used to overcome this drawback in several other processes. By continuously removing one of the products from the reaction mixture, the reaction progress in the direct way, in order to reach new equilibrium.

In conclusion, the utilization of carbon dioxide as feedstock is encouraged as a measure to reduce greenhouse gas emissions. In particular, the development of a sustainable process for the direct synthesis of DMC from carbon dioxide and methanol would be an important breakthrough for other utilization of carbon dioxide, and to introduce DMC as a benign chemical in further processes.

1.2. Objectives and Outline

The main objective of this thesis is to study the potential of a Simulated Moving Bed Reactor (SMBR) to enhance the direct synthesis of DMC at high pressure conditions. Thus, in order to achieve this goal it was necessary to address the following points: select an appropriate catalyst and adsorbent system; understand the physical behaviour of the reaction mixture at high pressure; modelling the reaction kinetics and equilibrium; determine and modelling the adsorption isotherms over the adsorbent; predict the mass transfer phenomenon along a fixed bed column; develop a SMBR model for further simulations; and, finally, design and optimize the SMBR unit for the production of DMC. Since there was no experimental set-up for the validation, the SMBR unit was designed and optimized through the simulation of a True Moving Bed Reactor (TMBR). Then, the present thesis was divided in seven chapters.

First, in **Chapter 2**, is summarized the state-of-the-art for DMC production in order to understand the advantages and disadvantages of the direct synthesis over the conventional and other alternative routes. It starts with a brief description of the applications of carbon dioxide as solvent and as C1 building block in organic chemistry, followed by an introduction about organic carbonates: properties and applications. In addition a deeper discussion about the properties of DMC is presented. Then, the main catalysts used so far, for the synthesis of DMC, are detailed, together with the operation conditions and catalyst performance; and it is also discussed the use of different dehydrating agents to increase DMC yield.

In order to understand and model high-pressure processes, the knowledge of phase equilibrium is essential. Therefore, in **Chapter 3**, the vapour-liquid equilibrium at low and high pressure condition was modelled based on the experimental data collected from literature. Herein, Soave-Redlich-Kwong equation of state with five different mixing rules (one fluid van der Walls modified first order Huron-Vidal, modified second order Huron-Vidal, linear combination of Vidal and Michelsen, and Wong-Sandler), was fitted to the vapour-liquid equilibrium, for the different binary mixture of the reaction system (carbon dioxide, methanol, water and dimethyl carbonate), in order to be able to predict physical equilibrium behaviour. Further, a ternary mixture (carbon dioxide, methanol, and water) was used to evaluate the performance of the best models.

In **Chapter 4** is presented a description of the experimental set-up, designed for high pressure reactions with dense carbon dioxide, where the direct synthesis of DMC was carried out in the presence of cerium oxide as catalyst. The experiments were conducted at different temperatures, carbon dioxide to methanol ratios, and pressures, in order to understand the effect of these parameters on the reaction kinetics and equilibrium. Then, two reaction rate expressions were considering, to modelling the reaction kinetic, based on Langmuir-Hinshelwood and Eley-Rideal mechanisms; and the kinetic and equilibrium parameters were adjusted to the experimental data.

Further, in **Chapter 5**, it was studied the adsorption equilibria of water and DMC over zeolite 3A, at high pressure conditions, by the analysis of pulse responses in a fixed bed column. The experiments were conducted in a Supercritical Fluid Chromatograph, which is also described elsewhere in the chapter. Moreover, a mathematical model to describe the pulse response, considering a linear adsorption isotherm, axial dispersion, and linear driving (for the mass transfer between the bulk and the particles pores) was developed in order to predict the experiments to find the Péclet number and the global mass transfer coefficients, by fitting the experimental data. Afterward, these parameters were estimated using different correlations, to check if predictions from “common” correlations are reliable at high pressure and for compressible liquid mixtures.

After collecting the physical chemistry models required, in **Chapter 6,** a TMBR unit is designed and optimized toward the enhancement of the direct synthesis of DMC. In addition, before the TMBR design, simpler configurations to enhance the DMC equilibrium yield will be explored: simultaneous reaction and adsorption in batch (Scenario 1); batch reactor with external adsorption (Scenario 2); alternating reaction and adsorption in fixed bed columns (Scenario 3). This work also aims to better understand and quantify the potential of zeolite 3A in process intensification. Then, a new methodology to design the TMBR is proposed,

concerning the maximization of reaction conversion and DMC purity (at the outlet stream), and minimization of the desorbent consumption together in a simple single-objective function. The approach is supported with numerical simulation to estimate the effect of mass transfer resistances; the simulations were based on the experimental data collected so far: mass transfer, adsorption over zeolite 3A, reaction kinetics over cerium oxide, and reaction equilibrium. Besides, the design is also supported by the volume separation method and contour maps of relevant performance variables inside the separation region. This approach attempts to obtain a quick assessment of the potentials and weaknesses of an SMBR process for the DMC production.

Finally, the major conclusions of this thesis are reviewed in **Chapter 7**, together with suggestions for possible future work.

References

[1] *BP Statistical Review Of World Energy June 2013, bp.com/statisticalreview*.

[2] Aresta, M.,Dibenedetto, A. Utilisation Of CO2 As A Chemical Feedstock: Opportunities And Challenges. *Dalton Transactions* **2007,** (28), 2975.

[3] Dibenedetto, A.,Angelini, A.,Stufano, P. Use Of Carbon Dioxide As Feedstock For Chemicals And Fuels: Homogeneous And Heterogeneous Catalysis. *Journal of Chemical Technology and Biotechnology* **2013,** *89*(3), 334.

[4] Schäffner, B.,Schäffner, F.,Verevkin, S.,Börner, A. Organic Carbonates As Solvents In Synthesis And Catalysis. *Chemical Reviews* **2010,** *110*(8), 4554.

[5] Delledonne, D.,Rivetti, F.,Romano, U. Developments In The Production And Application Of Dimethylcarbonate. *Applied Catalysis A: General* **2001,** *221*(1-2), 241.

[6] Pacheco, M.,Marshall, C. Review Of Dimethyl Carbonate (DMC) Manufacture And Its Characteristics As A Fuel Additive. *Energy and Fuels* **1997,** *11*(1), 2.

[7] Memoli, S.,Selva, M.,Tundo, P. Dimethylcarbonate For Eco-Friendly Methylation Reactions. *Chemosphere* **2001,** *43*(1), 115.

[8] Shaikh, A.,Sivaram, S. Organic Carbonates. *Chemical Reviews* **1996,** *96*(3), 951.

[9] Romano, U., Tesei, R., Cipriani, G., Micucci L. Method For The Preparation Of Esters Of Carbonic Acid. US 4218391, **1980**.

[10] Nishihira, K.,Yoshida, S.,Tanaka, S.,Asada, Y. Process For Continuously Producing Dimethyl Carbonate. US 5631396, **1997**.

[11] Monteiro, J. G. M. S.,De Queiroz Fernandes Araújo, O.,De Medeiros, J. L. Sustainability Metrics For Eco-Technologies Assessment, Part I: Preliminary Screening. *Clean Technologies and Environmental Policy* **2009,** *11*(2), 209.

[12] Kulprathipanja, S. *Reactive Separation Processes*; Taylor & Francis: **2001**.

Chapter 2. State-of-the-Art

"Adoramos a perfeição, porque não a podemos ter; repugná-la-íamos, se a tivéssemos. O perfeito é desumano, porque o humano é imperfeito." – Fernando Pessoa

This chapter is based on the following article: Santos, B., Silva, V., Loureiro, J., Rodrigues, Review for the Direct Synthesis of Dimethyl Carbonate. *ChemBioEng Reviews* **2014,** 1 (5), 214.

2.1. Chemistry of Carbon Dioxide

Since the industrial revolution, during the 18th century, the energy consumption increased exponentially; at the end of the 20th century the depletion of energy sources, especially from fossil fuels such as coal, petroleum and natural gas, became a serious issue. On the other hand, this high energy consumption has brought remarkable developments in several important sectors such as medicine, communication, transportation, etc.

However, the benefits in the human life quality, together with the increase of global population, have some negative consequences on the environment and consequently on human health. The emission of pollutant compounds, such SO_x, NO_x or particles, and the greenhouse gases, such as carbon dioxide and methane, due to the excessive consumption of fossil fuels, is the most direct issue for life in all its diversity. Besides, the high demand of energy is also responsible for the lack in carbon based fuel. Figure 2.1 shows the evolution of the carbon dioxide average concentration in the atmosphere since the 10th century, based on the analysis of ice core [1]. It can be observed that, after the 18th century, the carbon dioxide concentration followed the exponential tendency of energy consumption, which indicates a direct relation between them.

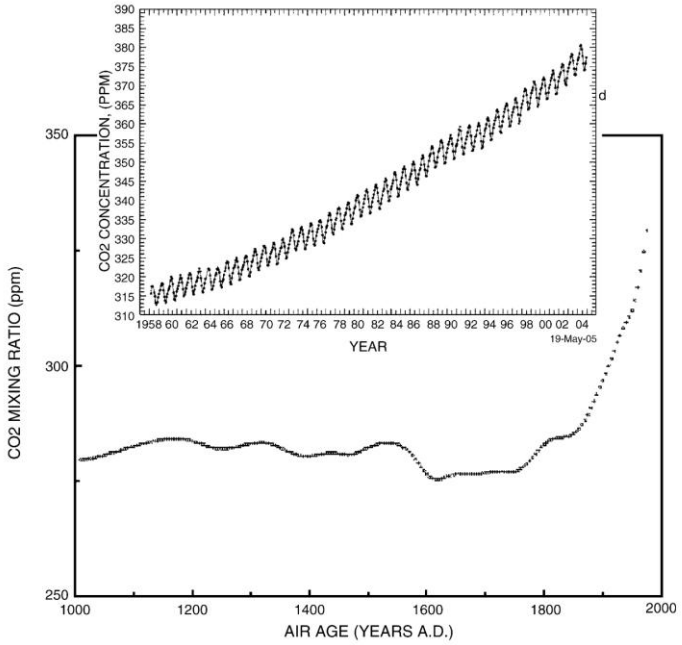

Figure 2.1: Atmospheric carbon dioxide concentration along time [1].

This continuous increase turns carbon dioxide in an important topic of discussion amongst the scientific community since it promotes global warming caused by the greenhouse effect. In order to decrease the carbon dioxide emissions, different methodologies can be applied, namely: energy (source) choice; energy efficiency; sequestration.

The energy choice consists in using different energy sources such as solar, nuclear, wind, hydroelectric to reach the required energy needs. Although these sources are not totally free of emissions due to several

reasons, such as transportation or materials production, the amount of carbon dioxide produced is much lower than from carbon based fuel. The decrease of consumption could be reached by increasing the efficiency of the process and transport of energy. The sequestration of carbon dioxide can be reached by the use of carbon dioxide as feedstock or by mineral carbonation [2]. The mineral carbonylation has a large capacity for carbon dioxide storage comparing to the first alternative. Since there is not a magic solution to reduce the carbon dioxide concentration, the contribution of the three methodologies is needed.

2.1.1. Carbon dioxide as solvent

Carbon dioxide is an important solvent in supercritical conditions. In spite of the high pressurization costs, carbon dioxide is easily separated by depressurization and its polarity can be tuned by addition of a co-solvent. Moreover, the low viscosity enhances mass transfer, which is the critical step in several processes. Biodiesel production [3-5] or caffeine extraction [6-9] are examples of the benefits of using supercritical carbon dioxide. For instance, Machmudac et al. [10] studied the simultaneous extraction and separation of chlorogenic acid (polar) and caffeine (non polar) from coffee beans, using supercritical carbon dioxide (non polar) in water (polar). Furthermore, they performed the extraction in three extractors with three different flow modes, semi-batch, co-current and counter-current.

2.1.2. Carbon dioxide as building block

The conversion of carbon dioxide into valuable chemicals, in large scale, aims to reduce carbon dioxide concentration in a sustainable way, since carbon dioxide is a non toxic, abundant and cheap reactant. However, the low reactivity of carbon dioxide caused by its high stability is presented as the major drawback in this strategy. Although high energy input is required in a global process, it can be compensated by the lower energy input needed for product-reactant separation, which eventually makes feasible several industrial applications based on carbon dioxide [1].

Therefore, the use of carbon dioxide might be advantageous for developing new sustainable processes. The versatility of carbon dioxide allows it to be used as a building block for many organic products [11, 12]. The carbonylation of monomeric compounds is an important process in the chemical industry. The carbonylation reaction leads to different products according to the kind of bond formed with the atomic carbon of carbon dioxide [1, 12].

The formation of C-C bonds leads to the production of acids, lactones, esters and pyrones [13]. For example, salicylic acid is produced by the carbonylation of phenol [12]:

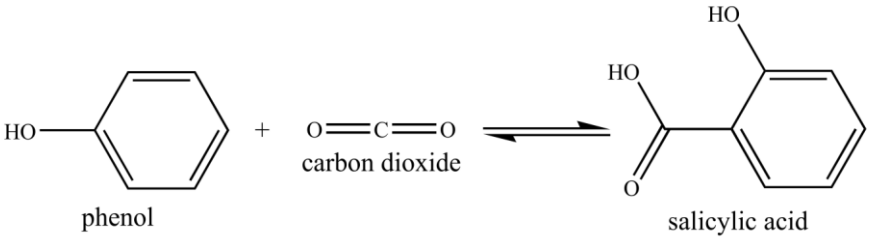

Scheme 2.1: C-C bond formation: synthesis of salicylic acid.

C-N bonds are formed to produce carbamate and isocyanates as in the production of urea from ammonia [13]:

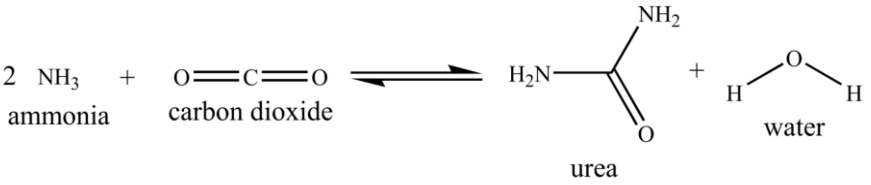

Scheme 2.2: C-N bond formation: synthesis of urea.

Carbon dioxide can also establish C-O bonds leading to the formation of organic carbonates [14, 15], as in the synthesis of dimethyl carbonate from its reaction with methanol [13]:

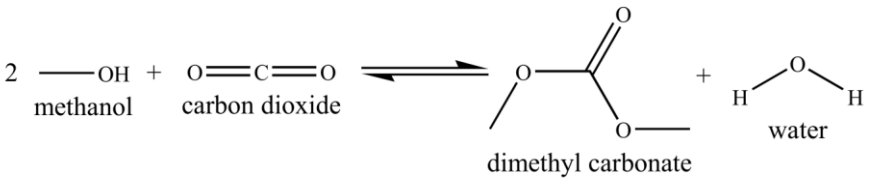

Scheme 2.3: C-O bond formation: synthesis of dimethyl carbonate.

Nowadays, in chemical industries, vast research efforts have been driven towards the development of environmentally-friendly processes based on the reduction of greenhouse and toxic gases emissions, as well as on lower energy and water consumptions. In this line, Anasta and Warner [16], proposed twelve principles in order to pave the way for the development of a sustainable green chemical process. According to these principles, the advantages of carbon dioxide are remarkable; in fact, the use of carbon dioxide as reactant and solvent encompasses three of the twelve principles of green chemistry:

- ❖ Safer solvents and auxiliaries (Principle 5)
- ❖ Use of renewable feedstock (Principle 7). Carbon dioxide could be considered renewable due to its high availability as well as its life cycle.
- ❖ Inherently safer chemistry for accidents prevention (Principle 12).

2.2. Organic Carbonates

Chemical industry is committed to develop or improve the hazardous traditional processes, responsible for the environmental problems referred before (emissions of greenhouse gases, particles, and toxic compounds), by more sustainable alternatives. Organic carbonates are an interesting organic family to be used as alternative in some of those alternative processes. Besides, organic carbonates, can be produced from carbon dioxide (carbon dioxide trap) [12, 13], and represent an important group of chemicals with large potential due to their polarity, viscosity, low toxicity and high degradability. Therefore, this class of compounds represents a key to replace some chemicals known as toxics, easy flammable and harmful for the environment and human health.

2.2.1. Organic carbonates – properties

Organic carbonates are mainly used as organic solvents and building blocks for organic compounds. According to several authors there are six important carbonates, based on their commercial value and characteristics. These organic carbonates are presented in Figure 2.2 and can be divided into two groups: linear carbonates (dimethyl carbonate (DMC) and diethyl carbonate (DEC)), and cyclic carbonates (ethylene carbonate (EC), propylene carbonate (PC), butylene carbonate (BC) and glycerol carbonate (GC)).

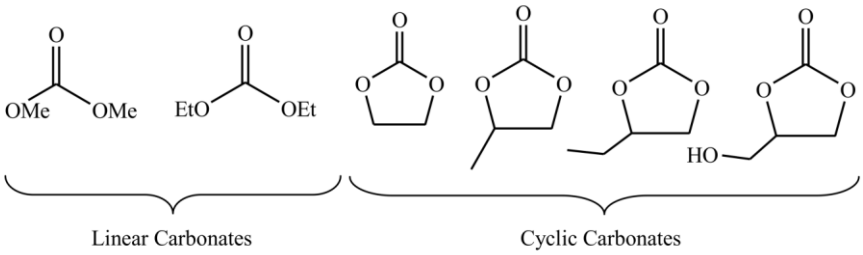

Figure 2.2: Principal organic carbonates, from the commercial point of view: linear and cyclic [17].

Some of the important properties of the organic carbonates previously referred are presented in Table 2.1. There are some relevant differences between cyclic and linear carbonates. In spite of these differences, due to their small size, all of them present high oxygen content, which also give to these compounds potential to be used as fuel additives. In particular, DMC is one of the most important carbonates to enhance the gasoline octane number: research and motor octane number [18]. Li et al. [19] studied the influence of DMC and DEC, as additives, in aviation fuels, specifically in the mixture volatility and flash point. They concluded that the presence of a small amount of carbonate increases substantially the volatility and decreases the flash point as well as the enthalpy of vaporization.

Table 2.1: Physical properties of linear and cyclic organic carbonates [17, 18].

Organic carbonate	Boiling point / K	Density$^{(293\ K)}$/ g·cm^{-3}	Viscosity$^{(298\ K)}$ / Pa·s	Biodegradability / day^{-1}	Oxygen content
DMC	363	1.07	5.90×10^{-4}	88%	53.3%
DEC	399	0.98	7.53×10^{-4}	75%	40.7%
EC	521	[a] 1.34	[a] 2.56×10^{-3}	Readily	54.5%
PC	515	1.20	2.50×10^{-3}	94%	47.1%
BC	524	1.14	3.14×10^{-3}	Readily	41.4%
GC	[b] 138	1.40	-	Readily	54.2%

[a] Under cooled liquid state; [b] at 66.7 Pa

2.2.2. Organic carbonates as solvents

In chemical industry, solvents have a remarkable action, stabilizing the solute, controlling the transition of states, among other important applications. Volatile organic compounds (VOC's) are by far the most used as solvents in chemical processes. The major disadvantages of conventional solvents are the high toxicity and the greenhouse effect promoted by their high volatility.

Ionic liquids, due to their low vapour pressure, emerged as substitutes for VOC's to overcome the toxic emissions [17]. However, ionic liquids are expensive and their biodegradability depends of the ionic interaction, which turns their use restricted for specified markets, as in pharmaceutical industries for the production of high valuable compounds. Supercritical carbon dioxide and organic carbonates have also become an attractive alternative. Organic carbonates are classified as aprotic highly dipolar solvents, similar to dimethyl sulfoxide (DMSO) and *N*,*N*-dimethyl formamide (DMF), considered volatile organic compounds.

Shäffner et al. [17] compared the toxicity and biodegradability of the main organic carbonates with those common solvents used in chemical processes: toluene, methanol (MeOH), tetrahydrofuran (THF), DMF, DMSO and dichloromethane. They concluded that organic carbonates have high biodegradability, between 75-100%, compared with conventional solvents, between 3.1% (DMSO) and 90% (MeOH). Furthermore, organic carbonates have faster decomposition rates and do not present median lethal dose (LD_{50}) values by inhalation (experiments performed in rats), with exception of DMC, which shows a median lethal dose of 140 mg·L^{-1} for exposure during 4 hours. However, some conventional solvents show lower lethal dose values such as dichloromethane (88 mg·L^{-1} for exposure during 30 minutes) and THF (54 mg·L^{-1} for exposure during 4 hours). Besides the general characteristics as solvents, organic carbonates are also interesting solvents for [16, 17]:

- Li-ion batteries: used as solvent for lithium salts due to their high dielectric constant.
- Electroanalytic systems: used as sensor to detect ammonia, thallium (III) among other applications.
- Polymerization: solvent for electropolymerization of polypyrrole, polythiophene and polyanilines.

Comparing cyclic and linear carbonates, a considerable difference between the viscosity values of each group can be observed, around three times higher for the cyclic carbonates, and also a large difference in the

boiling point, around 120 K higher for cyclic carbonates. However, the values of density are similar for all of them, with a maximum difference of 20%. These differences have some consequences for industrial applications: high viscosity leads to high pressure drop and can eventually influence the mass transfer resistances that increase with the viscosity of the solvent; and, high boiling point can be useful to guarantee a liquid state of the mixture but it can also lead to a waste of energy in the separation steps as in distillation.

2.2.3. Organic carbonates as building blocks

In spite of the high potential as solvents, organic carbonates have also a large applicability as building blocks for organic chemical products, which turn them into green substitutes for several processes. In particular, DMC can replace phosgene and dimethyl sulphate in carbonylation and methylation reactions, respectively. Indeed, DMC is an important alkylating agent for gas-liquid phase transfer catalysis. This reaction mechanism allows the alkylation of weak acids, such as phenols, thiophenols, aromatic amines, malonic acid esters, and arylacetonitriles [20]. Moreover, dimethyl and diethyl carbonate can be used for the production of urea, urethanes, and aliphatic carbonic acid esters. Diphenyl carbonate is a feedstock for low molecular weight monoisocyanates. Ethylene and propylene carbonates are used as monomers to produce polycarbonates [20].

Summarizing, their low toxicity, high degradability, and high versatility, emphasize the benefits of using organic carbonates for new sustainable processes. Besides, organic carbonates can also be considered as carbon dioxide traps since they can be produced from carbon dioxide.

2.3. Dimethyl Carbonate

Each organic carbonate has different performance depending on the application. However, this work will focus on DMC. DMC, the simplest organic carbonate, has an important role in chemical industry due to its versatility and large range of applications; moreover, its low toxicity for human health and other life forms turns DMC in a green chemical for sustainable processes. In the last 20 years the research involving DMC showed an exponential increase according to the SCOPUS data base. The main applications of DMC are as solvent, fuel additive and reactant.

2.3.1. Solvent and fuel additive

As solvent, DMC is a viable alternative for volatile organic solvents as non-polar aprotic solvent, reducing VOC's emissions. Its unique properties, low viscosity, low toxicity and its good solvency power, are pointed as the main advantages in many applications as solvent. In fact, DMC is an alternative for toxic compounds, such ketones or acetate esters in several applications, such as solvent for paints [21]. In addition, dimethyl carbonate became an important solvent for lithium rechargeable batteries applications [17].

In general, oxygenated compounds used as fuel additives produce less soot than hydrocarbon compounds. Westbrook et al. [22] observed a linear decrease of soot precursors with the fraction of oxygen content from a diesel engine. In particular, dimethyl carbonate has several physical properties to become a valuable additive either for gasoline or diesel: high blending octane number (105), low Reid vapour pressure, high oxygen content (53 *wt*%), reducing CO, SO_x and NO_x emissions [18]. Due its benign properties and since it also has required physical properties, DMC is an attractive compound to replace methyl-tert-butyl ether [18, 23].

2.3.2. Building block

Beyond the applications mentioned above, DMC is also considered a building block for many organic synthesis [24, 25], especially for carbonylation and methylation reactions, being an eco-friendly candidate to replace the current hazardous chemicals phosgene and dimethyl sulphate, respectively. Furthermore, DMC can be easily tuned as reactant by changing the operating conditions [26]; at lower temperature it usually acts as a carboxymethylating agent, but at higher temperatures it can behave as a methylating agent in the presence of several nucleophiles.

Methylation reactions can be performed using DMC as feedstock instead of the conventional toxic reactants, methyl sulphate or methyl halide. Moreover, there are three main methylation types, depending on the carbon bond, *C*-methylation, *O*-methylation and *N*-methylation. DMC can be used for the methylation of several organic groups [13, 27-30], such as phenols, arylacetonitriles, aromatic amines, thiols, aniline, nitrogen containing heterocycles and amides.

Instead of the toxic and hazardous route from phosgene, isocyanates, which are widely used for biomedical applications [31], DMC can be produced by methoxycarbonylation of amines into carbamates followed by decomposition to the corresponding isocyanate. Other important reaction is the methylation of phenol to produce dimethyl phenol, which is a feedstock for polycarbonates. DMC can also be applied in several methoxycarbonylation reactions such as the synthesis of phenylethenyl methyl carbonate from phenylacetaldehyde [32].

Esterification and transesterification reactions with carboxylic acids and alcohols are other important applications for the benign use of DMC as reactant. For example, unsymmetrical carbonates can be synthesized from DMC and alcohols [33]. Quaternary ammonium salts can also be produced from the reaction between DMC and aliphatic amines [34]. Reactions with metal oxides are other important reactions. Alkoxysilanes are important chemicals for the ceramic industry; in particular, tetramethoxysilane can be produced from DMC and silica [35]. Several works studied the application of DMC for fatty acid methyl esters (FAME's) production instead of the conventional process from methanol [36-39]. Besides the low price of methanol, the co-products formed from DMC (glycerol carbonate and citramalic acid) are more valuable than glycerol, co-product from the transesterification of triglycerides. Moreover, FAME's can also be produced by esterification of fatty acids in the presence of supercritical DMC. Based on this study, Tan et al. [40] optimized the FAME's production from DMC and vegetable oils at supercritical conditions. A maximum

FAME's yield of 91% was observed after 30 minutes at 653 K, 15-25 MPa, and a DMC to oil molar ratio of 39 to 1.

The main applications of DMC are summarized in Table 2.2. In spite of the large demand for DMC, the production is still much lower than the industrial needs. In 1997 the worldwide production was around 45 kton per year, while the US refineries estimated a demand from 5 to 10 times larger [18]. The global annual production and demand of DMC is hard to estimate. As mentioned, DMC has some physical properties required to replace several processes but this will strongly depend on its price, which is influenced by the global market and the available amount. However, the demand of DMC is much higher than the production [41]; hence, lots of efforts have been done in order to find a sustainable route to produce DMC in large scale.

Table 2.2: Main applications of dimethyl carbonate.

Application	Description	Ref.
Solvent	DMC is an alternative for ketones and acetate esters used as solvents for paint industries. DMC shows high performance as non-aqueous electrolyte for lithium batteries. DMC can be used as a generic solvent with low toxicity and low emissions.	[17, 21, 42]
Fuel additive	DMC enhances the performance of gasoline due to its high oxygen content (53.3%) and high octane number. It also promotes the performance of diesel and decreases the sulphur, aromatic and soot emissions.	[18, 19, 43]
Reactant	DMC is the base to produce aromatic polycarbonates through diphenyl carbonate. DMC is a reactant for carbonylation and methylation replacing the toxic and corrosive phosgene and dimethyl sulphate or methyl halide, respectively.	[20, 21, 44]

2.4. DMC Production

2.4.1. Conventional process

Until 1980 [21], DMC was only produced based on the phosgenation of methanol, which involves very toxic compounds as phosgene and other corrosive chemicals to recycle phosgene.

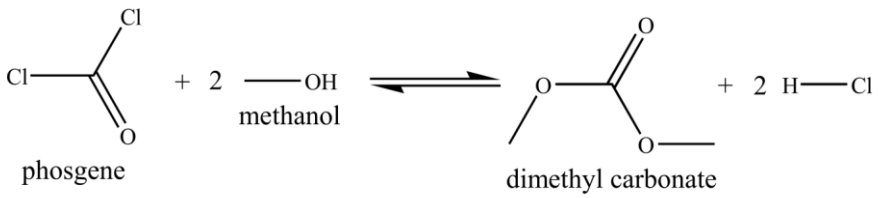

Scheme 2.4: Phosgenation of methanol

Then, the Italian company EniChem developed a novel route to produce dimethyl carbonate free of phosgene: the oxidative carbonylation (oxy-carbonylation) of methanol [45, 46]. The authors, Romano et al.

[46], claim the production of DMC from methanol, carbon monoxide and oxygen in a single *redox* reaction catalyzed by CuCl.

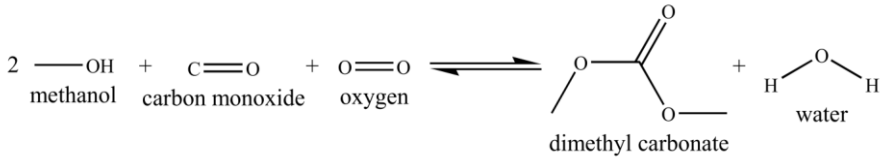

Scheme 2.5: Oxy-carbonylation of methanol

Several researches have been carried out in order to improve this process, in particular, the development of new catalysts [47-49] and understanding the reaction mechanisms of Cu based catalysts [50]. For instance, Ren et al. [51] tested a Cu catalyst supported in SiO_2–TiO_2, in order to reduce the corrosion. In spite of the corrosion reduction of around five times, it was observed higher selectivity and catalytic performance comparing with the conventional CuCl catalyst.

More recently, Ding et al. [52] proposed a novel catalyst to improve the selectivity (98% selectivity of DMC from CH_3OH, 70% selectivity of DMC from CO) and catalytic stability: $PdCl_2$-$CuCl_2$-KOAc/AC-AL_2O_3; furthermore, a gas-phase reaction mechanism was proposed. Meng et al. [53] also studied a bi-metallic Wacker type catalyst for the oxy-carbonylation of methanol: $CuCl_2$-$PdCl_2$. The major advantage of these catalysts is that palladium promotes the activation of carbon monoxide; however, palladium is very expensive, which makes these catalysts not attractive for industrial applications.

In spite of the great advance reached by this phosgene free route, it still involves risk of explosion and corrosive materials [54]. After, the transesterification of ethylene carbonate with methanol [55] was claimed by Texaco, for DMC production and it has been used until today. This route is responsible for a small fraction of the actual DMC production but is pointed as a sustainable alternative for the oxy-carbonylation process; it will be discussed in the following section in more detail.

Later, a Japanese company, Ube Industries, patented the oxidative carbonylation of methanol using NO_x , as oxidative agent, instead of O_2, to reduce the risk of explosion [56]. This route is also called carbonylation of methyl nitrite (MN); MN is first produced from the reaction between nitrogen oxides and methanol, and then it reacts with carbon monoxide to form DMC.

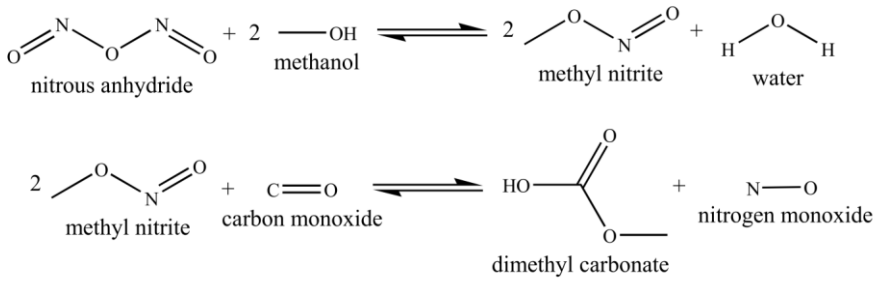

Scheme 2.6: Carbonylation of methyl nitrite

Recent researches are focused on the electrochemical oxy-carbonylation of methanol to avoid the use of hazardous oxidative agents [57]; however, this route was not industrially implemented yet. These two main

alternative processes for DMC production – oxy-carbonylation and carbonylation of methyl nitrite – have been replacing the traditional phosgenation of methanol. In the end of the 90's, Enichem and Ube were the largest DMC producers; each unit had a production capacity around 12 kton annually, which represented more than 25% of the worldwide production [1, 18, 58].

Nowadays, DMC is produced in other large chemical companies, such as General Electric, SNPE, Texaco, Mitsubishi, BASF, etc. In Table 2.3 are summarized some of the most relevant patents related to DMC production from 1979 until the present.

2.4.2. New alternative processes

In spite of the improvements achieved by the two phosgene free routes, they are still quite hazardous. The oxy-carbonylation involves the use of lethal carbon monoxide and oxygen streams, which increases the risk of explosion; the carbonylation of methyl nitrite (MN) arises as an alternative route to the phosgenation and oxy-carbonylation of methanol, although it also uses corrosive fluids to reactivate the catalyst [12]. Considerable efforts have been done to overcome the major issues of these conventional processes (phosgenation of methanol, and oxy-carbonylation of methanol, and carbonylation of methyl nitrite) through the development of new alternative routes to produce DMC, aiming the reduction of the environmental impacts and the minimization of the risks to the human health: transesterification of cyclic carbonates, transesterification of urea, carbonylation of methanol, and oxidation of dimethoxy methane.

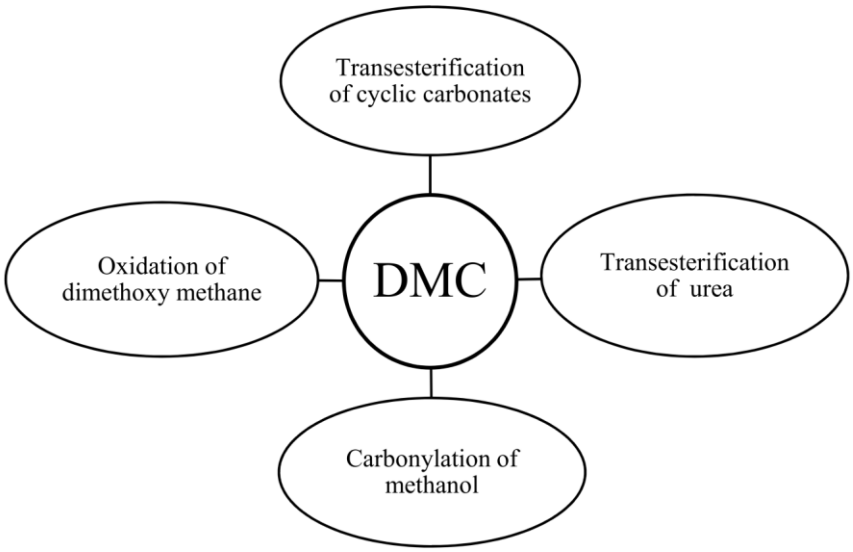

Scheme 2.7: New alternative routes for DMC synthesis.

Table 2.3: Patented processes for dimethyl carbonate production.

Year	Assignee	Summary of invention	Ref.
1979	BASF Aktiengesellschaft	This patent claims the separation of DMC from methanol stream, by distillation, with addition of aprotic organic liquid. Compounds with one or more ester group are preferred. The distillation of this ternary mixture eliminates the azeotropic mixture and removes the methanol in the head stream at 333 K, while the DMC and the extractive agent are recovered in the bottom stream at 523 K.	[59]
1980	Anic, S.p.A.	Anic S.p.A, current EniChem, developed the first industrial phosgene-free process for carbonic acid ester production. The carbonic acid esters (linear organic carbonates), are produced *via* oxy-carbonylation of methanol using a metal salt as catalyst, such as CuBr, CuCl, $CuClO_4$, $CuCl_2$, and $CuSO_4$. The reaction should be carried out between 343K and 473 K and a pressure higher than atmospheric.	[45]
1987	Texaco inc.	This patent presents the co-production of DMC and ethylene glycerol by transesterification of ethylene carbonate with methanol over heterogeneous organic catalysts. The preferred operating reactor conditions are: temperature 333-398 K; pressure 0.34-34 MPa; residence time 0.5-4 h; MeOH/EC 2-5. Weak basic, basic, weak acid and acid ion exchange resins, alkali and alkaline earth silicates and ammonium exchanged zeolites were proposed and tested as catalysts.	[55]
1988	Texaco inc.	This patent discloses the production of organic carbonates from carbon monoxide and the respective alcohol (ROH). The reactions are catalyzed by copper hydrocarbon halide in the presence of a promoter, such as BF_3, $CaCl_2$, $MgCl_2$, etc. The reaction carried out in excess of methanol at CO pressure of 2.7 MPa, 363 K during 4 hours reached a yield of 99% of DMC. This reaction was catalysed by Cu(OMe)Cl and $MgCl_2$ was used as promoter.	[60]
1988	Michael Burnside & Partners	In this patent is claimed the transesterification of ethylene carbonate with methanol to produce DMC and ethylene glycol catalyzed by zirconium, titanium and tin catalyst in salt or complex form. A temperature between 323 K and 423 K, a pressure above 0.34 MPa and an ethylene carbonate to methanol weight ratio of 2 to 5 are preferred to reach high selectivity and DMC yield. For instance, using zirconium acetylacetonate as catalyst, DMC selectivities of 98% and 86% were observed, based on the ethylene carbonate and methanol conversions, respectively.	[61]
1991	Ing. Barzanò & Zanardo Milano	A reactor design for the production of dimethyl carbonate from the oxidative carbonylation of methanol is disclosed in this patent. The reactor was designed to use cuprous chloride as catalyst and to operate in the temperature range of 353-473 K and pressure of 1-5 MPa. The reactor is composed by two tubes with a condenser coupled to the outlet stream where the liquid, rich in methanol, water and DMC, was separated from the gas stream, which is recycled to the reactor and mixed with fresh reactants.	[62]

Year	Assignee	Summary of invention	Ref.
1994	Ube Industries	The binary distillation between methanol and DMC is limited by the azeotrope compositions at 30 *wt*% of DMC. Addition of dimethyl oxalate eliminates the azeotrope, allowing the separation of pure methanol by distillation. A second distillation column should be used to remove the dimethyl oxalate from DMC. Water has to be pre-removed in order to avoid the decomposition of dimethyl oxalate.	[56]
1996	Mobil Oil Corp.	DMC is produced by transesterification of propylene carbonate catalyzed by an alkaline earth metal halide supported over a solid having high surface area and controlled surface hydroxyl concentration. Different methodologies to prepare the catalyst are presented. A conversion of 42% of propylene carbonate and DMC selectivity of 91%, were observed for the reaction performed at 423 K.	[63]
1997	Ube Industries	An industrial process to produce DMC from carbon monoxide and methyl nitrite is developed in this patent. Firstly, the reaction, catalyzed by palladium chloride and cupric chloride, occurs between 353 K and 423 K. After the DMC is removed by absorption in dimethyl oxalate, the residual methyl nitrite also present in the dimethyl oxalate steam is removed with carbon monoxide, before the purification of DMC by distillation. Some NO formed as by-product is regenerated in methyl nitrite by reacting with O_2 and MeOH, in order to be recycled into the reactor.	[64]
2001	General Electric Company	The use of a hydroxyl compound as extractive distillation is proposed to eliminate the azeotrope between methanol and DMC, and to obtain pure methanol at the bottom of the first column. An additional distillation column is required to separate DMC from the extractive agent, which is preferably phenol or anisole.	[65]
2002	ExxonMobil Chemical Patents Inc.	Dialkyl carbonate and diols are produced from alkylene oxide, carbon dioxide and aliphatic monohydric alcohol. Firstly, the alkylene oxide reacts with the carbon dioxide at 373-473 K and 2-9 MPa to produce the alkyl carbonate, with a yield around 90%. Secondly, the non reacted carbon dioxide is recycled by a flash separation and the alkyl carbonate with impurities follows to the second reactor in the same range conditions to produce the dialkyl carbonate and diol by transesterification with aliphatic monohydric alcohol.	[66]
2006	Hunton & Wiliams	The dimethyl carbonate was produced from urea and methanol in a catalytic rectification reactor, at 423-473 K and 0.5-3 MPa. The preparation of catalysts is also claimed. The catalyst suggested for this reaction system is composed by a support phase (20-50 *wt* %), α-alumina, γ-alumina, silica or molecular sieves, that activates the components, alkali metal, alkali-earth metal or transition elements. In spite of the advantages of this phosgene-free route, the DMC yield is still low.	[67]
2007	Maiwald	The transesterification of propylene carbonate catalyzed by a metal cyanide complex catalyst is described using several alcohols, methanol, ethanol, propanol, butanol, hexanol, or benzyl alcohol as feedstock. The catalyst showed selectivity of 82% for the reaction with methanol.	[68]

Year	Assignee	Summary of invention	Ref.
2007	Wenderoth, Lind & Ponack, L.L.P.	In this patent DMC is directly produced from methanol and carbon dioxide. Moreover, the authors disclose the co-production of methanol and DMC from the steam reforming of natural gas, essentially composed by methane. Therefore, hydrogen, carbon monoxide and carbon dioxide are formed during the reforming, and are used as feedstock for the methanol synthesis.	[69]
2008	Millen, White, Zelanio & Braginn, P.C.	This patent presents the performance of a catalyst for the oxidative carbonylation of methanol in the gas phase, in order to produce dimethyl carbonate. The catalyst is composed by Cu (1-20 *wt* %) supported on a zeolite. It was observed a DMC yield of 134 $kg \cdot m_{cat}^{-3} \cdot h^{-1}$ with selectivity of 73% .The reaction was carried out at 403 K.	[70]
2008	Marina Larson	The co-production of dimethyl carbonate and diphenyl carbonate is an interesting process since both have a high commercial value. In this patent the authors developed a reactor design that avoids the catalyst accumulation and the consequent clogging of transfer lines.	[71]
2010	Mitsubishi Heavy Industries	In this invention, solid acid catalysts, preferably Al_2O_3, ZrO_2 and TiO_2, loaded with strong acid are suggested for the DMC synthesis from carbon dioxide and dimethoxypropane. The SO_4^{2-} and PO_4^{3-} are preferably used to load the catalyst, between 2-4 *wt*%. A DMC yield of 27% was reached at 458 K and 30 MPa with 18 *wt*% of ZrO_2 loaded with PO_4^{3-} as catalyst, which represents a reaction activity five times higher than reached by the base catalyst.	[72, 73]

Nevertheless, researches on oxy-carbonylation of methanol and methyl nitrite are continually explored, since these routes are the main source of DMC industrial production, such as the development of new catalysts. Recently it was reported the use of Cl-free catalyst Cu/starch [74], or supported ionic liquid phase ([OMA][Br]) over polymer-based material in order to overcome the Cu deactivation [75].

In conclusion, a sustainable process for DMC production is necessary in order to develop new processes based on green chemistry principles capable to compete with the conventional toxic and hazardous processes.

Transesterification of cyclic carbonates

The transesterification of ethylene carbonate is by far the most studied alternative for DMC synthesis [76-84], mainly due to the high productivity, selectivity for DMC and also the co-generation of glycerol carbonate, which has a high commercial value. For instance, Sankar et al. [81] reached high selectivity (100%) for DMC and conversion (80%) of ethylene carbonate at mild temperatures and atmospheric pressure; furthermore, the authors reported the one-pot transesterification reaction, where the EC was produced *in situ* from carbonylation of ethylene oxide (EO); however, low selectivity was reached by this methodology.

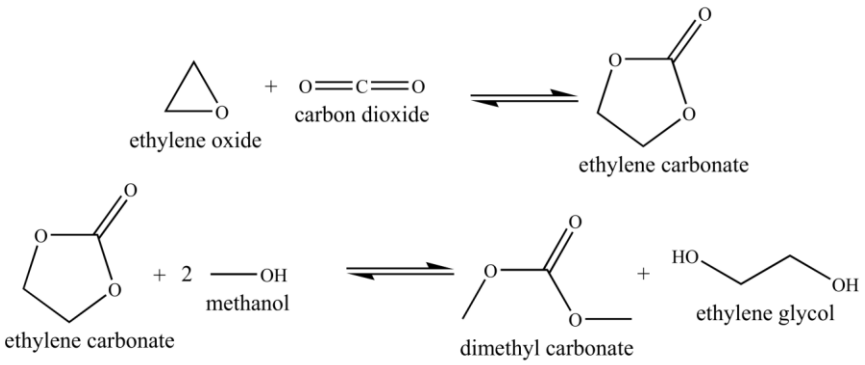

Scheme 2.8: Transesterification of ethylene carbonate

More recently, Liu et al. [83] reached high conversion of ethylene carbonate (94%), with also high selectivity towards DMC formation (99%) using a novel catalyst: *Penicillium expansum* lipase (PEL) supported over CMC-PVA polymer. In Table 2.4 is summarized the state-of-the-art for this reaction: operating conditions, yields, and selectivities of DMC for the transesterification of ethylene carbonate reached by the different catalysts.

The transesterification of propylene is also an interesting alternative for DMC synthesis because of the high value of propylene glycol, also produced by this reaction. Holtbruegge et al. investigated this route catalyzed by sodium methoxide [85] at 353 K; even though a large MeOH to propylene ratio was used (10/1), DMC yield was lower than 50%. Afterwards, Holtbruegge et al. [86] proposed a membrane-assisted reactive distillation process for the transesterification of PC, in order to overcome the thermodynamic constraints: reaction conversion and binary azeotrope (DMC-MeOH). Then, they designed and optimized a membrane-assisted reactive dividing wall column [87]; and compared this intensification process with the base case process (excess of MeOH followed by recycling), they concluded that a reduction around 35% for the investment and operating costs is expected. Huang et al. [88] also studied the transesterification of PC by

reactive distillation; however, they proposed a pressure-swing distillation process in order to eliminate the azeotrope.

The main drawbacks of this route are the high costs of cyclic carbonates, the considerable thermodynamic limitations, and the fact that cyclic carbonates be produced from hazardous reactants, such as ethylene oxide and propylene oxide.

Table 2.4: Summary of the state-of-the art for the transesterification of ethylene carbonate with methanol.

Catalyst	Operating Conditions	Time	Yield	Selec.	Ref.
MgO	V_R: 50 mL; n_{MeOH}/n_{EC}: 8/1; EC: 25 mmol; catalyst: 0.50 g; 423 K	4 h	66%	100%	[77]
Si:Mg:Na:K oxides	V_R: 50 mL; n_{MeOH}/n_{EC}: 8/1; EC: 25 mmol; catalyst: 0.25 g; 423 K	4 h	73%	90%	[76]
A-21	V_R:100 mL; n_{MeOH}/n_{EC}: 8/1; catalyst: 4.5 g; 398 K	4 h	30%	97%	[79]
$PVP_{(homogeneous)}$	V_R: 100 mL; n_{MeOH}/n_{EC}: 8/1; EC: 25 mmol; catalyst: 0.44 g; 413 K	4 h	96%	85%	[80]
$Na_2WO_4 \cdot H_2O$	n_{MeOH}/n_{EC}: 10/1; EC: 50 mmol; catalyst: 1 g; 298 K	5 h	80%	100%	[81]
Na-dawsonite	V_R: 50 mL; n_{MeOH}/n_{EC}: 4/1; catalyst: 10 *wt*% of EC; 3.4 MPa (CO_2); 343 K	4 h	65%	100%	[82]
PEL/CMC-PVA polymer	V_R: 25 mL; n_{MeOH}/n_{EC}: 16/1; catalyst: 2.2 g; 333 K	48 h	94%	99%	[83]

Transesterification of urea

Studies based on urea as feedstock for the production of DMC have been increasing in parallel with the transesterification of the ethylene carbonate route [89]. The synthesis of DMC is performed in two steps, where the first one corresponds to the conversion of urea into methyl carbamate (MC) by reacting with methanol followed by the transesterification of MC into DMC.

This route is very attractive due to the low toxicity of urea, although the low DMC yields forces the used of high MeOH/urea ratio; and, the low reactivity of urea requires high reaction temperature (over 423 K), which might lead to the decomposition of DMC. In Table 2.5 are summarized the main catalysts proposed in recent works for the transesterification of urea into DMC.

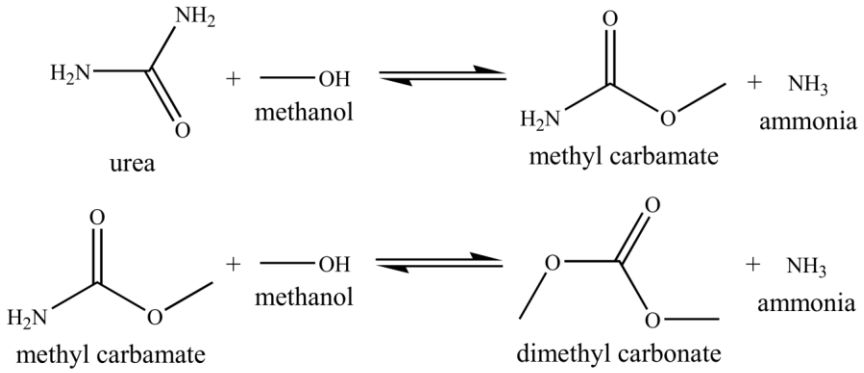

Scheme 2.9: Transesterification of urea

Table 2.5: Summary of the state-of-the-art for the transesterification of urea with methanol.

Catalyst	Operating Conditions	Time	Yield	Selec.	Ref.
ZnO	V_R: 250 mL; n_{MeOH}/n_{Urea}: 20/1; catalyst: 1 g; 453 K	9 h	37%	<100%	[90]
ZnO-CaO	n_{MeOH}/n_{Urea}: 20/1; Urea: 100 mmol; MeOH: 2 mol; catalyst: 0.4 g; 453 K	10 h	41%	81%	[91]
ZnO-Al_2O_3	n_{MeOH}/n_{Urea}: 20/1; Urea: 100 mmol; MeOH: 2 mol; catalyst: 0.4 g; 453 K	10 h	36%	-	[92]
Polyphosphoric acid	V_R: 750 mL; n_{MeOH}/n_{Urea}: 14/1; catalyst: 30 g; 0.8 MPa (CO_2 co-solvent); 423 K	4 h	67%	<100%	[93]
$C_{36}H_{70}O_4Zn$	V_R: 750 mL; n_{MeOH}/n_{Urea}: 15/1; catalyst: 9 g; 400 mL solvent (polyethylene glycol dimethyl ether); 423 K	10 h	29%	<100%	[94]
7ZnO-3CeO_2	V_R: 250 mL; n_{MeOH}/n_{Urea}: 2.7/1; catalyst: 0.25 g; 2 MPa (CO_2 solvent); 443 K	4 h	29%	-	[95]
None	V_R: 285 µL; n_{MeOH}/n_{Urea}: 14/1; 9.2 MPa; 538 K	2 h	97%	<100%	[96]

Direct carbonylation of methanol

Besides all the alternative routes presented for the DMC production, the simplest route is the direct conversion of methanol and carbon dioxide, producing dimethyl carbonate and water (Scheme 2.3). This route promotes the consumption of carbon dioxide, which is also non-toxic, non-flammable, non-corrosive and abundant. Methanol shows low toxicity comparing to the chemicals used on the other routes, and is also economically attractive since the price should round the 320 US dollar per ton (this price was estimated for production of methanol from coal in China in 2011 [97]). The low reaction rate and high thermodynamic limitations [98, 99] are the main barriers to the industrial implementation of this route. This route will be deeply discussed in the next section.

Oxidation of dimethoxy methane

This route was recently proposed by Ding et al. [100], consisting in the oxidation of dimethoxymethane (DMM).

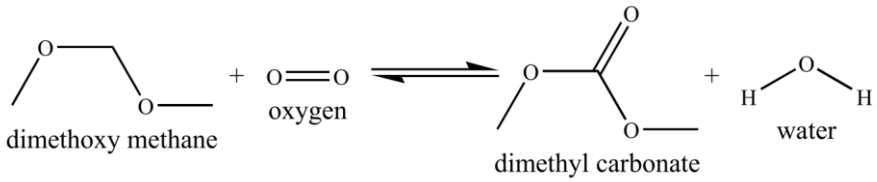

Scheme 2.10: Oxidation of dimethoxy methane

The reaction was performed at 413 K and 2 MPa, over CuO/SiO_2 based catalyst. The main advantages are the low toxicity of DMM and the high conversion, around 90%. However, this route is not completely selective towards DMC formation and needs *N*-hydroxyphthalimide, as radical initiator, which will represent a contamination of the products. In spite of the good results accomplished, this route should be further explored in order to be able to be compared to the others routes.

Comparing the routes

These are the main routes for DMC synthesis, although it is not clear which one might become the most sustainable for industrial production. Some of them were not developed enough to predict their potential. All the routes show advantages and disadvantages; therefore, the choice of the best route should be determined by the weight of the different factors such as economical, environmental, operating as well as safety and human health impact. Nowadays, the choice of a new process is also determined by its environmental impact, such as greenhouse gases emissions and human health consequences, but still has to be profitable. In spite of the advantages/disadvantages presented, it is not possible to conclude, based on those qualitative differences, which one is the most sustainable route to produce DMC. In Table 2.6 are summarized the main advantages and disadvantages of all the routes.

In order to assess the sustainability of each route, Monteiro et al. [101] used some measuring tools to quantify the economical and environmental aspects; the oxidation of dimethoxy methane and transesterification of propylene carbonate were out of the scope of this work. For the economical assessment they compared the price of the product with the reactants cost in stoichiometric conditions, while for environmental assessment they considered two factors: the toxicity and the environmental impact. The environmental impact was measured by a waste reduction algorithm [102].

Table 2.6: Comparison of different routes for the synthesis of dimethyl carbonate: advantages and disadvantages [21, 42, 103].

Reaction	Catalyst	Advantages	Disadvantages
Phosgenation of methanol	Pyridine	High yield	Very Toxic, corrosive, acid waste
Oxy-carbonylation of methanol	CuCl, KCl	No phosgene, high yield	Use of CO, risk of explosion, corrosive
Carbonylation of methyl nitrite	Pd(II) based	No phosgene or O_2, high yield	Use of CO, corrosive
Transesterification of ethylene carbonate (or propylene carbonate)	Metal basis oxides, MgO	CO_2 instead of CO, production of EG	Toxic, risk of explosion, low yield
Transesterification of urea	Metal basis oxides	Low toxicity	Low yield
Carbonylation of methanol	$Bu_2Sn(OMe)_2$, ZrO_2, CeO_2 based	Low toxicity, promotes CO_2 use, low cost of reactants	Very low yield
Oxidation of dimethoxy methane	Cu based	High yield	Medium selectivity, risk of explosion

Table 2.7 presents the total score, which is inversely proportional to the sustainability of the process. It was considered an equal weight factor for the three indicators. The phosgenation of methanol is by far the worst solution, while carbonylation of methanol and methanol oxy-carbonylation present the best score, 0.12 and 0.07, respectively. However, the authors considered the transesterification of methyl carbamate and ethylene carbonate as the most sustainable, since methanol oxy-carbonylation does not involve carbon dioxide sequestration and rejected carbonylation of methanol due to being not feasible industrially; similar conclusions were reported by Kongpanna et al. [104]. Then, a more detailed comparison of those two routes was accomplished by the authors using Life Cycle Analysis [105].

Table 2.7: Sustainability of the different routes to produce DMC [101].

Route	Total score	Final Rating
Methanol oxy-carbonylation	0.07	First
Carbonylation of methanol	0.12	Second
Transesterification of methyl nitrite	0.37	Third
Transesterification of ethylene carbonate	0.49	Fourth
Transesterification of urea	0.77	Fifth
Phosgenation of methanol	3.00	Sixth

The transesterification of propylene carbonate would have similar sustainability as the transesterification of ethylene carbonate, since the process and the chemicals involved are very alike; while the sustainability of the oxidation of dimethoxy methane is hard to guess without further information.

2.5. Direct Synthesis of DMC from Carbonation of Methanol

In spite of the drawbacks associated to the thermodynamic limitations of the direct synthesis of DMC, this route is still one of the most promising routes for DMC synthesis due to environmental and economical reasons. The challenge of this route is to overcome the kinetic and thermodynamic limitations, which have been catching the attention of researchers all over the world, namely in the development of novel catalysts or *in situ* water removal techniques, to shift the reaction equilibrium towards DMC production. The state-of-the-art will be discussed along this section. In Table 2.8 is shown the main physical properties for the components presented in this route.

Table 2.8: Main physical properties for CO_2, MeOH, Water and DMC (DIPPR^{TM}).

Property	CO_2	MeOH	Water	DMC
Molecular weight / g·mol^{-1}	44.01	32.04	18.02	90.08
Melting point / K	216.58	175.47	273.15	273.15
Normal boiling point / K	-	337.85	373.15	363.4
Vaporization Enthalpy (298 K) / J·kmol^{-1}	5.31×10^{6}	3.75×10^{7}	4.40×10^{7}	3.71×10^{7}
Critical temperature / K	304.21	512.5	647.096	548*
Critical pressure / MPa	7.383	8.084	22.064	4.50*
Acentric factor	0.2236	0.5658	0.3449	0.3846
Liquid density (298 K) / kmol·m^{-3}	-	24.65	55.22	11.08
Viscosity (298 K) / Pa·s	1.50×10^{-5}	5.39×10^{-4}	9.16×10^{-4}	5.83×10^{-4}
Dielectric constant (298 K)	1.449	33	80.1	3.087
Dipole moment / C·m	0.0	5.67×10^{-30}	6.17×10^{-30}	3.0×10^{-30}
Flash point / K	-	284.15	-	289.85

* Predicted

2.5.1. Thermodynamic and kinetic limitations

As previously discussed, the main issue of the direct production of dimethyl carbonate from methanol and carbon dioxide is the low yield of DMC. This low DMC yield is caused by thermodynamic limitations. Figure 2.3 shows the methanol conversion as a function of the temperature, at equilibrium conditions, as estimated by Zhao et al. [99].

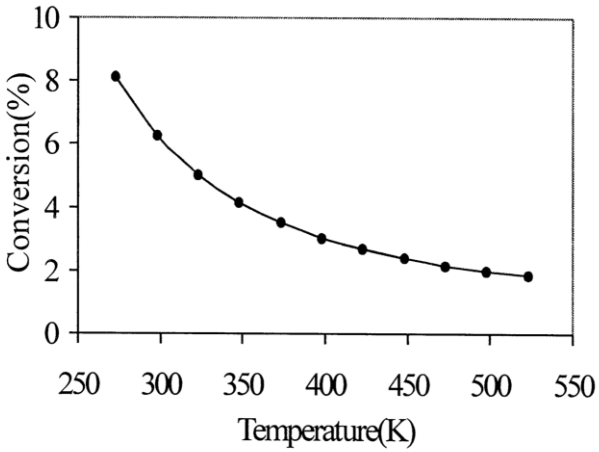

Figure 2.3: Estimated conversion of methanol for DMC synthesis at equilibrium conditions. Volume: 80 mL; methanol: 100 mmol; reaction pressure: 7 MPa [99].

Leino et al. and Cai et al. [106, 107] estimated the standard enthalpy and Gibbs free energy changes of reaction ($\Delta_r H^o$ and $\Delta_r G^o$). These values are shown in Table 2.9, together with the standard heat capacity (C_p), standard enthalpy of formation ($\Delta_f H^o$), and standard Gibbs free energy of formation ($\Delta_f G^o$), for all the compounds.

Table 2.9: Thermodynamic properties of the components for direct DMC production [106].

Component	$\Delta_f H^o$ / kJ·mol^{-1}	$\Delta_f G^o$/ kJ·mol^{-1}	C_p/ J·mol^{-1}·K^{-1}	$\Delta_r H^o$ / kJ·mol^{-1}	$\Delta_r G^o$ / kJ·mol^{-1}
DMC	-613.78	-464.23	109.50		
Water	-285.83	-237.14	75.30	-27.90	26.21
CO_2	-393.51	-394.38	37.10	(298K)	(298 K)
MeOH	-239.10	-166.60	81.59		

Besides the low equilibrium yields, the reaction rate reported is also low due to the low activity of carbon dioxide; however, the reaction rate can in principle be improved by developing new catalysts. Therefore, the catalyst activity seems to be the key solution to overcome the kinetic limitation.

2.5.2. Homogenous catalysis

Organotin alkoxides compounds have been investigated as catalysts for this reaction due to the high selectivity for DMC. The dibutyltin dimethoxide is a well known catalyst for this route. However, in the presence of water the dibutyltin dimethoxide decomposes itself [108]: $Bu_2Sn(OCH_3) + H_2O \rightleftharpoons Bu_2SnO + CH_3OH$.

Ballivet-Tkatchenko et al. [109] have carried out the reaction catalysed by dibutyltin dimethoxide at 423 K and 20 MPa. In these conditions, the authors reached a conversion around 1%, and it was observed a decrease to half of the activity between the first and second reactions. The deactivation of dibutyltin dimethoxide with water can be overcome by the regeneration of Bu_2SnO with methanol in the presence of a dehydrating alcohol, such as 2,2-dimethoxypropane (DMP), as proposed by Kohno et al. [110], at high carbon dioxide pressure and excess of DMP. The effects of the dehydrating alcohol are deeply discussed in the next section. They also achieved the DMC synthesis [111] in the same conditions with a Ti-catalyst in the presence of polyether-type ligands, reaching a DMC yield of 41%, which is higher than the 28% obtained with the organotin catalyst [112].

In order to avoid the organotin catalyst, Zhao et al. [109] synthesized DMC using nickel acetate at moderated temperatures (305 K) and 10 MPa, reaching a DMC yield of 3%. This new catalyst showed higher activity in the presence of water. However, the selectivity of this catalyst strongly depends on temperature and pressure, leading to the production of methyl acetate (MA) as secondary product.

Fang et al. [113] performed the direct synthesis of DMC using an alkaline catalyst, and CH_3I as promoter, at 5 MPa and temperatures between 353 and 373 K. The promoter is responsible for donating the second methyl group to the DMC molecule. Furthermore, dimethyl ether (DME) was produced by a side reaction; however, the decrease of temperature from 373 to 353 K allowed the increase of DMC selectivity from 68% to 93%.

Hong et al. [114] also studied the performance of basic catalysts, metal hydroxide and metal-carbonates, with metals from the first group (potassium, sodium and lithium) in the presence of CH_3I as a promoter. Furthermore, a dehydrating agent, DMP, was added to the reaction mixture with the aim of understanding the influence of this compound in the reaction. They found optimum amounts of CH_3I and DMP that maximize the DMC yield. Comparing the performance of the several catalysts, it was observed that the yield reached by potassium carbonate (12%), was four times higher than with potassium hydroxide, sodium hydroxide, or sodium carbonate. Lithium hydroxide and lithium carbonate showed very poor activity for this reaction, with yields below 0.3%.

Cao et al. [115] also studied the reaction catalyzed by K_2CO_3 and promoted by CH_3I. The maximum conversion of DMC was reached at 403-413 K and 20 MPa using K_2CO_3 as catalyst, CH_3I as promoter, and DMP as a dehydrating agent. The addition of promoter showed good effects on the DMC production. Cai et al. [107] observed similar behaviour of CH_3I as promoter when compared the performance of three different catalysts: CH_3OK, KOH, and K_2CO_3. Moreover, a kinetic study, at 353 K, showed first-order dependence on the CO_2 and they concluded that the activity of the catalyst decreases in the following order: CH_3OK, KOH and K_2CO_3, with the kinetic constant of 0.0204, 0.0161 and 0.00721 h^{-1}, respectively.

Recently, Lim et al. [116] studied the direct synthesis of dimethyl carbonate, and other organic carbonates, from carbon dioxide and the respective alcohol, catalyzed by an alkaline metal-free organic catalyst (1,8-Diazabicyclo[5.4.0]undec-7-ene) and using dibromomethane as solvent; in addition, a hydrophobic ionic liquid (bmif-PF_6) was used to enhance the solubility of carbon dioxide. A DMC yield of 46% was reached at

the following reaction conditions: 343 K, 1 MPa, with 500 mmol of methanol, 0.1 mL of bmif-PF_6, 0.5 M of dibromomethane, and 2 equivalents of catalyst.

2.5.3. Heterogeneous catalysis

According to the green chemistry principles, the use of heterogeneous catalysts instead of the homogeneous is preferred, since the catalyst separation is easily done by filtration, avoiding the use of solvents to recover the catalyst or another hazardous and expensive separation process.

Zirconium oxide is a well known alternative for organotin catalysts in the direct synthesis of DMC. Tomishige et al. [117, 118] observed a DMC yield of 1%, at 433 K and at a CO_2 pressure of 5 MPa using a commercial zirconium hydroxide ($ZrO_2 \cdot xH_2O$) calcined at 673 K. In order to understand the influence of the metal oxide structure, Jung et al. [119] compared the performance of monoclinic and tetragonal zirconia. The higher performance of monoclinic zirconia is mainly explained by the high strength and amount of basic sites. Ballivet-Tkatchenko et al. [120] compared the performance of the ZrO_2 and SnO_2 supported on SiO_2, with the respective metal oxide particles, for the direct DMC conversion at 423 K and 20 MPa. The experiments showed an improvement of ten times in the activity of the supported catalysts.

Cerium oxide is also a reference catalyst for the synthesis of DMC, showing higher activity than ZrO_2 as demonstrated by Yoshida et al. [121]. They observed a proportional relation between specific area and activity above a calcination temperature of 873 K. However, Tomishige et al. [122, 123] observed an increase of activity when using a mixture of CeO_2/ZrO_2. The reaction was carried out at 383 K and 0.6 MPa reaching a DMC yield of 0.83% after 4 h. This synergetic effect was also observed by La et al. [124] for the $Ce_xTi_{1-x}O_2$ mixture prepared by sol-gel method, with a maximum activity for 10% of cerium. Moreover, they observed an improvement on the activity by doping the previous structure with $H_3PW_{12}O_{40}$, due to the increase of acidity.

The direct production of DMC from methanol and carbon dioxide was also performed by Wu et al. [125] at moderate pressure (0.6 MPa) using a phosphoric acid modified V_2O_5 catalyst. The impregnation of H_3PO_4 over V_2O_5 led to an improvement of activity around 8 times, reaching a DMC yield of 0.18% with a selectivity of 92%. The impregnation with phosphoric acid to enhance the activity of the catalyst was already performed by Yoshida et al. [126, 127], over zirconium oxide, which led to an increase of activity around 100%.

In addition, Wu et al. [128] also studied the influence of temperature and pressure for a similar catalyst, Cu-Ni/V_2O_5-SiO_2. Besides the kinetic study, the authors compared the performance of the catalyst prepared in different conditions. In spite of the high activity observed at medium pressure, 0.9 MPa, the selectivity reached was lower than 87%; dimethoxymethane (DMM) was the main by-product observed.

Wang et al. [129] conducted the reaction in a photoreactor using copper modified (Ni, V, O) catalysts. Furthermore, they studied the effect of UV irradiation and observed an increase between 30% and 60% in DMC yield. However, the radiation leads to a decrease of DMC selectivity producing methoxy metallic acid and carbon monoxide as secondary products.

Fan et al. [130] tested the organotin compound immobilized on silica support, to use as heterogeneous catalyst, in order to overcome the drawback of the conventional homogenous catalysis. The reaction was carried out at 18 MPa and 453 K, and, a DMC yield of 0.41 $mol_{DMC} \cdot mol_{Sn}^{-1}$ was reached after 10 hours. This value is half of the value reported by Choi et al. [112] for homogeneous catalysis.

Bian et al. [131] performed the DMC synthesis using $CuCl_2$ supported on activated carbon (AC),which is a conventional catalyst in the oxy-carbonylation of methanol. The reaction was carried out at 373-413 K and 1-1.4 MPa. A selectivity of 91% for DMC was reached, producing methyl formate (MF) and DME as side products. Moreover, Bian et al. [132] compared the activity of a Cu-Ni catalyst supported on activated carbon, thermally expanded graphite, multi-walled carbon nanotubes and graphene nanotubes (GNS), at 393 K and 1.2 MPa. The catalyst supported on GNS showed the highest activity with a selectivity of 83%, which increases to 90% for temperatures below 353 K.

Aouissi et al. [133] reported the direct synthesis of DMC catalyzed by several Keggin-type heteropolyoxometalates: $Fe_{1.5}PW_{12}O_{40}$, $Co_{1.5}PW_{12}O_{40}$, $Cu_{1.5}PW_{12}O_{40}$, $Zn_{1.5}PW_{12}O_{40}$. The highest performance was observed by using cobalt as cation. Furthermore, they also compared tungsten and molybdenum as the addenda atom, and concluded that the molybdenum reaches higher DMC yields and selectivity, around 70% and 1%, respectively, leading to the production of two by-products, MF and DMM. Higher selectivity and DMC yield were observed by carrying out the reaction at 473 K and atmospheric pressure [134]: 7.6% and 86%, respectively.

Lee et al. reached 1.2% and 2.3% of DMC after 3 hours using $H_3PW_{12}O_{40}$ [135] and Ga_2O_3 [136], respectively, supported in a mixture composed by $Ce_xZr_{1-x}O_2$, at 443 K and 6 MPa. It was observed a linear relation between the activity and the amount of acidity and basicity. A maximum catalyst activity was reached using $5 \cdot Ga_2O_3/Ce_{0.6}Zr_{0.4}O_2$, which also showed the highest basicity and acidity. All catalysts were calcined at 773 K during 3 hours.

Apart from the conventional homogenous and heterogeneous catalysis, Lu et al. [137] proposed the electrochemical conversion of carbon dioxide and methanol into DMC. They reported a DMC yield of 1.06% with a selectivity of 94.3% in the following operating conditions: 298 K, 3.5 V (cathode: graphite), 494 mmol of MeOH, and 24 mmol of ionic liquid (ApmimBr: 1-(3-aminopropyl)-3-methylimidazolium bromide). In addition, Garcia-Herrero et al. [138] also proposed the electrochemical valorisation of carbon dioxide, using potassium methoxide and an ionic liquid ([bmin][Br]), in a filter-press cell to mitigate the need of high temperatures and pressures.

In conclusion, both acid and basic sites are needed to produce DMC. The basic sites are responsible for producing the methoxy groups and for the activation of carbon dioxide, which generates the methoxy carbonate anion that will react with the methyl group formed in the acid sites to finally produce DMC [114, 136, 139]. Table 2.10 summarizes the operating conditions and the performance of the discussed catalysts for the direct synthesis of DMC.

Table 2.10: Catalysts performance for direct synthesis of DMC

Catalyst	Operating Conditions	Time	Yield/Selec.	Side products	Ref.	Year
K_2CO_3	V_R: 70 mL; MEOH: 192 mmol; CO_2: 200 mmol; CH_3I[a]: 24 mmol; K_2CO_3: 3 mmol; 405K	2 h	12/93%	Dimethyl ether	[113]	1996
ZrO_2	V_R: 30 mL; MeOH: 82 mmol; CO_2: 250 mmol; catalyst: 0.04 g; 433K	16 h	1.0/100%	-	[117, 118]	1999
$Ni(CH_3COO)_2{\cdot}4H_2O$	V_R: 80 mL; MeOH: 100 mmol; catalyst: 4 mmol; 413 K; 7 MPa	12 h	2.1/45%	Methyl acetate	[99]	2000
$Bu_2Sn(OMe)_2$[e]	V_R: 20 mL; MeOH: 100 mmol; catalyst: 2 mmol; 453 K; 30 MPa	24 h	2/100%	-	[112]	2002
CeO_2-ZrO_2	V_R: 70 mL; MeOH: 192 mmol; CO_2: 200 mmol; catalyst: 0.5 g; 383 K; 6 MPa	4 h	0.8/100%	-	[122]	2002
H_3PO_4/V_2O_5	n_{MeOH}/n_{CO_2}: 2/1; catalyst: 0.5 g; 453 K; 0.6 MPa	-[b]	1.8/93%	-	[125]	2005
Cu-Ni/ V_2O_5-SiO_2	n_{MeOH}/n_{CO_2}2/1; catalyst: 0.5 g; 413 K; 0.9 MPa	-[b]	2.4/87%	Dimethoxymethane	[128]	2006
n-$Bu_2Sn(OMe)_2$[e]	V_R: 125 mL; MeOH: 500 mmol; CO_2: 820 mmol; catalyst: 4 mmol; 20 MPa; 423 K	15 h	1.4/100%	-	[109]	2006
K_2CO_3	V_R: 95 mL; MeOH: 312 mmol; CH_3I[a]: 2 ml; catalyst: 1.73 g; 408 K; 20 MPa	4 h	9.7/100%	-	[114]	2006
CeO_2	V_R: 70 mL; MeOH: 192 mmol; CO_2: 200 mmol; catalyst: 0.1 g; 403 K	5 h	0.8/100%	-	[121]	2006
Cu (Ni, V, O) [c]	393 K; 1.2 MPa	-	4.5/90%	Carbon monoxide	[129]	2007
Cu (Ni, V, O)	393 K; 1.2 MPa	-	3.5/93%	Carbon monoxide	[129]	2007
$H_3PW_{12}O_{40}/Ce_{0.1}Ti_{0.9}O_2$	V_R: 100 mL; MeOH: 200 mmol; catalyst: 0.5 g; 443 K; 5 MPa (initial)	12 h	5/100%	-	[124]	2007
ZrO_2/SiO_2	V_R: 120 mL; MeOH: 10 mL; CO_2: 40 g; catalyst: 0.10-0.55 g; 423 K; 20 MPa	80 h	6[d]/100%	-	[120]	2010
$CuCl_2$/AC	n_{MeOH}/n_{CO_2}: 2/1; catalyst: 3 g (Cu 7 *wt*%); 398 K; 1.2 MPa	4 h[c]	- /90%	Dimethyl ether Methyl formate Carbon monoxide	[131]	2010

Catalyst	Operating Conditions	Time	Yield/Selec.	Side products	Ref.	Year
$Co_{1.5}PW_{12}O_{40}$	MeOH: 20 mL; catalyst: 0.1 g; 353 K; 0.25 MPa	5 h	1.1/69%	Dimethoxymethane Methyl formate	[133]	2010
$Co_{1.5}PW_{12}O_{40}$	n_{MeOH}/n_{CO_2}: 1/1.9; catalyst: 0.1 g; 473 K; 0.1 MPa	-[c]	7.6/86.5%	Dimethoxymethane Methyl formate	[134]	2010
$H_3PW_{12}O_{40}/Ce_{0.6}Zr_{0.4}O_2$	V_R: 75 mL; MeOH: 30 mL; catalyst: 0.7 g; 443 K; 6 MPa	3 h	1.2/100%	-	[135]	2011
$5Ga_2O_3/Ce_{0.6}Zr_{0.4}O_2$	V_R: 75 mL; MeOH: 30 mL; catalyst: 0.7 g; 443 K; 6 MPa	3 h	2.3/100%	-	[136]	2011
Cu-Ni/GNS	n_{MeOH}/n_{CO_2}: 2/1; catalyst: 3 g; 373 K; 0.12 MPa	3 h[c]	5/92%	-	[132]	2011
Mo-Cu-Fe/SiO_2	Saturated MeOH with CO_2; catalyst: 2 g; 393 K; 0.6 MPa	-[c]	7/88%	Dimethyl ether Formaldehyde Carbon monoxide	[140]	2013
Mg-Al Hydrotalcite/SiO_2	n_{MeOH}/n_{CO_2}: 1/25; flow: 0.047 mL·min^{-1}; catalyst: 0.25 g; 363 K	2 h[c]	14/~100%	Dimethyl ether	[141]	2013
Choline hydroxide	V_R: 250 mL; MeOH: 625 mmol; CO_2: 312 mmol; catalyst: 8 g; 413 K;	6 h	0.55/95%	Dimethoxymethane	[142]	2013

[a] Promoter [b] Continuous reactor [c] UV Radiation [d] DMC/cat. molar ratio [e] Precursor

2.5.4. Dehydrating agents

As mentioned before, the water formation is one of the main drawbacks of the carbonylation of methanol. Several strategies [112] were proposed to overcome this issue, such as water adsorption (using molecular sieves or MgO) or the use of a dehydrating agent, that quickly reacts with the water produced during the reaction. Choi et al. [112] compared the performance of these two strategies (DMP *vs.* molecular sieves), and observed that using molecular sieves to remove the water could reach the same yield of DMC by adding 6 times more catalyst in the same conditions (453K, 30 MPa). Moreover, dimethyl carbonate can be directly produced from acetal or orthoesters avoiding the formation of water.

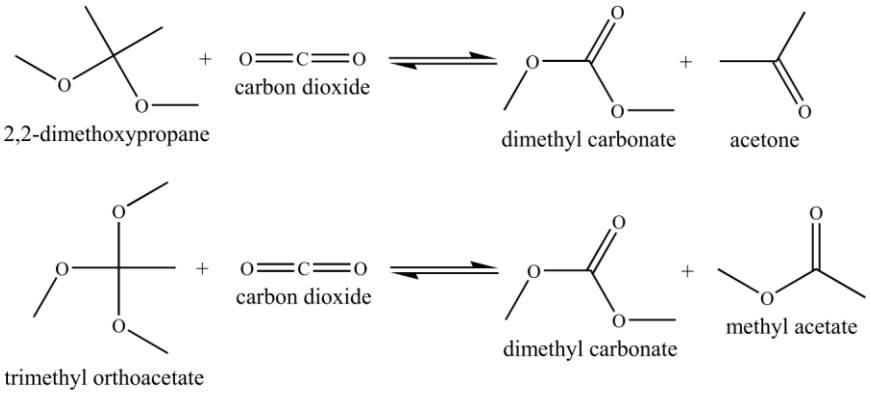

Scheme 2.11: DMC production from CO_2 and ketal or orthoesters.

The dehydrating agent can be after recycled by the reaction between the respective co-product (ketone or ester) and methanol. Although orthoesters are more reactive than ketals [108], it is hard to regenerate them from methyl acetate and methanol. Sakakura et al. [108] achieved the formation of DMC by trimethyl orthoacetate (TMOAc). They have reached a yield of DMC around 20% with 93% of selectivity, and methyl acetate was produced as a secondary product. Besides, orthoesters are expensive, which turn ketals much more attractive due to the low cost and the easy recycle. Sakakura et al. have carried the reaction using a ketal [143, 144], DMP, which is cheaper and also produces acetone that can be easily recycled into DMP by reacting with methanol. The conversion of DMC reached using DMP is much higher than from the direct methanol carbonylation: 88% at 453 K and 200 MPa after 24 h; Nevertheless, methanol addition is necessary by the mechanism suggested by Sakakura [143] (Figure 2.4).

Sakakura et al. [143] also compared the performance of different ketals. Table 2.11 contains the DMC yield reached, by each ketal, for the reactions carried out at 453 K, 30 MPa, during 24 h with 10 mmol of ketals and 8.1 mL of methanol. The higher yields were observed for 2,2-dimethoxypropane and 3,3-dimethoxypentane. In spite of the similar performance of both ketals, the 2,2-dimethoxypropane is a more attractive feedstock due to its lower price [145]. Acetals are also suggested to be a potential dehydrating agent for this reaction, due to its low price and the aldehyde formed by hydrolysis is easily reconverted to acetal [139]. Choi et al. [146] observed that the performance of DMP as dehydrating agent can be improved by the addition of ammonium triflates (Tf ≡ $CF_3SO_3^-$) as acid co-catalyst, such as $[Ph_2NH_2]$OTf. In addition, DMC yield increased from 17% to 40% in the presence of ammonium triflates at 453K and 30 MPa.

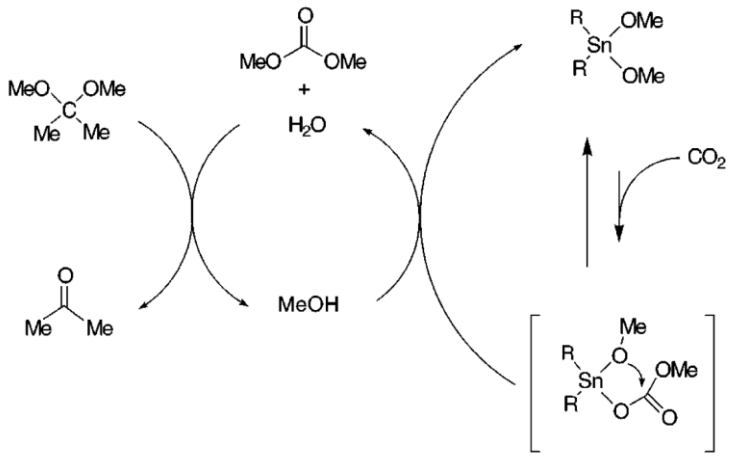

Figure 2.4: Mechanism suggested by Sakakura for DMC synthesis from DMP [143].

Table 2.11: Performance of ketals for DMC production [143].

Ketals	DMC yield
2,2-dimethoxypropane	26/57% [a]
3,3-dimethoxypentane	26/58% [b]
1,1-dimethoxicyclohexane	23%
Dimethoxy phenyl methane	14%

[a)] after 96 h [b)] after 72 h

Tomishige and Kunimori [122] reached a DMC yield of 1.4% with high selectivity, 99.3% at 383 K using a mixture of zirconium and cerium oxide as catalyst. Honda et al. [147, 148] reported carbonylation of methanol using acetonitrile as dehydrating agent instead of a ketal. They reached a DMC yield of 3% at 0.5 MPa and 423 K with a selectivity of 96%. The dehydrating agent reacts with water producing acetamide (Step 1: $CH_3CN + H_2O \rightleftharpoons CH_3(CO)NH_2$) that will react with methanol to produce ammonia and methyl acetate (Step 2: $CH_3(CO)NH_2 + CH_3OH \rightleftharpoons CH_3COOCH_3 + NH_3$); however, the ammonia can react with DMC to produce methyl nitrite (Step 3: $NH_3 + DMC \rightleftharpoons CH_3O(CO)NH_2 + CH_3OH$).

Other dehydrating agents can be used for the same purpose. Eta et al. [149] proposed the use of butylene oxide (BO) as dehydrating agent and observed a high reaction rate. The reaction was carried out at 423 K and 9.5 MPa, catalyzed by ZrO_2 doped with KCl and ZrO_2-MgO. A methanol conversion of 10% was reached; however, low selectivity was observed for DMC and butylene glycol, around 48% each, producing 1,2-butylene carbonate (BC) and methoxybutanol (MB) in parallel. They also reached high selectivity (around 80%) by using ZrO_2-MgO as catalyst [150]. Cyclohexene, was also used to remove water from the reaction mixture [151], producing DMC and 1,2-cyclohexanediol, and 2-methoxycyclohexanol as side product.

Moreover, Eta et al. [152] observed an improvement on the selectivity (around 90%) with ZrO_2-MgO at 393 K and 7.5 MPa in the presence of an alkoxide ionic liquid with high water removal potential. Fan et al.

[130] compared the efficiency of 3 different dehydrating agents, zeolite 3A, DMP and tetramethyl orthosilicate. DMP showed the higher effectiveness, reaching a DMC yield 7 times higher than the others.

Recently, 2-cyanopyridine was successfully used as dehydrating agent, by Honda et al. [153], reaching high DMC yield around 94% with 96% of selectivity in the presence of CeO_2. Furthermore, 2-cyanopyridine was recovered (96%) by dehydration of 2-picolinamide, produced by the hydration of 2-cyanopyridine, catalysed by Na_2O/SiO_2, showing a yield of 84% and a selectivity higher than 99%. In addition, 2-cyanopyridine was also successfully used to enhance the direct synthesis of propylene carbonate [15] (yield >99%) over cerium oxide, which can also be used for the direct synthesis of cyclic carbonates from carbon dioxide and the respective diol [154, 155].

Table 2.12 summarizes the operating conditions and the main results for the reaction carried out with a dehydrating agent. In addition, Honda et al. [156] recently published a review for the direct synthesis of DMC using dehydrating systems to increase the carbon dioxide conversion, where this topic is also discussed.

2.5.5. Side reactions

As previously mentioned, DMC synthesis can lead to the formation of side products. Those products can come from a side reaction of methanol or by the thermal decomposition of DMC. Fu et al. [157] studied the thermal decomposition of DMC over different solid catalysts, MgO (strong solid base), H-ZSM-5 (strong solid acid), SiO_2 (mostly neutral with very weak acidity), γ-Al_2O_3 (amphoteric with the acid sites stronger than the basic sites), ZnO (amphoteric with the basic sites stronger and the acid sites weaker than γ-Al_2O_3). In Table 2.13 are presented the results obtained for each catalyst. It was observed that for strong solid base (MgO) the decomposition of DMC becomes significant above 373 K, while for strong solid acid (H-ZSM-5) or amphoteric solids with strong acid sites (γ-Al_2O_3) the decomposition starts from 323 K. Contrarily, for SiO_2 and ZnO, DMC stays stable at temperatures between 473 K and 573 K, respectively.

Methanol and DME were reported as the main products of the thermal decomposition of DMC; however, other organic compounds were produced during the direct synthesis of DMC, such as MF, DMM and MA. Those products can also be produced by the selective oxidation of methanol, in presence of oxygen [139]. Therefore, DME is the most concerning by-product, since it can also be produced, in the absence of oxygen or other oxidant species, by the dehydration of methanol: $2CH_3OH \rightleftharpoons CH_3OCH_3 + H_2O$.

This reaction is essentially conducted in the presence of strong acid catalysts such as zeolites [158], silica-aluminas [159], silicoaluminophosphates [160], metal oxides [161] or sulphonic acid ion exchange resins [162], at moderate pressures and temperatures lower than 573 K to minimize the decomposition of DME into different hydrocarbons. The reaction can be also performed by catalytic distillation [163, 164] in order to minimize the investment cost and the energy consumption. Besides the synthesis from methanol, DME can also be produced by direct reaction between carbon monoxide and hydrogen (syngas), around 523 K and 5 MPa, where carbon dioxide can be formed by a side reaction [165, 166].

Table 2.12: Catalysts performance for DMC synthesis using dehydrating agents.

Catalyst	Dehydrating agent	Operating Conditions	Time	Yield[a] / Selec.	Side products	Ref.	Year
$Bu_2Sn(OMe)_2$	Molecular Sieves 3A	V_R: 20 mL; MeOH: 100 mmol; catalyst: 2 mmol; 453 K; 30 MPa	24 h	28/100%	-	[112]	2002
Cu-Ni/Zeolite 4A	Molecular Sieves 4A	n_{MeOH}/n_{CO_2} 10/1; catalyst: 4.5 g; 393 K; 1.1 MPa	5h	7/87%	Dimethyl ether; CO; formaldehyde	[167]	2013
n-$Bu_2Sn(OMe)_2$	2,2-Dimethoxypropane (DMP)	V_R: 20 mL; DMP: 10 mmol; MeOH: 200 mmol; catalyst: 0.17 mmol; 453 K; 200 MPa	24 h	88/100%	-	[143]	1999
n-$Bu_2Sn(OMe)_2$	DMP	V_R: 20 mL; 10 mmol DMP; MeOH: 100 mmol; catalyst: 0.2 mmol; 453 K; 30 MPa	24 h	28/100%	-	[112]	2002
CeO_2-ZrO_2	DMP	V_R: 70 mL; MeOH: 192 mmol; DMP: 30 mmol; CO_2: 200 mmol; catalyst: 0.5 g; 383 K; 6 MPa	48 h	16.3/96%	Dimethyl ether	[122]	2002
K_2CO_3	DMP	V_R: 95 mL; MeOH: 10 g; CH_3I[b]: 2 ml; DMP: 2 mL; catalyst: 1.73 g; 408 K; 20 MPa	4 h	12/100%	-	[114]	2006
Bu_2SnO	DMP	V_R: 20 mL; DMP: 50 mmol; MeOH: 100 mmol; catalyst: 2 mmol; 453 K; 30 MPa	24 h	17/-%	-	[146]	2008
Bu_2SnO	DMP	V_R: 20 mL; DMP: 50 mmol; MeOH: 100 mmol; catalyst: 2 mmol; co-catalyst ($[Ph_2NH_2]OTf$): 0.2 mmol; 453 K; 30 MPa	24 h	40/97%	-	[146]	2008
$Ti(OiPR)_4$-Ligand	DMP	V_R: 20 mL; DMP: 10 mmol; MeOH: 200 mmol; catalyst: 0.2 mmol; ligand (decyl-18-crown-6): 0.2 mmol; 453 K; 30 MPa	24h	41/-%	-	[111]	2008
CeO_2	DMP	V_R: 190 mL; MeOH: 100 mmol; DMP: 20 mmol; catalyst: 0.17 g; 423 K; 0.5 MPa	24 h	1.5/60%	Dimethyl ether	[147]	2009
n-$Bu_2Sn(OMe)_2$	Trimethyl orthoacetate	V_R: 20 mL; TMOAc: 50 mmol; catalyst: 0.85 mmol; 453 K; 30 MPa	24 h	20/93%	Methyl acetate	[108]	1998

Catalyst	Dehydrating agent	Operating Conditions	Time	Yield[a] / Selec.	Side products	Ref.	Year
CeO_2	Acetonitrile	V_R: 190 mL; MeOH: 100 mmol; acetonitrile: 420 mmol; catalyst: 0.17 g; 423 K; 0.5 MPa	2 h	3.5/95%	Methyl acetate, methyl carbamate	[147]	2009
CeO_2	Benzonitrile	V_R: 190 mL; MeOH: 100 mmol; benzonitrile: 420 mmol; catalyst: 0.17 g; 423 K; 0.5 MPa	2 h	9.4/99%	Methyl carbamate; methyl benzoate	[168]	2011
ZrO_2-KCl	Butylene oxide	V_R 300 mL; BO: 14.5 mmol; MeOH: 463 mmol; catalyst: 1 g; CO_2: 490 mmol; 423 K; 9.5 MPa	8 h	10/47%	1,2-butylene carbonate; methoxy butanol	[149]	2010
ZrO_2-MgO	Butylene oxide	V_R: 300 mL; BO: 21 mmol; MeOH: 695 mmol; catalyst: 1 g; 423 K; 9 MPa	8 h	12/80%	1,2-butylene carbonate; methoxy butanol	[150]	2011
K_2CO_3	Cyclohexene oxide	Cyclohexene oxide: 50 mmol; MeOH: 250 mmol; catalyst: 2 mmol; 423 K; 2.6 MPa	6 h	39/48%	2-methoxycyclohexanol	[151]	2013
ZrO_2-MgO	Ionic liquid – 1-butyl-3-methylimidazolium methoxide	V_R: 300 mL; ionic liquid: 4 g; MeOH: 247 mmol; catalyst: 0.5 g; 393 K; 7.5 MPa	9 h	12/90%	Dimethyl ether	[152]	2011
CeO_2	2-cyanopyridine	V_R: 190 mL; MeOH: 100 mmol; 2-cyanopyridine: 50 mmol; catalyst: 0.34 g; 393 K; 5 MPa	12 h	94/96%	Methyl carbamate	[153]	2013

[a)] Yield based on dehydrating agent.

Table 2.13: Thermal decomposition of DMC [157].

Catalyst	Temperature	Conversion	Main products
MgO	373 K	2.1%	DME(81%), MeOH
	473 K	76.4%	DME(99%), MeOH
H-ZSM-5	323 K	1.0%	DME(33%), MeOH
	373 K	32.9%	DME(79%), MeOH
γ-Al_2O_3	323 K	8.8%	DME(2%), MeOH
	373 K	53.0%	DME(78%), MeOH
SiO_2	473 K	1.0%	DME(2%), MeOH
	573 K	9.3%	DME(72%), MeOH
ZnO	573 K	1.5%	DME, MeOH
	623 K	3.0%	DME, methane, MeOH

2.6. Conclusions

The valorisation of carbon dioxide as building block for several organic compounds is an essential measure in order to minimize its negative impacts on the environment and on human health. However, the high stability of carbon dioxide turns this goal into an enormous challenge, because usually the reactions have low yields and rates, due to thermodynamic and kinetic limitations, respectively. Nevertheless, lot of efforts were done so far, and should continue, to achieve sustainable processes able to transform carbon dioxide into valuable products in the long term.

Among those organic compounds, organic carbonates could play an important role in the development of more sustainable chemical processes, since they are environmentally friendly and very versatile (as solvents, fuel additives, or reactants). The high price of organic carbonates is the main barrier for their industrial incorporation as a commodity, which could be significantly reduced using carbon dioxide (cheap and abundant) as feedstock.

In particular, DMC has a large potential to replace hazardous compounds, such as phosgene and dimethyl sulphate in carbonylation and methylation reactions, respectively. Several alternatives have emerged in order to overcome the weaknesses of the conventional routes. The transesterification of ethylene (or propylene) carbonate is by far the most mature alternative; however, the production of cyclic carbonates from epoxides also involves hazardous compounds and risk of explosion.

The direct synthesis of DMC from carbon dioxide and methanol is the most dreamed route, since it promotes the capture of carbon dioxide and uses less toxic reactants. However, this route is extremely constrained by thermodynamic limitations. Nevertheless, great efforts have been done in the development of novel catalysts ($Ce_xZr_{(1-x)}O_2$ based catalysts show high activity and selectivity), and in the search of more efficient, preferably *in situ*, water removal agents to enhance the DMC yield (molecular sieves, ketals,

epoxides, nitriles). In conclusion, advances reached so far are fundamental to continue to open new horizons for reutilization of carbon dioxide for other organic synthesis.

Nomenclature

Symbols

C_p	Molar heat capacity at constant pressure ($J \cdot mol^{-1} \cdot K^{-1}$)
$\Delta_f H^o$, $\Delta_r H^o$	Standard enthalpy change of formation and reaction ($J \cdot mol^{-1}$)
$\Delta_f G^o$, $\Delta_r G^o$	Standard Gibbs energy change of formation and reaction ($J \cdot mol^{-1}$)
n	Molar amount (mol)
V_r	Reactor volume (m^3)

Abbreviations

AC	Activated carbon	GNS	Graphene nanotubes
BC	Butylene carbonate	LD_{50}	Median lethal dose
DEC	Diethyl carbonate	MA	Methyl acetate
DMC	Dimethyl carbonate	MB	Methoxybutanol
DME	Dimethyl ether	MC	Methyl carbamate
DMF	*N*,*N*-dimethyl formamide	MeOH	Methanol
DMM	Dimethoxymethane	MF	Methyl formate
DMP	2,2-Dimethoxypropane	MN	Methyl nitrite
DMSO	Dimethyl sulfoxide	PC	Propylene carbonate
EC	Ethylene carbonate	PEL	Penicillium expansum lipase
EO	Ethylene oxide	THF	Tetrahydrofuran
FAME's	Fatty acid methyl esters	TMOAc	Trimethyl orthoacetate
GC	Glycerol carbonate	VOC's	Volatile organic compounds

References

[1] Song, C. Global Challenges And Strategies For Control, Conversion And Utilization Of CO2 For Sustainable Development Involving Energy, Catalysis, Adsorption And Chemical Processing. *Catalysis Today* **2006,** *115*(1-4).

[2] Zevenhoven, R.,Eloneva, S.,Teir, S. Chemical Fixation Of CO2 In Carbonates: Routes To Valuable Products And Long-Term Storage. *Catalysis Today* **2006,** *115*(1-4), 73.

[3] Maçaira, J.,Santana, A.,Recasens, F.,Angeles Larrayoz, M. Biodiesel Production Using Supercritical Methanol/Carbon Dioxide Mixtures In A Continuous Reactor. *Fuel* **2010,** *90*(6), 2280.

[4] Maçaira, J.,Santana, A.,Costa, A.,Ramirez, E.,Larrayoz, M. A. Process Intensification Using CO2 As Cosolvent Under Supercritical Conditions Applied To The Design Of Biodiesel Production. *Industrial and Engineering Chemistry Research* **2014,** *53*(10), 3985.

[5] Wei, C. Y.,Huang, T. C.,Yu, Z. R.,Wang, B. J.,Chen, H. H. Fractionation For Biodiesel Purification Using Supercritical Carbon Dioxide. *Energies* **2014,** *7*(2), 824.

[6] Banchero, M.,Pellegrino, G.,Manna, L. Supercritical Fluid Extraction As A Potential Mitigation Strategy For The Reduction Of Acrylamide Level In Coffee. *Journal of Food Engineering* **2013,** *115*(3), 292.

[7] Chen, Y.,Brown, P. H.,Hu, K.,Black, R. M.,Prior, R. L.,Ou, B.,Chu, Y. F. Supercritical CO2 Decaffeination Of Unroasted Coffee Beans Produces Melanoidins With Distinct NF-Kb Inhibitory Activity. *Journal of Food Science* **2011,** *76*(7), H182.

[8] MacHmudah, S.,Kitada, K.,Sasaki, M.,Goto, M.,Munemasa, J.,Yamagata, M. Simultaneous Extraction And Separation Process For Coffee Beans With Supercritical Co2 And Water. *Industrial and Engineering Chemistry Research* **2011,** *50*(4), 2227.

[9] Tan, H. P.,Li, H. P.,Guan, C.,Song, H.,Xu, Y.,Ran, L. P.,Tang, X. K. Study On The Extraction Of Natural Essence From Green Tea Leaf By Supercritical CO2. In *Advanced Materials Research*, **2013**; Vol. 781-784, pp 869-874.

[10] Machmudah, S.,Kitada, K.,Sasaki, M.,Goto, M.,Munemasa, J.,Yamagata, M. Simultaneous Extraction and Separation Process for Coffee Beans with Supercritical CO_2 and Water. *Industrial & Engineering Chemistry Research* **2011**.

[11] Aresta, M.,Dibenedetto, A. The Contribution Of The Utilization Option To Reducing The CO2 Atmospheric Loading: Research Needed To Overcome Existing Barriers For A Full Exploitation Of The Potential Of The CO2 Use. *Catalysis Today* **2004,** *98*(4), 455.

[12] Aresta, M.,Dibenedetto, A. Utilisation Of CO2 As A Chemical Feedstock: Opportunities And Challenges. *Dalton Transactions* **2007,** (28), 2975.

[13] Sakakura, T.,Choi, J. C.,Yasuda, H. Transformation Of Carbon Dioxide. *Chemical Reviews* **2007,** *107*(6), 2365.

[14] Adeleye, A. I.,Patel, D.,Niyogi, D.,Saha, B. Efficient And Greener Synthesis Of Propylene Carbonate From Carbon Dioxide And Propylene Oxide. *Industrial & Engineering Chemistry Research* **2014,** *x*(x), xx.

[15] Honda, M.,Tamura, M.,Nakao, K.,Suzuki, K.,Nakagawa, Y.,Tomishige, K. Direct Cyclic Carbonate Synthesis From CO2 And Diol Over Carboxylation/Hydration Cascade Catalyst Of CeO2 With 2-Cyanopyridine. *ACS Catalysis* **2014,** *4*(6), 1893.

[16] Anastas, P.,Warner, J. *Green Chemistry: Theory And Practice*; 1st ed.; Oxford University Press: New York, **1998**.

[17] Schäffner, B.,Schäffner, F.,Verevkin, S.,Börner, A. Organic Carbonates As Solvents In Synthesis And Catalysis. *Chemical Reviews* **2010,** *110*(8), 4554.

[18] Pacheco, M.,Marshall, C. Review Of Dimethyl Carbonate (DMC) Manufacture And Its Characteristics As A Fuel Additive. *Energy and Fuels* **1997,** *11*(1), 2.

[19] Li, D.,Fang, W.,Xing, Y.,Guo, Y.,Lin, R. Effects Of Dimethyl Or Diethyl Carbonate As An Additive On Volatility And Flash Point Of An Aviation Fuel. *Journal of Hazardous materials* **2009,** *161*(2-3), 1193.

[20] Shaikh, A.,Sivaram, S. Organic Carbonates. *Chemical Reviews* **1996,** *96*(3), 951.

[21] Delledonne, D.,Rivetti, F.,Romano, U. Developments In The Production And Application Of Dimethylcarbonate. *Applied Catalysis A: General* **2001,** *221*(1-2), 241.

[22] Westbrook, C. K.,Pitz, W. J.,Curran, H. J. Chemical Kinetic Modeling Study Of The Effects Of Oxygenated Hydrocarbons On Soot Emissions From Diesel Engines†. *Journal of Physical Chemistry A* **2006,** *110*(21), 6912.

[23] Bardin, M. E.,Ivanov, E. V.,Nilsson, E. J. K.,Vinokurov, V. A.,Konnov, A. A. Laminar Burning Velocities Of Dimethyl Carbonate With Air. *Energy and Fuels* **2013,** *27*(9), 5513.

[24] Chankeshwara, S. V. Dimethyl Carbonate (DMC): A Versatile And Environmentally Benign Building Block. *Synlett* **2008,** (4), 624.

[25] Ono, Y. Catalysis In The Production And Reactions Of Dimethyl Carbonate, An Environmentally Benign Building Block. *Applied Catalysis A: General* **1997,** *155*(2), 133.

[26] Tundo, P.,Selva, M. The Chemistry Of Dimethyl Carbonate. *Accounts of Chemical Research* **2002,** *35*(9), 706.

[27] He, X.,Li, Z.,Su, K.,Cheng, B.,Ming, J. Study On The Reaction Between Bisphenol A And Dimethyl Carbonate Over Organotin Oxide. *Catalysis Communications* **2013,** *33*, 20.

[28] Ji, Y.,Sweeney, J.,Zoglio, J.,Gorin, D. J. Catalytic Methyl Transfer From Dimethylcarbonate To Carboxylic Acids. *Journal of Organic Chemistry* **2013,** *78*(22), 11606.

[29] Li, L. L.,Janik, M. J.,Nie, X. W.,Song, C. S.,Guo, X. W. Reaction Mechanism Of Toluene Methylation With Dimethyl Carbonate Or Methanol Catalyzed By H-ZSM-5. *Acta Physico - Chimica Sinica* **2013,** *29*(7), 1467.

[30] Sun, L. Y.,Zhu, K. Synthesis Of Methyleugenol With Dimethyl Carbonate As Methylating Agent. *Chemistry and Industry of Forest Products* **2013,** *33*(2), 139.

[31] Hadba, A. R.,Belcheva, N.,Jones, F.,Abuzaina, F.,Calabrese, A.,Kapiamba, M.,Skalla, W.,Taylor, J. L.,Rodeheaver, G.,Kennedy, J. Isocyanate-Functional Adhesives For Biomedical Applications. Biocompatibility And Feasibility Study For Vascular Closure Applications. *Journal of Biomedical Materials Research - Part B Applied Biomaterials* **2011,** *99 B*(1), 27.

[32] Wu, D.,Chen, Z. Synthesis Of Phenylethenyl Methyl Carbonate By Methoxycarbonylation Of Phenylacetaldehyde With Dimethyl Carbonate. *Chemical Engineering and Technology* **2013,** *36*(7), 1125.

[33] Kumar, S.,Jain, S. L. An Easy Base-Assisted Synthesis Of Unsymmetrical Carbonates From Alcohols With Dimethyl Carbonate. *Monatshefte fur Chemie* **2014,** *145*(5), 791.

[34] Zhang, P. B.,Fan, M. M.,Wei, X. Q.,Zeng, Y. N. A Novel Quaternary Ammonium Salt Synthesis With Dimethyl Carbonate As Alkylating Agent. *Optoelectronics and Advanced Materials, Rapid Communications* **2011,** *5*(2), 164.

[35] Lewis, L. N.,Schattenmann, F. J.,Jordan, T. M.,Carnahan, J. C.,Flanagan, W. P.,Wroczynski, R. J.,Lemmon, J. P.,Anostario, J. M.,Othon, M. A. Reaction Of Silicate Minerals To Form Tetramethoxysilane. *Inorganic Chemistry* **2002,** *41*(9), 2608.

[36] Ilham, Z.,Saka, S. Dimethyl Carbonate As Potential Reactant In Non-Catalytic Biodiesel Production By Supercritical Method. *Bioresource Technology* **2009,** *100*(5), 1793.

[37] Kai, T.,Mak, G. L.,Wada, S.,Nakazato, T.,Takanashi, H.,Uemura, Y. Production Of Biodiesel Fuel From Canola Oil With Dimethyl Carbonate Using An Active Sodium Methoxide Catalyst Prepared By Crystallization. *Bioresource Technology* **2014,** *163*.

[38] Rathore, V.,Tyagi, S.,Newalkar, B.,Badoni, R. P. Glycerin-Free Synthesis Of Jatropha And Pongamia Biodiesel In Supercritical Dimethyl And Diethyl Carbonate. *Industrial and Engineering Chemistry Research* **2014,** *53*(26).

[39] Shuzhen, S.,Liping, Z.,Xin, M.,Cong, M.,Zhong, X. Biodiesel Production By Transesterification Of Corn Oil With Dimethyl Carbonate Under Heterogeneous Base Catalysis Conditions Using Potassium Hydroxide. *Chemistry and Technology of Fuels and Oils* **2014,** *In Press*.

[40] Tan, K. T.,Lee, K. T.,Mohamed, A. R. Optimization Of Supercritical Dimethyl Carbonate (SCDMC) Technology For The Production Of Biodiesel And Value-Added Glycerol Carbonate. *Fuel* **2010,** *89*(12), 3833.

[41] Bertilsson, F.,Karlsson, H. T. CO2 Utilization Options, Part II: Assessment Of Dimethyl Carbonate Production. *Energy Conversion and Management* **1996,** *37*(12), 1733.

[42] Sakakura, T.,Kohno, K. The Synthesis Of Organic Carbonates From Carbon Dioxide. *Chemical Communications* **2009,** (11), 1312.

[43] Rounce, P.,Tsolakis, A.,Leung, P.,York, A. P. E. A Comparison Of Diesel And Biodiesel Emissions Using Dimethyl Carbonate As An Oxygenated Additive. *Energy and Fuels* **2010,** *24*(9), 4812.

[44] Memoli, S.,Selva, M.,Tundo, P. Dimethylcarbonate For Eco-Friendly Methylation Reactions. *Chemosphere* **2001,** *43*(1), 115.

[45] Romano, U., Tesei, R., Cipriani, G., Micucci L. Method For The Preparation Of Esters Of Carbonic Acid. US 4218391, **1980**.

[46] Romano, U.,Tesel, R.,Mauri, M. M.,Rebora, P. Synthesis Of Dimethyl Carbonate From Methanol, Carbon Monoxide, And Oxygen Catalyzed By Copper Compounds. *Industrial and Engineering Chemistry Product Research and Development* **1980,** *19*(3), 396.

[47] Wang, R.,Li, Z. Surface Reactions Of CuCl2 And HY Zeolite During The Preparation Of CuY Catalyst For The Oxidative Carbonylation Of Methanol. *Chinese Journal of Catalysis* **2014,** *35*(1), 134.

[48] Merza, G.,László, B.,Oszkó, A.,Pótári, G.,Baán, K.,Erdohelyi, A. The Direct Synthesis Of Dimethyl Carbonate By The Oxicarbonylation Of Methanol Over Cu Supported On Carbon Nanotube. *Journal of Molecular Catalysis A: Chemical* **2014,** *393*.

[49] Yan, B.,Huang, S.,Wang, S.,Ma, X. Catalytic Oxidative Carbonylation Over Cu2O Nanoclusters Supported On Carbon Materials: The Role Of The Carbon Support. *ChemCatChem* **2014,** *In Press*.

[50] Ren, J.,Wang, W.,Wang, D.,Zuo, Z.,Lin, J.,Li, Z. A Theoretical Investigation On The Mechanism Of Dimethyl Carbonate Formation On Cu/AC Catalyst. *Applied Catalysis A: General* **2014,** *472*, 47.

[51] Ren, J.,Liu, S.,Li, Z.,Xie, K. Structural Feature And Catalytic Performance Of Cu-SiO2-TiO2 Cogelled Xerogel Catalysts For Oxidative Carbonylation Of Methanol To Dimethyl Carbonate. *Catalysis Communications* **2010,** *12*(5), 357.

[52] Ding, X.,Dong, X.,Kuang, D.,Wang, S.,Zhao, X.,Wang, Y. Highly Efficient Catalyst PdCl2-CuCl2-KOAc/AC@Al2O3 For Gas-Phase Oxidative Carbonylation Of Methanol To Dimethyl Carbonate: Preparation And Reaction Mechanism. *Chemical Engineering Journal* **2014,** *240*, 221.

[53] Meng, Q.,Wang, S.,Shen, Y.,Yan, B.,Wu, Y.,Ma, X. Surface Structure And Reaction Property Of CuCl2-PdCl2 Bimetallic Catalyst In Methanol Oxycarbonylation: A DFT Approach. *Applied Surface Science* **2014,** *292*, 117.

[54] Anderson, S. A.,Root, T. W. Kinetic Studies Of Carbonylation Of Methanol To Dimethyl Carbonate Over $Cu^{+}X$ Zeolite Catalyst. *Journal of Catalysis* **2003,** *217*(2), 396.

[55] Duranleau, R. G.,Nieh, E. C. Y.,Knifton, J. F. Process For Production Of Ethylene Glycol And Dimethyl Carbonate. US 4691041, **1987**.

[56] Nishihira, K.,Yoshida, S.,Tanaka, S. Process For Purifying Dimethyl Carbonate. US 5292917, **1994**.

[57] Yu, Y.,Liu, X.,Zhang, W.,Zhang, Y.,Li, L.,Cao, Z.,Guo, Z.,Wang, H.,Jia, G.,Pan, Y.,Gao, Y. Electrosynthesis Of Dimethyl Carbonate From Methanol And Carbon Monoxide Under Mild Conditions. *Industrial & Engineering Chemistry Research* **2013,** *52*(21), 6901.

[58] Buysch, H.-J. Ullmann's Encyclopedia Of Industryal Chamestry. In *Carbonic Esters*, 6th ed.; John Wiley and Sons, I., Ed. **2012**; Vol. 7, pp 45-71.

[59] Himmele, W.,Fischer, K.,Kaibel, G.,Schneider, K.,Irnich, R. Preparation Of Pure Dimethyl Carbonate. US 4162200, **1979**.

[60] Bhattacharya, A. K., Hopewell Junction, N.Y. Preparation Of Dimethyl Carbonate. US 4785130, **1988**.

[61] Knifton, J. F. Process For Cosynthesis Of Ethylene Glycol And Dimethyl Carbonate. EP 255252, **1988**.

[62] Paret, G.,Donati, G.,Ghirardini, M. Process For Producing Dimethyl Carbonate And Apparatus Suitable For Such Purpose. US 5536864 A, **1991**.

[63] Shih, S. S.,Wu, M. M.,Yan, T. Y. Process For Producing Dialkylcarbonates. US 5498743, **1996**.

[64] Nishihira, K.,Yoshida, S.,Tanaka, S.,Asada, Y. Process For Continuously Producing Dimethyl Carbonate. US 5631396, **1997**.

[65] Nisoli, A.,Bouwens, S. M.,Doherty, M. F.,Malone, M. F. Method Of Separating Dimethyl Carbonate And Methanol. US 6315868, **2001**.

[66] Buchanan, J. S.,Jiang, Z.,Kowalski, J. A.,Santiesteban, J. G. Integrated Process For Preparing Dialkyl Carbonates And Diols. US 20130225850 A1, **2002**.

[67] Sun, Y.,Wei, W.,Zhao, N.,Sun, B.,Zhang, B.,Chen, Y. Catalyst For The Synthesis Of Dimethyl Carbonate From Urea And Methanol, Preparation And Use Thereof. US 20060047136, **2006**.

[68] Darbha, S.,Srivastava, R.,Ratnasamy, P. A Process For The Preparation Of Dialkyl Carbonate. EP 1777212 A1, **2007**.

[69] Kobayashi, K.,Osora, H.,Seiki, Y.,Iijima, M. Method And Device For Manufacturing Dimethyl Carbonate. US 20070037998, **2007**.

[70] Eckelt, R.,Fait, M. J. G.,Fricke, R.,Richter, M. Catalyst For The Synthesis Of Dimethyl Carbonate In The Gas Phase. US 20080249327, **2008**.

[71] Fernandez, I. V.,Fillion, B.,Murthy, V.,Nair, V. S.,Perez Collado, M. Process For Manufacturing Dimethyl Carbonate. US 20080200713, **2008**.

[72] Osora, H. Catalyst For Dimethyl Carbonate Synthesis. US 7674742, **2010**.

[73] Osora, H.,Kobayashi, K.,Seiki, Y.,Yasutake, T.,Iijima, M.,Oguchi, A. Method For Dimethyl Carbonate Synthesis. US 07790914, **2010**.

[74] Ren, J.,Guo, C.,Yang, L.,Li, Z. Synthesis Of Dimethyl Carbonate Over Starch-Based Carbon-Supported Cu Nanoparticles Catalysts. *Chinese Journal of Catalysis* **2013,** *34*(9), 1734.

[75] Schneider, M. J.,Haumann, M.,Stricker, M.,Sundermeyer, J.,Wasserscheid, P. Gas-Phase Oxycarbonylation Of Methanol For The Synthesis Of Dimethyl Carbonate Using Copper-Based Supported Ionic Liquid Phase (SILP) Catalysts. *Journal of Catalysis* **2013,** *309*, 71.

[76] Bhanage, B.,Fujita, S.,He, Y.,Ikushima, Y.,Shirai, M.,Torii, K.,Arai, M. Concurrent Synthesis Of Dimethyl Carbonate And Ethylene Glycol Via Transesterification Of Ethylene Carbonate And Methanol Using Smectite Catalysts Containing Mg And/Or Ni. *Catalysis Letters* **2002,** *83*(3-4), 137.

[77] Bhanage, B.,Fujita, S.,Ikushima, Y.,Arai, M. Synthesis Of Dimethyl Carbonate And Glycols From Carbon Dioxide, Epoxides, And Methanol Using Heterogeneous Basic Metal Oxide Catalysts With High Activity And Selectivity. *Applied Catalysis A: General* **2001,** *219*(1-2), 259.

[78] Bhanage, B.,Fujita, S.,Ikushima, Y.,Torii, K.,Arai, M. Synthesis Of Dimethyl Carbonate And Glycols From Carbon Dioxide, Epoxides And Methanol Using Heterogeneous Mg Containing Smectite Catalysts: Effect Of Reaction Variables On Activity And Selectivity Performance. *Green Chemistry* **2003,** *5*(1), 71.

[79] Dhuri, S.,Mahajani, V. Studies In Transesterification Of Ethylene Carbonate To Dimethyl Carbonate Over Amberlyst A-21 Catalyst. *Journal of Chemical Technology and Biotechnology* **2006,** *81*(1), 62.

[80] Jagtap, S. R.,Bhor, M. D.,Bhanage, B. M. Synthesis Of Dimethyl Carbonate Via Transesterification Of Ethylene Carbonate With Methanol Using Poly-4-Vinyl Pyridine As A Novel Base Catalyst. *Catalysis Communications* **2008,** *9*(9), 1928.

[81] Sankar, M.,Nair, C. M.,Murty, K. V. G. K.,Manikandan, P. Transesterification Of Cyclic Carbonates With Methanol At Ambient Conditions Over Tungstate-Based Solid Catalysts. *Applied Catalysis A: General* **2006,** *312*(1-2), 108.

[82] Stoica, G.,Abelló, S.,Pérez-Ramírez, J. Na-Dawsonite Derived Aluminates For DMC Production By Transesterification Of Ethylene Carbonate. *Applied Catalysis A: General* **2009,** *365*(2), 252.

[83] Liu, J.,Guo, H.,Zhou, Q.,Wang, J.,Lin, B.,Zhang, H.,Gao, Z.,Xia, C.,Zhou, X. Highly Efficient Enzymatic Preparation For Dimethyl Carbonate Catalyzed By Lipase From Penicillium Expansum Immobilized On CMC-PVA Film. *Journal of Molecular Catalysis B: Enzymatic* **2013,** *141*(4).

[84] Xu, J.,Long, K. Z.,Wu, F.,Xue, B.,Li, Y. X.,Cao, Y. Efficient Synthesis Of Dimethyl Carbonate Via Transesterification Of Ethylene Carbonate Over A New Mesoporous Ceria Catalyst. *Applied Catalysis A: General* **2014,** *484*.

[85] Holtbruegge, J.,Leimbrink, M.,Lutze, P.,Górak, A. Synthesis Of Dimethyl Carbonate And Propylene Glycol By Transesterification Of Propylene Carbonate With Methanol: Catalyst Screening, Chemical Equilibrium And Reaction Kinetics. *Chemical Engineering Science* **2013,** *104*, 347.

[86] Holtbruegge, J.,Wierschem, M.,Lutze, P. Synthesis Of Dimethyl Carbonate And Propylene Glycol In A Membrane-Assisted Reactive Distillation Process: Pilot-Scale Experiments, Modeling And Process Analysis. *Chemical Engineering and Processing: Process Intensification* **2014**.

[87] Holtbruegge, J.,Kuhlmann, H.,Lutze, P. Process Analysis And Economic Optimization Of Intensified Process Alternatives For Simultaneous Industrial Scale Production Of Dimethyl Carbonate And Propylene Glycol. *Chemical Engineering Research and Design* **2014**.

[88] Huang, Z.,Li, J.,Wang, L.,Jiang, H.,Qiu, T. Novel Procedure For The Synthesis Of Dimethyl Carbonate By Reactive Distillation. *Industrial & Engineering Chemistry Research* **2014,** *53*(8), 3321.

[89] Chang, Y.,Luo, H.,Shi, C. Advances In Synthesis Of Dimethyl Carbonate By Alcoholysis Of Urea. *Speciality Petrochemicals* **2010,** *27*(2), 78.

[90] Zhao, X. Q.,Wang, Y. J.,Shen, Q. B.,Yang, H. J.,Zhang, J. Y. Synthesis Of Dimethyl Carbonate From Urea And Methanol Over Metal Oxide Catalysts. *Acta Petrolei Sinica, Petroleum Processing Section* **2002,** *18*(5), 47.

[91] Wu, X.,Kang, M.,Zhao, N.,Wei, W.,Sun, Y. Dimethyl Carbonate Synthesis Over ZnO-CaO Bi-Functional Catalysts. *Catalysis Communications* **2014,** *46*, 46.

[92] Wu, X.,Kang, M.,Yin, Y.,Wang, F.,Zhao, N.,Xiao, F.,Wei, W.,Sun, Y. Synthesis Of Dimethyl Carbonate By Urea Alcoholysis Over Zn/Al Bi-Functional Catalysts. *Applied Catalysis A: General* **2014,** *473*, 13.

[93] Sun, J.,Yang, B.,Wang, X.,Wang, D.,Lin, H. Synthesis Of Dimethyl Carbonate From Urea And Methanol Using Polyphosphoric Acid As Catalyst. *Journal of Molecular Catalysis A: Chemical* **2005,** *239*(1-2), 82.

[94] Yang, B.,Wang, D.,Lin, H.,Sun, J.,Wang, X. Synthesis Of Dimethyl Carbonate From Urea And Methanol Catalyzed By The Metallic Compounds At Atmospheric Pressure. *Catalysis Communications* **2006,** *7*(7), 472.

[95] Joe, W.,Lee, H. J.,Hong, U. G.,Ahn, Y. S.,Song, C. J.,Kwon, B. J.,Song, I. K. Synthesis Of Dimethyl Carbonate From Urea And Methanol Over ZnO(X)-CeO2(1-X) Catalysts Prepared By A Sol-Gel Method. *Journal of Industrial and Engineering Chemistry* **2012,** *18*(3), 1018.

[96] Hou, Z.,Luo, L.,Liu, K.,Liu, C.,Wang, Y.,Dai, L. High-Yield Synthesis Of Dimethyl Carbonate From The Direct Alcoholysis Of Urea In Supercritical Methanol. *Chemical Engineering Journal* **2014,** *236*, 415.

[97] Su, L.-W.,Li, X.-R.,Sun, Z.-Y. Flow Chart Of Methanol In China. *Renewable and Sustainable Energy Reviews* **2013,** *28*, 541.

[98] Hofmann, H. J.,Brandner, A.,Claus, P. CO2-Folgechemie: Direktsynthese Von Dimethylcarbonat Durch Carboxylierung Von Methanol An Cer-Basierten Mischoxiden

CO2 Subsequent Chemistry: Direct Synthesis Of Dimethyl Carbonate By Carboxylation Of Methanol With Cerium-Based Mixed Oxides. *Chemie Ingenieur Technik* **2011,** *83*(10), 1711.

[99] Zhao, T.,Han, Y.,Sun, Y. Novel Reaction Route For Dimethyl Carbonate Synthesis From CO2 And Methanol. *Fuel Processing Technology* **2000,** *62*(2), 187.

[100] Ding, Y.,Kong, A.,Zhang, H.,Shen, H.,Sun, Z.,Huang, S. D.,Shan, Y. A Novel Synthetic Approach For Preparing Dimethyl Carbonate From Dimethoxymethane And O2 Over Cu-MCM-48. *Applied Catalysis A: General* **2013,** *455*.

[101] Monteiro, J. G. M. S.,De Queiroz Fernandes Araújo, O.,De Medeiros, J. L. Sustainability Metrics For Eco-Technologies Assessment, Part I: Preliminary Screening. *Clean Technologies and Environmental Policy* **2009,** *11*(2), 209.

[102] Young, D.,Scharp, R.,Cabezas, H. The Waste Reduction (WAR) Algorithm: Environmental Impacts, Energy Consumption, And Engineering Economics. *Waste Management* **2000,** *20*(8), 605.

[103] Peng, W.,Zhao, N.,Xiao, F.,Wei, W.,Sun, Y. Recent Progress In Phosgene-Free Methods For Synthesis Of Dimethyl Carbonate. *Pure and Applied Chemistry* **2012,** *84*(3), 603.

[104] Kongpanna, P.,Pavarajarn, V.,Gani, R.,Assabumrungrat, S. Techno-Economic Evaluation Of Different CO2-Based Processes For Dimethyl Carbonate Production. *Chemical Engineering Research and Design* **2014,** *In Press*.

[105] Monteiro, J. G. M. S.,de Queiroz Fernandes Araújo, O.,de Medeiros, J. L. Sustainability Metrics For Eco-Technologies Assessment, Part II. Life Cycle Analysis. *Clean Technologies and Environmental Policy* **2009,** *11*(4), 459.

[106] Leino, E.,Mäki-Arvela, P.,Eta, V.,Murzin, D. Y.,Salmi, T.,Mikkola, J. P. Conventional Synthesis Methods Of Short-Chain Dialkylcarbonates And Novel Production Technology Via Direct Route From Alcohol And Waste CO2. *Applied Catalysis A: General* **2010,** *383*(1-2), 1.

[107] Cai, Q.,Lu, B.,Guo, L.,Shan, Y. Studies On Synthesis Of Dimethyl Carbonate From Methanol And Carbon Dioxide. *Catalysis Communications* **2009,** *10*(5), 605.

[108] Sakakura, T.,Saito, Y.,Okano, M.,Choi, J.,Sako, T. Selective Conversion Of Carbon Dioxide To Dimethyl Carbonate By Molecular Catalysis. *Journal of Organic Chemistry* **1998,** *63*(20), 7095.

[109] Ballivet-Tkatchenko, D.,Chambrey, S.,Keiski, R.,Ligabue, R.,Plasseraud, L.,Richard, P.,Turunen, H. Direct Synthesis Of Dimethyl Carbonate With Supercritical Carbon Dioxide: Characterization Of A Key Organotin Oxide Intermediate. *Catalysis Today* **2006,** *115*(1-4), 80.

[110] Kohno, K.,Choi, J.-C.,Ohshima, Y.,Yili, A.,Yasuda, H.,Sakakura, T. Reaction of dibutyltin oxide with methanol under CO_2 pressure relevant to catalytic dimethyl carbonate synthesis. *Journal of Organometallic Chemistry* **2008,** *693*(7).

[111] Kohno, K.,Choi, J. C.,Ohshima, Y.,Yasuda, H.,Sakakura, T. Synthesis Of Dimethyl Carbonate From Carbon Dioxide Catalyzed By Titanium Alkoxides With Polyether-Type Ligands. *ChemSusChem* **2008,** *1*(3), 186.

[112] Choi, J.,He, L.,Yasuda, H.,Sakakura, T. Selective And High Yield Synthesis Of Dimethyl Carbonate Directly From Carbon Dioxide And Methanol. *Green Chemistry* **2002,** *4*(3), 230.

[113] Fang, S.,Fujimoto, K. Direct Synthesis Of Dimethyl Carbonate From Carbon Dioxide And Methanol Catalyzed By Base. *Applied Catalysis A: General* **1996,** *142*(1), L1.

[114] Hong, S.,Park, H.,Lim, J.,Lee, Y.,Anpo, M.,Kim, J. Synthesis Of Dimethyl Carbonate From Methanol And Supercritical Carbon Dioxide. *Research on Chemical Intermediates* **2006,** *32*(8), 737.

[115] Cao, F. H.,Fang, D. Y.,Liu, D. H.,Ying, W. Y. Catalytic Esterification Of Carbon Dioxide And Methanol For The Preparation Of Dimethyl Carbonate. In *ACS Division of Fuel Chemistry, Preprints*, **2002**; Vol. 47, pp 295-297.

[116] Lim, Y. N.,Lee, C.,Jang, H. Y. Metal-Free Synthesis Of Cyclic And Acyclic Carbonates From CO2 And Alcohols. *European Journal of Organic Chemistry* **2014,** *2014*(9), 1823.

[117] Tomishige, K.,Sakaihori, T.,Ikeda, Y.,Fujimoto, K. A Novel Method Of Direct Synthesis Of Dimethyl Carbonate From Methanol And Carbon Dioxide Catalyzed By Zirconia. *Catalysis Letters* **1999,** *58*(4), 225.

[118] Tomishige, K.,Ikeda, Y.,Sakaihori, T.,Fujimoto, K. Catalytic Properties And Structure Of Zirconia Catalysts For Direct Synthesis Of Dimethyl Carbonate From Methanol And Carbon Dioxide. *Journal of Catalysis* **2000,** *192*(2).

[119] Jung, K. T.,Bell, A. T. Effects Of Catalyst Phase Structure On The Elementary Processes Involved In The Synthesis Of Dimethyl Carbonate From Methanol And Carbon Dioxide Over Zirconia. *Topics in Catalysis* **2002,** *20*(1), 97.

[120] Ballivet-Tkatchenko, D.,dos Santos, J. H. Z.,Philippot, K.,Vasireddy, S. Carbon Dioxide Conversion To Dimethyl Carbonate: The Effect Of Silica As Support For SnO2 And ZrO2 Catalysts. *Comptes Rendus Chimie* **2010,** *14*(7-8), 780.

[121] Yoshida, Y.,Arai, Y.,Kado, S.,Kunimori, K.,Tomishige, K. Direct Synthesis Of Organic Carbonates From The Reaction Of CO2 With Methanol And Ethanol Over CeO2 Catalysts. *Catalysis Today* **2006,** *115*(1-4), 95.

[122] Tomishige, K.,Kunimori, K. Catalytic And Direct Synthesis Of Dimethyl Carbonate Starting From Carbon Dioxide Using CeO2-ZrO2 Solid Solution Heterogeneous Catalyst: Effect Of H2O Removal From The Reaction System. *Applied Catalysis A: General* **2002,** *237*(1-2), 103.

[123] Tomishige, K.,Furusawa, Y.,Ikeda, Y.,Asadullah, M.,Fujimoto, K. CeO2-ZrO2 Solid Solution Catalyst For Selective Synthesis Of Dimethyl Carbonate From Methanol And Carbon Dioxide. *Catalysis Letters* **2001,** *76*(1-2), 71.

[124] La, K. W.,Jung, J. C.,Kim, H.,Baeck, S. H.,Song, I. K. Effect Of Acid-Base Properties Of H3PW12O40/CexTi(1-x)O2 Catalysts On The Direct Synthesis Of Dimethyl Carbonate From Methanol And Carbon Dioxide: A TPD Study Of H3PW12O40/CexTi(1-x)O2 Catalysts. *Journal of Molecular Catalysis A: Chemical* **2007,** *269*(1-2), 41.

[125] Wu, X. L.,Xiao, M.,Meng, Y. Z.,Lu, Y. X. Direct Synthesis Of Dimethyl Carbonate On H3PO4 Modified V2O5. *Journal of Molecular Catalysis A: Chemical* **2005,** *238*(1-2), 158.

[126] Ikeda, Y.,Sakaihori, T.,Tomishige, K.,Fujimoto, K. Promoting Effect Of Phosphoric Acid On Zirconia Catalysts In Selective Synthesis Of Dimethyl Carbonate From Methanol And Carbon Dioxide. *Catalysis Letters* **2000,** *66*(1-2).

[127] Ikeda, Y.,Asadullah, M.,Fujimoto, K.,Tomishige, K. Structure Of The Active Sites On H3PO4/ZrO2 Catalysts For Dimethyl Carbonate Synthesis From Methanol And Carbon Dioxide. *The Journal of Physical Chemistry B* **2001,** *105*(43).

[128] Wu, X. L.,Meng, Y. Z.,Xiao, M.,Lu, Y. X. Direct Synthesis Of Dimethyl Carbonate (DMC) Using Cu-Ni/VSO As Catalyst. *Journal of Molecular Catalysis A: Chemical* **2006,** *249*(1-2), 93.

[129] Wang, X. J.,Xiao, M.,Wang, S. J.,Lu, Y. X.,Meng, Y. Z. Direct Synthesis Of Dimethyl Carbonate From Carbon Dioxide And Methanol Using Supported Copper (Ni, V, O) Catalyst With Photo-Assistance. *Journal of Molecular Catalysis A: Chemical* **2007,** *278*(1-2), 92.

[130] Fan, B.,Li, H.,Fan, W.,Zhang, J.,Li, R. Organotin Compounds Immobilized On Mesoporous Silicas As Heterogeneous Catalysts For Direct Synthesis Of Dimethyl Carbonate From Methanol And Carbon Dioxide. *Applied Catalysis A: General* **2009,** *372*(1), 94.

[131] Bian, J.,Wei, X. W.,Jin, Y. R.,Wang, L.,Luan, D. C.,Guan, Z. P. Direct Synthesis Of Dimethyl Carbonate Over Activated Carbon Supported Cu-Based Catalysts. *Chemical Engineering Journal* **2010,** *165*(2), 686.

[132] Bian, J.,Wei, X. W.,Wang, L.,Guan, Z. P. Graphene Nanosheet As Support Of Catalytically Active Metal Particles In DMC Synthesis. *Chinese Chemical Letters* **2011,** *22*(1), 57.

[133] Aouissi, A.,Apblett, A. W.,Al-Othman, Z. A.,Al-Amro, A. Direct Synthesis Of Dimethyl Carbonate From Methanol And Carbon Dioxide Using Heteropolyoxometalates: The Effects Of Cation And Addenda Atoms. *Transition Metal Chemistry* **2010,** *35*(8), 1.

[134] Aouissi, A.,Al-Othman, Z. A.,Al-Amro, A. Gas-Phase Synthesis Of Dimethyl Carbonate From Methanol And Carbon Dioxide Over Co1.5PW12O40 Keggin-Type Heteropolyanion. *International Journal of Molecular Sciences* **2010,** *11*(4), 1343.

[135] Lee, H. J.,Park, S.,Jung, J. C.,Song, I. K. Direct Synthesis Of Dimethyl Carbonate From Methanol And Carbon Dioxide Over H3PW12O40/CexZr(1-X)O2 Catalysts: Effect Of Acidity Of The Catalysts. *Korean Journal of Chemical Engineering* **2011,** *28*(7), 1518.

[136] Lee, H. J.,Park, S.,Song, I. K.,Jung, J. C. Direct Synthesis Of Dimethyl Carbonate From Methanol And Carbon Dioxide Over Ga2O3/Ce0.6Zr0.4O2 Catalysts: Effect Of Acidity And Basicity Of The Catalysts. *Catalysis Letters* **2011,** *141*(4), 1.

[137] Lu, B.,Wang, X.,Li, Y.,Sun, J.,Zhao, J.,Cai, Q. Electrochemical Conversion Of CO2 Into Dimethyl Carbonate In A Functionalized Ionic Liquid. *Journal of CO2 Utilization* **2013,** *3-4*, 98.

[138] Garcia-Herrero, I.,Alvarez-Guerra, M.,Irabien, A. CO2 Electro-Valorization To Dimethyl Carbonate From Methanol Using Potassium Methoxide And The Ionic Liquid [bmim][Br] In A Filter-Press Electrochemical Cell. *Journal of Chemical Technology & Biotechnology* **2014,** *In Press*.

[139] Keller, N.,Rebmann, G.,Keller, V. Catalysts, Mechanisms And Industrial Processes For The Dimethylcarbonate Synthesis. *Journal of Molecular Catalysis A: Chemical* **2010,** *317*(1-2), 1.

[140] Zhou, Y. J.,Xiao, M.,Wang, S. J.,Han, D. M.,Lu, Y. X.,Meng, Y. Z. Effects Of Mo Promoters On The Cu-Fe Bimetal Catalysts For The DMC Formation From CO2 And Methanol. *Chinese Chemical Letters* **2013,** *24*(4), 307.

[141] Stoian, D. C.,Taboada, E.,Llorca, J.,Molins, E.,Medina, F.,Segarra, A. M. Boosted CO2 Reaction With Methanol To Yield Dimethyl Carbonate Over Mg-Al Hydrotalcite-Silica Lyogels. *Chemical Communications* **2013,** *49*(48), 5489.

[142] Sun, J.,Lu, B.,Wang, X.,Li, X.,Zhao, J.,Cai, Q. A Functionalized Basic Ionic Liquid For Synthesis Of Dimethyl Carbonate From Methanol And CO2. *Fuel Processing Technology* **2013,** *115*, 233.

[143] Sakakura, T.,Choi, J.,Saito, Y.,Masuda, T.,Sako, T.,Oriyama, T. Metal-Catalyzed Dimethyl Carbonate Synthesis From Carbon Dioxide And Acetals. *Journal of Organic Chemistry* **1999,** *64*(12), 4506.

[144] Sakakura, T.,Choi, J. C.,Saito, Y.,Sako, T. Synthesis Of Dimethyl Carbonate From Carbon Dioxide: Catalysis And Mechanism. *Polyhedron* **2000,** *19*(5), 573.

[145] Polienko, J. F.,Schanding, T.,Voinov, M. A.,Grigor'ev, I. A. Improved synthesis of 1-hydroxy-2,2,5,5-tetramethyl-3-imidazoline 3-oxide (HTIO). *Synthetic Communications* **2006,** *36*(19).

[146] Choi, J.,Kohno, K.,Ohshima, Y.,Yasuda, H.,Sakakura, T. Tin- Or Titanium-Catalyzed Dimethyl Carbonate Synthesis From Carbon Dioxide And Methanol: Large Promotion By A Small Amount Of Triflate Salts. *Catalysis Communications* **2008,** *9*(7), 1630.

[147] Honda, M.,Suzuki, A.,Noorjahan, B.,Fujimoto, K. I.,Suzuki, K.,Tomishige, K. Low Pressure CO2 To Dimethyl Carbonate By The Reaction With Methanol Promoted By Acetonitrile Hydration. *Chemical Communications* **2009,** (30), 4596.

[148] Honda, M.,Kuno, S.,Begum, N.,Fujimoto, K. I.,Suzuki, K.,Nakagawa, Y.,Tomishige, K. Catalytic Synthesis Of Dialkyl Carbonate From Low Pressure CO2 And Alcohols Combined With Acetonitrile Hydration Catalyzed By CeO2. *Applied Catalysis A: General* **2010,** *384*(1-2), 165.

[149] Eta, V.,Mäki-Arvela, P.,Leino, A.-R.,Kordás, K.,Salmi, T.,Murzin, D.,Mikkola, J.-P. Synthesis Of Dimethyl Carbonate From Methanol And Carbon Dioxide: Circumventing Thermodynamic Limitations. *Industrial & Engineering Chemistry Research* **2010,** *49*(20), 9609.

[150] Eta, V.,Mäki-Arvela, P.,Wärnå, J.,Salmi, T.,Mikkola, J. P.,Murzin, D. Y. Kinetics Of Dimethyl Carbonate Synthesis From Methanol And Carbon Dioxide Over ZrO2-MgO Catalyst In The Presence Of Butylene Oxide As Additive. *Applied Catalysis A: General* **2011,** *404*(1-2), 39.

[151] Yang, Q.,Wang, H.,Ding, X.,Yang, X.,Wang, Y. One-Pot Synthesis Of Dimethyl Carbonate From Carbon Dioxide, Cyclohexene Oxide, And Methanol. *Research on Chemical Intermediates* **2013**, 1.

[152] Eta, V.,Mäki-Arvela, P.,Salminen, E.,Salmi, T.,Murzin, D. Y.,Mikkola, J. P. The Effect Of Alkoxide Ionic Liquids On The Synthesis Of Dimethyl Carbonate From CO2 And Methanol Over ZrO2-MgO. *Catalysis Letters* **2011,** *141*(9), 1254.

[153] Honda, M.,Tamura, M.,Nakagawa, Y.,Sonehara, S.,Suzuki, K.,Fujimoto, K. I.,Tomishige, K. Ceria-Catalyzed Conversion Of Carbon Dioxide Into Dimethyl Carbonate With 2-Cyanopyridine. *ChemSusChem* **2013,** *6*(8), 1341.

[154] Tomishige, K.,Yasuda, H.,Yoshida, Y.,Nurunnabi, M.,Li, B.,Kunimori, K. Novel Route To Propylene Carbonate: Selective Synthesis From Propylene Glycol And Carbon Dioxide. *Catalysis Letters* **2004,** *95*(1-2).

[155] Tamura, M.,Honda, M.,Nakagawa, Y.,Tomishige, K. Direct Conversion Of CO2 With Diols, Aminoalcohols And Diamines To Cyclic Carbonates, Cyclic Carbamates And Cyclic Ureas Using Heterogeneous Catalysts. *Journal of Chemical Technology & Biotechnology* **2014,** *89*(1).

[156] Honda, M.,Tamura, M.,Nakagawa, Y.,Tomishige, K. Catalytic CO2 Conversion To Organic Carbonates With Alcohols In Combination With Dehydration System. *Catalysis Science & Technology* **2014,** *4*(9).

[157] Fu, Y.,Zhu, H.,Shen, J. Thermal Decomposition Of Dimethoxymethane And Dimethyl Carbonate Catalyzed By Solid Acids And Bases. *Thermochimica Acta* **2005,** *434*(1-2), 88.

[158] Laugel, G.,Nitsch, X.,Ocampo, F.,Louis, B. Methanol Dehydration Into Dimethylether Over ZSM-5 Type Zeolites: Raise In The Operational Temperature Range. *Applied Catalysis A: General* **2011,** *402*(1-2), 139.

[159] Moradi, G. R.,Yaripour, F.,Vale-Sheyda, P. Catalytic Dehydration Of Methanol To Dimethyl Ether Over Mordenite Catalysts. *Fuel Processing Technology* **2010,** *91*(5), 461.

[160] Yaripour, F.,Baghaei, F.,Schmidt, I.,Perregaard, J. Catalytic Dehydration Of Methanol To Dimethyl Ether (DME) Over Solid-Acid Catalysts. *Catalysis Communications* **2005,** *6*(2), 147.

[161] Fu, Y.,Hong, T.,Chen, J.,Auroux, A.,Shen, J. Surface Acidity And The Dehydration Of Methanol To Dimethyl Ether. *Thermochimica Acta* **2005,** *434*(1-2), 22.

[162] Spivey, J. J. Review: Dehydration Catalysts For The Methanol/Dimethyl Ether Reaction. *Chemical Engineering Communications* **1991,** *110*(1), 123.

[163] An, W.,Chuang, K. T.,Sanger, A. R. Dehydration Of Methanol To Dimethyl Ether By Catalytic Distillation. *Canadian Journal of Chemical Engineering* **2004,** *82*(5), 984.

[164] Lei, Z.,Zou, Z.,Dai, C.,Li, Q.,Chen, B. Synthesis Of Dimethyl Ether (DME) By Catalytic Distillation. *Chemical Engineering Science* **2011,** *66*(14), 3195.

[165] Ogawa, T.,Inoue, N.,Shikada, T.,Ohno, Y. Direct Dimethyl Ether Synthesis. *Journal of Natural Gas Chemistry* **2003,** *12*(4), 219.

[166] Stiefel, M.,Ahmad, R.,Arnold, U.,Döring, M. Direct Synthesis Of Dimethyl Ether From Carbon-Monoxide-Rich Synthesis Gas: Influence Of Dehydration Catalysts And Operating Conditions. *Fuel Processing Technology* **2011,** *92*(8), 1466.

[167] Chen, H.,Wang, S.,Xiao, M.,Han, D.,Lu, Y.,Meng, Y. Direct Synthesis Of Dimethyl Carbonate From CO2 And Ch3OH Using 0.4 nm Molecular Sieve Supported Cu-Ni Bimetal Catalyst. *Chinese Journal of Chemical Engineering* **2012,** *20*(5), 906.

[168] Honda, M.,Kuno, S.,Sonehara, S.,Fujimoto, K.-i.,Suzuki, K.,Nakagawa, Y.,Tomishige, K. Tandem Carboxylation-Hydration Reaction System From Methanol, CO2 And Benzonitrile To Dimethyl Carbonate And Benzamide Catalyzed By CeO2. *ChemCatChem* **2011,** *3*(2), 365.

Chapter 3. Vapour-Liquid Equilibrium for the Direct Synthesis of DMC

"Two things are infinite: the universe and human stupidity; and I'm not sure about the universe." – Albert Einstein

This chapter is based on the following article: Santos, B., Silva, V., Loureiro, J., Barbosa, D., Rodrigues, A. Modeling Of Physical And Chemical Equilibrium For The Direct Synthesis Of Dimethyl Carbonate At High Pressure Conditions. *Fluid Phase Equilibria* **2012,** *336*, 41.

3.1. Introduction

Thermodynamics is a fundamental discipline of chemical engineering; it is an important tool to predict physical properties or simulate several phenomena such as phase equilibrium or reaction equilibrium. These phenomena are essential to model and design chemical units as distillation columns, multiphase reactors or heat exchangers. Therefore, the knowledge of thermodynamic properties is essential in order to understand and model the phase behaviour for high-pressure processes.

3.1.1. Cubic equation of state for pure compounds

Cubic equations of state (EoS) are widely used to predict the thermodynamic properties of a mixture at high-pressure conditions [1]. Cubic EoS, and in particular Peng-Robinson (PR) [2] EoS and Soave-Redlich-Kwong (SRK) [3] EoS, are probably the most used due to their simplicity, since those models just depend on the critical properties of the components: critical pressure (P_c), critical temperature (T_c) and acentric factor (ω). An equation of state relates the pressure (P), temperature (T), and molar volume (V_M) of given compound or mixture. Other equations of state available in literature, such as Schmidt-Wenzel [4], Petal-Teja [5] and Peng-Robinson-Stryjek-Vera [6] have also been satisfactorily used in predicting high pressure phase equilibrium.

Peng-Robinson EoS

As mentioned above, thermodynamic properties can be predicted by cubic equations of state based on the critical properties of pure components. The Peng-Robinson equation of state has two parameters (a and b), dependent on the critical properties; and a function of the reduced temperature ($f[T_r]$).

$$P = \frac{R \cdot T}{V_M - b} - \frac{a \cdot f[T_r]}{V_M^2 + 2V_M - b^2} \tag{3.1}$$

$$a = 0.45724 \frac{R^2 \cdot {T_c}^2}{P_c} \tag{3.2}$$

$$f[T_r] = \left[1 + (0.37464 + 1.54226\omega - 0.26992\omega^2) \cdot \left(1 - \sqrt{T_r}\right)\right]^2 \tag{3.3}$$

$$b = 0.07780 \frac{R \cdot T_c}{P_c} \tag{3.4}$$

Soave-Redlich-Kwong EoS

Similarly to Peng-Robinson, the Soave-Redlich-Kwong equation of state also depends on the same parameters (a, b) and $f[T_r]$ which are related to the critical properties and reduced temperature.

$$P = \frac{R \cdot T}{V_M + \ b} - \frac{a \cdot f[T_r]}{V_M(V_M + b)} \tag{3.5}$$

$$a = 0.42747 \frac{R^2 T_C^2}{P_C} \tag{3.6}$$

$$f[T_r] = \left[1 + (0.480 + 1.574\omega - 0.176\omega^2) \cdot \left(1 + \sqrt{T_r}\right)\right]^2 \tag{3.7}$$

$$b = 0.08664 \frac{R \cdot T_c}{P_c} \tag{3.8}$$

3.1.2. Mixing rules for cubic equations of state

The previous equations of state for pure compounds can also be extended for multicomponent mixtures by considering an adequate mixing rule. The reliability of these cubic equations of state depends essentially on the mixing rule chosen, as well as the availability of the binary parameters, which are normally fitted to experimental data (such as vapour-liquid equilibrium). The classic van der Waals one-fluid mixing rule (1PVDW) [1] is based on attractive and repulsive forces theory, and it is widely used for mixtures composed by heavy hydrocarbons and non-polar mixtures. The model presents two binary interaction parameters, k_{ij} and l_{ij}, usually set equal to zero, but that can be fitted from experimental data in order to correct small deviations not predicted by the simple assumptions of this model. Different modifications of the classic van der Waals mixing rule were proposed by other authors [7-9], in order to extend the rule to asymmetric systems and mixtures containing polar components.

However, for more complex mixtures, other mixing rules have also been proposed based on the excess Gibbs free energy. Huron and Vidal (HV) [10] suggested a mixing rule depending on the excess Gibbs free energy at infinite pressure. In spite of the good results reached, this model has difficulties to predict the mixture properties in the presence of nonpolar compounds. The major weakness of the HV mixing rule is the estimation of the excess Gibbs free energy at infinite pressure by the activity coefficients models for low pressure, such as NRTL, Wilson or UNIQUAQ. Hence, Michelsen [11] developed a model known as modified first order Huron-Vidal mixing rule (mHV1), based on the excess Gibbs free energy at zero pressure, in order to overcome this weakness. After, Holderbaum and Gmehling [12] suggested a similar mixing rule; however, they used a group contribution method, UNIFAC, to estimate the excess Gibbs free energy: the predictive Soave-Redlich-Kwong equation of state (PSRK). This mixing rule allows the prediction of physical properties when VLE data are not available. Other modifications of the Huron-Vidal mixing rule were

proposed, such as the modified second order Huron-Vidal (mHV2) by Dahl and Michelsen [13], or the linear combination of Vidal and Michelsen (LCVM) by Boukouvalas et al. [14].

Wong and Sandler [15] developed a mixing rule (WS) based on the excess Helmholtz free energy at infinite pressure and considering a quadratic dependence on the second virial coefficient (B). The Helmholtz energy is almost not affected by pressure changes, which allows its estimation based on low pressure models [16]. Orbey and Sandler [17] proposed a modification of this rule in order to incorporate the van der Waals mixing rule. This mixing rule have been successfully used for binary mixtures between carbon dioxide and n-alcohols [18].

In Table 3.1 are presented, in detail, the mixing rules discussed above, where z_i represents the molar fraction of each component in the mixture; and, in Table 3.2 are displayed the constants of each mixing rule for the Peng-Robinson and Soave-Redlich-Kwong equations of state. Other equations of state and mixing rules already used in several systems can be found elsewhere [19-24]. In particular, new generation of cubic-plus-association equations of state [25-27] have been extensively studied due to their high ability to account with stronger interactions such as hydrogen bonds and ionic interactions.

In this chapter it is aimed to optimize and compare the performance of five different mixing rules (1PVDW, mHV1, mHV2, LCVM and WS) coupled with Soave-Redlich-Kwong equation of state for modelling the vapour-liquid equilibrium for the reaction system (carbon dioxide, methanol, water, and dimethyl carbonate) at high and low pressure conditions. Although the Peng-Robinson equation of state is discussed along the chapter, it was not considered for the fitting because its performance is very similar to that of the Soave-Redlich-Kwong equation. Besides, PSRK and HV are also out of the scope of this work: the use of PSRK is encouraged when there are no experimental data available; mHV1 and mHV2 emerged to correct some inconsistency of the original HV mixing rule, and will be used instead.

The excess Gibbs energy was modelled by the UNIQUAC activity coefficient model [28]. UNIQUAC has been successfully applied to several systems and its binary interaction parameters are not strongly temperature dependent, which turns this model acceptable for large temperature range. The UNIQUAC model is given by the following mathematical equations:

$$\frac{G_0^E}{R \cdot T} = \sum_i x_i \cdot \ln \gamma_i \tag{3.9}$$

$$\ln \gamma_j = \ln \gamma_j^{C(\text{Combinatorial})} + \ln \gamma_j^{R(\text{Residual})} \tag{3.10}$$

$$\ln \gamma_j^C = \ln \frac{\Phi_j}{x_j} + \frac{z}{2} q_j \ln \frac{\theta_j}{\Phi_j} + l_j - \frac{\Phi_j}{x_j} \sum_i x_i \cdot l_i \tag{3.11}$$

$$l_j = 5\left(r_j - q_j\right) - \left(r_j - 1\right) \tag{3.12}$$

$$\theta_j = \frac{q_j \cdot x_j}{\sum_i q_i \cdot x_i} \tag{3.13}$$

$$\Phi_j = \frac{r_j \cdot x_j}{\sum_i r_i \cdot x_i} \tag{3.14}$$

$$\tau_{ij} = \exp\left(-\frac{A_{ij}}{R \cdot T}\right) \tag{3.15}$$

3.2. Modelling Phase Equilibrium

3.2.1. Thermodynamic model

The vapour liquid equilibrium for a mixture is characterized by the equality of the fugacities of each species in the liquid ($\hat{f}_i^l$) and vapour ($\hat{f}_i^v$) phases [29]. This condition can be expressed in terms of the fugacity coefficient ($\hat{\varphi}_i$) and the corresponding mole fraction (Eq. 3.16): φ-φ model. The fugacity coefficient can be calculated by the next equation, where n and Z represent the number of moles and the compressibility factor, respectively (Eq. 3.17). In addition, Silva [16] derived the analytic solution for the fugacity of each component for the Soave-Redlich-Kwong equation of state (Eq. 3.18), and the respective parameters for each compound for the different mixing rules ($\bar{\alpha}_\iota$ and $\bar{b}_\iota$).

$$\hat{f}_i^v = \hat{f}_i^l \Leftrightarrow \; y_i \cdot \hat{\varphi}_i^v[T, P, y_i] = x_i \cdot \hat{\varphi}_i^l[T, P, x_i] \tag{3.16}$$

$$ln\,\hat{\varphi}_i = \int_0^P \left[\frac{\partial(n \cdot Z - n)}{\partial n_i}\right]_{P,T,n_{j\neq i}} \frac{dP}{P} \tag{3.17}$$

$$\ln\cdot\,\hat{\varphi}_i^{(v/l)} = \frac{\bar{b}_\iota}{b}\left(\frac{P \cdot V_M^{(v/l)}}{R \cdot T} - 1\right) - \ln\left[\frac{P(V_M^{(v/l)} - b)}{R \cdot T}\right] - \bar{\alpha}_\iota \ln\left(1 + \frac{b}{V_M^{(v/l)}}\right) \tag{3.18}$$

In Table 3.3 are displayed the two parameters, $\bar{b}_\iota$ and $\bar{\alpha}_\iota$ for each mixing rule for the Soave-Redlich-Kwong equation of state. The derived parameter, $\bar{\alpha}_\iota$, depends directly of the activity coefficient (γ_i), which is related with the excess Gibbs free energy [29].

Table 3.1: Some mixing rules for the calculation of cubic equations of state parameters [1, 10-15, 17].

Mixing rule	$a^* = a \cdot f[T_r]$ (3.19)	b (3.20)
1PVDW	$a^* = \sum_i \sum_j a_{ij}^* \cdot z_i \cdot z_j$ where, $a_{ij}^* = \sqrt{a_i^* \cdot a_j^*}(1 - k_{ij})$	$b = \sum_i \sum_j b_{ij} \cdot z_i \cdot z_j$ where, $b_{ij} = \frac{b_i + b_j}{2}(1 - l_{ij})$
HV	$\frac{a^*}{b \cdot R \cdot T} = \frac{1}{C_{HV}} \cdot \frac{G_\infty^E}{R \cdot T} + \sum_i z_i \cdot \frac{a_i^*}{b_i \cdot R \cdot T}$	$b = \sum_i z_i \cdot b_i$
MHV1	$\frac{a^*}{b \cdot R \cdot T} = \frac{1}{C_{MHV1}} \cdot \left[\frac{G_0^E}{R \cdot T} + \sum_i z_i \cdot \ln\frac{b}{b_i}\right] + \sum_i z_i \cdot \frac{a_i^*}{b_i \cdot R \cdot T}$	$b = \sum_i z_i \cdot b_i$
PSRK (UNIFAC)	$\frac{a^*}{b \cdot R \cdot T} = \frac{1}{C_{PSRK}} \cdot \left[\frac{G_0^E}{R \cdot T} + \sum_i z_i \cdot \ln\frac{b}{b_i}\right] + \sum_i z_i \cdot \frac{a_i^*}{b_i \cdot R \cdot T}$	$b = \sum_i z_i \cdot b_i$
MHV2	$C_{1,MHV2}\left[\alpha - \sum_i z_i \cdot \alpha_i\right] + C_{2,MHV2}\left[\alpha^2 - \sum_i z_i \cdot \alpha_i^2\right] = \frac{G_0^E}{R \cdot T} + \sum_i z_i \cdot \ln\frac{b}{b_i}$ where, $\alpha = \frac{a^*}{b \cdot R \cdot T}$ and $\alpha_i = \frac{a_i^*}{b_i \cdot R \cdot T}$	$b = \sum_i z_i \cdot b_i$
LCVM	$\frac{a^*}{b \cdot R \cdot T} = \frac{1}{C_{1,LCVM}} \cdot \frac{G_0^E}{R \cdot T} + C_{1,LCVM} \sum_i z_i \cdot \ln\frac{b}{b_i} + \sum_i z_i \cdot \frac{a_i^*}{b_i \cdot R \cdot T}$	$b = \sum_i z_i \cdot b_i$
WS	$\frac{a^*}{b \cdot R \cdot T} = \frac{1}{C_{WS}} \cdot \frac{A_\infty^E}{R \cdot T} + \sum_i z_i \cdot \frac{a_i^*}{b_i \cdot R \cdot T}$ where, $A_\infty^E \cong G_0^E$	$b = \frac{\sum_i \sum_j B_{ij} \cdot z_i \cdot z_j}{1 - \left[\frac{1}{C_{WS}} \cdot \frac{A_\infty^E}{R \cdot T} + \sum_i z_i \cdot \alpha_i\right]}$ where, $B[T] = b - \frac{a^*}{R \cdot T}$ and $B_{ij} = \frac{B_i + B_j}{2} \cdot (1 - k_{ij})$

Table 3.2: Mixing rules constants [1, 10-15, 17].

Constant	PR EoS	SRK EoS
C_{HV}	-0.623	-0.693
C_{MHV1}	-0.5275	-0.593
C_{PSRK}	-0.578	-0.647
$C_{1,MHV2}$	-0.477	-0.478
$C_{2,MHV2}$	-0.0020	-0.0047
$C_{1,LCVM}$	-0.558	-0.625
$C_{2,LCVM}$	-1.213	-1.079
C_{WS}	-0.623	-0.693

Table 3.3: Mixing rules parameters to calculate the fugacity coefficient of each compound [16].

Mixing rule	$\bar{\alpha}_i$ parameter (3.21)	$\bar{b}_i$ parameter (3.22)
1PVDW	$-\frac{a^*}{b \cdot R \cdot T}\left[\frac{2}{b}\sum_i z_j \cdot b_{ij} - \frac{2}{a^*}\sum_i z_j \cdot a^*_{ij} - 1\right]$	$2\sum_j z_j \cdot b_{ij}$
HV	$\frac{1}{C_{HV}} \cdot \ln\gamma_i + \alpha_i$	b_i
mHV1	$\frac{1}{C_{MHV1}}\left[\ln\gamma_i + \ln\frac{b}{b_i} + \frac{b_i}{b} - 1\right] + \alpha_i$	b_i
PSRK	$\frac{1}{C_{PSRK}}\left[\ln\gamma_i + \ln\frac{b}{b_i} + \frac{b_i}{b} - 1\right] + \alpha_i$	b_i
mHV2	$\frac{\left[\ln\gamma_i + \ln\frac{b}{b_i} + \frac{b_i}{b} - 1\right] + C_{1,MHV2} \cdot \alpha_i + C_{2,MHV2}(\alpha_i^2 + \alpha^2)}{C_{1,MHV2} + 2 \cdot C_{2,MHV2} \cdot \alpha}$	b_i
LCVM	$\frac{\ln\gamma_i}{C_{1,LCVM}} + C_{2,LCVM}\left[\ln\frac{b}{b_i} + \frac{b_i}{b} - 1\right] + \alpha_i$	b_i
WS	$\frac{\ln\gamma_i}{C_{WS}} + \alpha_i$	$\frac{2\sum_j z_j B_{ij}}{1-\alpha} - \frac{B(1-\bar{\alpha}_i)}{(1-\alpha)^2}$

In Table 3.4 are depicted the physical properties (critical properties and UNIQUAC parameters) used in our calculations.

Table 3.4: Physical properties and UNIQUAC parameters for pure components (DIPPR™).

Component	M / g.mol^{-1}	T_c / K	P_c / MPa	ω	r	q
CO_2	44.01	304.2	7.383	0.223621	1.29862	1.292
MeOH	32.04	512.6	8.097	0.563991	1.43110	1.432
DMC	90.60	548.0	4.500	0.384621	3.04812	2.816
H_2O	18.02	647.1	22.055	0.344861	0.92000	1.400

A MatLab routine was developed in order to calculate the vapour-liquid equilibrium, which was based on a convergence algorithm, proposed by Anderson and Prausnitz [30], to solve the φ-φ model at high pressure. This algorithm is described in Figure 3.1.

3.2.2. Experimental data collected

Several works are available in the literature with experimental data for the vapour-liquid equilibrium (VLE) of all the binary and ternary mixtures relevant for the direct synthesis of dimethyl carbonate (DMC). In Table 3.5 are summarized the publications from where the experimental data, used in this work, were collected. In addition, the thermodynamic models used by each author are also displayed: Patel-Teja (PT), Peng-Robinson, modified Peng-Robinson (mPR), Peng-Robinson-Stryjek-Vera (PRSV), SRK, Redlich-Kwong-Aspen (RKA) and statistical associating fluid theory for potentials of variable attractive range (SAFT-VR) equations of state, coupled with 1PVDW, mVH2, Panagiotopoulos and Reid (PgR) and WS mixing rules, have been used to describe the phase behaviour of these systems. Other works related to the physical equilibrium between the compounds involved in the direct synthesis of DMC can be found elsewhere [31-43].

3.3. Results

3.3.1. Model optimization

In order to optimize the equation of state, the binary parameters related to each mixing rule were fitted to the experimental data: k_{ij} for 1PVDW and WS mixing rules; UNIQUAC parameters A_{ij} for the prediction of excess of Gibbs free energy. The parameter k_{ij} was considered to be linearly dependent of the temperature ($k_{ij} = k_{ji} = k_{ij}^1 + k_{ij}^2 \cdot T$), while l_{ij} was considered equal to zero. In Table 3.6 and 3.7 are displayed the values for these binary interaction parameters obtained by fitting the experimental data through the following objective function:

$$F_{Obj} = min\left\{\left[\sum_{i=1}^{NP}\frac{abs(P^{model} - P^{exp.})}{P^{exp.}} + \sum_{i=1}^{NP}\frac{abs(y^{model} - y^{exp.})}{y^{exp.}}\right]\Big/NP\right\} \quad (3.23)$$

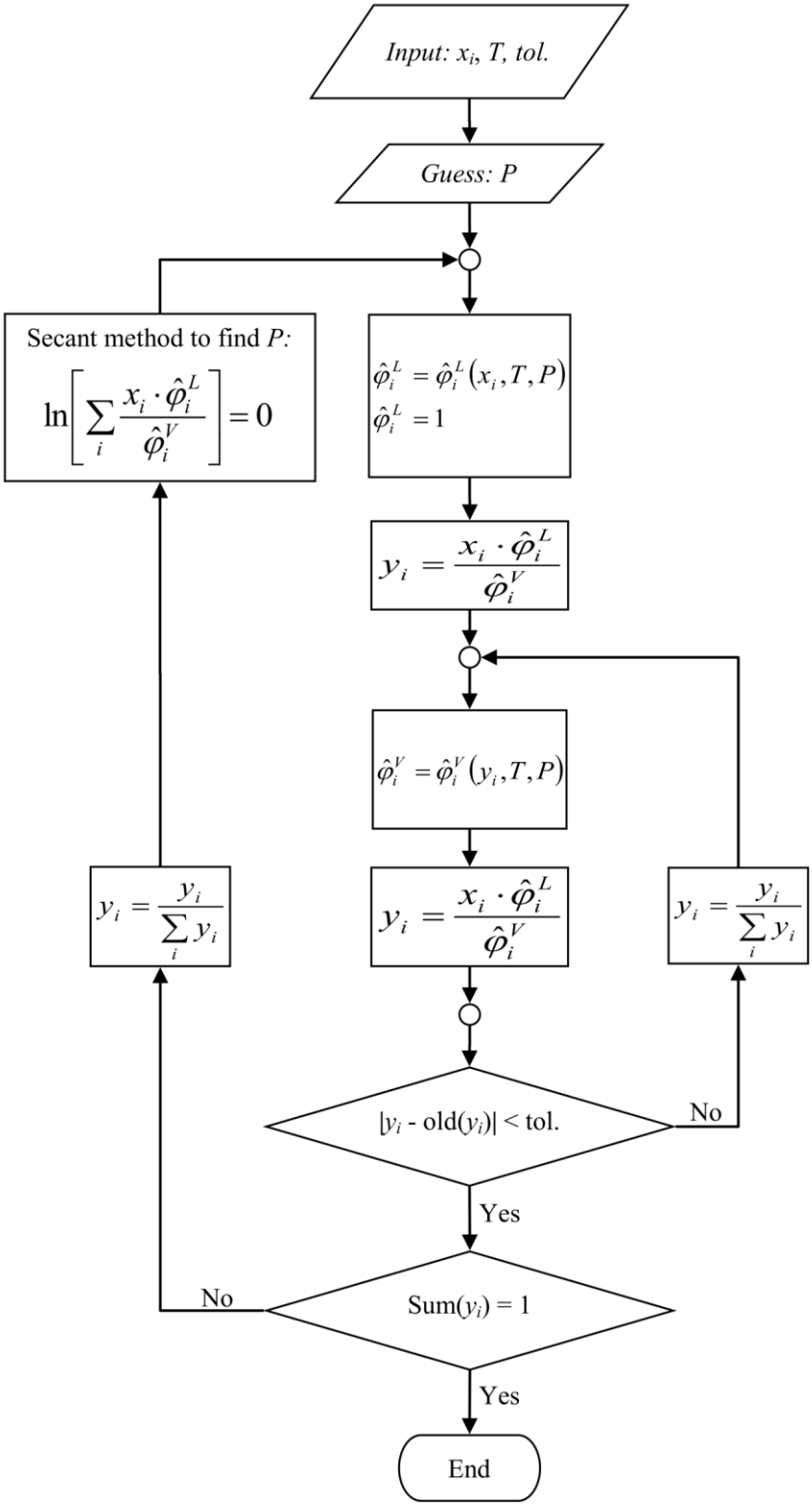

Figure 3.1: Algorithm for the calculation of the vapour liquid equilibrium (bubble point calculation).

Table 3.5: Experimental VLE data published in literature for the systems relevant to the production of DMC.

Mixture	Temperature/ Pressure	Models	Parameters	References
CO_2-MeOH	291-313 K	PR/1PVDW	2	Chang et al. (1998) [44]
		PT/1PVDW	2	
	363-373 K	PRSV/WS	1	Naidoo et al. (2008) [45]
CO_2-DMC	310- 340 K	PR/1PVDW	2	Im et al. (2003) [46]
	310- 423 K	RKA/1PVDW	2	Ciccolini et al. (2010) [47]
CO_2-H_2O	278- 378 K	PR/1PVDW	3	Valtz et al. (2004) [48]
		PR/WS	3	
		SAFT-VR	5	
	323- 353 K	PR/PgR	2	Bamberger et al. (2000) [49]
MeOH-H_2O	308-338 K	-	-	McGlashan et al. (1976) [50]
MeOH-DMC	337- 428 K	mPR/1PVDW	1	Yunhai et al. (2005) [51]
DMC-H_2O	1.01 kPa	SRK/mHV2	2	Camy et al. (2003) [52]
CO_2-MeOH-H_2O	7.0- 12.0 MPa	SRK/mHV2	2	Yoon et al. (1993) [53]
		SRK/PgR	2	
		PT/HV	2	
		PT/Wilson	2	

Since the experimental data available for the binary mixture between dimethyl carbonate and water only show the values for the bubble point curve, a different objective function was used:

$$F_{Obj} = min\left\{\left[\sum_{i=1}^{NP} abs(x^{model} - x^{exp.})/x^{exp.}\right]\Big/ NP\right\} \tag{3.24}$$

The optimization was carried out using an intrinsic function of MatLab (*fminsearch*) based on the Nelder-Mead simplex direct search method, with an absolute tolerance of 10^{-6}.

In Figures 3.2 and 3.3 are shown the overall relative deviations between the experimental data, from literature (Table 3.5), and the values predicted by the models; these deviations are shown for mole fractions and pressure, respectively, and for all the binary systems using the different thermodynamic models. In general it can be observed similar deviations in predicting the vapour mole fraction (liquid mole fraction for DMC-water), showing a higher deviation for the MeOH-water mixture, around 10%, while for the other mixtures the deviations were lower than 5%. However, for the pressure deviations a different behaviour was observed; indeed, higher discrepancy between the models was observed, as well as larger deviations. In particular for carbon dioxide-water mixture, deviations higher than 5% were obtained for all models, especially when using the SRK/mHV1 (21%) and SRK/LCVM (22%) models.

Table 3.6: UNIQUAC binary interaction parameters A_{ij} / J·mol^{-1}.

i,j	1PVDW	mHV1	LCVM	mHV2	WS
CO_2, MeOH	-	3150.9	3235.3	2220.8	11908.8
MeOH, CO_2	-	-700.8	-605.0	382.8	-739.8
CO_2, DMC	-	1386.6	1129.9	-653.3	2583.8
DMC, CO_2	-	-1529.2	-1137.9	688.8	-1150.9
CO_2, H_2O	-	13529.0	122678.3	9793.4	14781.4
H_2O, CO_2	-	1909.9	2264.3	4111.6	-159.7
MeOH, DMC	-	1587.0	1732.1	1586.3	1533.1
DMC, MeOH	-	170.6	269.9	90.6	-502.8
MeOH, H_2O	-	2068.0	2526.4	1747.3	1782.2
H_2O, MEOH	-	-1028.0	-436.1	-680.4	2086.5
DMC, H_2O	-	4827.0	5010.6	4507.1	6261.7
H_2O, DMC	-	279.5	1119.2	556.5	1219.1

Table 3.7: Binary interaction parameters k_{ij}^1 and k_{ij}^2.

i,j	1PVDW	mHV1	LCVM	mHV2	WS
		k_{ij}^1			
CO_2, MeOH	-1.926×10^{-1}	-	-	-	-3.606×10^{-1}
CO_2, DMC	8.830×10^{-2}	-	-	-	1.598×10^{-1}
CO_2, H_2O	-4.920×10^{-1}	-	-	-	9.564×10^{-1}
MeOH, DMC	7.444×10^{-2}	-	-	-	1.000×10^{0}
MeOH, H_2O	-6.481×10^{-2}	-	-	-	-5.647×10^{-1}
DMC, H_2O	-7.238×10^{0}	-	-	-	2.352×10^{-1}
		k_{ij}^2			
CO_2, MeOH	7.710×10^{-4}	-	-	-	1.708×10^{-3}
CO_2, DMC	-3.135×10^{-4}	-	-	-	6.604×10^{-4}
CO_2, H_2O	1.170×10^{-3}	-	-	-	2.172×10^{-4}
MeOH, DMC	-8.970×10^{-5}	-	-	-	-1.691×10^{-3}
MeOH, H_2O	-3.634×10^{-5}	-	-	-	3.960×10^{-4}
DMC, H_2O	2.046×10^{-2}	-	-	-	1.584×10^{-4}

It was already expected that the water-carbon dioxide system was the most difficult to model since there is a large difference on the polarity between the molecules; besides, water can also establish hydrogen bonds which contributes to increase the complexity of the system. The models are not perfectly adaptable to these phenomena, and this can be traduced by the high values of the UNIQUAC binary interaction parameters that try to force the model to fit the experimental data. In spite of this difficulty, the models show excellent ability to estimate the effect of high pressure conditions. Nevertheless, the performance observed for SRK/ 1PVDW,

SRK/mHV1, and SRK/WS for all the binary systems is quite reasonable, considering the complexity of the system.

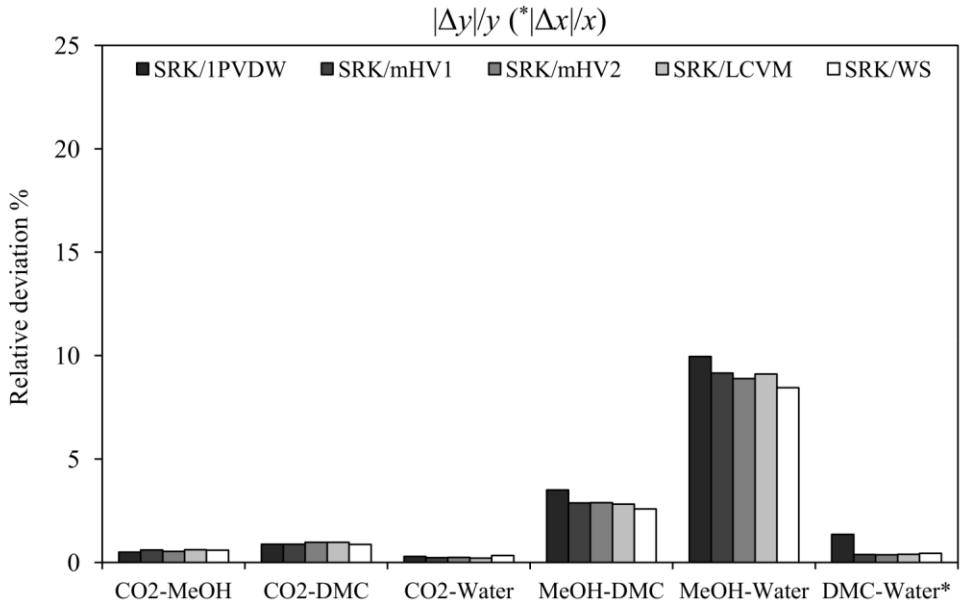

Figure 3.2: Relative molar fraction deviation, between the model and the experimental data, for the binary systems.

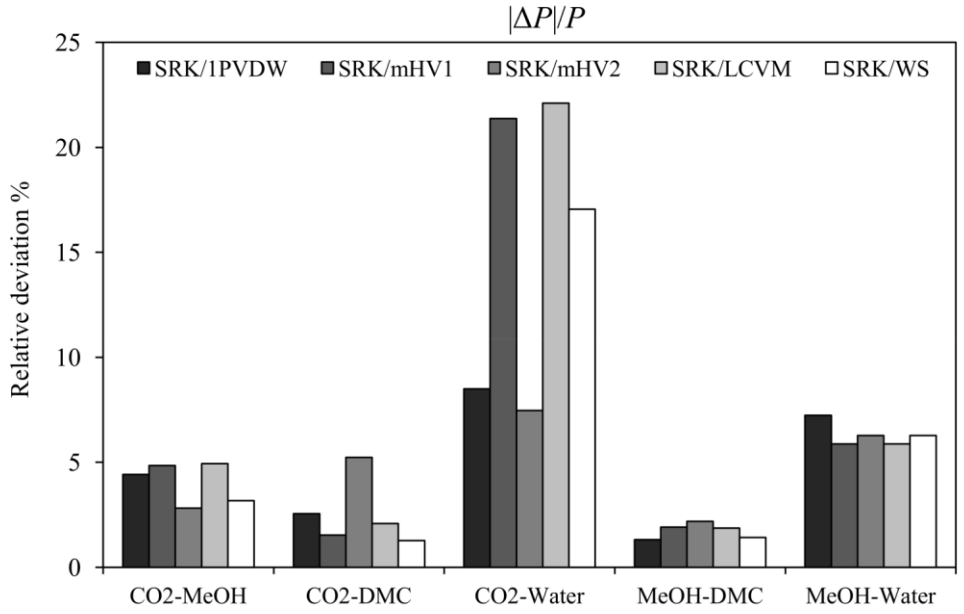

Figure 3.3: Relative pressure deviation, between the model and the experimental data, for the binary systems.

3.3.2. Ternary validation

Figure 3.4 shows the ternary diagram for the sub-system carbon dioxide-MeOH-water at 313.15 K, and 7.0, 10 and 12 MPa. This diagram includes the equilibrium lines predicted by the SRK/1PVDW, SRK/mHV2 and

SRK/WS models. The SRK/mHV1 and SRK/LCVM were not considered in this analysis because they showed higher deviations for the binary systems. As can be seen in the figure, the SRK/mHV2 and SRK/WS models give a better prediction of the phase equilibria than the SRK/1PVDW model. In spite of giving similar results, SRK/mHV2 is recommended rather than SRK/WS because of its simplicity (it has two, instead of four, binary parameters). This model has already been applied to this system by Camy et al. [52]. Piñero et al. [54] used the PT/1PVDW and PRSV/1PVDW models to describe this same system, obtaining higher deviations than those found with the SRK/mHV2 model.

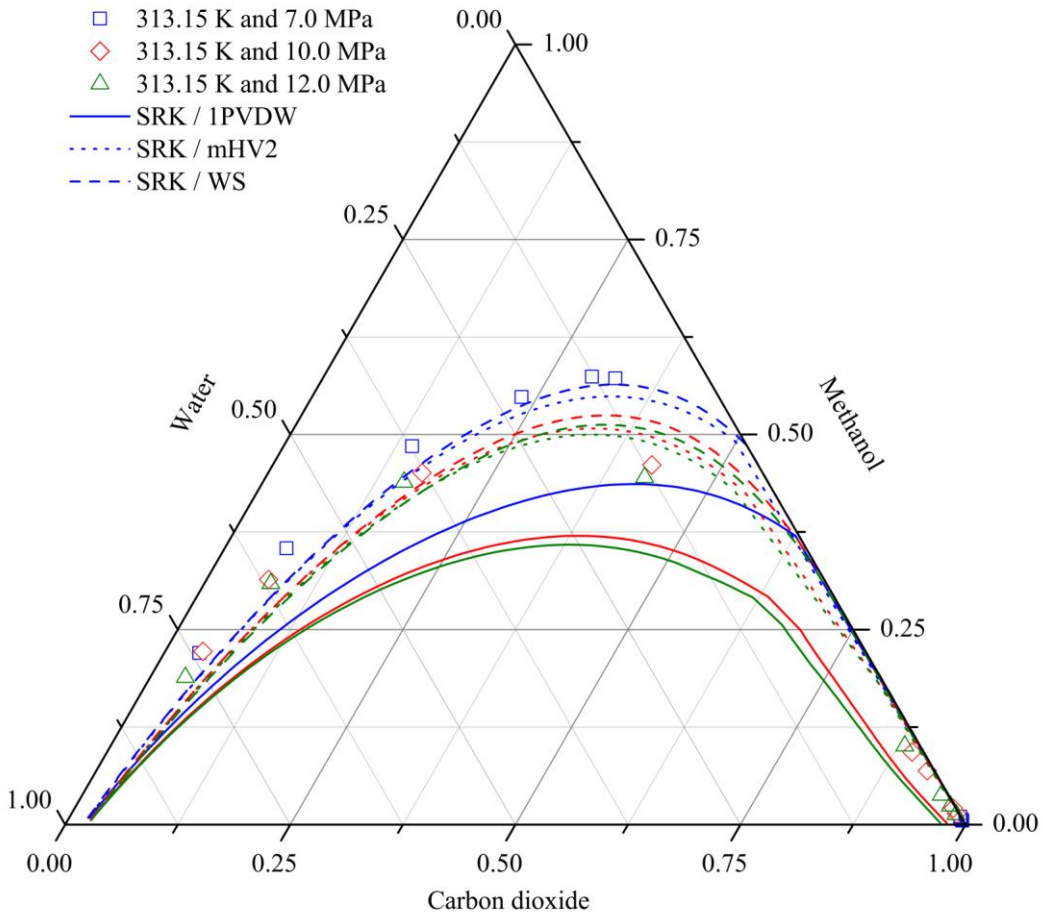

Figure 3.4: Vapour-liquid ternary diagram for carbon dioxide-methanol-water system: simulation and experimental data [53].

3.3.3. Simulation of binary equilibrium

Figures 3.5-3.10 show the VLE diagrams predicted by the SRK/mHV2, which was found to be the best model, together with the respective experimental data, for all the binary systems: carbon dioxide-MeOH, carbon dioxide-DMC, carbon dioxide-water, MeOH-DMC, MeOH-water, and DMC-water, respectively. In spite of small deviations, the model shows high consistency, showing high performance for the prediction of vapour-liquid equilibrium for all the binary systems, with exception for the prediction of the vapour composition for the water-carbon dioxide mixture.

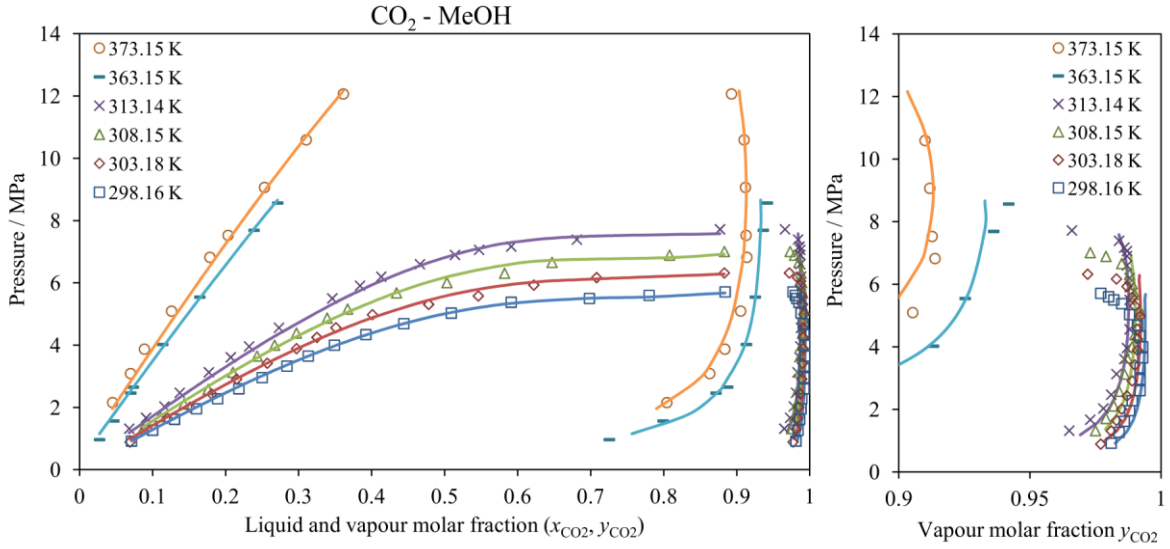

Figure 3.5: Experimental (points) [44, 45] and estimated VLE at different temperatures based on SRK/mHV2 EoS (curves) for CO_2-MEOH binary mixture.

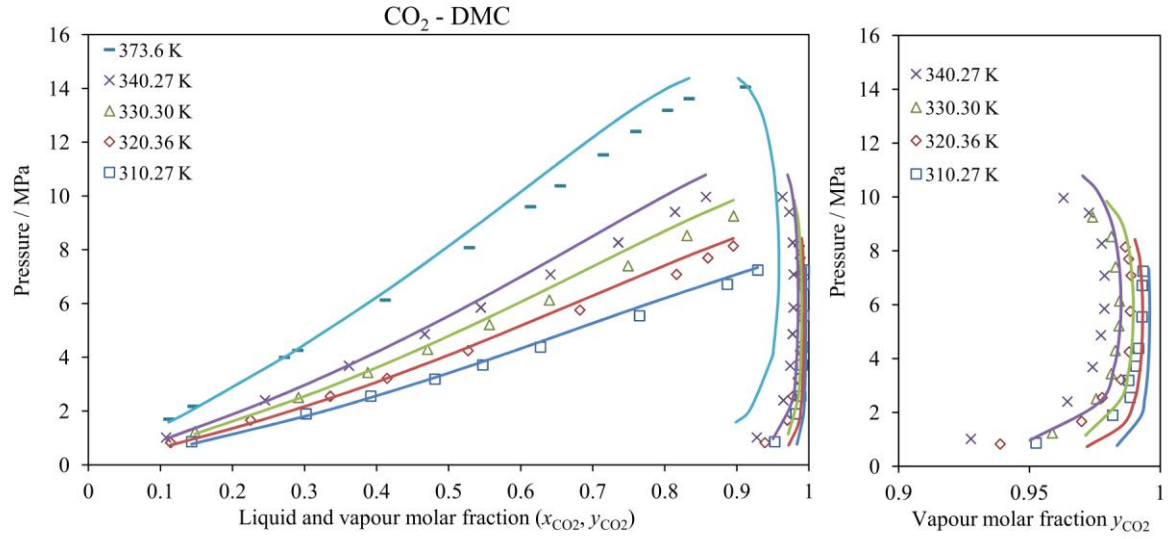

Figure 3.6: Experimental (points) [46, 47] and estimated VLE at different temperatures based on SRK/mHV2 EoS (curves) for CO_2-DMC binary mixture.

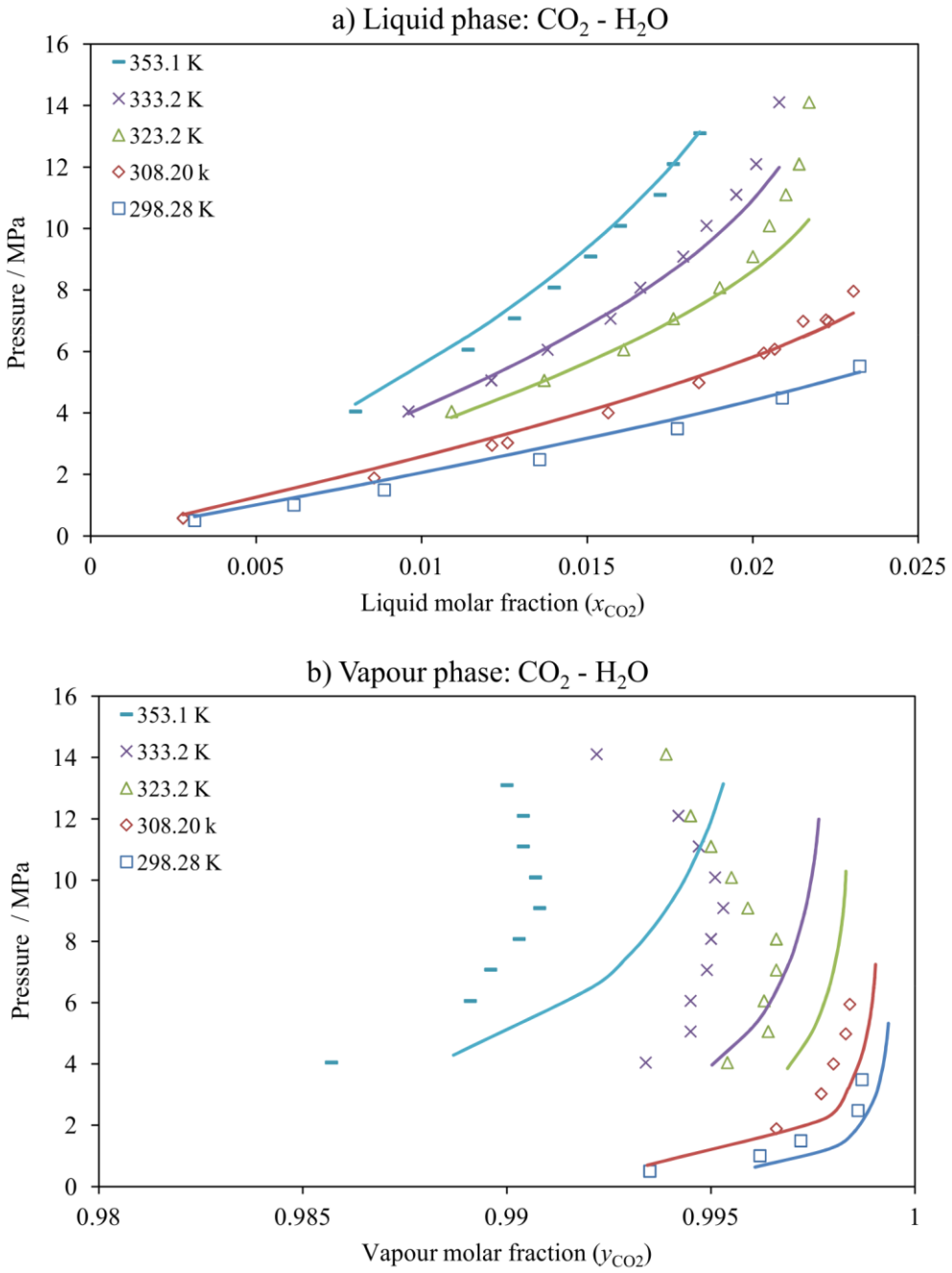

Figure 3.7: Experimental (points) [48, 49] and estimated VLE at different temperatures based on SRK/mHV2 EoS (curves) for CO_2-H_2O: a) liquid saturation curve; b) vapour saturation curve.

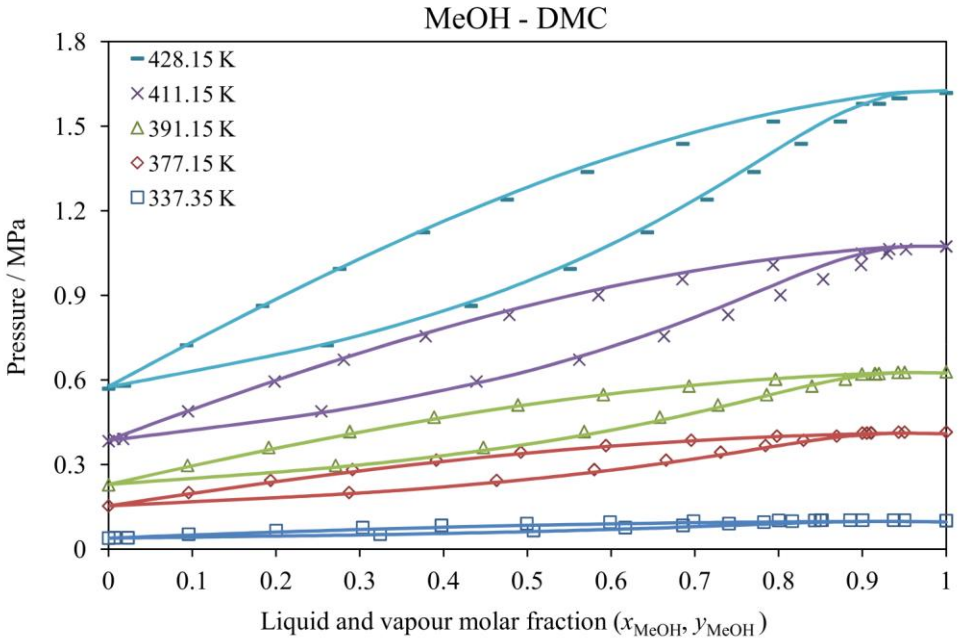

Figure 3.8: Experimental (points) [51] and estimated VLE at different temperatures based on SRK/mHV2 EoS (curves) for MeOH-DMC binary mixture.

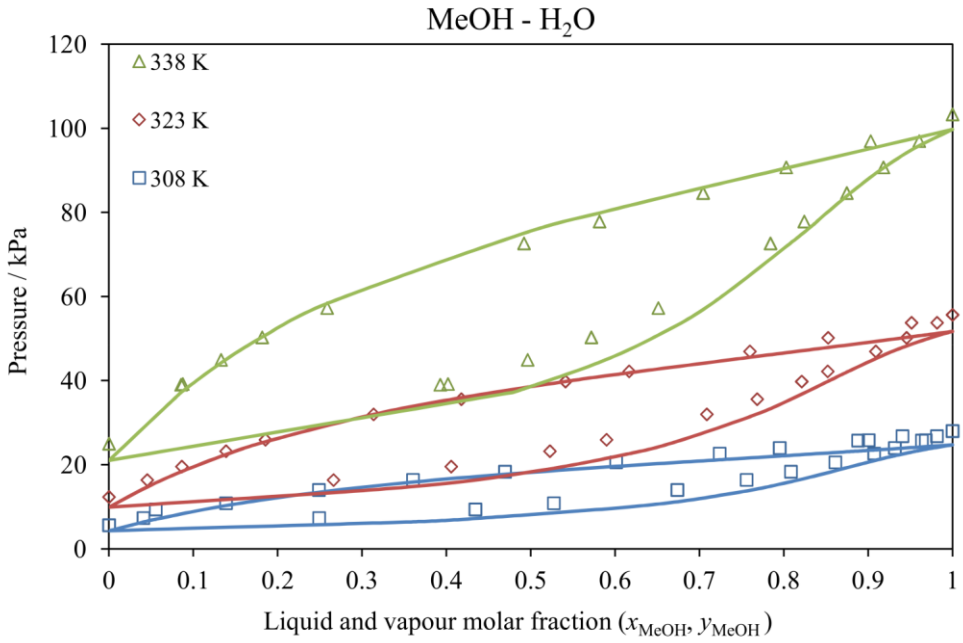

Figure 3.9: Experimental (points) [50] and estimated VLE at different temperatures based on SRK/mHV2 EoS (curves) for MeOH-H_2O binary mixture.

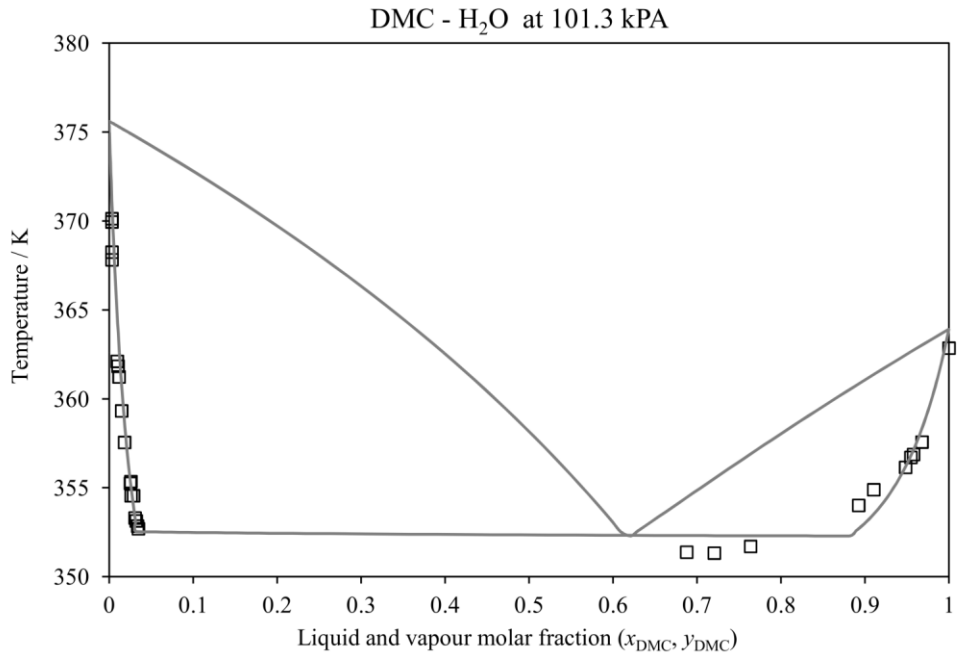

Figure 3.10: Experimental (points) [52] and estimated VLE at different temperatures based on SRK/mHV2 EoS (curves) for DMC-H_2O binary mixture.

3.4. Simulation of Pressure-Temperature Diagram

In the further works it will be needed to understand the physical behaviour of the reaction system; therefore, the pressure-temperature diagram for MeOH-carbon dioxide was predicted based on the SRK/mHV2, so it will be possible to estimate if the system is at vapour, liquid, or supercritical state. Since the reaction yield for the direct synthesis is too low, water and DMC will be present in small amount, which make this approach reasonable. The pressure-temperature diagram was computed through the calculation of bubble (with $x = z$) and dew (with $y = z$) pressure (Figure 3.1) at different temperature.

Then, in Figure 3.11 is depicted the pressure-temperature diagram for the binary system carbon dioxide-MeOH, at different carbon dioxide concentrations. As can be seen in this figure the critical temperature increases with the decrease in carbon dioxide concentration up to the critical temperature of pure methanol (512 K), while the critical pressure reaches a maximum value near 20 MPa, for a carbon dioxide mole fraction around 0.7 and then tends to decrease till the critical pressure of pure methanol (8.08 MPa).

Therefore, assuming that these tendencies are still valid for a quaternary system, with diluted water and DMC, we may expect that above 20 MPa the reaction mixture may be in the liquid or supercritical state, depending on the system temperature.

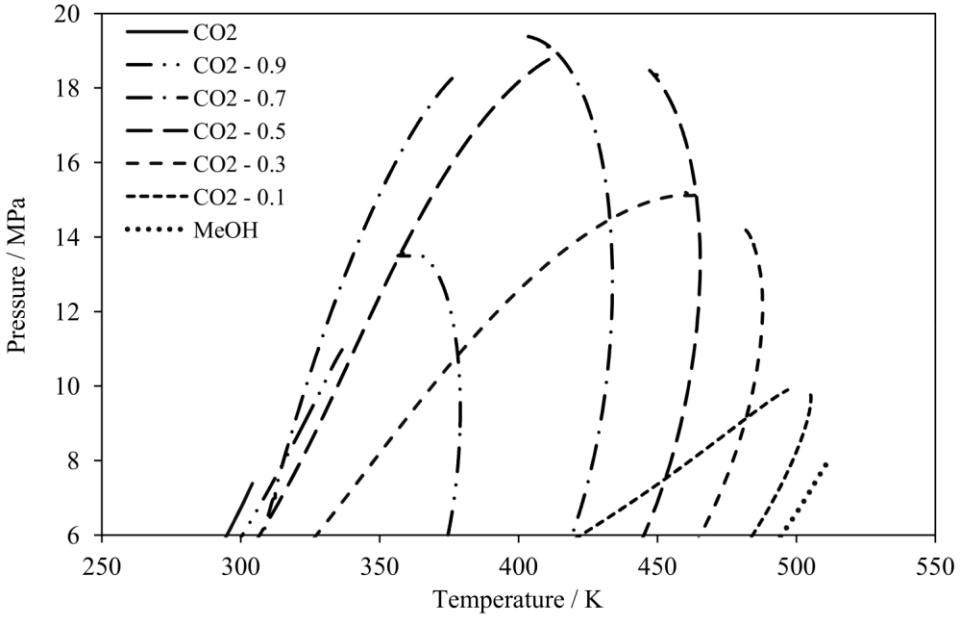

Figure 3.11: Simulation of pressure-temperature diagram using SRK/mHV2 EoS for carbon dioxide-methanol system, at different carbon dioxide molar fractions.

3.5. Conclusions

The five mixing rules studied showed to be suitable to predict the VLE for all the binary mixtures relevant to DMC synthesis, with the exception of the system carbon dioxide-water, which presented high deviations for LCVM and mHV1 mixing rules. Among the mixing rules optimized for the Soave-Redlich-Kwong equation of state, the mHV2, with only two fitted parameters, was found to be the best model, showing high performance for the estimation of vapour liquid equilibrium for all the binary systems, as well as for the ternary mixture between carbon dioxide, MeOH, and water.

Furthermore, from the simulated pressure-temperature diagram, for MeOH and carbon dioxide mixtures, a maximum value of the critical pressure, around 20 MPa, was estimated. Hence, and neglecting the effect of small amounts of DMC and water, above this pressure, the reaction is expected to be carried out in the liquid or supercritical phase, depending on the reaction temperature.

Nomenclature

Symbols

a, a^*	EoS parameter ($J \cdot mol^{-1}$)
A_{ij}	UNIQUAC binary parameter between species i and j ($J \cdot mol^{-1}$)
α	EoS temperature dependent parameter ($mol \cdot m^{-3}$)

b	EoS parameter ($m^3 \cdot mol^{-1}$)
B	Second virial coefficient ($m^3 \cdot mol^{-1}$)
γ	Activity coefficient
f_i^o	Standard fugacity of pure species i (Pa)
$\hat{f}_i^l, \hat{f}_i^v$	Fugacity of species i in the liquid and vapour phase (Pa)
F_{Obj}	Objective function
$f[T_r]$	EoS temperature dependent function
G^E	Excess Gibbs free energy ($J \cdot mol^{-1}$)
k_{ij}	1PVDW and WS binary interaction parameter
M	Molar mass ($g \cdot mol^{-1}$)
n	Molar amount (mol)
NP	Number of points
l_{ij}	1PVDW binary interaction parameter
P, P_c, P^o	Absolute, critical, and standard pressure (Pa)
q	UNIQUAC pure compound parameter
r	UNIQUAC pure compound parameter
R	Ideal gas constant ($J \cdot mol^{-1} \cdot K^{-1}$)
T, T_c, T_r, T^o	Absolute, critical, reduced and reference temperature (K)
V_M	Molar volume ($m^3 \cdot mol^{-1}$)
$\hat{\varphi}_i^v, \hat{\varphi}_i^l$	Fugacity coefficient of species i in the liquid and in the vapour phase
x	Liquid mole fraction
y	Vapour mole fraction
ω	Acentric factor
z	Mixture molar fraction
Z	Compressibility factor

Abbreviations

1PVDW	Van der Waals one-fluid mixing rule
DMC	Dimethyl carbonate
EoS	Equation of state
HV	Huron-Vidal mixing rule
LCVM	Linear combination of Vidal and Michelsen mixing rules
MeOH	Methanol
mHV1	Modified first-order Huron-Vidal mixing rule
mHV2	Modified second-order Huron-Vidal mixing rule
mPR	Modified Peng-Robinson
PgR	Panagiotopoulos and Reid mixing rule
PR	Peng-Robinson
PRSV	Peng-Robinson-Stryjek-Vera
PT	Patel-Teja
RKA	Redlich-Kwong-Aspen
SAFT-VR	Statistical Associating Fluid Theory for Potentials of Variable Attractive Range
SRK	Soave-Redlich-Kwong
VLE	Vapour-liquid equilibrium
WS	Wong-Sandler mixing rule

References

[1] Vetter, A. B. G. *High Pressure Process Technology: Fundamentals And Applications*; First ed.; Elsevier Science B.V.: Amsterdam, **2001**; Vol. 9.

[2] Peng, D. Y.,Robinson, D. B. A New Two-Constant Equation Of State. *Industrial and Engineering Chemistry Fundamentals* **1976,** *15*(1), 59.

[3] Soave, G. Equilibrium Constants From A Modified Redlich-Kwong Equation Of State. *Chemical Engineering Science* **1972,** *27*(6), 1197.

[4] Schmidt, G.,Wenzel, H. A Modified Van Der Waals Type Equation Of State. *Chemical Engineering Science* **1980,** *35*(7), 1503.

[5] Patel, N. C.,Teja, A. S. A New Cubic Equation Of State For Fluids And Fluid Mixtures. *Chemical Engineering Science* **1982,** *37*(3), 463.

[6] Stryjek, R.,Vera, J. H. PRSV: An Improved Peng-Robinson Equation Of State For Pure Compounds And Mixtures. *Canadian Journal of Chemical Engineering* **1986,** *64*(2), 323.

[7] Adachi, Y.,Sugie, H. A New Mixing Rule-Modified Conventional Mixing Rule. *Fluid Phase Equilibria* **1986,** *28*(2), 103.

[8] Panagiotopoulos, A. Z.,Reid, R. C. In *New Mixing Rule For Cubic Equations Of State For Highly Polar, Asymmetric Systems*, American Chemical Society: **1986**; pp 571-582.

[9] Sandoval, R.,Wilczek-Vera, G.,Vera, J. H. Prediction Of Ternary Vapor-Liquid Equilibria With The PRSV Equation Of State. *Fluid Phase Equilibria* **1989,** *52*(C), 119.

[10] Huron, M. J.,Vidal, J. New Mixing Rules In Simple Equations Of State For Representing Vapour-Liquid Equilibria Of Strongly Non-Ideal Mixtures. *Fluid Phase Equilibria* **1979,** *3*(4), 255.

[11] Michelsen, M. L. A Modified Huron-Vidal Mixing Rule For Cubic Equations Of State. *Fluid Phase Equilibria* **1990,** *60*(1-2), 213.

[12] Holderbaum, T.,Gmehling, J. PSRK: A Group Contribution Equation Of State Based On Unifac. *Fluid Phase Equilibria* **1991,** *70*(2-3), 251.

[13] Dahl, S.,Michelsen, M. L. High-Pressure Vapor-Liquid Equilibrium With A UNIFAC-Based Equation Of State. *AIChE Journal* **1990,** *36*(12), 1829.

[14] Boukouvalas, C.,Spiliotis, N.,Coutsikos, P.,Tzouvaras, N.,Tassios, D. Prediction Of Vapor-Liquid Equilibrium With The LCVM Model: A Linear Combination Of The Vidal And Michelsen Mixing Rules Coupled With The Original UNIF. *Fluid Phase Equilibria* **1994,** *92*(C), 75.

[15] Hill Wong, D. S.,Sandler, S. I. Theoretically Correct Mixing Rule For Cubic Equations Of State. *AIChE Journal* **1992,** *38*(5), 671.

[16] Silva, M. I. d. G. V. M. d. Estudo Do Equilíbrio De Fases De Sistemas Relevantes Para O Processo De Desalcoolização De Vinho Por Extracção Supercrítica. Tese de doutoramento, Faculdade de Engenharia da Universidade do Porto Porto, **2002**.

[17] Orbey, H.,Sandler, S. I. Reformulation Of Wong-Sandler Mixing Rule For Cubic Equations Of State. *AIChE Journal* **1995,** *41*(3), 683.

[18] Valderrama, J. O.,Zavaleta, J. Generalized Binary Interaction Parameters In The Wong-Sandler Mixing Rules For Mixtures Containing N-Alkanols And Carbon Dioxide. *Fluid Phase Equilibria* **2005,** *234*(1-2), 136.

[19] Anderko, A. Equation-Of-State Methods For The Modelling Of Phase Equilibria. *Fluid Phase Equilibria* **1990,** *61*(1-2), 145.

[20] Han, X.,Wang, Q.,Chen, G. The Vapor Liquid Equilibrium Mixing Rules Based On Excess Free Energy Models. *Chemistry Bulletin / Huaxue Tongbao* **2006,** *69*(2), 95.

[21] Salim, P. H.,Trebble, M. A. An Evaluation Of Mixing Rules For The Trebble-Bishnoi-Salim Equation Of State. *Industrial and Engineering Chemistry Research* **1995,** *34*(9), 3112.

[22] Valderrama, J. O. The State Of The Cubic Equations Of State. *Industrial and Engineering Chemistry Research* **2003,** *42*(8), 1603.

[23] Wei, Y. S.,Sadus, R. J. Equations Of State For The Calculation Of Fluid-Phase Equilibria. *AIChE Journal* **2000,** *46*(1), 169.

[24] Zheng, X. Y.,Li, P.,Iwai, Y.,Arai, Y. Comparison Of Several Mixing Rules In Equations Of State For Calculating Solid-Solubilities In Supercritical Fluids. *Memoirs of the Kyushu University, Faculty of Engineering* **1997,** *57*(2), 52.

[25] Kontogeorgis, G. M.,Michelsen, M. L.,Folas, G. K.,Derawi, S.,Von Solms, N.,Stenby, E. H. Ten Years With The Cpa (Cubic-Plus-Association) Equation Of State. Part 1. Pure Compounds And Self-Associating Systems. *Industrial and Engineering Chemistry Research* **2006,** *45*(14), 4855.

[26] Kontogeorgis, G. M.,Michelsen, M. L.,Folas, G. K.,Derawi, S.,Von Solms, N.,Stenby, E. H. Ten Years With The Cpa (Cubic-Plus-Association) Equation Of State. Part 2. Cross-Associating And Multicomponent Systems. *Industrial and Engineering Chemistry Research* **2006,** *45*(14), 4869.

[27] Xiang, H. W.,Montel, F.,Graciaa, A.,Mendiboure, B.,Miqueu, C. In *Generalized Cubic-Plus-Association Equation Of State*, AIChE Annual Meeting, Conference Proceedings, **2005**; p 572.

[28] Poling, B. E.,Prausnitz, J. M.,O'Connell, J. P. *The Properties Of Gases And Liquids*; 5 ed.; McGraw-Hill: **2001**.

[29] Smith, J. M.,Ness, H. C. V.,Abbott, M. M. *Introduction To Chemical Engineering Thermodynamics*; 6th ed.; McGraw-Hill: New York, **2005**.

[30] Anderson, T. F.,Prausnitz, J. M. Computational Methods For High-Pressure Phase Equilibria And Other Fluid-Phase Properties Using A Partition Function - 2. Mixtures. *Industrial and Engineering Chemistry, Process Design and Development* **1980,** *19*(1), 9.

[31] Chen, X.,Cai, F.,Wu, X.,Asumana, C.,Yu, G. Isobaric Vapor-Liquid Equilibrium For Methanol + Dimethyl Carbonate + 1-Butyl-3-Methylimidazolium Dibutylphosphate. *Journal of Chemical and Engineering Data* **2013,** *58*(5), 1186.

[32] Cho, H.,Yim, J. H.,Lim, J. S. Measurement Of Vle Data Of Carbon Dioxide (CO2) + Methyl Iodide (CH3I) System For The Direct Synthesis Of Dimethyl Carbonate Using Supercritical CO2 And Methanol. *Journal of Supercritical Fluids* **2013,** *81*, 7.

[33] Lazzaroni, M. J.,Bush, D.,Brown, J. S.,Eckert, C. A. High-Pressure Vapor−Liquid Equilbria Of Some Carbon Dioxide + Organic Binary Systems. *Journal of Chemical and Engineering Data* **2004,** *50*(1), 60.

[34] Lee, M. H.,Yim, J.-H.,Kang, J. W.,Lim, J. S. Measurement Of Vle Data Of Carbon Dioxide + Dimethyl Carbonate System For The Direct Synthesis Of Dimethyl Carbonate Using Supercritical CO2 And Methanol. *Fluid Phase Equilibria* **2012,** *318*, 77.

[35] Ma, X.-B.,Liu, X.-G.,Li, Z.-H.,Xu, G.-H. Vapor-Liquid Equilibria For The Ternary System Methanol + Dimethyl Carbonate + Dimethyl Oxalate And Constituent Binary Systems At Different Temperatures. *Fluid Phase Equilibria* **2004,** *221*(1-2), 51.

[36] Pappa, G. D.,Perakis, C.,Tsimpanogiannis, I. N.,Voutsas, E. C. Thermodynamic Modeling Of The Vapor-Liquid Equilibrium Of The CO2/H2O Mixture. *Fluid Phase Equilibria* **2009,** *284*(1), 56.

[37] Rodríguez, A.,Canosa, J.,Domínguez, A.,Tojo, J. Vapour-Liquid Equilibria Of Dimethyl Carbonate With Linear Alcohols And Estimation Of Interaction Parameters For The UNIFAC And ASOG Method. *Fluid Phase Equilibria* **2002,** *201*(1), 187.

[38] Sako, T.,Sugeta, T.,Nakazawa, N.,Otake, K.,Sato, M.,Ishihara, K.,Kato, M. High Pressure Vapor-Liquid And Vapor-Liquid-Liquid Equilibria For Systems Containing Supercritical Carbon Dioxide, Water And Furfural. *Fluid Phase Equilibria* **1995,** *108*(1-2), 293.

[39] Soujanya, J.,Satyavathi, B.,Vittal Prasad, T. E. Experimental (Vapour + liquid) Equilibrium Data Of (Methanol + water), (Water + glycerol) And (Methanol + glycerol) Systems At Atmospheric And Sub-Atmospheric Pressures. *Journal of Chemical Thermodynamics* **2010,** *42*(5), 621.

[40] Tsivintzelis, I.,Musko, N. E.,Baiker, A.,Grunwaldt, J.-D.,Kontogeorgis, G. M. Experimental Determination And Modeling Of The Phase Behavior For The Direct Synthesis Of Dimethyl Carbonate From Methanol And Carbon Dioxide. *The Journal of Supercritical Fluids* **2013,** *84*, 155.

[41] Wiebe, R.,Gaddy, V. L. The Solubility Of Carbon Dioxide In Water At Various Temperatures From 12 To 40° And At Pressures To 500 Atmospheres. Critical Phenomena*. *Journal of the American Chemical Society* **1940,** *62*(4), 815.

[42] Yang, C.,Zeng, H.,Yin, X.,Ma, S.,Sun, F.,Li, Y.,Li, J. Measurement Of (Vapor + Liquid) Equilibrium For The Systems {Methanol + Dimethyl Carbonate} And {Methanol + Dimethyl Carbonate + Tetramethylammonium Bicarbonate} At P = (34.43, 67.74) kPa. *Journal of Chemical Thermodynamics* **2012,** *53*, 158.

[43] Yoon, J. H.,Lee, H. S.,Lee, H. High-Pressure Vapor-Liquid Equilibria For Carbon Dioxide + Methanol, Carbon Dioxide + Ethanol, And Carbon Dioxide + Methanol + Ethanol. *Journal of Chemical and Engineering Data* **1993,** *38*(1), 53.

[44] Chang, C. J.,Chiu, K.-L.,Day, C.-Y. A New Apparatus For The Determination Of P-x-y Diagrams And Henry's Constants In High Pressure Alcohols With Critical Carbon Dioxide. *Journal of Supercritical Fluids* **1998,** *12*(3), 223.

[45] Naidoo, P.,Ramjugernath, D.,Raal, J. D. A New High-Pressure Vapour-Liquid Equilibrium Apparatus. *Fluid Phase Equilibria* **2008,** *269*(1-2), 104.

[46] Im, J.,Kim, M.,Lee, J.,Kim, H. Vapor−Liquid Equilibria Of Binary Carbon Dioxide + Alkyl Carbonate Mixture Systems. *Journal of Chemical and Engineering Data* **2003,** *49*(2), 243.

[47] Ciccolini, R. P.,Madlinger, A. C.,Rogers, S. A.,Tester, J. W. Vapor−Liquid Equilibrium Data And Predictive Correlations For The Carbon Dioxide−Dimethyl Carbonate Binary Mixture. *Journal of Chemical and Engineering Data* **2010,** *55*(8), 2673.

[48] Valtz, A.,Chapoy, A.,Coquelet, C.,Paricaud, P.,Richon, D. Vapour-Liquid Equilibria In The Carbon Dioxide-Water System, Measurement And Modelling From 278.2 To 318.2 k. *Fluid Phase Equilibria* **2004,** *226*, 333.

[49] Bamberger, A.,Sieder, G.,Maurer, G. High-Pressure (Vapor+Liquid) Equilibrium In Binary Mixtures Of (Carbon Dioxide+Water Or Acetic Acid) At Temperatures From 313 To 353 K. *Journal of Supercritical Fluids* **2000,** *17*(2), 997.

[50] McGlashan, M. L.,Williamson, A. G. Isothermal Liquid-Vapor Equilibriums For System Methanol-Water. *Journal of Chemical and Engineering Data* **1976,** *21*(2), 196.

[51] Yunhai, S.,Honglai, L.,Kun, W.,Wende, X.,Ying, H. Measurements Of Isothermal Vapor-Liquid Equilibrium Of Binary Methanol/Dimethyl Carbonate System Under Pressure. *Fluid Phase Equilibria* **2005,** *234*(1-2), 1.

[52] Camy, S.,Pic, J. S.,Badens, E.,Condoret, J. S. Fluid Phase Equilibria Of The Reacting Mixture In The Dimethyl Carbonate Synthesis From Supercritical CO2. *Journal of Supercritical Fluids* **2003,** *25*(1), 19.

[53] Yoon, J. H.,Chun, M. K.,Hong, W. H.,Lee, H. High-Pressure Phase Equilibria For Carbon Dioxide-Methanol-Water System: Experimental Data And Critical Evaluation Of Mixing Rules. *Industrial and Engineering Chemistry Research* **1993,** *32*(11), 2881.

[54] Piñero, R.,García, J.,Sokolova, M.,Cocero, M. J. Modelling Of The Phase Behaviour For The Direct Synthesis Of Dimethyl Carbonate From CO2 And Methanol At Supercritical Or Near Critical Conditions. *Journal of Chemical Thermodynamics* **2007,** *39*(4), 536.

Chapter 4. Direct Synthesis of DMC over CeO_2 at High Pressure Conditions

"*Nothing in life is to be feared, it is only to be understood. Now it is time to understand more, so that we may fear less.*" – Marie Curie

This chapter is based on the following article: Santos, B., Pereira, C., Silva, V., Loureiro, J., Rodrigues, A. Kinetic Study For The Direct Synthesis Of Dimethyl Carbonate From Methanol And CO2 Over CeO2 At High Pressure Conditions. *Applied Catalysis A: General* **2013,** *455*, 219.

4.1. Introduction

As concluded in Chapter 2, the direct synthesis ($CO_2 + 2 \cdot MeOH \rightleftharpoons DMC + H_2O$) is considered to be one of the most promising routes for DMC production based on economical and environmental features [1]. However, this route shows high thermodynamic limitations even at high pressure conditions. Several approaches have been studied in order to overcome this issue, such as the use of dehydrating agents, which will react with the water, to shift the equilibrium towards the DMC production, such as ketals [2-7], orthoesters [8], acetonitrile [9, 10], butylene oxide [11] or ionic liquids [12].

Apart from the thermodynamic limitations, carbon dioxide is also a stable molecule with low reactivity leading to low reaction rates. The direct synthesis of DMC is achieved in the presence of an acid-base catalyst. In spite of the large variety of catalysts (see Chapter 2), those based on zirconium oxide (ZrO_2) and/or cerium oxide (CeO_2) are still showing the higher activity and selectivity [6, 10, 13-19]. In spite of the huge efforts done in searching for novel catalysts and dehydrating agents, there is a lack of kinetic data, which is essential to design and evaluate novel processes for DMC production and turn this route competitive in comparison with the conventional processes.

In this chapter, it will be presented a detailed kinetic and equilibrium model for the direct synthesis over cerium oxide at high pressure conditions. Cerium oxide was chosen due to its high activity and selectivity, and also because it is easy to prepare from calcination of cerium hydroxide ($Ce(OH)_4$); the preparation of novel catalysts is out of the scope of this thesis. Then, two reaction rate expressions will be considered based on Langmuir-Hinshelwood and Eley-Rideal mechanisms. In order to fit the kinetic parameters, the effect of several variables on the reaction rate will be studied: temperature, initial carbon dioxide to MeOH molar ratio, and pressure. Furthermore, the enthalpy, Gibbs free energy, and entropy change of reaction will be adjusted from the experimental data.

4.2. Experimental

4.2.1. Materials and analytical method

Cerium oxide was prepared from cerium hydroxide ($Ce(OH)_4$, Sigma-Aldrich®) by calcination. Anhydrous methanol (99.9%, AcroSeal®), carbon dioxide (99.995%, Linde®) and dimethyl carbonate (99%, Sigma-Aldrich®) were used without further purification. The water used was deionised in our laboratory.

All the samples were analyzed by GC chromatography (GC2010 plus, Shimadzu®) using a fused silica capillary column, Chrompack CP-Wax 52 CB (25 m × 0.25 mm × 1.2 μm) to separate the compounds coupled with a thermal conductivity detector and a flame ionization detector. Helium N50 was used as carrier gas at a constant linear velocity of 30 $cm \cdot s^{-1}$ with a split ratio equal to 30 for 2 μL of sample injected. The temperature of the injector and detectors was set at 573 K, while the oven temperature was set at 348 K during the 5 min of analyzing time. An example of the analytic method development can be found in Annex A.

4.2.2. Experimental set-up

Figure 4.1 shows the sketch of the experimental set-up where all the experiments were conducted. The set-up is composed by an autoclave reactor (HP reactor 4575A, Parr®) coupled with temperature (±1K) and stirrer speed control, and a pressure gauge (±0.01 MPa) (4848 reactor controller, Parr®); the HPLC pump (K-1900 100mL head, Knauer®) is cooled with an external cooling bath at 278 K in order to keep carbon dioxide in the liquid state; the feed cylinder is used to add other chemicals to the reactor through the carbon dioxide stream. The depressurization of the system is easily done through a metering valve into a trap cylinder to expand the carbon dioxide; moreover, the valve is heated by an external resistance thereby avoiding freezing. A more detailed description of the experimental set-up can be found in Annex B.

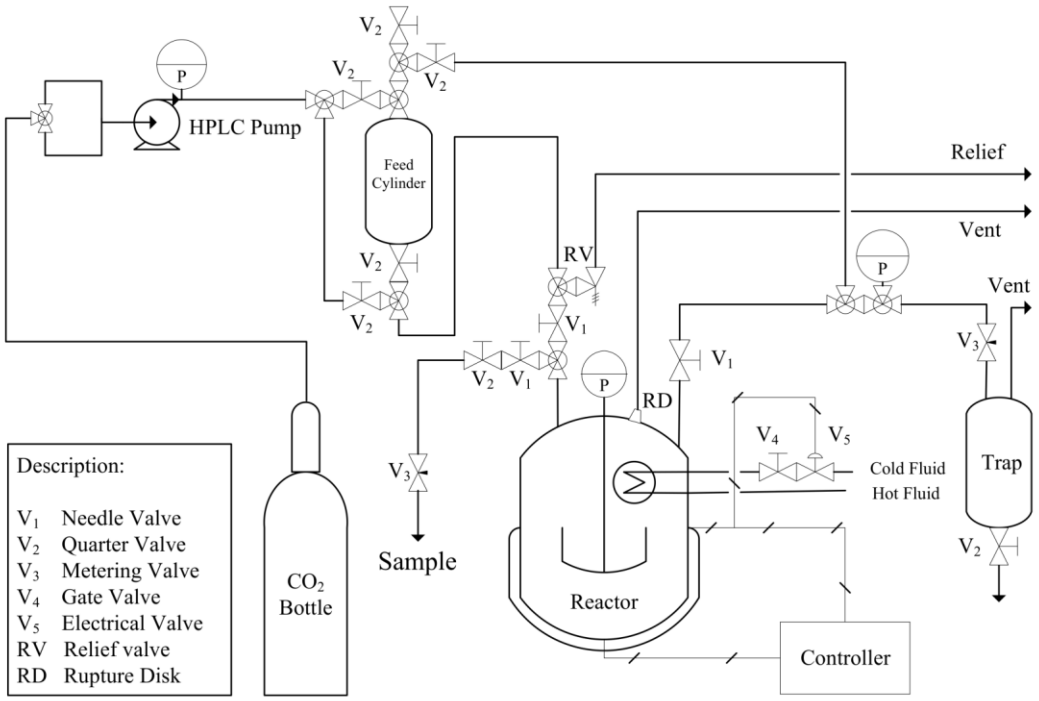

Figure 4.1: Sketch of the experimental set-up for high pressure reactions.

4.2.3. Experimental procedure

The catalyst is firstly added to the reactor and, then, the reactor is closed; the loss of catalyst is avoided by the use of a filter. Afterwards, the reactor is filled with carbon dioxide, through the feed cylinder, at environmental temperature around 1 MPa and heated until 413 K, followed by depressurization. This procedure is used to reduce the initial water content in the reactor, which is present on the tubes and reactor walls, due to the humidity of the air inside the reactor. With this approach, an average of initial water contents around 0.5% was reached. Afterwards, the methanol is dragged through the feed cylinder by the carbon dioxide stream. Finally, the temperature is set followed by the pressurization with carbon dioxide to the desired pressure. The samples are carefully collected through the sample line (2 mL) by a metering valve to reach a slow depressurization and a complete condensed sample (without carbon dioxide). Then the pressure

drop (around 0.4 MPa for each sample) is compensated with carbon dioxide that also cleans the line for the next sample. In the end of the reaction, the reaction mixture is cooled until 300 K and the reactor is slowly depressurized improving the condensation of the reaction mixture (without carbon dioxide).

Before the experiments, six standard solutions (50-60 mL), with known concentrations of DMC diluted in MeOH, from 0.1% to 0.3%, were added to the reactor with the purpose of validating the sampling method. Two samples were collected: one from the sampling line and other after depressurization. Both methods showed good agreement with the real concentration inside the reactor, with an average absolute deviation of 0.03%. These experiments are depicted in Figure 4.2.

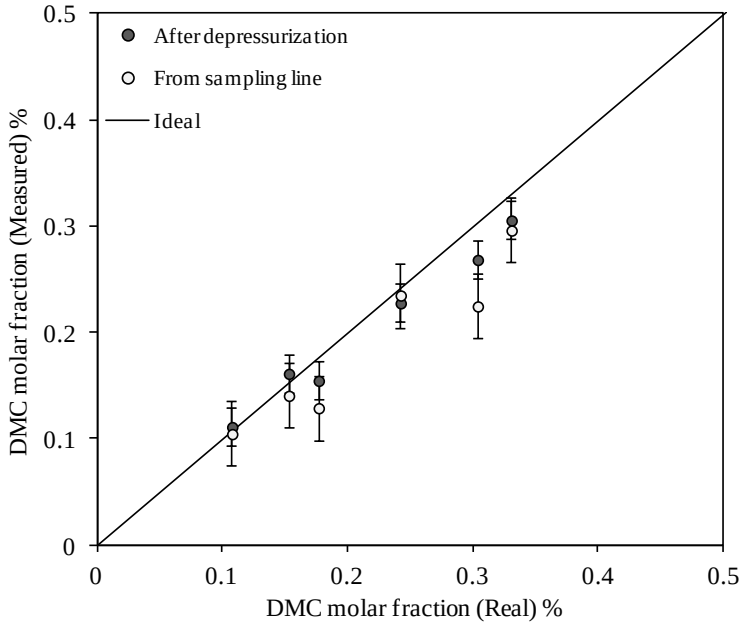

Figure 4.2: Validation of the sampling systems: from the sampling line and after depressurization.

Table 4.1 presents the reaction operating conditions held for all the experiments. Several experiments were carried out with the objective of studying the effect of different physical parameters on the reaction rate and/or equilibrium yield: external mass transfer (between 200 rpm and 400 rpm), temperature (between 378 K and 408K), carbon dioxide to MeOH molar ratio (between 1.1 and 4.0) and pressure (between 15 MPa and 20 MPa).

Table 4.1: Experimental conditions for kinetic and/or equilibrium experiments.

Run	T / K	P / MPa	n_{CO_2}/n_{MeOH}	$x_{H_2O}^{initial}$ (CO_2 free basis)	$m_{Catalyst}$ / g	Stirrer / rpm
1	398	20.0	2.5	0.42%	4.6	200
2	398	20.0	2.5	0.57%	4.6	200
3	398	20.0	2.5	0.34%	4.6	400
4	408	20.0	2.4	0.72%	4.4	200
5	403	20.0	2.5	0.35%	4.6	200
6	393	20.0	2.6	0.56%	4.6	200
7	388	20.0	2.7	0.57%	4.7	200
8	388	20.0	2.7	0.37%	4.7	200
9	383	20.0	2.9	0.58%	4.6	200
10	378	20.0	2.9	0.74%	4.4	200
11	398	20.0	1.1	0.17%	4.7	200
12	398	20.0	1.6	0.18%	4.6	200
13	398	20.0	1.8	0.28%	4.6	200
14	398	20.0	4.0	1.06%	4.6	200
15	398	20.0	4.0	0.78%	4.5	200
16	398	17.5	2.5	0.54%	4.6	200
17	398	15.0	2.5	0.86%	4.5	200

4.3. Experimental Results

4.3.1. Catalyst characterization

As mentioned before, cerium oxide was prepared by calcination of cerium hydroxide, as reported by Yoshida et al. [19]. They observed that above 873 K the reaction rate was proportional to the surface area; however for 673 K the activity was lower than expected, probably due to insufficient water removal. The calcination temperature should be as low as possible in order to minimize the decrease of surface area by sintering but ensuring the maximum water removal. Cerium oxide was, then, prepared from the calcination of cerium hydroxide at 923 K during 4 hours at a rate of 5 $K \cdot min^{-1}$, in order to guarantee a complete water removal. Furthermore, a BET area of 36 $m^2 \cdot g^{-1}$ was determined, which is in accordance with the values reported at this temperature using cerium hydroxide as precursor [19]. Helium pycnometry was carried out to determine the solid density (6345 $kg \cdot m^3$) and the particle porosity (0.66).

The catalyst was analysed by X-ray diffractometry (Cu Kα) – XRD PANalytical X'Pert Pro and detector X´Celerator – in order to determine its crystal structure. In Figure 4.3 is shown the X-ray diffraction patterns for cerium oxide after calcination. The peaks positions reveal crystallinity similar to cubic fluorite structure,

with a lattice parameter of 54.09 Å predicted from the Reitveld refinement (PowderCell 2.3); however, low crystallinity was observed.; the low crystallinity was also observed by Yoshida et al. [19]. They observed an increase of crystallinity with the increase of temperature, although the increase of temperature leads to a decrease of surface area.

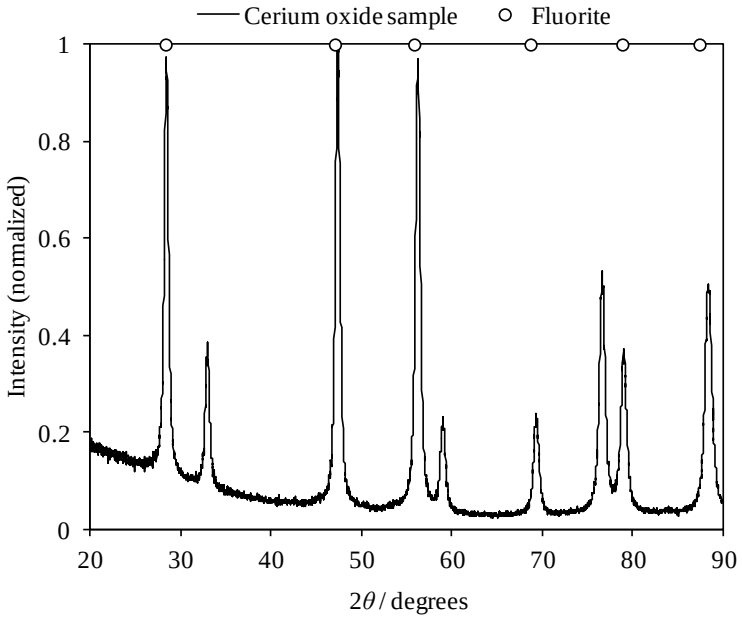

Figure 4.3: XRD patterns of cerium oxide prepared by calcination. Crystal structure: fluorite (○).

Furthermore, in Figure 4.4 is shown the particle size distribution determined by light scattering granulometry, where it can be seen a trimodal size distribution (0.06 μm, 0.50 μm, and 2.20 μm).

4.3.2. Reproducibility and external resistance to mass transfer

In order to evaluate the reproducibility of our experiments, two reactions were carried out at almost the same operating conditions (run 1 and 2 from Table 4.1). The small difference in the initial water contents between the two reactions has negligible effect on the initial reaction rate. In Figure 4.5 is represented the DMC molar fraction along the time for the two runs, where it can be observed a good reproducibility since the curves are coincident within experimental errors.

Then, in order to evaluate the external mass transfer resistance, two reactions were held at the same conditions, again with small differences in the initial water content, but varying the stirrer speed. Figure 4.6 shows the DMC produced along time. Since, in both runs, the initial reaction rates are similar, the external resistance to mass transfer is negligible above 200 rpm.

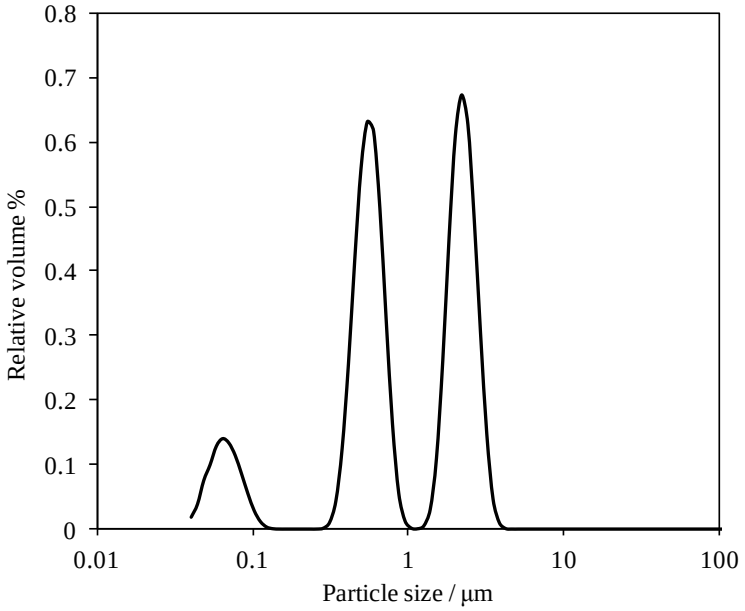

Figure 4.4: Particle size distribution for cerium oxide.

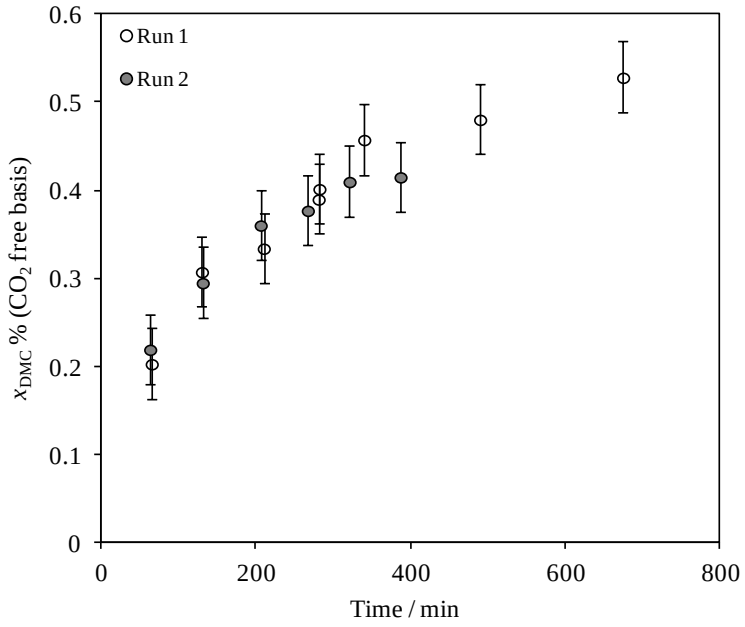

Figure 4.5: Reproducibility: experimental DMC molar fraction along time.

Reaction conditions: 20 MPa, 398 K, 200 rpm, 4.6 g CeO_2, n_{CO_2}/n_{MeOH}: 2.54/1.

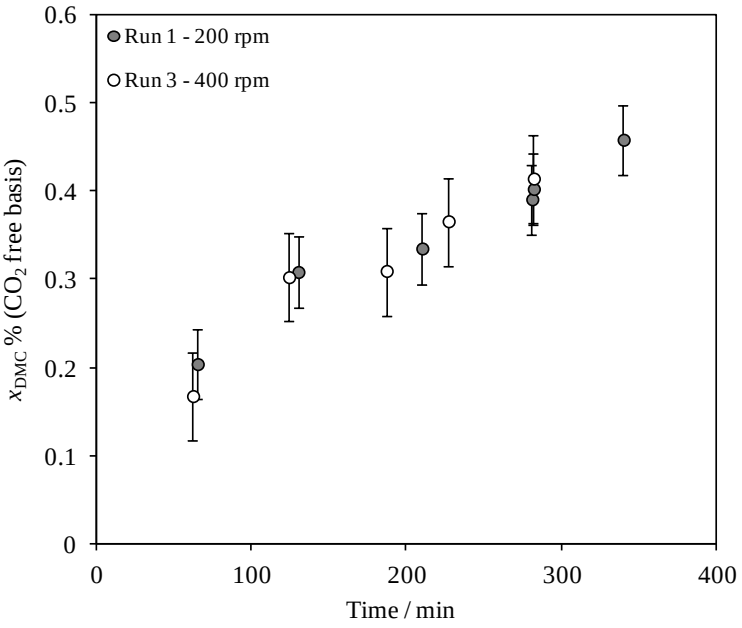

Figure 4.6: Experimental DMC molar fraction along time for different stirrer speeds.
Reaction conditions: 20 MPa, 398 K, 4.6 g CeO_2, n_{CO_2}/n_{MeOH}: 2.54/1.

4.3.3. Chemical equilibrium

Once guaranteed a good reproducibility and negligible external mass transfer resistance, the kinetic modelling can be optimized; however, the reaction equilibrium data is needed for the kinetic model. The equilibrium constant can be calculated based on the fugacity of each compound ($\hat{f}_i$) by the following equation [20]:

$$K_{eq} = \prod_{i=1}^{NC}\left(\frac{\hat{f}_i}{f_i^o}\right)^{\vartheta_i} = \prod_{i=1}^{NC}\left(\frac{x_i \cdot \hat{\varphi}_i \cdot P}{P^o}\right)^{\vartheta_i} \tag{4.1}$$

For ideal gas the fugacity coefficient is equal to one ($\hat{\varphi}_i = 1$). Besides, the equilibrium constant can also be calculated based on the thermodynamic properties of reaction (standard enthalpy ($\Delta_r H^o$), Gibbs energy ($\Delta_r G^o$) and heat capacity ($\Delta_r C_p^o$) change of reaction):

$$\ln K_{eq} = \left[\frac{-\Delta_r G_{T_0}^o}{R \cdot T_0}\right] + \left[\frac{\Delta_r H_{T_0}^o}{R \cdot T_0}\left(1 - \frac{T_0}{T}\right)\right] + \left[-\frac{1}{R \cdot T}\int_{T_0}^{T} \Delta_r C_p^o \cdot dT + \frac{1}{R}\int_{T_0}^{T} \frac{\Delta_r C_p^o}{T} \cdot dT\right] \tag{4.2}$$

Herein, the enthalpy and Gibbs energy of reaction are adjusted from our experimental data for ideal and real gas mixture by minimization of the maximum relative deviation; this objective function gives a more homogenous distribution of the relative deviation:

$$F_{obj} = \min\left\{max\left[\frac{\left|x_{DMC}^{model} - x_{DMC}^{exp.}\right|}{x_{DMC}^{exp.}}\right]\right\} \tag{4.3}$$

The Soave-Redlich-Kwong (SRK) equation of state coupled with the modified Huron-Vidal second order (mHV2) mixing rule, with the binary energetic parameter optimized in the previous Chapter 3, was used to describe the fugacity of the real gas. All the other physical properties were collected from DIPPR™. Table 4.2 contains the standard enthalpy and Gibbs energy of reaction adjusted for ideal and real gas; note that these values are slightly different from the predicted by Hofmann et al. [21], -17.99 and 37.31 kJ·mol^{-1}, respectively. Moreover, the standard entropy change of reaction ($\Delta_r S^o$) at 298.15 K was also computed ($G = H - T \cdot S$), together with the respective uncertainty.

Table 4.2: Standard Enthalpy and Gibbs energy change of reaction adjusted from the reaction experimental data.

Model	$\Delta_r H^o_{298\ \mathrm{K}}$ / kJ·mol^{-1}	$\Delta_r S^o_{298\ \mathrm{K}}$ / J·K^{-1}·mol^{-1}	$\Delta_r G^o_{298\ \mathrm{K}}$ / kJ·mol^{-1}
Ideal Gas	-20±2	-174±8	31±1
Real gas (SRK / mHV2)	-22±3	-180±9	32±1

Now, in Table 4.3 are presented the experimental DMC molar fractions at equilibrium conditions as well as the values estimated by both the ideal and the real gas models. Contrarily to the expected, considering an ideal gas mixture leads to a lower deviation than using SRK/mHV2 to predict the fugacity. This may be explained by the deviation of the real gas model near supercritical conditions, since the model was adjusted based on liquid-vapour equilibrium, at temperatures and pressures below the critical point of the mixture.

Table 4.3: Experimental and predicted DMC molar fractions (carbon dioxide free basis) at equilibrium for several reaction conditions.

Run	x_{DMC}% Experimental	Equilibrium conversion %	x_{DMC}% Ideal gas	Relative deviation %	x_{DMC}% Real gas	Relative deviation %
1	0.57	1.1	0.52	-9.5%	0.50	-13.9%
4	0.33	0.7	0.37	11.3%	0.35	6.4%
5	0.57	1.1	0.52	-10.5%	0.49	-15.3%
6	0.52	1.0	0.51	-3.0%	0.49	-7.2%
7	0.59	1.2	0.54	-10.1%	0.51	-14.7%
12	0.58	1.2	0.56	-2.9%	0.64	9.2%
13	0.51	1.0	0.54	5.4%	0.59	12.9%
15	0.39	0.8	0.44	12.2%	0.35	-10.3%
16	0.43	0.9	0.44	1.8%	0.43	0.6%
17	0.33	0.7	0.31	-5.6%	0.31	-5.0%

4.4. Kinetic Models

The reaction rate expression can be obtained from the reaction mechanism [22]. Two mechanisms were considered for the direct synthesis of DMC over acid-base catalysts: the first one is a Langmuir-Hinshelwood mechanism, where all the species adsorb on the catalyst surface and the surface reaction is considered as the controlling step; the second is based on an Eley-Rideal mechanism, where one of the reactants does not adsorb and the formation of an intermediate species, methyl carbonate (MC), is considered the controlling step. This last mechanism was already proposed by Eta et al. [23] to model the synthesis of DMC, although they used a dehydrating agent to remove the water. In Table 4.4 are shown in detail the two reaction mechanisms proposed.

Table 4.4: Reaction mechanism based on Langmuir-Hinshelwood and Eley-Rideal methodology.

Step	Mechanism 1	Mechanism 2 [23]
1	CO_2 + * ↔ CO_2*	MeOH + * ↔ MeOH*
2	MeOH + * ↔ MeOH*	MeOH* + CO_2 ↔ MC*
3	2·MeOH* + CO_2* ↔ DMC* + H_2O* + *	MC* + MeOH* ↔ DMC + H_2O + *
4	DMC* ↔ DMC + *	-
5	H_2O* ↔ H_2O + *	-
	Controlling step: 3	Controlling step: 2

* Active center

The reaction rate expressions (r) can be deduced from the mechanisms considering each step as an elementary reaction and defining the controlling step. The following equations express the reaction rate, for mechanisms 1 and 2, respectively, as function of the kinetic constant (k), partial pressure (P_i), standard pressure (P^o), adsorption constants (K_{ads}) and (global) reaction equilibrium constant (K_{eq}):

$$r = \frac{k \cdot \left[P_{CO2} \cdot {P_{MeOH}}^2 - \frac{P_{DMC} \cdot P_{H2O}}{K_{eq}/P^o} \right]}{\left[1 + \sum K_{ads,i} \cdot \frac{P_i}{P^o} \right]^3} \tag{4.4}$$

$$r = \frac{k \cdot \left[P_{CO2} \cdot {P_{MeOH}}^2 - \frac{P_{DMC} \cdot P_{H2O}}{K_{eq}/P^o} \right]}{\frac{P_{MeOH}}{P^o} \left[1 + K_{ads,1} \cdot \frac{P_{MeOH}}{P^o} + K_{ads,2} \cdot \frac{P_{MeOH}}{P^o} \cdot \frac{P_{CO2}}{P^o} \right]} \tag{4.5}$$

The adsorption constants were considered as not depending of temperature for the studied temperatures range, because a large number of parameters drastically increases the complexity of the optimization and may lead to unrealistic values for the adsorption enthalpy; these values ought to be measured by adsorption

experiments. However, the kinetic constant was considered function of temperature following an Arrhenius equation:

$$k = k_0 \cdot e^{-E_a/R \cdot T} \tag{4.6}$$

The activation energy (E_a) reflects the effect of temperature on the reaction rate; k_0 is the pre-exponential factor. For a batch reaction the dependence of molar reaction conversion (X_c) with time is expressed by the following equation:

$$\frac{dX_c}{dt} = m_{cat}\frac{\vartheta_{Lim.}}{n_{Lim.(t=0)}}r, \qquad Initial\ condition: X_c(t=0) = 0 \tag{4.7}$$

where m_{cat} is the catalyst mass, ϑ_{Lim} is the stoichiometric coefficient of the limiting reactant, and $n_{Lim(t=0)}$ is the initial molar amount of the limiting reactant.

4.5. Parameters Optimization

Firstly, the activation energy was estimated by the linearization of the logarithm of the initial reaction rate as function of the inverse of the temperature: 107 kJ·mol^{-1}, which is higher than the reported by Hoffmann et al. [21] for 0.8·CeO_2-0.2·ZrO_2 (around 75 kJ·mol^{-1}). The higher activity of 0.8·CeO_2-0.2·ZrO_2 and the precursor used for the synthesis of cerium oxide might be the reasons for this difference in the activation energy. The precursor and the thermal treatment will also define the activity of the catalyst due to the effects on the physical properties, specially the amount and strength of the acid-base sites and the amount of Ce^{3+} on the surface that is responsible for the loss of activity. This Arrhenius plot is depicted in Figure 4.7, where the initial reaction rate was calculated by the slope of the linear line fitted to the first reaction experimental points. Then, the kinetic parameters were adjusted from the experimental data by minimization of the maximum average deviation of each run by the following objective function:

$$F_{obj} = \min\left\{max\left[\sum_{i=1}^{NP}\frac{\left|x_{DMC}^{model} - x_{DMC}^{exp.}\right|}{x_{DMC}^{exp.}}/NP\right]\right\} \tag{4.8}$$

Among the runs presented in Table 4.1, just some of them were used for parameters optimization; the others were used only for equilibrium purposes, or to measure the initial reaction rate (lowest temperature); the pressure effect was not taken into account for these parameters optimization but only to evaluate its effect afterwards.

The ordinary differential equation, which constitutes an initial value problem, was solved using a Runge-Kutta method implemented in Matlab ® (subroutine *ODE45*), with a relative tolerance of 10^{-5}; moreover, *fminsearch* was used to solve the optimization problem. In Table 4.5 are presented the kinetic parameters optimized from the experimental data for the models based on mechanisms 1 and 2; furthermore, the model

based on mechanism 1 was optimized considering a real gas ($\hat{f}_i \leftrightarrow P_i$). The model based on the mechanism 1 (Langmuir-Hinshelwood) was chosen for further calculations; in spite of the equal overall deviation (17%) when compared to the model based on mechanism 2, the activation energy (106 kJ·mol^{-1}) value is similar to the predicted by the initial reaction rate (107 kJ·mol^{-1}). The third model, based on mechanism 1 but considering the fugacity to predict the deviation of ideal gas (by SRK/mHV2 model), showed a slight lower overall deviation (16%); however, the uncertainties related to the fitted parameters are much higher. Therefore, there are not relevant advantages in using this more complex model. Finally, in Figure 4.8 is shown the average deviation, for the runs considered in the optimization (for each model), as well as the respective standard deviation for each run.

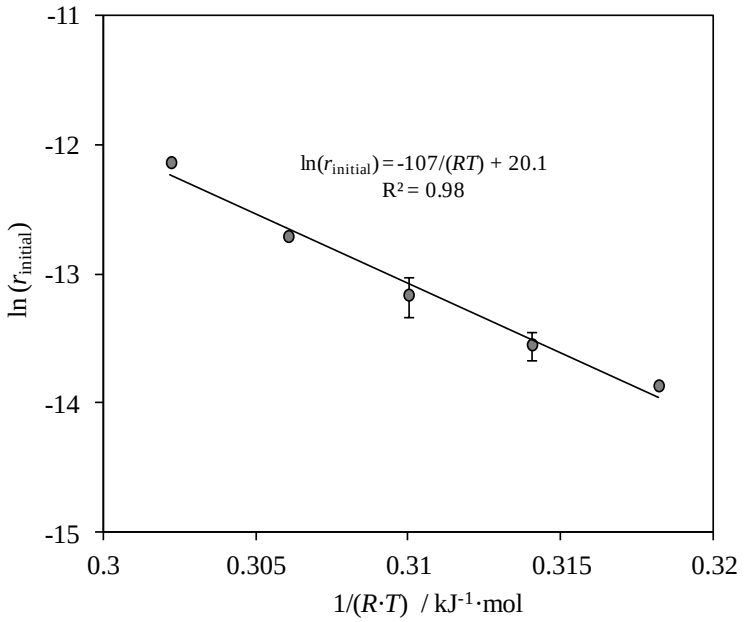

Figure 4.7: Arrhenius plot: logarithm of initial reaction rate as function of the inverse of temperature.

Table 4.5: Kinetic parameters optimized from the kinetic experiments.

Model	E_a / kJ·mol^{-1}	Error %	k_0×10^{11}/ mol·Pa^{-3}·g^{-1}·min^{-1}	Error %	$K_{ads,1}$×10^3	Error %	$K_{ads,2}$×10^3	Error %	Overall deviation
Mechanism 1	106	1	0.463	2	23	2	60	22	17%
Mechanism 2	117	1	1.94	3	1.2	3	-	-	17%
Mechanism 1: Fugacity	101	1	0.3	33	1.7	33	190	15	16%

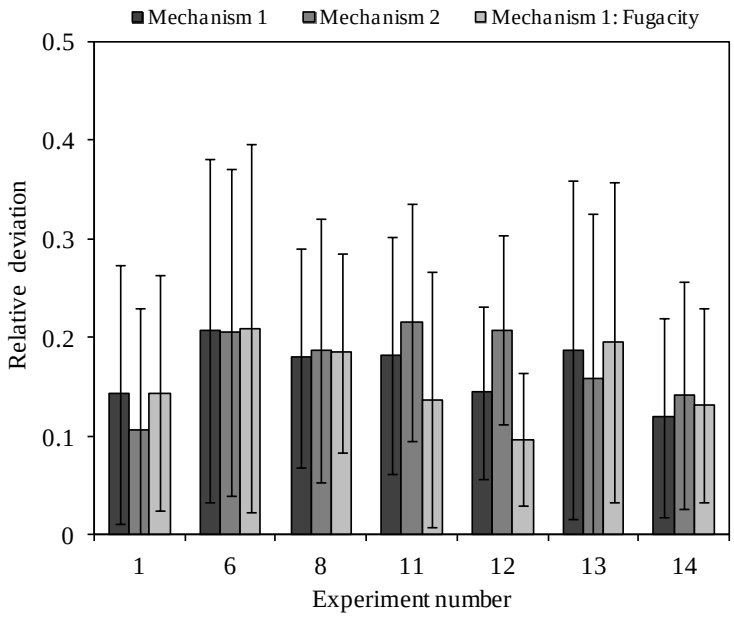

Figure 4.8: Average deviation from the experimental data for each experiment.

4.6. Simulation

Herein are presented the main simulation results for the kinetic modelling at high pressure conditions. In Figure 4.9 is presented the evolution of DMC molar fraction along the time at three different temperatures. It can be observed from the graph a good fitting for the experimental data, with exception of the last point for 388 K. The major drawback in the experiments is the estimation of the initial amount of water that is predicted based on the final amounts of water and DMC, since there is some water present on the walls of the tubes and vessel that are mixed with the stream of MeOH and carbon dioxide. Thus, this uncertainty may lead to relative high deviations for the equilibrium, which also explains some deviations observed on the equilibrium prediction. However, this has almost no effect on the initial reaction rate as predicted from the model.

In Figure 4.10 is represented the DMC molar fraction as function of the time at the same conditions for 4 different carbon dioxide to MeOH molar ratios. These results are the most important to validate the reaction rate expression, while the variation of temperature is mainly useful for the determination of the activation energy almost independently of the reaction rate expression. In all graphs, the model shows a good fitting to the experimental data. It is important to mention that the initial water content is different for each run (see Table 4.1), which affects the DMC molar fraction at equilibrium conditions.

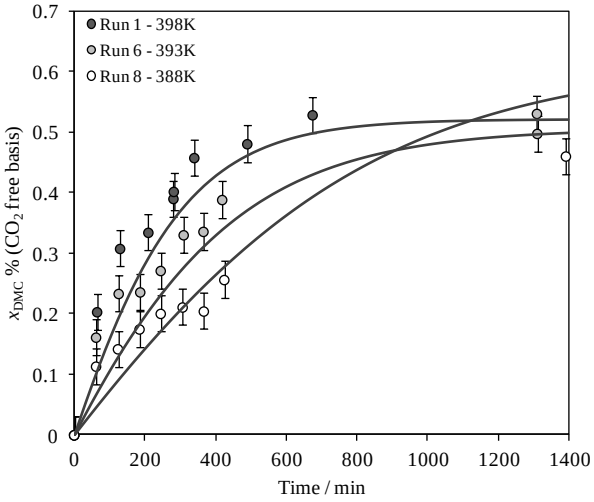

Figure 4.9: Experimental DMC molar fraction along the time at different temperatures.

Reaction conditions: 20 MPa, 200 rpm, ~4.6 g CeO_2, n_{CO_2}/n_{MeOH}: ~2.6/1.

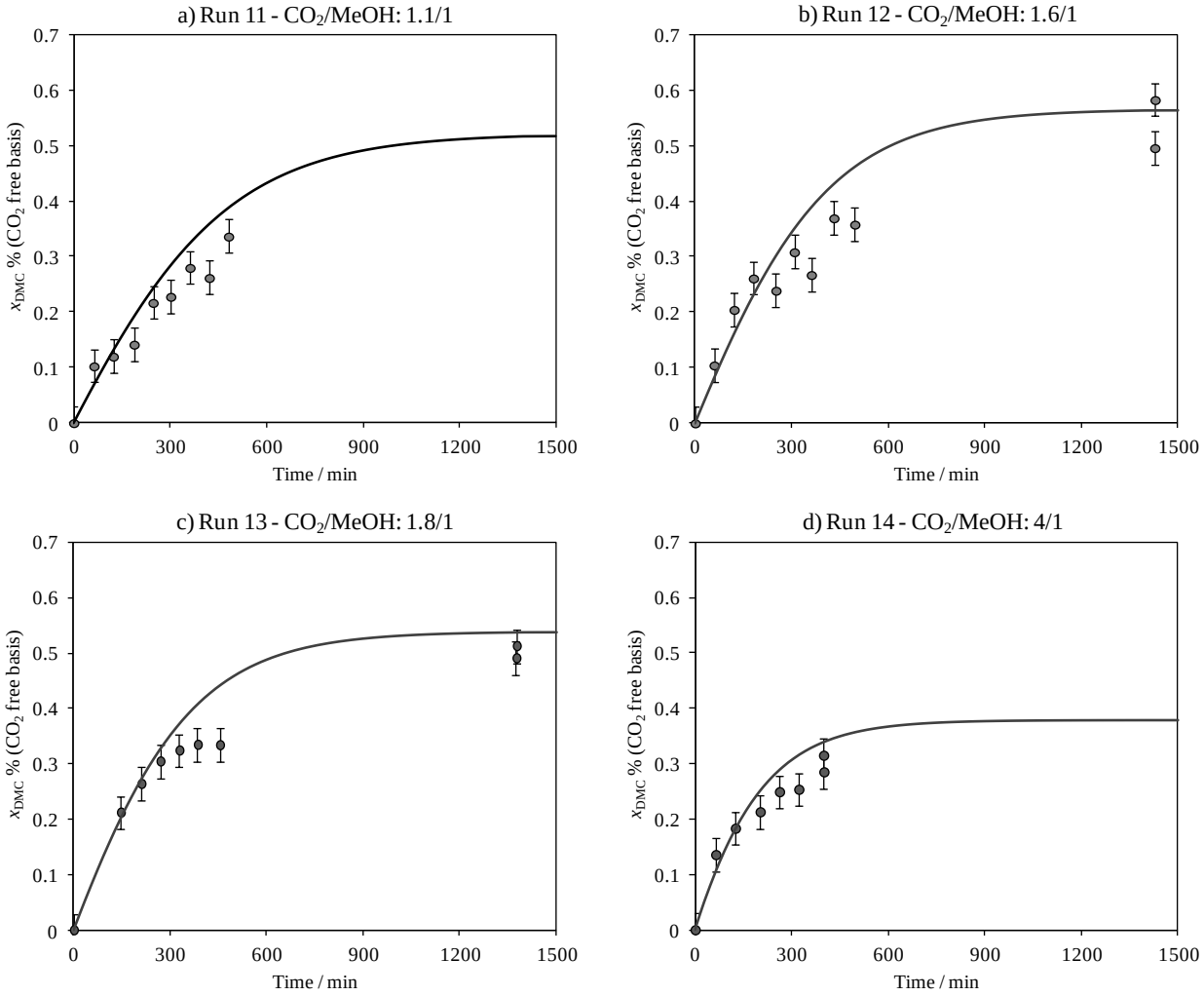

Figure 4.10: Experimental DMC molar fraction along the time at different n_{CO_2}/n_{MeOH}.

Reaction conditions: 20 MPa, 398 K, 200 rpm, ~4.6 g CeO2.

The reaction rate is also affected by the pressure since it affects the equilibrium yield or by changing the partial pressure of each compound (Equations 4.4 and 4.5). However, the pressure also affects the kinetic constant. The activation volume ($\Delta v^{\#}$) is the physical parameter that describes this effect, similarly to the activation energy on the temperature effect [24]:

$$k = k_0 \cdot e^{-\frac{E_a}{R \cdot T}} \cdot e^{-\frac{\Delta v^{\#} \cdot (P - P_{ref})}{R \cdot T}} \tag{4.9}$$

The activation volume of -0.4±0.2 $dm^3 \cdot mol^{-1}$ was adjusted from our experimental data (Runs 1, 16, and17) using the same objective function; the reference pressure (P_{ref}) was set at 20 MPa. In Figure 4.11 are represented the experimental and the predicted DMC molar fractions along the time for three different pressures.

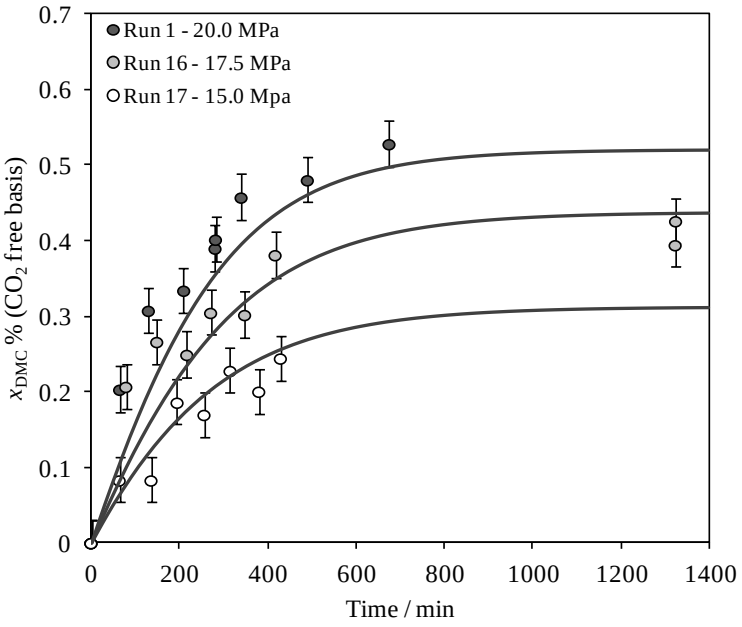

Figure 4.11: Experimental DMC molar fraction along the time at different pressures.
Reaction conditions: 398 K, 200 rpm, ~4.6 g CeO_2, $\boldsymbol{n_{CO_2}/n_{MeOH}}$: ~2.5/1.

4.7. Conclusions

In this chapter the kinetics for the direct synthesis of DMC over cerium oxide was investigated under high pressure conditions. The reaction experiments performed showed high reproducibility and were conducted under conditions that guarantee negligible external mass transfer resistances.

The kinetic and equilibrium experiments were better modelled as ideal gas than considering real gas behaviour, using the SRK/mHV2 thermodynamic model (developed in Chapter 3), probably due to the difficulty to predict the fugacity above the critical point. Furthermore, a standard enthalpy, a Gibbs free

energy, and an entropy change of reaction were adjusted from reaction equilibrium data: -20±2 kJ·mol^{-1}, 31±1 kJ·mol^{-1}, and -174±8 J·K^{-1}·mol^{-1}, respectively.

The reaction rate model based on Langmuir-Hinshelwood mechanism showed similar deviations compared to the model based on Eley-Rideal mechanism. An activation energy of 107 kJ·mol^{-1} was estimated from the initial reaction rate for the direct synthesis of DMC over cerium oxide, which is in accordance with the value fitted for the model based on the Langmuir- Hinshelwood mechanism (106 kJ·mol^{-1}).

Finally, the effect of pressure on the reaction rate revealed an activation volume equal to -0.4±0.2 dm^3·mol^{-1} (also adjusted from the experimental data).

4.8. Nomenclature

Symbols

$\Delta_r C_p^o$	Heat capacity change of reaction (J·mol^{-1}·K^{-1})
E_a	Activation energy (J·mol^{-1})
f_i^o	Standard fugacity of pure species *i* (Pa)
$\widehat{f_i}$	Fugacity of species *i* in the mixture (Pa)
F_{Obj}	Objective function
$\Delta_r G^o$	Standard Gibbs free energy change of reaction (J·mol^{-1})
$\Delta_r H^o$	Standard Enthalpy change of reaction (J·mol^{-1})
k	Kinetic constant (mol·Pa^{-3}·g^{-1}·s^{-1})
k_0	Pre-exponential factor of kinetic constant (mol·Pa^{-3}·g^{-1}·s^{-1})
K_{ads}	Adsorption equilibrium constant over cerium oxide
K_{eq}	Reaction Equilibrium constant
$\vartheta_{Lim.}$	Stoichiometric coefficient of the limiting reactant
m_{cat}	Catalyst mass (g)
$n_{Lim.}$	Molar amount of the limiting reactant (mol)
P, P_{ref}, P^o, P_i	Absolute, reference, standard, and partial pressure of species *i* (Pa)
$\hat{\varphi}_i$	Fugacity coefficient of species *i*
r	Reaction rate (mol·g^{-1}·s^{-1})
R	Ideal gas constant (J·mol^{-1}·K^{-1})

t	Time (min)
T	Temperature (K)
$\Delta v^{\#}$	Activation volume ($m^3 \cdot mol^{-1}$)
x	Molar fraction
X_c	Molar reaction conversion

Abbreviations

DMC	Dimethyl carbonate
MeOH	Methanol
mHV2	Modified Huron-Vidal second order mixing rule
MC	Methyl carbonate
NC	Number of compounds
NP	Number of points
SEM	Scanning Electron Microscope
SRK	Soave-Redlich-Kwong equation of state

4.9. References

[1] Monteiro, J. G. M. S.,De Queiroz Fernandes Araújo, O.,De Medeiros, J. L. Sustainability Metrics For Eco-Technologies Assessment, Part I: Preliminary Screening. *Clean Technologies and Environmental Policy* **2009,** *11*(2), 209.

[2] Sakakura, T.,Choi, J.,Saito, Y.,Masuda, T.,Sako, T.,Oriyama, T. Metal-Catalyzed Dimethyl Carbonate Synthesis From Carbon Dioxide And Acetals. *Journal of Organic Chemistry* **1999,** *64*(12), 4506.

[3] Choi, J.,Kohno, K.,Ohshima, Y.,Yasuda, H.,Sakakura, T. Tin- Or Titanium-Catalyzed Dimethyl Carbonate Synthesis From Carbon Dioxide And Methanol: Large Promotion By A Small Amount Of Triflate Salts. *Catalysis Communications* **2008,** *9*(7), 1630.

[4] Hong, S.,Park, H.,Lim, J.,Lee, Y.,Anpo, M.,Kim, J. Synthesis Of Dimethyl Carbonate From Methanol And Supercritical Carbon Dioxide. *Research on Chemical Intermediates* **2006,** *32*(8), 737.

[5] Kohno, K.,Choi, J. C.,Ohshima, Y.,Yasuda, H.,Sakakura, T. Synthesis Of Dimethyl Carbonate From Carbon Dioxide Catalyzed By Titanium Alkoxides With Polyether-Type Ligands. *ChemSusChem* **2008,** *1*(3), 186.

[6] Tomishige, K.,Kunimori, K. Catalytic And Direct Synthesis Of Dimethyl Carbonate Starting From Carbon Dioxide Using CeO2-ZrO2 Solid Solution Heterogeneous Catalyst: Effect Of H2O Removal From The Reaction System. *Applied Catalysis A: General* **2002,** *237*(1-2), 103.

[7] Fan, B.,Li, H.,Fan, W.,Zhang, J.,Li, R. Organotin Compounds Immobilized On Mesoporous Silicas As Heterogeneous Catalysts For Direct Synthesis Of Dimethyl Carbonate From Methanol And Carbon Dioxide. *Applied Catalysis A: General* **2009,** *372*(1), 94.

[8] Sakakura, T.,Saito, Y.,Okano, M.,Choi, J.,Sako, T. Selective Conversion Of Carbon Dioxide To Dimethyl Carbonate By Molecular Catalysis. *Journal of Organic Chemistry* **1998,** *63*(20), 7095.

[9] Honda, M.,Kuno, S.,Begum, N.,Fujimoto, K. I.,Suzuki, K.,Nakagawa, Y.,Tomishige, K. Catalytic Synthesis Of Dialkyl Carbonate From Low Pressure CO2 And Alcohols Combined With Acetonitrile Hydration Catalyzed By CeO2. *Applied Catalysis A: General* **2010,** *384*(1-2), 165.

[10] Honda, M.,Suzuki, A.,Noorjahan, B.,Fujimoto, K. I.,Suzuki, K.,Tomishige, K. Low Pressure CO2 To Dimethyl Carbonate By The Reaction With Methanol Promoted By Acetonitrile Hydration. *Chemical Communications* **2009,** (30), 4596.

[11] Eta, V.,Mäki-Arvela, P.,Leino, A.-R.,Kordás, K.,Salmi, T.,Murzin, D.,Mikkola, J.-P. Synthesis Of Dimethyl Carbonate From Methanol And Carbon Dioxide: Circumventing Thermodynamic Limitations. *Industrial & Engineering Chemistry Research* **2010,** *49*(20), 9609.

[12] Eta, V.,Mäki-Arvela, P.,Salminen, E.,Salmi, T.,Murzin, D. Y.,Mikkola, J. P. The Effect Of Alkoxide Ionic Liquids On The Synthesis Of Dimethyl Carbonate From CO2 And Methanol Over ZrO2-MgO. *Catalysis Letters* **2011,** *141*(9), 1254.

[13] Ballivet-Tkatchenko, D.,dos Santos, J. H. Z.,Philippot, K.,Vasireddy, S. Carbon Dioxide Conversion To Dimethyl Carbonate: The Effect Of Silica As Support For SnO2 And ZrO2 Catalysts. *Comptes Rendus Chimie* **2010,** *14*(7-8), 780.

[14] Honda, M.,Kuno, S.,Sonehara, S.,Fujimoto, K.-i.,Suzuki, K.,Nakagawa, Y.,Tomishige, K. Tandem Carboxylation-Hydration Reaction System From Methanol, CO2 And Benzonitrile To Dimethyl Carbonate And Benzamide Catalyzed By CeO2. *ChemCatChem* **2011,** *3*(2), 365.

[15] Honda, M.,Tamura, M.,Nakagawa, Y.,Sonehara, S.,Suzuki, K.,Fujimoto, K. I.,Tomishige, K. Ceria-Catalyzed Conversion Of Carbon Dioxide Into Dimethyl Carbonate With 2-Cyanopyridine. *ChemSusChem* **2013,** *6*(8), 1341.

[16] Lee, H. J.,Park, S.,Jung, J. C.,Song, I. K. Direct Synthesis Of Dimethyl Carbonate From Methanol And Carbon Dioxide Over H3PW12O40/CexZr(1-X)O2 Catalysts: Effect Of Acidity Of The Catalysts. *Korean Journal of Chemical Engineering* **2011,** *28*(7), 1518.

[17] Lee, H. J.,Park, S.,Song, I. K.,Jung, J. C. Direct Synthesis Of Dimethyl Carbonate From Methanol And Carbon Dioxide Over Ga2O3/Ce0.6Zr0.4O2 Catalysts: Effect Of Acidity And Basicity Of The Catalysts. *Catalysis Letters* **2011,** *141*(4), 1.

[18] Tomishige, K.,Sakaihori, T.,Ikeda, Y.,Fujimoto, K. A Novel Method Of Direct Synthesis Of Dimethyl Carbonate From Methanol And Carbon Dioxide Catalyzed By Zirconia. *Catalysis Letters* **1999,** *58*(4), 225.

[19] Yoshida, Y.,Arai, Y.,Kado, S.,Kunimori, K.,Tomishige, K. Direct Synthesis Of Organic Carbonates From The Reaction Of CO2 With Methanol And Ethanol Over CeO2 Catalysts. *Catalysis Today* **2006,** *115*(1-4), 95.

[20] Smith, J. M.,Ness, H. C. V.,Abbott, M. M. *Introduction To Chemical Engineering Thermodynamics*; 6th ed.; McGraw-Hill: New York, **2005**.

[21] Hofmann, H. J.,Brandner, A.,Claus, P. CO2-Folgechemie: Direktsynthese Von Dimethylcarbonat Durch Carboxylierung Von Methanol An Cer-Basierten Mischoxiden

CO2 Subsequent Chemistry: Direct Synthesis Of Dimethyl Carbonate By Carboxylation Of Methanol With Cerium-Based Mixed Oxides. *Chemie Ingenieur Technik* **2011,** *83*(10), 1711.

[22] Figueiredo, J. L.,Ribeiro, F. R.,Orfão, J. J. M.,Lemos, F.,Guisnet, M. *Catálise Heterogénea*; 2ª ed. rev. e actualizada ed.; Fundação Calouste Gulbenkian. Serviço de Educação e Bolsas: Lisboa, **2007**.

[23] Eta, V.,Mäki-Arvela, P.,Wärnå, J.,Salmi, T.,Mikkola, J. P.,Murzin, D. Y. Kinetics Of Dimethyl Carbonate Synthesis From Methanol And Carbon Dioxide Over ZrO2-MgO Catalyst In The Presence Of Butylene Oxide As Additive. *Applied Catalysis A: General* **2011,** *404*(1-2), 39.

[24] Vetter, A. B. G. *High Pressure Process Technology: Fundamentals And Applications*; First ed.; Elsevier Science B.V.: Amsterdam, **2001**; Vol. 9.

Chapter 5. Adsorption of Water and DMC over Zeolite 3A in Fixed Bed Column at High Pressure Conditions

"Rien ne se perd, rien ne se crée, tout se transforme." – Antoine Lavoisier

This chapter is based on the following article: Santos, B., Silva, V., Loureiro, J., Rodrigues, A. Adsorption Of H2O And Dimethyl Carbonate At High Pressure Over Zeolite 3A In Fixed Bed Column. *Industrial & Engineering Chemistry Research* **2014,** *53*(6), 2473.

5.1. Introduction

In Chapter 2 was discussed the thermodynamic limitation of the synthesis of DMC from MeOH and carbon dioxide. The water removal *in situ* from the reaction mixture was pointed as a key solution for the direct synthesis of DMC. The main efforts done to overcome this challenge were on the search of more efficient dehydrating chemicals [1-14], which led to successful results. Recently, Honda et al. reached a high DMC yield of 94% with 96% selectivity by adding 2-cyanopyridine to react with the water produced by reaction. Besides the great achievements reached, the addition of dehydrating agents leads to a loss of selectivity and will add another reaction step for the regeneration of the dehydrating agent. Therefore, the use of molecular sieves, proposed by Choi et al. [3], is an interesting alternative since it avoids the formation of more species keeping the high selectivity. By using an external loop to remove the water from the batch reaction system the authors reached a DMC yield around 40%. These results show a huge potential of this methodology to design a novel continuous process for direct DMC synthesis, which could be more environmentally friendly.

However, there is a lack of adsorption data for water in carbon dioxide and MeOH solutions. The dehydration of ethanol is the most similar process to compare with; and since carbon dioxide is a non-polar molecule with low interaction forces with polar adsorbents used to catch the water, it is probably acceptable to assume that most of the adsorbents with high efficiency, for dehydration of alcohols, will also be efficient for our reaction system. The separation of ethanol and water is one of the most studied binary systems; this system shows an azeotropic point at 95 *wt.*% of ethanol (101 kPa). Several processes can be used to purify ethanol, such as extractive distillation or, pervaporation or adsorption processes. The last one has been providing evidence of sustainability for ethanol dehydration. In 1983 it was patented the first continuous process using 3A molecular sieves to remove water from ethanol vapour (>80 *wt.*% EtOH around 363 K) [15]. The adsorption temperature should be around 10 K higher than the boiling point of the mixture in order to avoid condensation in the solid bed. Afterwards, several studies have been developed in order to improve this separation, using different absorbents, from zeolites to natural starchy materials, or new processes, from batch to pressure swing adsorption, either in vapour or liquid phase [16-29].

The state of the art for ethanol dehydration, through adsorption, is summarized in Table 5.1; most of the works were performed in vapour phase, but there also are few studies in liquid phase. Molecular sieves (zeolites), especially 3A molecular sieves, aluminosilicate also referred as zeolite LTA-K or zeolite 3A, show high selectivity towards water uptake for ethanol dehydration. Nevertheless, there has been an increase of researching on bio-adsorbents, in order to compete with these synthesized materials. In particular, some starch-based materials have high water capacity, in some cases similar to 3A molecular sieves, with even higher selectivity [24]. In addition, starch-based materials can be regenerated at lower temperatures (353 K) compared with 3A molecular sieves (around 473 K) [19], but most of them begin to disaggregate at water content above 10% (volume). Cellulose and hemi-cellulose have also shown high affinity to water [19, 22-24]. Nevertheless, in spite of the high potential of starch-based adsorbent, commercial molecular sieves are still

very important since they are a reliable material and show high selectivity to water, excellent reproducibility and high mechanical stability.

Moreover, the same type of adsorbent material was used for dehydration of other similar systems: benzyl alcohol/water (4A, 5A) [30], isopropanol/water (3A, 4A, Palm stone) [31], cyclohexane/water (3A, 13X) [32], carbon dioxide/water (3A, AW500, Coal) [33-35], or adsorption of pure water vapour (Activated carbon) [36]. In conclusion, these works reinforce the initial idea that the adsorbents for ethanol dehydration might also be applied for adsorption of water in carbon dioxide and methanol streams. The objective of this chapter is to experimentally determine the equilibrium isotherms of DMC and water in carbon dioxide/MeOH medium over 3A molecular sieves (zeolite 3A) at high pressure conditions, as well as the enthalpy and entropy change of adsorption of each compound, which is essential to develop the SMBR model afterwards. Moreover, the hydrodynamics and the mass transfer kinetics in fixed bed column will be studied at the same conditions. Then, a mathematical model will be proposed in order to fit the dynamic behaviour of a pulse response.

5.2. Experimental Procedure

5.2.1. Chemicals

In order to perform the experiments, the following chemical compounds were purchased and used without further treatment: dimethyl carbonate at 99% from Sigma-Aldrich® (Ref. D152927), vanillin at 99% from Sigma-Aldrich® (Ref. V1104), and carbon dioxide at 99.995% from Linde®; carbon dioxide was supplied in pressurized bottle with a siphon in order to guarantee the supply of liquid carbon dioxide to the HPLC pump. Water was deionised in our laboratories; anhydrous methanol at 99.9% from Acros Organics® (Ref. 50-344-214) was filtrated at vacuum and degasified in an ultrasound bath during 30 min in order to be used in the HPLC pump. The 3A molecular sieve (beads, 8-12 mesh) was purchased from Sigma-Aldrich® (Ref. 208582); moreover, the zeolite was first activated, at 583 K during 24 hours with a temperature ramp of 1 $K \cdot min^{-1}$, in order to remove some water or other volatile contaminations that could be present on the zeolite.

5.2.2. Set-up

A supercritical fluid chromatograph (SFC), from Thar®, was used to carry out the experiments and reach the objective proposed. In brief, the SFC is composed by: two delivery pumps (for the carbon dioxide and the co-solvent), a column oven (where the column is kept at the settled temperature), an automated back pressure regulator (ABPR) (to maintain the desired pressure in the column), an auto sampler module (for injection of sample), and a collector module (for semi-preparative mode). Moreover, for analytical applications, the set-up is equipped with two detectors: UV spectrophotometer (2998 Photodiode Array Detector, Waters®) and an Evaporative Light Scattering Detector (2424 ELSD Water®). The adsorption experiments were carried out in a fixed bed column filled with Zeolite 3A. Figure 5.1 displays a photography of the set-up and another of the column (inside the oven); the specifications of the fixed bed column are summarized in Table 5.2.

Table 5.1: State of the art for ethanol dehydration through adsorption processes.

Process	Adsorbents	Conditions	Capacity*/ $g_{H2O} \cdot g^{-1}$	EtOH Purity* *wt.*%	Year	Ref.
Adsorptive distillation	Zeolite 3A	Vapour	-	99.9	1987	[16]
Equilibrium isotherms	Zeolites Na-ZSM5	Vapour; 293 K; 99-100 *wt.*% H_2O	0.042	-	1989	[17]
Adsorptive distillation	Zeolite 4A	Vapour; 10 *wt.*% H_2O	-	>98	1999	[18]
Capacity screening	Zeolite 3A; silica gel; synthesized starch; corn grits	Liquid; 303 K; 1-20 *wt.*% H_2O	0.11	-	2001	[19]
Adsorptive distillation	Zeolite 3A; Zeolite 4A; Zeolite 5A; palm stone; corncobs; oak	Vapour; 356 K; 5-12 *wt.* % H_2O	0.12-0.23	>99	2004	[20]
Adsorptive distillation	Phillipsite\$CaCl_2$	Vapour; 5 *wt.*% H_2O	0.1	>99	2009	[21]
Adsorptive distillation	Corn, elephant ear and cassava starch; sugar cane bagasse	Vapour; 8 *wt.*% H_2O	0.19	99.5	2009	[22]
Equilibrium isotherms	Natural clinoptilolite	Liquid; 293 K	0.16	-	2009	[23]
Equilibrium isotherms	Zeolite 3A; potato, corn and cassava starch; cellulose	Vapour; pure compounds; 297 K	0.16	-	2010	[24]
Fixed bed adsorption	Cassava starch	Vapour; 353-373 K; 6 *wt.*% H_2O,	0.016	>99.5	2011	[25]
Adsorption kinetic	Cassava: starch, pellet and shred; modified starch.	Liquid; 301 K; 10 *wt.*% H_2O	0.0004	-	2011	[26]
Pressure Swing Adsorption	Canola meal	Vapour; 358 K; 8 *wt.*% H_2O	0.025	>99	2012	[27]
Equilibrium isotherms	Zeolites: LTA-K; LTA-Na; LTA-Ca; FAU-Na	Vapour; 298 K; 90 kPa	0.25	-	2012	[28]
Pressure Swing Adsorption	Canola meal	Vapour; 373 K; 200 kPa; 5 *wt.*% H_2O	0.026	>99	2013	[29]

*These results correspond to the underlined adsorbents, which showed higher water capacity

a)

b)

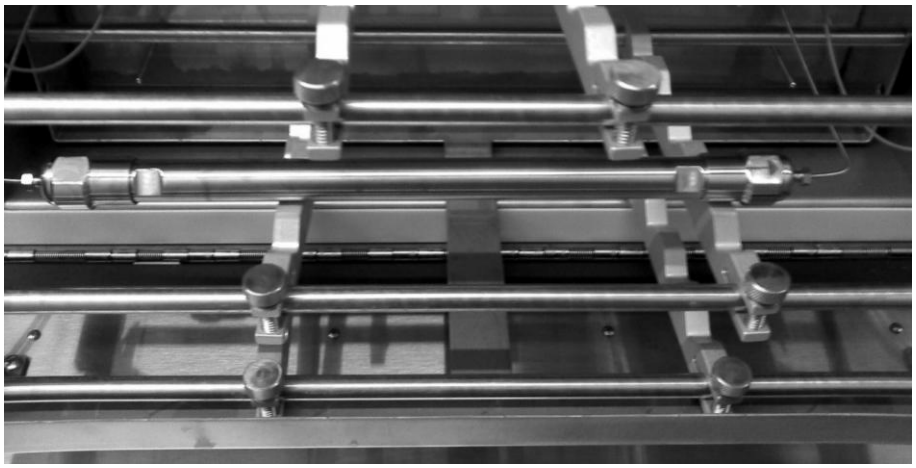

Figure 5.1: Photography of: a) SFC Thar® Unit; b) fixed bed column.

Table 5.2: Specification of fixed bed column.

Properties	Value
Inner diameter / cm	1
Average Particle diameter / mm	2
Length / cm	25
Volume / mL	19.6
Porosity	0.43
Weight of zeolite / g	13.36

The system has the versatility to operate in analytic or semi-preparative mode. In the analytic mode, the sample is injected, carried with the eluent through the column, measured in the detector, recorded and finally it

follows for the residues container. When operating in semi-preparative mode, instead of being wasted, the sample is recovered in a solvent after depressurization (to avoid loss of sample by evaporation), in the collector vessels (up to 6), during the run at different times.

Other important feature is the injection modes of the sample, which are classified as: full-loop mode, partial-loop mode, and μL-mode. In the first one, full loop mode, the sample is pushed by a syringe and it completely fills the loop; an excess of sample is wasted in order to guarantee that the loop is full. The partial-loop mode allows settling the volume of sample (less than the loop volume); the remainder volume is filled by air. In its turn, in μL-loop mode, the remainder is filled by the cleaning solvent, which is usually the same used as co-solvent. The selection of the injection mode, as well as the operating mode – analytic or semi preparative – should be defined according to the requirements of each application.

For this work the analytic mode was used to perform the experiments. In Figure 5.2 is depicted a simple scheme of the equipment in analytic mode; the main specifications of each module are described below:

- Fluid Delivery Module:

  Two HPLC pumps: carbon dioxide and co-solvent

  Carbon dioxide flow: 0.1-10 $g \cdot min^{-1}$ (±0.1 $g \cdot min^{-1}$)

  Co-solvent flow: 0.01-10 $mL \cdot min^{-1}$ (±0.01 $mL \cdot min^{-1}$)

  Co-solvent fraction: 0-100%

  Up to 6 co-solvents

- Endurance Auto Sampler:

  Plate: 48 vials

  Loop volume: 5-200 μL

- Column Oven:

  Up to 6 columns

  Range: 278-363 K (±0.1 K)

- ELSD:

  Light source: LED 480 nm

  Detector: Photomultiplier tube

- UV spectrophotometer:

  UV Lamp: Deuterium

  Range: 190-400 nm (±1.0 nm)

  Max. Pressure: 40 MPa

❖ ABPR:

Pressure control: 0.5-40 MPa

Minimum 0.3 MPa of pressure drop

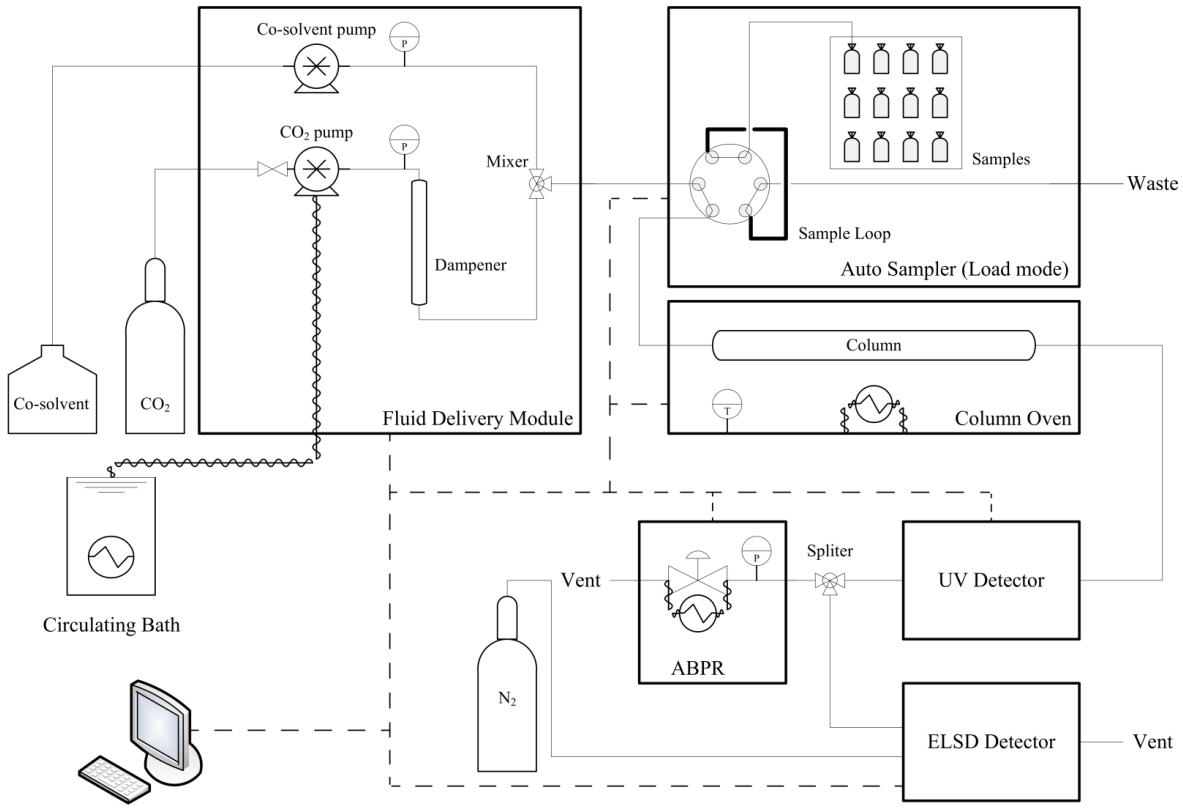

Figure 5.2: Simplified diagram flow for the experimental set-up SFC Thar® in analytic mode.

5.2.3. Methodology

The main goal of this chapter is to study the adsorption of DMC and water over the zeolite 3A at high pressure conditions using MeOH and carbon dioxide as eluent. Adsorption batch experiments are not easy to perform in supercritical state for several reasons: sampling promotes depressurization and might lead to small deviations of the overall concentration; if the differences of concentrations, from initial to equilibrium state, are small comparing to the quantification method, it may lead to drastic errors in adsorption amount by mass balance calculation; it is often difficult to guarantee that the equilibrium was reached.

Therefore, the equilibrium isotherms were measured by analysis of the pulse responses from the injection of small pulses (100-200 µL) of water and DMC in a fixed bed column filled with zeolite 3A. The use of small pulses instead of large pulses is due to equipment limitations since no large amount of water should be injected in the presence of liquid/supercritical carbon dioxide; the depressurization lead to very low temperature that could freeze the water (not soluble in carbon dioxide) and damage the automatic back pressure regulator valve.

During the experiments, the detector signal of the outlet stream (proportional to the solute concentration) was recorded along the time, allowing the calculation of the retention time (first moment of the chromatographic peak); afterwards, the retention time is used to compute the slope of the adsorption equilibrium isotherm.

The main drawback of this methodology is the fact that the slope of the adsorption equilibrium isotherm is measured indirectly from the retention time of the dynamic pulse response, which can be slightly affected by several variables, such as temperature, flow, etc. Besides, a narrow concentration range will be covered due to the small injected volume. Considering the complexity of these issues, a convenient model should be adopted. For the equilibrium adsorption, a linear isotherm seems to be more appropriate since pulse response experiments were conducted at diluted concentration of the solute and then the slope of the adsorption equilibrium isotherm can be calculated from the retention time, independently of other phenomena. Moreover, the shape of a pulse response curve allows quantifying the dispersive phenomena: mass transfer and the hydrodynamics in the fixed bed column.

The experiments – injection of pulses of DMC and water – were carried out in a stainless steel column, previously described, at 20 MPa; a mixture of MeOH and carbon dioxide (with 40 % (*v/v*)) was used as solvent at a flow rate of 10-12 $mL \cdot min^{-1}$; different temperatures were achieved, 313 K, 333 K and 353 K, in order to determine the enthalpy and entropy change of adsorption. Also, three different volumes were used (100 μL, 150 μL, and 200 μL), in order to study the effect of concentration.

In addition, to develop a mathematical model to describe the hydrodynamics and distinguish the effect of hydrodynamics and mass transfer resistance on the curve dispersion, tracer experiments were carried out. In order to assess the hydrodynamics, tracer experiments were conducted in the same conditions for water and DMC pulse injections. Thus, an equal column (L = 25 cm; D = 1 cm), filled with non-porous glass particles (spherical) with a diameter of 2 mm (similar to the zeolite beads) was used. Vanillin (~1 mg/L in MeOH) was chosen as tracer since it is easily detected by the UV detector with a linear response between 50 μL and 200 μL. The linear relation, between the UV peak area – with wavelength of 254 nm and a resolution of 1.2 nm – and the volume of Vanillin (solution), is depicted in Figure 5.3.

In addition, DMC was analyzed by UV detector, with a resolution of 1.2 nm and a wavelength of 210 nm, while water was analyzed by ELSD, since UV detector has low sensitivity for water. ELSD was used, in order to quantify the amount of water, with the following operating conditions: drift tube temperature of 323 K, nitrogen as nebulizer gas at 275 kPa. During depressurization, carbon dioxide vaporizes and small drops of water are formed due to the low temperatures induced by carbon dioxide depressurization which avoid water to vaporize completely. These drops scatter the light and the intensity received in the detector falls down creating a signal function of the number of particles and falsifying the measured concentration. Although ELSD is mostly used for low volatile solutes, such as sugars, a linear response between peak areas and injected volumes was obtained for water; however, as expected, the signal shows a low intensity and some noise, which were minimized by further smoothing techniques.

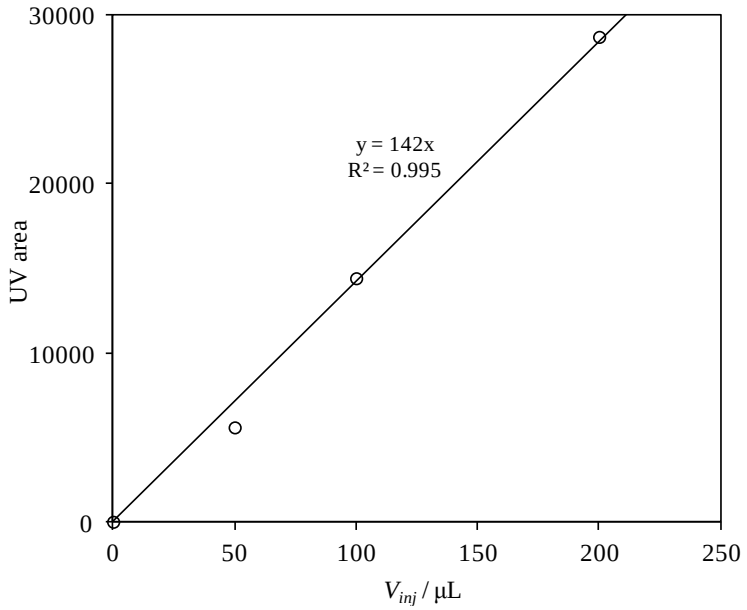

Figure 5.3: UV peak area (254 nm) versus injected volume of Vanillin solution (~1 mg/L in MeOH); Operating conditions: Glass column, 20 MPa, 353 K; reference flow of 10 mL·min^{-1}, CO_2/MeOH (40% MeOH (*v/v*)), and µL-loop mode injection.

The linear responses obtained for water and DMC are depicted in Figure 5.4 and 5.5, respectively. In both graphs are shown relative small deviations from the linear tendency. For DMC, these deviations are probably caused by some inaccuracy of the partial-loop injection mode, and not because of any lack of linearity of the detector, which shows very reproducible results with a perfect linear tendency when the µL-loop mode is used. However, the deviations observed for water are not just caused by the same phenomenon, but also due to the low water sensitivity of ELSD.

As explained earlier, the partial loop avoids the injection of eluent by pushing air into the sampling loop; although, for large loops (e.g., 200 µL) there is some compression of air when pushing the sample that leads to an inaccurate sampling. In consequence, the amount of sample is slightly lower than the settled. Nevertheless, since a linear adsorption isotherm is assumed, due to the low concentrations involved, the injection amount should not have any effect on the retention time.

5.2.4. Adsorbent characterization

The zeolite 3A ($K_nNa_{12-n}[(AlO_2)_{12}(SiO_2)_{12}]$) used for the experiments was purchased from Sigma-Aldrich with spherical shape (diameter 1.68-2.38 mm). The macro and meso porosities were assessed by Hg porosimetry and He pycnometry, in order to determine the particle porosity and density. The adsorption of N_2 at 77 K was accomplished; however, the information about the microporous structure is not reliable, since the unit cell access windows have an average diameter of 3 Å, which represents an obstacle for N_2 molecule since its kinetic diameter is 3.64 Å. In fact, a microporous area of 4.5 $m^2 \cdot g^{-1}$ was measured by N_2 adsorption, which is much less than expected. Nevertheless, the results from N_2 adsorption were useful to assess the surface area

of the mesopores (22 $m^2 \cdot g^{-1}$) and validate the results obtained from Hg porosimetry (21 $m^2 \cdot g^{-1}$), for meso and macro pores.

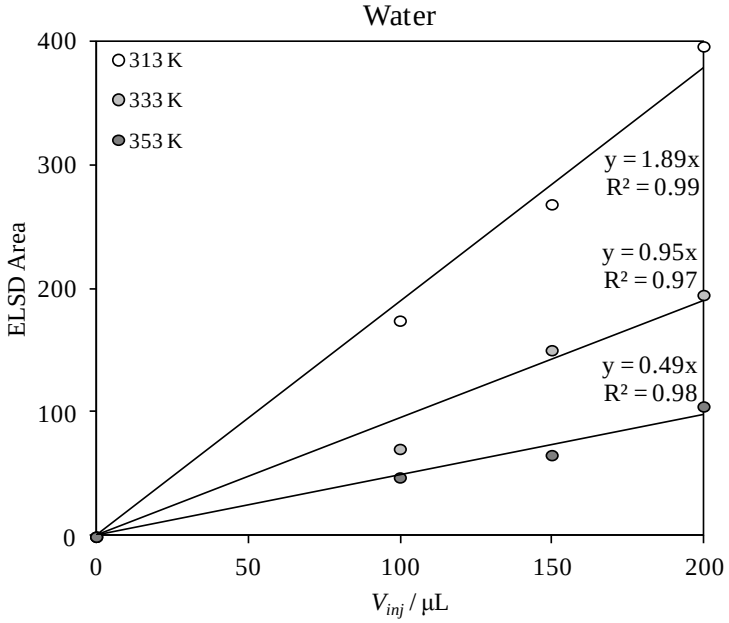

Figure 5.4: ELSD peak area as function of the volume injected at different temperatures; operating conditions: zeolite 3A column, 20 MPa, reference flow of 10 $mL \cdot min^{-1}$, CO_2/MeOH (40% MeOH (*v/v*)), and partial-loop injection mode.

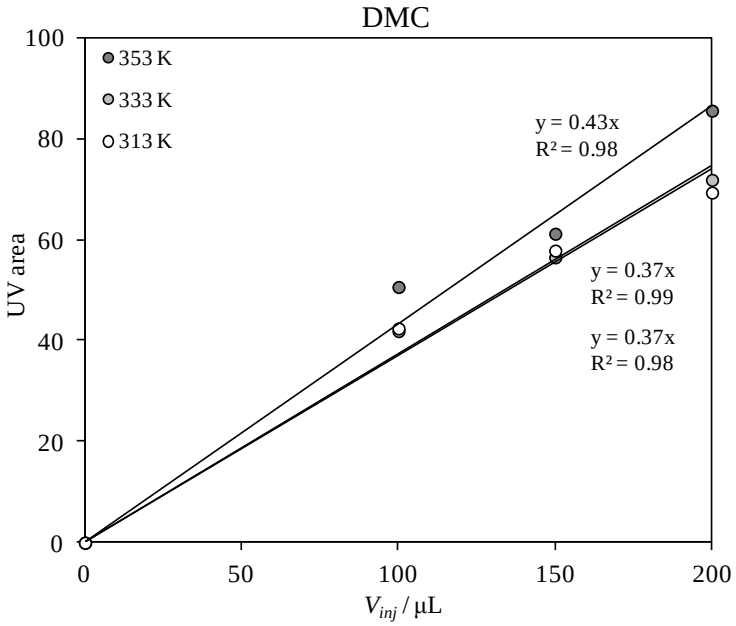

Figure 5.5: UV peak area (210 nm) as function of the volume injected at different temperatures; operating conditions: zeolite 3A column, 20 MPa, reference flow of 10 $mL \cdot min^{-1}$, CO_2/MeOH (40% MeOH (*v/v*)), and partial-loop injection mode.

The zeolite was, after milled, analysed by X-ray diffractometry (Cu Kα) – XRD PANalytical X'Pert Pro and detector X´Celerator – in order to determine its crystal structure. The XRD pattern for the zeolite powder is shown in Figure 5.6. The peaks positions are consistent with standard Linde Type A (LTA) cubic structure; the lattice parameter, a of 24.60 Å, and the average crystallite size of 100 nm were predicted from the Reitveld refinement (PowderCell 2.3). Moreover, some traces of quartz were also detected from the XRD pattern.

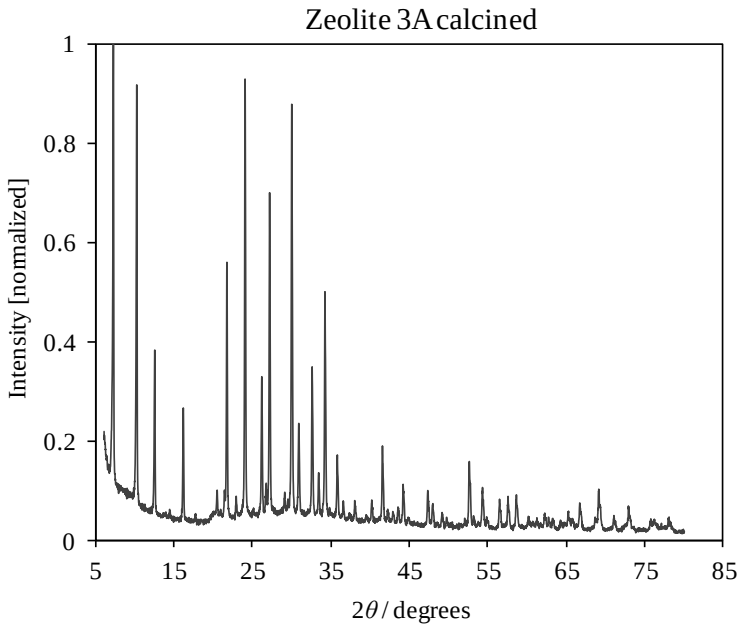

Figure 5.6: XRD pattern of zeolite 3A. X-ray source Cu Kα.

Afterwards, the zeolite was analyzed by Scanning Electron Microscopy (SEM) with Energy Dispersive X-ray Spectroscopy (EDS) – JEOL JSM 6301/Oxford INCA Energy 350 – in order to understand the textural structure and quantify the elemental composition. The SEM images are shown in Figure 5.7; it can be seen that the pellet is mainly composed by well defined cubic crystals, as expected (Zone 1 – Z1), although these crystals are surrounded by a binder, needle shaped crystals (Zone 2 – Z2), which have higher percentage of Si (17% atomic) and Mg (3% atomic). A generic chemical formula close to $K_6Na_6[(AlO_2)_{12}(SiO_2)_{12}]$ was determined by the EDS results for the cubic crystals (Zone 1 – Z1). The cubic crystals show a crystal size around 1 μm, which is much larger than the estimated by Reitveld refinement (0.1 μm); this difference is probably caused by the fact that XRD was done on a mixture of both crystals (cubic and needles), giving an average cristalite size. In Table 5.3 are summarized the main physical properties of this zeolite 3A.

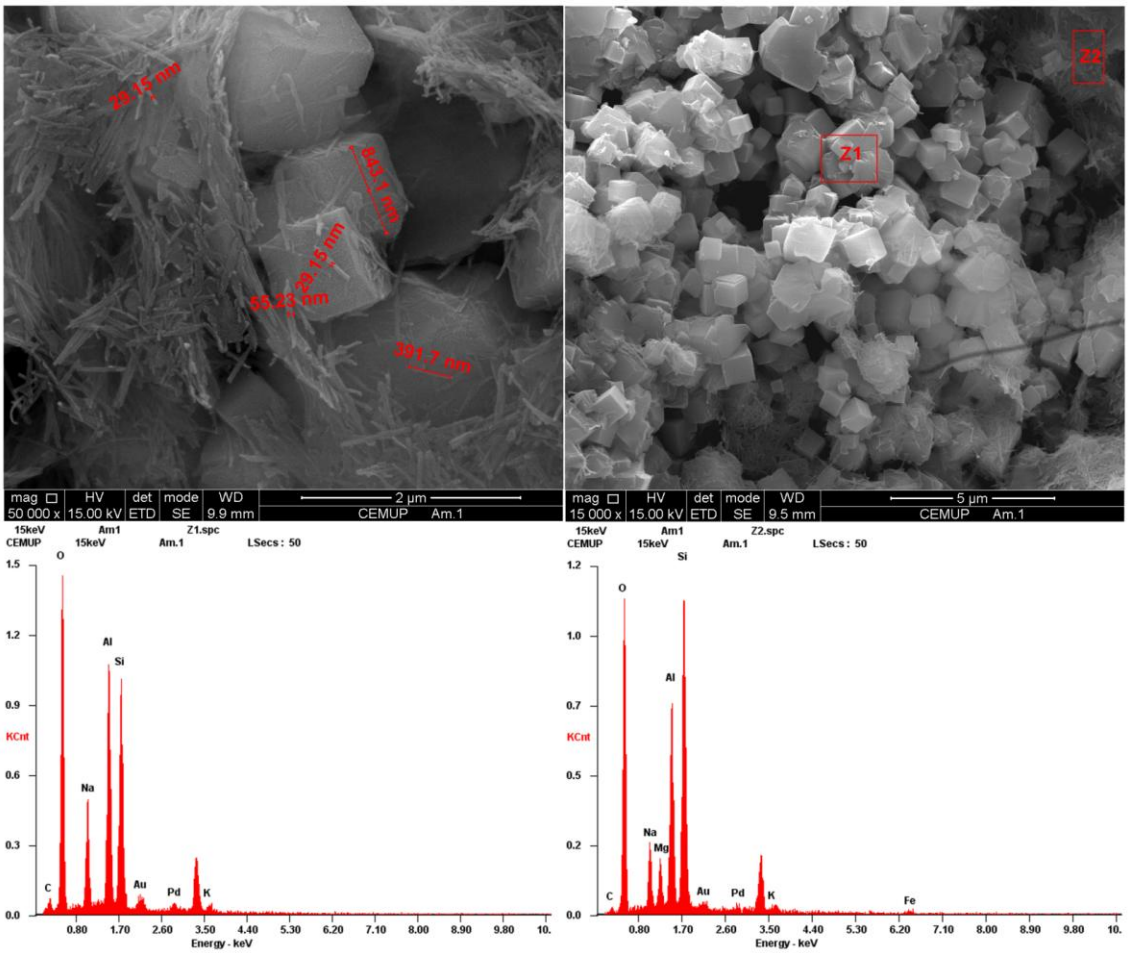

Figure 5.7: SEM images of zeolite 3A and EDS results for Zone 1 and Zone 2 (Z1-Z2).

Table 5.3: Physical properties of zeolite 3A.

Properties	Value
Chemical formula	$K_6Na_6[(AlO_2)_{12}(SiO_2)_{12}]$
Size / mm	1.7-2.4
Crystal size / µm	~1
Real density / $kg \cdot m^{-3}$	2361
Apparent density/ $kg \cdot m^{-3}$	1189
Pore diameter / nm	55
Porosity (meso)	36%
Surface area / $m^2 \cdot g^{-1}$	22

5.3. Modelling

5.3.1. Mathematical model

A mathematical model is necessary in order to fit the dynamic response to inlet perturbations taking into account several phenomena: hydrodynamics, mass transfer from the bulk to the micropores, equilibrium and

kinetics of adsorption on the zeolite 3A surface. Due to the complexity of these phenomena, compared to the simple experimental methodology, a simple model is encouraged, in order to avoid unrealistic parameters just to force the fitting. Nevertheless, the simplicity of the model is limited by a reasonable ability of fitting the experimental data. The proposed model, based on some experimental observations, has the following assumptions:

- The fixed bed hydrodynamics is represented by axial dispersion model.
- Mass transfer is modelled by a linear driving force.
- The adsorption equilibrium is reached instantaneously.
- Linear adsorption equilibrium isotherms: Henry's law.
- The velocity, temperature and pressure are constant.
- Danckwerts boundary conditions.

Based on the assumptions previously mentioned, the molar balance to an infinitesimal fraction of the column leads to the following partial differential equations:

Bulk balance:
$$\varepsilon_b \frac{\partial C_i}{\partial t} + \varepsilon_b \cdot u \frac{\partial C_i}{\partial x} + (1-\varepsilon_b)\frac{3}{r_p} k_L\left(C_i - \bar{C}_{p,i}\right) = \varepsilon_b \cdot D_{ax} \frac{\partial^2 C_i}{\partial x^2} \quad (5.1)$$

Particle balance:
$$\frac{3}{r_p} k_L\left(C_i - \bar{C}_{p,i}\right) = \varepsilon_p \frac{\partial \bar{C}_{p,i}}{\partial t} + \left(1-\varepsilon_p\right)\frac{\partial q_i\left(\bar{C}_p\right)}{\partial t} \quad (5.2)$$

where C represents the bulk concentration, t the time, x the axial position, D_{ax} the axial dispersion coefficient, ε_b the bulk porosity, ε_p the particle porosity, $\bar{C}_p$ the average concentration in the particle porous medium, k_L the global mass transfer coefficient, q the adsorbed amount per volume of solid, u the intersticial velocity and r_p the particle radius.

These balances are often written as function of the dimensionless axial position ($z = x/L$ (Column length)), Péclet number ($Pe = u \cdot L/\, D_{ax}$), volumetric flow (Q) and column volume (V). In Table 5.4 this model is detailed with its respective initial and boundary conditions, where K_{ads} is the slope of the adsorption equilibrium isotherm.

5.3.2. MatLab® resolution

This system of partial differential equations (PDEs) was solved by the *pdepe* function, from Matlab® library. This function was designed to solve initial-boundary problems for parabolic/elliptic PDEs along one-dimension (x^*) and time (t^*). After discretization of x^*, into a mesh ($xmesh^*$) the ordinary differential equations (ODEs) for each cell are solved by a stiff ODEs solver, the *ode115s*, also from the same library with a relative tolerance of 10^{-5}.

Table 5.4: Mathematical model for adsorption in a fixed bed column with axial dispersion and linear driving force.

Bulk molar balance:	$\frac{V \cdot \varepsilon_b}{Q}\left[\frac{\partial C_i}{\partial t} + \frac{(1-\varepsilon_b)}{\varepsilon_b} \cdot \frac{3}{r_p} \cdot k_L \cdot \left(C_i - \overline{C_{p,i}}\right)\right] + \frac{\partial C_i}{\partial z} = \frac{1}{Pe} \cdot \frac{\partial^2 C_i}{\partial z^2}$	(5.3)
Particle molar balance:	$\frac{3}{r_p} \cdot k_{L,i} \cdot \left(C_i - \overline{C_{p,i}}\right) = \varepsilon_p \cdot \frac{\partial C_{p,i}}{\partial t} + \left(1-\varepsilon_p\right) \cdot \frac{\partial q_i(\overline{C_{p,i}})}{\partial t}$	(5.4)
Initial conditions:	$C_i(t=0, \forall z) = \overline{C_{p,i}}(t=0, \forall z) = C_i^{Eluent}$	(5.5)
Boundary conditions:	$C_i(\forall t, z=0) = C_i^{Feed}(t) + \frac{1}{Pe} \cdot \frac{\partial C_i}{\partial z}\Big\|_{\forall t, z=0}$	(5.6)
	$\frac{\partial C_i}{\partial z}\Big\|_{\forall t, z=1} = 0$	(5.7)
Feed composition:	$C_i^{Feed}(t) = \begin{cases} C_i^{Inj}(t) & , t \le t^{Inj} \\ C_i^{Eluent} & , t > t^{Inj} \end{cases}$	(5.8)
Adsorption equilibrium:	$q_i = K_{ads,i} \cdot \overline{C_{p,i}}$	(5.9)

The MatLab® syntax is the following: *sol = pdepe* (*m*, *pdefun*, *icfun*, *bcfun*, $xmesh^*$, $tspan^*$). After converging, the solver gives the numerical solution (*sol*), which corresponds to the dependent variables, u^*at each x^* defined in the $xmesh^*$ and at each specified time, $tspan^*$; where m^* is the parameter corresponding to the problem symmetry , assuming the value of 0 for slab, 1 for cylindrical and 2 for spherical geometries, respectively; *pdefun*, *icfun*, *bcfun*, are functions where the PDEs, initial and boundary conditions, are respectively defined:

$$[c^*,\ f^*,\ s^*] = pdefun\left(x^*, t^*, u^*, \frac{\partial u^*}{\partial x^*}\right)$$

$$u_0^* = icfun(x^*)$$

$$[p_l^*,\ q_l^*, p_r^*, q_r^*] = bcfun(x_l^*, u_l^*, x_r^*,\ u_r^*, t^*)$$

where c^*, f^*, s^*, u_0^*, p^* and q^*, are parameterizable vector functions to be adapted to different problems. The PDE problem has to be expressed in the format described in Table 5.5, with the respective initial and boundary conditions.

In order to parameterize according to our mathematical model, for the adsorption model in a fixed bed column, previously presented, the independent variables, $x^*$and t^*, correspond to our axial dimension variable, z = [0, 1], and time, t = [0, t_{final}], while the depended variable, u^*, was related to concentration in bulk and particles. Other important parameter is the $xmesh^*$ vector, which divides the axial interval in several cells; in each cell the problem is reduced to an ordinary differential equations problem, where the u^* is not function of x^*. In principle, the number of cells should be as large as possible; however, this leads to long time for converging, and sometimes is impossible to converge or the results are not more accurate than when using

fewer cells. Therefore, the $xmesh^*$ should be adapted to each problem in order to have satisfactory results in a reasonable time. The parameterization of the *pdepe* function to our mathematical model is described in Table 5.6.

Table 5.5: Description of PDEs format of *pdepe* solver from MatLab® library.

Partial Differential Equations:

$$c^*\left(x^*, t^*, u^*, \frac{\partial u^*}{\partial x^*}\right) \cdot \frac{\partial u^*}{\partial x^*} = x^{*-m^*} \cdot \frac{\partial}{\partial x^*} \cdot \left[x^{*m^*} \cdot f^*\left(x^*, t^*, u^*, \frac{\partial u^*}{\partial x^*}\right)\right] + s^*\left(x^*, t^*, u^*, \frac{\partial u^*}{\partial x^*}\right), m = 0 \quad (5.10)$$

Initial Conditions:

$$u^*(\forall\, x^*, t^* = 0) = u_0^*(x^*) \quad (5.11)$$

Boundary Conditions:

Left Condition:
$$p_l^*(x_l^*, t^*, u_l^*) + q_l^*(x_l^*, t^*) \cdot f^*\left(x_l^*, t^*, u_l^*, \frac{\partial u_l^*}{\partial x_l^*}\right) = 0 \quad (5.12)$$

Right Condition:
$$p_r^*(x_r^*, t^*, u_r^*) + q_r^*(x_r^*, t^*) \cdot f^*\left(x_r^*, t^*, u_r^*, \frac{\partial u_r^*}{\partial x_r^*}\right) = 0 \quad (5.13)$$

5.4. Results and Discussion

5.4.1. Tracer experiments

Experiments were carried out at 20 MPa, 10 mL·min^{-1}, using carbon dioxide and MeOH as eluent (40% MeOH (*v/v*)) at different temperatures. Before each experiment the equipment was running for 1 hour in order to stabilize the detectors signals and the oven temperature. A dead volume, of 1.1±0.1 mL, was previously measured from a small pulse injection with a bypass to the detector, without passing through the column. Then 50 μL of tracer were injected to the column to compute the residence time distribution. The signal, which is proportional to the concentration, was recorded and both the residence time distribution ($E(t)$) and the mean residence time ($\bar{t}_{res}$), were then calculated:

$$E(t) = \frac{C(t)}{\int_0^\infty C(t) \cdot dt} = \frac{Signal(t)}{\int_0^\infty Signal(t) \cdot dt} \quad (5.14)$$

$$\bar{t}_{res} = \int_0^\infty E(t) \cdot t\, dt \quad (5.15)$$

These experiments allowed measuring the flow rate, which was slightly different from the set value (10 mL·min^{-1}) mainly at 313 K (12 mL·min^{-1}); the flow rates were calculated by the following relation:

$$\bar{t_r} = \frac{V \cdot \varepsilon_b}{Q} \quad (5.16)$$

Table 5.6: Parameterization of *pdepe* functions according to our mathematical model.

$c^*\{i\} = \begin{cases} \dfrac{V \cdot \varepsilon_b}{Q}, & i = 1{:}NC \\ \varepsilon_p + (1-\varepsilon_p) \cdot K_{ads,i}, & i = NC+1{:}2NC \end{cases}$	(5.17)
$f^*\{i\} = \begin{cases} \dfrac{1}{Pe} \cdot \dfrac{\partial u^*(i)}{\partial x^*}, & i = 1{:}NC \\ 0, & i = NC+1{:}2NC \end{cases}$	(5.18)
$s^*\{i\} = \begin{cases} -\dfrac{V}{Q} \cdot (1-\varepsilon_b) \cdot \dfrac{3}{r_p} \cdot k_L \cdot \left(u^*(i) - u^*(i+NC)\right) - \dfrac{\partial u^*(i)}{\partial x^*}, & i = 1{:}NC \\ \dfrac{3}{r_p} \cdot k_{L,i} \cdot \left(u^*(i) - u^*(i+NC)\right), & i = NC+1{:}2NC \end{cases}$	(5.19)
$u^*\{i\} = \begin{cases} C_i, & i = 1{:}NC \\ \overline{C_{p,i}}, & i = NC+1{:}2NC \end{cases}$	(5.20)
$u_0^*\{1{:}NC\} = u_0^*\{NC+1{:}2NC\} = C^{Eluent}\{1{:}NC\}$	(5.21)
$q_l\{i\} = q_r\{i\} = \begin{cases} 1, & i = 1{:}NC \\ 0, & i = NC+1{:}2NC \end{cases}$	(5.22)
$p_l{}^*\{i\} = \begin{cases} C^{Feed}\{i\}(t) - u_l^*\{i\}, & i = 1{:}NC \\ 0, & i = NC+1{:}2NC \end{cases}$	(5.23)
$p_r{}^*\{i\} = 0, \quad i = 1{:}2NC$	(5.24)

The HPLC pump is a positive displacement pump and the set flow rate is calculated based on the piston volume times the frequency; at 313 K the carbon dioxide is relatively close to its critical temperature which may affect its compressibility and then promote some change in the fluid flow rate delivered by the pump.

The dispersion of the curve around the mean residence time is a consequence of axial dispersion – assumed in the model – which is quantified by the Péclet number (Pe). Some expressions are available to calculate Péclet number from the variance of the curve; however, this hydrodynamic parameter was fitted to the experimental data by the objective function presented below.

$$F_{Obj} = min\left\{\sum^{Nexp}\left(\sum^{NP}\frac{\left(E^{Model} - E^{Exp.}\right)^2}{NP}\right)\Big/ Nexp\right\} \tag{5.25}$$

Nevertheless, the column with zeolite pellets has different porosity, and therefore it will have different Péclet number by the changing of intersticial velocity; at the same conditions, Péclet number is inversely

proportional to the bulk porosity ($Pe_1 \cdot \varepsilon_{b,1} = Pe_2 \cdot \varepsilon_{b,2}$). In Table 5.7 is shown the Péclet number for the column with glass particles – fitted from the experimental data – and the Péclet number estimated for the column with zeolite 3A. Furthermore, the table shows the eluent flow rates used at each temperature. A decrease of Pe number was observed when decreasing temperature.

Table 5.7: Péclet values adjusted from tracer experiments.

T / K	Q / mL·min^{-1}	Glass column Pe (ε_b=0.5)	Zeolite 3A column Pe (ε_b=0.43)
313	12.0	31±1	36
333	10.0	59±1	69
353	10.4	79±1	92

The residence time distributions for the tracer experiments, model and experimental data, are displayed in Figure 5.8. No adsorption and particle pores were considered for the model. As the figure shows, an excellent fitting was obtained between the experimental data and the model. Therefore, it can be concluded that the hydrodynamics for the fixed bed column used in these conditions can be accurately described by the axial dispersion model.

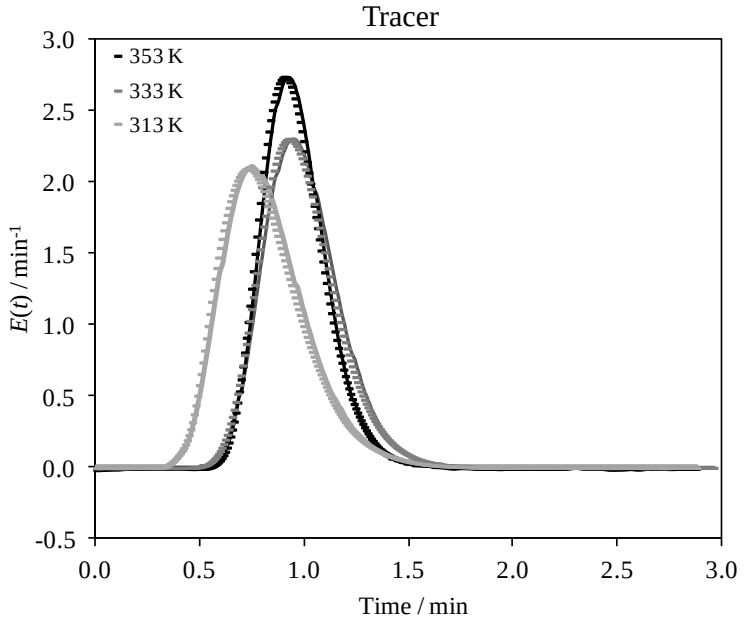

Figure 5.8: Residence time distribution for tracer pulses (50 µL Vanillin) at different temperatures: experimental (points) and model (line). Operating conditions: 20 MPa, reference flow rate 10 mL·min^{-1}, CO_2/MeOH (40% MeOH (*v/v*)).

5.4.2. DMC and water pulses

Afterwards, adsorption isotherms and mass transfer were estimated by the analysis of the dynamic response of injections of small pulses of water and DMC in a fixed bed filled with zeolite 3A. The experiments were carried out at the same conditions of the tracer experiments since the axial dispersion effects are known in those conditions. The slope of the adsorption isotherm was calculated based on the retention time:

$$t_r = \frac{V}{Q}\left(\varepsilon_b + (1-\varepsilon_b)\cdot\varepsilon_p + (1-\varepsilon_b)\cdot\left(1-\varepsilon_p\right)\cdot K_{ads}\right) \tag{5.26}$$

In turn, the global mass transfer coefficients were fitted from the experimental data by minimizing the squared difference of the maximum peak time, which is related to the dispersion for a non Gaussian curve:

$$F_{Obj} = min\left\{\left(t^{Model}_{(peak\ max)} - t^{Exp.}_{(peak\ max)}\right)^2\right\} \tag{5.27}$$

The main results for DMC and water are summarized in Tables 5.8 and 5.9, respectively. For linear adsorption isotherms, the retention time should be independent of the amount injected to the column; however, it was observed a slight increase on retention time with the volume injected, which suggests a deviation from linearity in the form of an anti-Langmuir isotherm. Nevertheless, the adsorption isotherms are difficult to measure by small pulses since the saturation is not reached. As an alternative, the isotherm could be fitted to the pulse response data, although the low range of concentrations covered may lead to unacceptable extrapolations for higher concentrations experiments.

One inaccuracy of the linear isotherm is that competitive adsorption is neglected; however, for these conditions this assumption is reasonable: the first reason is the fact that, at low concentration, the interaction between DMC and water can be neglected, and, since the adsorbent capacity would not be reached, the number of active centers would be enough for each species, without much competition; second, most of the adsorption occurs in the micropores, which are highly selective for water, since DMC molecules do not access the micropores; thus, the effect of DMC concentration on water adsorption, in the micropores, would not be significant. Nevertheless, some competition could occur, which could lead to a slight deviation from the predicted by the non-competitive model.

There is lack of data for the adsorption of water in the presence of carbon dioxide and MeOH. However, Yamamoto et al. [28] reported the adsorption of water dissolved in ethanol (liquid phase) at atmospheric pressure, which is the more comparable with water in methanol. At 298 K the authors reported a slope of the adsorption equilibrium isotherm around 10 $m^3_{fluid}\cdot m^{-3}_{solid}$; while, based on this work, a value around 6 $m^3_{fluid}\cdot m^{-3}_{solid}$ is expected.

The global mass transfer coefficient includes contributions of external and internal mass transfer resistances; the values of the coefficients for DMC (1.9×10^{-5}-2.8×10^{-5} $m\cdot s^{-1}$) are 30-50% lower than for water (2.8×10^{-5}-3.9×10^{-5} $m\cdot s^{-1}$). The quality of the fitting was quantified by the degree of explanation:

$$R^2 = 1 - \frac{\sum\left(C(t)^{Model} - C(t)^{Exp.}\right)^2}{\sum\left(C(t)^{Model} - \overline{C(t)^{Exp.}}\right)^2} \tag{5.28}$$

High values for the degree of explanation parameter, over 87%, were obtained, which indicates a reasonable fitting quality; however, lower values (81% and 83%) were obtained for water pulses at 313 K and 333 K. In spite of the relative low degree of explanation, these results are reasonable considering the simple assumptions considered. A more complex model could be used, but the confidence of the results would be restricted to narrow operating conditions ranges.

Table 5.8: Main results obtained from DMC pulses response.

T / K	K_{ads} (Calculated)			K_{ads} (average)	$k_L \times 10^5$ / m·s^{-1}	R^2
	100 µL	150 µL	200 µL		(Fitted)	
313	1.23	1.38	1.61	1.4±0.2	2.8±0.6	87%
333	0.63	0.83	0.88	0.8±0.1	1.9±0.6	97%
353	0.46	0.63	0.82	0.6±0.2	2.2±0.6	98%

Table 5.9: Main results obtained from water pulses response.

T / K	K_{ads} (Calculated)			K_{ads} (average)	$k_L \times 10^5$ / m·s^{-1}	R^2
	100 µL	150 µL	200 µL		(Fitted)	
313	2.92	3.40	3.62	3.3±0.4	3.9±0.6	81%
333	1.57	1.96	2.05	1.9±0.3	2.8±0.6	83%
353	0.78	1.28	1.33	1.1±0.3	3.3±0.6	93%

The experimental pulse response data and the predicted by the model for water and DMC pulses are displayed in Figures 5.9 and 5.10. As already anticipated by the degree of explanation values, excellent fittings are shown by the graphs at 353 K and 333 K (for DMC), while higher deviations ate observed at 333 K (for water) and 313 K (for both compounds). The deviation of the experimental data from the expected for a linear isotherm – which also causes more dispersive effects - may be the main reason for these deviations; however, as mentioned above, large errors would have been made if a non linear isotherm had been considered, because a narrow concentration range was covered by the experiments. Therefore, besides this approach may eventually lead to a better fitting, the reliability of the isotherms for higher concentrations would be poor, leading to predictions of adsorption amounts out of the studied range.

In addition, the assumption of the linear driving force model for the mass transfer resistance may also lead to slight deviations from the experimental data. However, considering the limitations of the experimental data, it can be concluded that the model shows reasonable performance for fitting the experimental data.

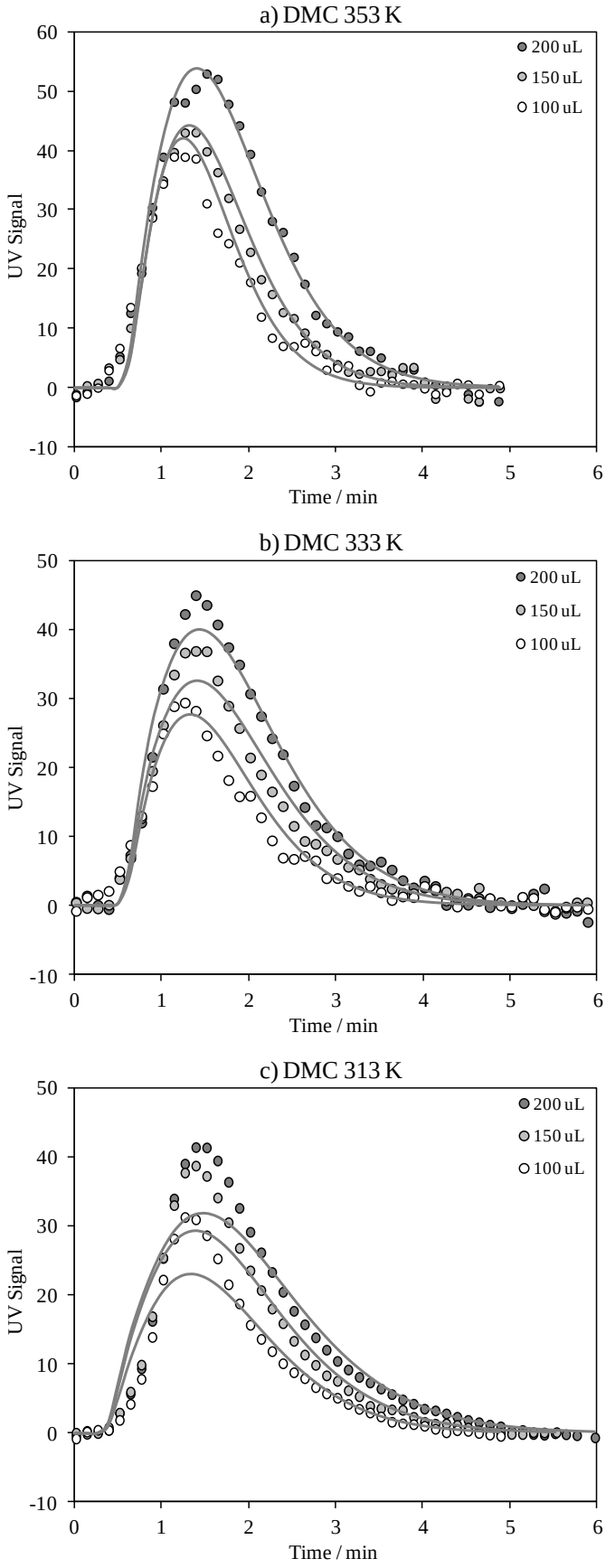

Figure 5.9: DMC pulses responses at different temperatures: experimental (points) and model (lines). Operating conditions: 20 MPa, reference flow rate 10 mL·min^{-1}, CO_2/MeOH (40% MeOH (*v/v*)).

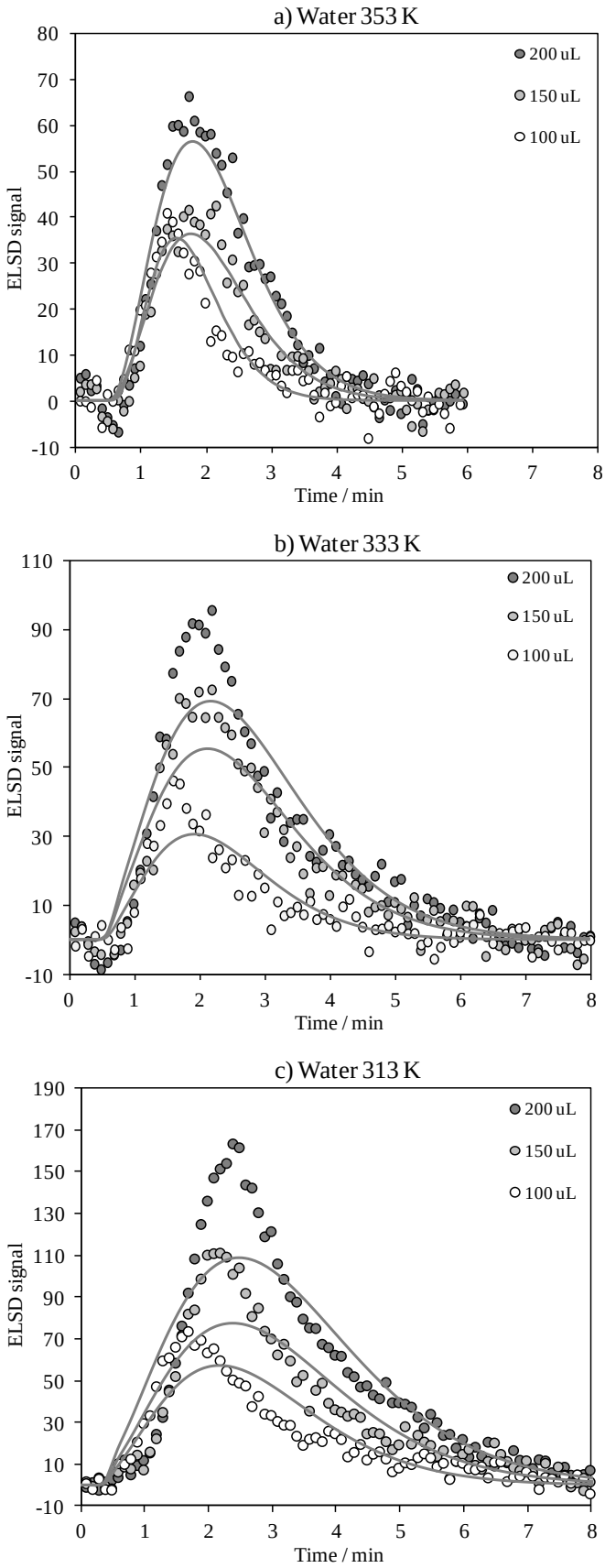

Figure 5.10: Water pulses responses at different temperatures: experimental (points) and model (lines). Operating conditions: 20 MPa, reference flow rate 10 mL·min^{-1}, CO_2/MeOH (40% MeOH (*v/v*)).

The experiments were held at three different temperatures in order to study the effect of temperature on the slope of the adsorption equilibrium isotherm. This effect is shown in Figure 5.11, where the logarithm of the equilibrium constant is plotted against the inverse of the absolute temperature. It can be observed an increase of the slope of the adsorption equilibrium isotherm with the inverse of temperature, which indicates an exothermic phenomenon, as expected for adsorption. Moreover, a linear fitting was performed using the Van't Hoff equation:

$$\ln(K_{ads}) = -\frac{\Delta H_{ads}}{R \cdot T} + \frac{\Delta S_{ads}}{R} \tag{5.29}$$

where ΔH_{ads} and ΔS_{ads} are the enthalpy and entropy changes of adsorption, T is the temperature and R is the ideal gas constant.

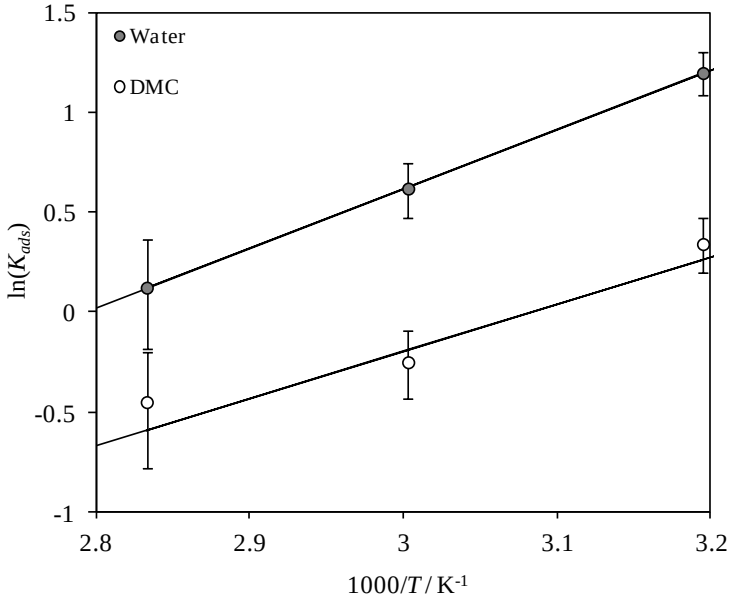

Figure 5.11: Ln(K_{ads}) *versus* the inverse of temperature for water and DMC.

The enthalpy, entropy, and Gibbs free energy changes ($G = H - T \cdot S$) of adsorption, – with the respective standard deviations – estimated from the Van't Hoff equation for the slope of the adsorption equilibrium isotherm, are displayed in Table 5.10. The parameters were determined using each pair of points and the standard deviation was calculated based on the theory of uncertainties propagation.

Table 5.10: Van't Hoff parameters for the slope of the adsorption equilibrium isotherm.

Compound	ΔH_{ads} / kJ·mol^{-1}	ΔS_{ads} / J·mol^{-1}·K^{-1}	$\Delta G_{ads}^{298\,K}$ / kJ·mol^{-1}
Water	-25± 6	-69±4	-4±6
DMC	-20±6	-60±4	-2±6

The enthalpy of adsorption of water in the zeolite is higher than the estimated for DMC. This higher enthalpy for water was expected since its high polarity contributes to a stronger interaction with the solid surface; for less polar molecules, lower interaction forces are expected which leads to lower enthalpy of adsorption. The enthalpy of adsorption values obtained (-25 $kJ \cdot mol^{-1}$) is lower than the reported in the literature, where enthalpies of adsorption equal to 44 $kJ \cdot mol^{-1}$ [28], 58 $kJ \cdot mol^{-1}$ [37], 52-72 $kJ \cdot mol^{-1}$ [38] are reported by other authors for water vapour adsorption on zeolite 3A. The adsorption enthalpy observed may be an average of several phenomena. For instance, the binder that surrounds the LTA crystals may also adsorb some amount of water; then the adsorption enthalpy observed would be a weighted average of both materials. This also justifies the fact of DMC adsorption be considerable, which was not predicted, since DMC should not enter into zeolite 3A micropores due to its large molecule size, when compared to the cage window size (3 Å). Moreover, if some physical adsorption occurred it would decrease the adsorption enthalpy, since physical adsorption usually shows enthalpy changes lower than chemical adsorption.

In Figure 5.12 is depicted the selectivity of zeolite for water adsorption at different temperatures. The slope of adsorption isotherm of water is around 2 times higher than for DMC with a moderate decrease with the increase of temperature. Again, the higher selectivity for water is explained by the small size of the cage windows of LTA crystals, which blocks the access to the cage for molecules larger than 3 Å, allowing water molecules to enter while DMC molecules are kept out of the cages. Based on the assumption that DMC is mainly adsorbed in the unknown crystals, it can be concluded that, for a pure crystal, the selectivity for water would drastically increased. The high selectivity for water is essential for the separation of DMC and water in SMBR technology.

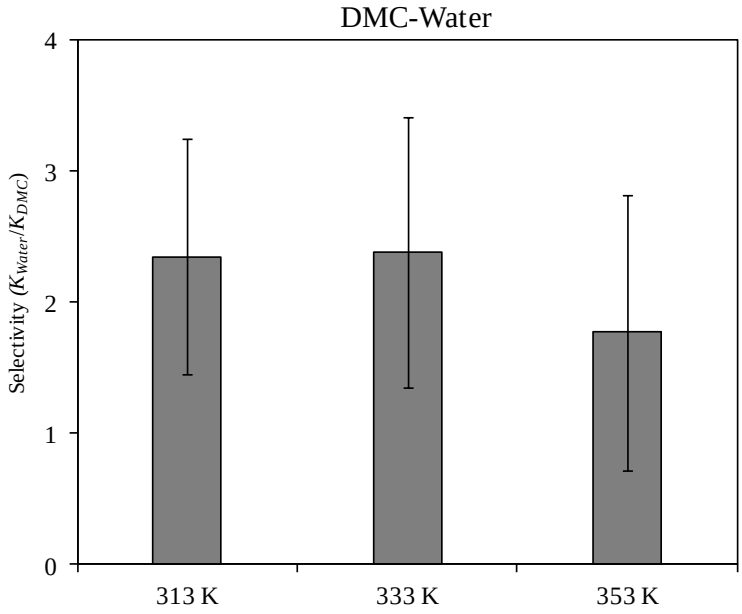

Figure 5.12: Zeolite selectivity for water adsorption at different temperatures.

Zeolite 3A is mainly composed by LTA crystals, agglomerated similar to well defined cubic crystallites, the major responsible for water adsorption; however, as mentioned before, the zeolite also presents a secondary structure (binder), where it is believed that the adsorption of DMC occurs. The effect on DMC adsorption, promoted by small differences in the binder, would be hard to predict. However, even with a DMC adsorption variation of 20%, the selectivity of water will still be high (1.67-2.5), which is the main feature for the development of a new process combining water adsorption to enhance the DMC yield.

5.5. Prediction of Mass Transfer

In the beginning of this section, some mass transfer properties were measured from experiments: the Péclet number and the global mass transfer for the linear driving force model. But how reliable are these parameters? And how can they be used to predict the mass transfer phenomena for other conditions? The mass transfer is the third pillar for building the SMBR model, along with reaction kinetics and adsorption equilibrium. In order to understand how reliable empirical correlations are, at high pressure conditions, several correlations, available from the literature, were used to predict the mass transfer phenomena in a fixed bed column: axial dispersion, pore diffusion, and external film mass transfer.

Viscosity and Density

Most of the correlations are related to the physical properties of the solvent, specially density and viscosity. For pure carbon dioxide, the density can be predicted by a cubic Equation of State while the viscosity can be predicted by a correlation proposed by Stephan and Lucas [39]. However, for carbon dioxide and MeOH mixtures, the predictions are more complex leading to higher errors. In this work, the mixture density was estimated using the Soave-Redlich-Kwong Equation of State with modified second order Huron-Vidal mixing rule, and UNIQUAQ to compute the excess of Gibbs free energy (Chapter 3). In turn, the viscosity was estimated using the following correlations available from literature for high pressure gases: Dean and Stiel (1965) [40], Stiel and Thodos [41], and Chung et al. [42]. In Table 5.11 are summarized the viscosity (μ) estimated by each correlation and the density (ρ) estimated by the equation of state. The standard deviation between the three correlations is around 0.01 mPa·s, which is within the correlation errors (10%).

Table 5.11: Viscosity of CO_2-MeOH mixtures estimated from correlations.

T / K	x_{MeOH}	ρ / kg·m^{-3}	μ / mPa·s (Dean-Stiel)	μ / mPa·s (Stiel-Thodos)	μ / mPa·s (Chung)	μ / mPa·s (Average)
313	0.42	786	0.093	0.082	0.111	0.10±0.01
333	0.53	721	0.084	0.074	0.098	0.09±0.01
353	0.57	666	0.070	0.062	0.082	0.07±0.01

Linear driving force model

In our model, a linear driving force was assumed to model the mass transfer from the bulk to the particle pores. Nevertheless, this global mass transfer model lumps contributions of the external mass transfer as well as of the internal mass transfer in the pores, as sketched in Figure 5.13. Therefore, a resistance in series model is proposed for the global mass transfer resistance:

$$\frac{1}{k_L} = \frac{1}{k_{ext}} + \frac{1}{k_{int}} \tag{5.30}$$

where k_L represents the global mass transfer coefficient, k_{ext} is the external mass transfer coefficient, and k_{int} is the internal mass transfer coefficient. Glueckauf et al. [43] proposed that the internal mass transfer coefficient can be related to the effective diffusion coefficient (D_{eff}) by the following relation:

$$k_{int} = \frac{5D_{eff}}{r_p} \tag{5.31}$$

where the effective diffusion can be calculated from the particle porosity, tortuosity (τ) and molecular diffusion coefficient (D_{12}):

$$D_{eff} = \frac{\varepsilon_p \cdot D_{12}}{\tau} \tag{5.32}$$

Da Silva and Rodrigues [44] observed a value of 2.2 for the tortuosity of zeolite 4A, which should be similar to zeolite 3A.

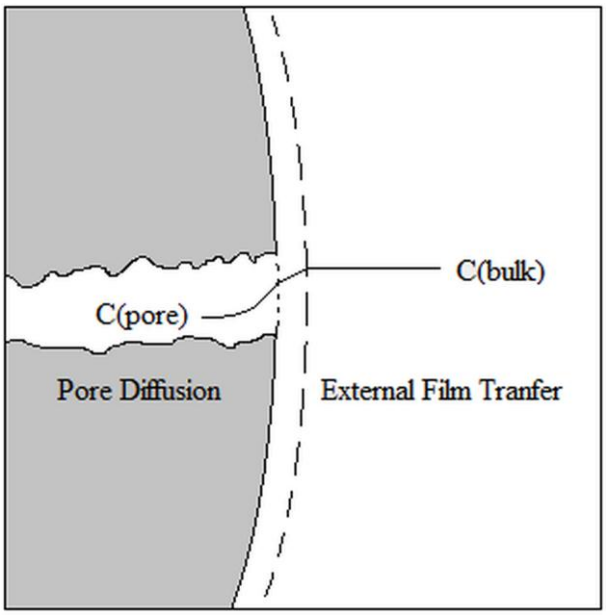

Figure 5.13: Scheme of internal and external mass transfer in a porous material.

Molecular Diffusion

The diffusion coefficient for diluted water and DMC in carbon dioxide-MeOH mixtures was estimated by the Wilke and Chang equation [45], slightly modified, since it was already used with high performance for high pressure carbon dioxide [46] and carbon dioxide - MeOH [47]:

$$D_{12} = 8.6 \times 10^{-15} \cdot \frac{T \cdot \sqrt{M_2}}{\mu \cdot {V_{M,1}}^{0.6}} \tag{5.33}$$

where D_{12} is the molecular diffusion coefficient of solute (1) diluted in the solvent (2), M_2 is the molecular weight of the solvent, and $V_{M,1}$the molar volume of the solute. The diffusion coefficients were estimated using the viscosity estimated by each previous model. Moreover, the $D_{12}$was also estimated by a simpler method proposed by He and Yu [48], in order to compare to the previous correlation, since this method is not function of the viscosity of the fluid; although it could lead to higher errors it is still a good reference to evaluate the reasonability of our estimation:

$$D_{12} = \left[14.882 + 0.005908 \cdot \frac{T_{c,2} \cdot V_{c,2}}{M_2} + 2.0821 \times 10^{-6} \cdot \left(\frac{T_{c,2} \cdot V_{c,2}}{M_2}\right)^2\right] \times 10^{-5} \cdot \cdot \sqrt{\left(\frac{T}{M_1}\right)} \cdot \exp\left(-\frac{0.3887}{V_{r,2} - 0.23}\right) \tag{5.34}$$

where D_{12} is the diffusion coefficient in $cm^2 \cdot s^{-1}$, $T_{c,2}$ is the critical temperature of the solvent in K, $V_{c,2}$ is the critical molar volume of the solvent in $cm^3 \cdot mol^{-1}$, M_1 and M_2 are the molecular weight of solute and solvent in $g \cdot mol^{-1}$, respectively, and $V_{r,2}$ is the reduced molar volume of the solvent. The molecular diffusion coefficients, for DMC and water, estimated by the correlations, are presented in Table 5.12 and 5.13, as well as the average value and the standard deviation between them; the correlations show a variation between 15 and 20%; values of diffusion coefficients between 10^{-4} and 10^{-3} $cm^2 \cdot s^{-1}$ were estimated, which are typically of supercritical fluids, according to Schoenmakers and Uunk [49]. From the Wilke and Chang equation, the diffusion coefficient is inversely proportional to the viscosity, and therefore different values were found using the three different values of viscosity previously estimated. The average value will be used for further calculations, since there is no information about the accuracy of each correlation.

Table 5.12: Diffusion coefficient of DMC in CO_2-MeOH, $10^4 \cdot D_{DMC}$ ($cm^2 \cdot s^{-1}$)

T / K	He-Yu	Wilke-Chang \ Chung (μ)	Wilke-Chang \ Dean-Stiel (μ)	Wilke-Chang \ Stiel-Thodos (μ)	Average
313	0.91	1.06	1.26	1.43	1.2±0.2
333	1.07	1.24	1.45	1.65	1.4±0.2
353	1.32	1.57	1.84	2.10	1.7±0.3

Table 5.13: Diffusion coefficient of water in CO_2, $10^4 \cdot D_W$ ($cm^2 \cdot s^{-1}$)

T / K	He-Yu	Wilke-Chang \ Chung (μ)	Wilke-Chang \ Dean-Stiel(μ)	Wilke-Chang \ Stiel-Thodos (μ)	Average
313	2.56	2.67	3.19	3.61	3.0±0.5
333	2.90	3.14	3.67	4.17	3.5±0.6
353	3.40	3.97	4.64	5.30	4.3±0.8

External and global mass transfer

External mass transfer, over the particle surface, is drastically conditioned by the hydrodynamics of the system itself. Several correlations are available in the literature to predict the external mass transfer in a fixed bed column. Most of them are written using some dimensionless numbers: Sherwood (Sh) and Stanton (St) numbers as function of Reynolds (Re) and Schmidt (Sc) numbers:

$$Sh = \frac{k_{ext} \cdot d_p}{D_{12}} \tag{5.35}$$

$$St = \frac{k_{ext}}{u \cdot \varepsilon_p} \tag{5.36}$$

$$Re = \frac{u \cdot \varepsilon_p \cdot \rho \cdot d_p}{\mu} \tag{5.37}$$

$$Sc = \frac{\mu}{\rho \cdot D_{12}} \tag{5.38}$$

Table 5.14 shows the correlations used in this work to estimate the external mass transfer, which are appropriated for the range of Reynolds (2.7-3.7) and Schmidt (2.9-4.5) numbers; the average viscosity and molecular diffusion were used in calculating the dimensionless numbers.

All the correlations are very similar, and therefore similar results were obtained with a variation between 25% and 30%. In Table 5.15 are displayed the average external and global mass transfer coefficients, calculated based on the external mass transfer and diffusion, for each of our experimental conditions. Moreover, it was calculated the percent contribution of the diffusion resistance to the global mass transfer resistance, and it was concluded that the diffusion phenomenon represents around 90% of the global mass transfer resistance. Thus, it is hard to point out which correlation for the external mass transfer is more appropriated since it has low effect on the global mass transfer.

In Figure 5.14 are depicted the global mass transfer coefficients predicted by the previous correlations and the values obtained by adjusting the model to the experimental data. It can be observed a reasonable prediction from the correlations used, especially for water, with exception of 313 K where the values predicted are considerably lower than the experimentally estimated values. However, the values obtained by the fitting at 313 K are not in agreement with the expected for a diffusion controlled regime, since diffusion should increase

with temperature. This effect might also be caused by the deviation from linear isotherms, which are more accentuated at 313 K, affecting the curve shape that is modelled by the global mass transfer. Thus, the global mass transfer probably includes contributions of the true mass transfer and of the slight deviation from Henry's law.

Table 5.14: Correlations for external mass transfer in a fixed bed column.

Authors	Ref.	Correlation	Range	Eq.
Wilson-Geankoplis	[50]	$Sh = \frac{1.09}{\varepsilon_b} \cdot Re^{0.33} \cdot Sc^{0.33}$	$0.0015 < Re < 55$	(5.39)
Kataoka	[51]	$Sh = 1.89 \cdot \left(\frac{1-\varepsilon_b}{\varepsilon_b}\right)^{1/3} \cdot Re^{1/3} \cdot Sc^{1/3}$	$Re < 100$	(5.40)
Sherwood-Pigford-Wilke	[52]	$St = 1.17 \cdot Re^{-0.415}$	$10 < Re < 2500$	(5.41)
Ranz-Marshall	[53]	$Sh = 2 + 0.6 \cdot Re^{1/3} \cdot Sc^{1/2}$		(5.42)
Wakao-Funazkri	[54]	$Sh = 2 + 1.1 \cdot Re^{0.6} \cdot Sc^{1/3}$	$3 < Re < 10^4$	(5.43)
Petrovic-Thodos	[55]	$Sh = \frac{0.357}{\varepsilon_b} \cdot Re^{0.64} \cdot Sc^{0.33}$	$3 < Re < 2000$	(5.44)
Tan-Liou	[56]	$Sh = 0.3 \cdot Re^{0.83} \cdot Sc^{1/3}$	$2 < Re < 40$ $2 < Sc < 20$	(5.45)

Table 5.15: Estimation of external and global mass transfer coefficients.

T / K	$10^4 \times k_{ext,W}$/ m·s^{-1}	$10^4 \cdot k_{L,W}$/ m·s^{-1}	Diff.	$10^4 \times k_{ext,DMC}$/ m·s^{-1}	$10^4 \times k_{L,DMC}$/ m·s^{-1}	Diff.
313	20±5	2.2±0.4	89%	11±3	0.9±0.2	92%
333	20±5	2.5±0.5	88%	11±3	1.0±0.2	90%
353	24±6	3.1±0.7	87%	13±3	1.3±0.3	90%

In spite of the deviations observed, it can be concluded that the correlations used showed excellent performance to predict the global mass transfer for a binary solvent near critical conditions. Moreover, similar results can be obtained by using Dean and Stiel correlation for viscosity, Wilke and Chang for the molecular diffusion, and any correlation for the external mass transfer, instead of the average values, which avoids a large number of calculations.

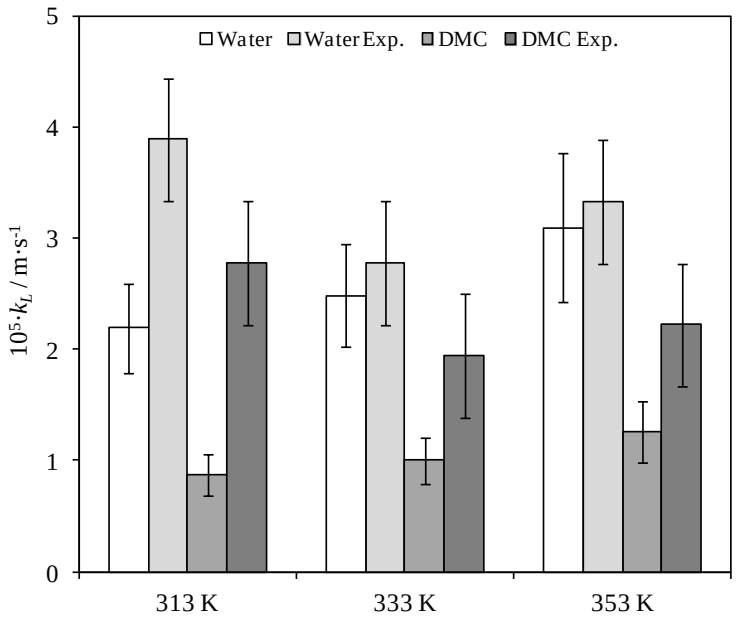

Figure 5.14: Global mass transfer coefficient: Experimental and predicted.

Axial dispersion

As explained before, the axial dispersion was quantified by a pulse response of vanillin in a fixed bed filled with glass particles in the same conditions of the pulse response of DMC and water over zeolite 3A in a similar column: 20 MPa, 10-12 ml·min^{-1}, and 313-353 K, with CO_2-MeOH (40 % (*v/v*) of MeOH). The Péclet number, fitted to the experimental data, is depicted in Figure 5.15 for each temperature. A linear relation between the Péclet number and the temperature can be seen from the graph.

The axial dispersion is a contribution of molecular diffusion and convective dispersion [53]; therefore, this trend indicates that the axial dispersion is mainly controlled by convective dispersion. Since the molecular diffusion increases with temperature, a decrease of Péclet number with temperature was expected if the convective dispersion change was neglected. Then, the change of viscosity and density of the mixture might have caused the increase of Péclet number with the temperature, as it was observed by Tan and Liou [57] for a pulse dispersion of methane in supercritical carbon dioxide.

Several correlations were tested in order to predict the axial dispersion: Tan and Liou [57] (Pe = [56, 63, 86] for T = [313 K, 333 K, 353 K]), Catchpole [58] (Pe = 13), Chung and Wen [59] (Pe = 66), Hsu-Haynes [60] (Pe = 35), and Edwards and Richardson [61] (Pe = 250); these correlations, based on the Péclet number of the particle ($Pe_p = \frac{u \cdot d_p}{Dax}$), are depicted in Table 5.16. It was observed a large discrepancy between the correlations presented, probably due to the differences on the application range of each correlation [62], although it was found that Tan-Liou correlation showed the same trend with temperature with similar Péclet values. In spite of the good prediction for vanillin axial dispersion, this correlation predicts that an increase in the molecular diffusion leads to an increase of Péclet number, which do not seems reasonable, but it is still the best correlation to predict the axial dispersion here observed.

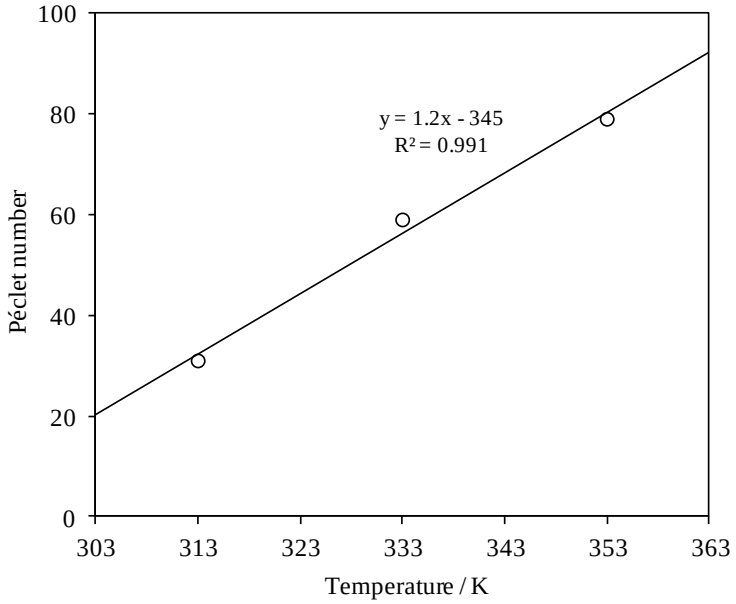

Figure 5.15: Effect of temperature on Pe observed from the tracer experiments.

Table 5.16: Correlations for Péclet number in a fixed bed column.

Authors	Ref.	Correlation	Eq.
Tan-Liou	[57]	$Pe_p = 1.634 \cdot \left(\frac{Re}{\varepsilon_b}\right)^{0.265} \cdot Sc^{-0.919}$	(5.46)
Catchpole	[58]	$Pe_p = \frac{0.018}{Re} + \frac{10}{1 + 0.7/Re}$	(5.47)
Chung-Wen	[59]	$Pe_p = \frac{1}{\varepsilon_b} \cdot (0.2 + 0.011 \cdot Re^{0.48})$	(5.48)
Hsu-Haynes	[60]	$\frac{1}{Pe_p} = \frac{0.7}{Re \cdot Sc} + \frac{1}{0.28 \cdot (1 + 0.63/(Re \cdot Sc))}$	(5.49)
Edwards-Richardson	[61]	$\frac{1}{Pe_p} = \frac{0.73}{Re \cdot Sc} + \frac{1}{13 \cdot (1 + 9.49/(Re \cdot Sc))}$	(5.50)

5.6. Conclusions

In this chapter was studied the adsorption of DMC and water over zeolite 3A surface. These data were assessed by pulse response experiments in a fixed bed column using 10-12 ml·min^{-1} of carbon dioxide and MeOH (40% (*v*/*v*)) as eluent at 20 MPa between 313 K and 353 K.

The axial dispersion model for a fixed bed column showed excellent ability to fit the tracer experiments carried in a column filled with glass particles; Pe values of 79±1 (353 K), 59±1 (333 K), and 31±1 (313 K) were estimated.

The injection of small pulses of DMC and water allowed estimating the slopes of the adsorption equilibrium isotherms, considering linear isotherms, from the retention time of the peaks: 0.6±0.2 (333 K), 0.8±0.1 (333 K), and 1.4±0.2 (313K) for DMC; and 1.1±0.3 (353 K), 1.9±0.3 (333 K), and 3.3±0.4 (313 K) for water. These results reveal a high selectivity factor for water, around 2, which is a crucial feature for the development of novel processes, based on water removal from the reaction mixture, in order to enhance the DMC yield.

Moreover, the enthalpies of adsorption were estimated using Van't Hoff equation. Enthalpies of -25±6 kJ·mol^{-1} and -20±6 kJ·mol^{-1} were estimated for water and DMC, respectively.

The global mass transfer coefficients, for a binary solvent (CO_2-MeOH) at high pressure condition, were usefully predicted by the average values obtained from common correlations available in the literature. Tan-Liou correlation was successfully used to predict the axial dispersion behaviour of vanillin pulses in high pressure carbon dioxide-MeOH mixtures.

Nomenclature

Symbols

C_i	Bulk concentration of each compound *i* (mol·m$_{bulk}^{-3}$)
$\overline{C_{p,i}}$	Average pores concentration of each compound (mol·m$_{pores}^{-3}$)
C_i^{Eluent}	Eluent concentration of each compound (mol·m^{-3})
C_i^{Feed}	Feed concentration of each compound (mol·m^{-3})
D	Column diameter (m)
D_{12}	Molecular diffusion coefficient of diluted solute (1) in solvent (2) (m^2·s^{-1})
D_{ax}	Axial dispersion coefficient (m^2·s^{-1})
D_{eff}	Effective diffusion coefficient (m^2·s^{-1})
d_p	Particle diameter (m)
E	Residence time distribution (s^{-1})
ε_b	Bulk porosity (m$_{bulk}^{-3}$·m$_{total}^{-3}$)
ε_p	Particle porosity (m$_{pores}^{-3}$·m$_{particle}^{-3}$)

F_{Obj}	Objective Function (s^{-2})
ΔG_{ads}	Gibbs free energy change of adsorption ($J \cdot mol^{-1}$)
ΔH_{ads}	Enthalpy change of adsorption ($J \cdot mol^{-1}$)
k_{int}, k_{ext}, k_L	Internal, external and global mass transfer coefficient ($m \cdot s^{-1}$)
K_{ads}	Slope of the adsorption equilibrium isotherm ($m_{pores}^3 \cdot m_{solid}^{-3}$)
L	Length (m)
M	Molecular weight ($g \cdot mol^{-1}$)
μ	Viscosity ($Pa \cdot s$)
NC	Number of compounds (-)
N_{exp}	Number of experiments (-)
NP	Number of points (-)
Pe (Pe_p)	Péclet number (Particle) (-)
q_i	Adsorbed amount ($mol \cdot m_{solid}^{-3}$)
Q	Volumetric flow rate ($m^3 \cdot s^{-1}$)
r_p	Particle radius (m)
R	Ideal gas constant ($J \cdot K^{-1} \cdot mol^{-1}$)
R^2	Degree of explanation (-)
Re	Reynolds number (-)
ρ	Density ($kg \cdot m^{-3}$)
Sc	Schmidt number (-)
Sh	Sherwood number (-)
St	Stanton number (-)
ΔS_{ads}	Entropy change of adsorption ($J \cdot K^{-1} \cdot mol^{-1}$)
t	Time (s)
t^{inj}	Injection time frame (s)
t_r	Retention time (s)
$\bar{t}_{res}$	Mean residence time (s)
T	Temperature (K)

T_c	Critical temperature (K)
τ	Tortuosity (-)
u	Intersticial velocity ($m \cdot s^{-1}$)
V	Column volume (m^3)
V_c	Critical molar volume ($m^3 \cdot mol^{-1}$)
V_M	Molar volume ($m^3 \cdot mol^{-1}$)
V_r	Reduced molar volume (-)
x	Axial position (m)
z	Dimensionless axial position (-)

Abbreviations

ABPR	Automated Back Pressure Regulator
BET	Brunauer–Emmett–Teller
EDS	Energy-dispersive X-ray Spectroscopy
LTA	Linde Type A
ODE	Ordinary Differential Equation
PDE	Partial Differential Equation
SEM	Scanning Electron Microscopy
SFC	Supercritical Fluid Chromatography

Acknowledgements

I would like to acknowledge the excellent services provided, in the characterization of the zeolite 3A, by Centro de Materiais da Universidade do Porto, financially supported by Fundação para a Ciência e Tecnologia (REEQ/1062/CTM/2005 and REDE/1512/RME/2005), for the SEM and XPS analysis, Unidade de Microscopia Electrónica da Universidade de Trás-os-Montes e Alto Douro for the XRD analysis, and Laboratory of Catalysis Materials of the University of Porto for the adsorption isotherms of nitrogen over zeolite 3A. These analyses were very helpful to characterize the material and to better understand the physical phenomenon observed.

References

[1] Sakakura, T.,Saito, Y.,Okano, M.,Choi, J.,Sako, T. Selective Conversion Of Carbon Dioxide To Dimethyl Carbonate By Molecular Catalysis. *Journal of Organic Chemistry* **1998,** *63*(20), 7095.

[2] Sakakura, T.,Choi, J. C.,Saito, Y.,Sako, T. Synthesis Of Dimethyl Carbonate From Carbon Dioxide: Catalysis And Mechanism. *Polyhedron* **2000,** *19*(5), 573.

[3] Choi, J.,He, L.,Yasuda, H.,Sakakura, T. Selective And High Yield Synthesis Of Dimethyl Carbonate Directly From Carbon Dioxide And Methanol. *Green Chemistry* **2002,** *4*(3), 230.

[4] Tomishige, K.,Kunimori, K. Catalytic And Direct Synthesis Of Dimethyl Carbonate Starting From Carbon Dioxide Using CeO2-ZrO2 Solid Solution Heterogeneous Catalyst: Effect Of H2O Removal From The Reaction System. *Applied Catalysis A: General* **2002,** *237*(1-2), 103.

[5] Hong, S.,Park, H.,Lim, J.,Lee, Y.,Anpo, M.,Kim, J. Synthesis Of Dimethyl Carbonate From Methanol And Supercritical Carbon Dioxide. *Research on Chemical Intermediates* **2006,** *32*(8), 737.

[6] Choi, J.,Kohno, K.,Ohshima, Y.,Yasuda, H.,Sakakura, T. Tin- Or Titanium-Catalyzed Dimethyl Carbonate Synthesis From Carbon Dioxide And Methanol: Large Promotion By A Small Amount Of Triflate Salts. *Catalysis Communications* **2008,** *9*(7), 1630.

[7] Kohno, K.,Choi, J. C.,Ohshima, Y.,Yasuda, H.,Sakakura, T. Synthesis Of Dimethyl Carbonate From Carbon Dioxide Catalyzed By Titanium Alkoxides With Polyether-Type Ligands. *ChemSusChem* **2008,** *1*(3), 186.

[8] Honda, M.,Suzuki, A.,Noorjahan, B.,Fujimoto, K. I.,Suzuki, K.,Tomishige, K. Low Pressure CO2 To Dimethyl Carbonate By The Reaction With Methanol Promoted By Acetonitrile Hydration. *Chemical Communications* **2009,** (30), 4596.

[9] Eta, V.,Mäki-Arvela, P.,Leino, A.-R.,Kordás, K.,Salmi, T.,Murzin, D.,Mikkola, J.-P. Synthesis Of Dimethyl Carbonate From Methanol And Carbon Dioxide: Circumventing Thermodynamic Limitations. *Industrial & Engineering Chemistry Research* **2010,** *49*(20), 9609.

[10] Honda, M.,Kuno, S.,Begum, N.,Fujimoto, K. I.,Suzuki, K.,Nakagawa, Y.,Tomishige, K. Catalytic Synthesis Of Dialkyl Carbonate From Low Pressure CO2 And Alcohols Combined With Acetonitrile Hydration Catalyzed By CeO2. *Applied Catalysis A: General* **2010,** *384*(1-2), 165.

[11] Eta, V.,Mäki-Arvela, P.,Salminen, E.,Salmi, T.,Murzin, D. Y.,Mikkola, J. P. The Effect Of Alkoxide Ionic Liquids On The Synthesis Of Dimethyl Carbonate From CO2 And Methanol Over ZrO2-MgO. *Catalysis Letters* **2011,** *141*(9), 1254.

[12] Eta, V.,Mäki-Arvela, P.,Wärnå, J.,Salmi, T.,Mikkola, J. P.,Murzin, D. Y. Kinetics Of Dimethyl Carbonate Synthesis From Methanol And Carbon Dioxide Over ZrO2-MgO Catalyst In The Presence Of Butylene Oxide As Additive. *Applied Catalysis A: General* **2011,** *404*(1-2), 39.

[13] Honda, M.,Kuno, S.,Sonehara, S.,Fujimoto, K.-i.,Suzuki, K.,Nakagawa, Y.,Tomishige, K. Tandem Carboxylation-Hydration Reaction System From Methanol, CO2 And Benzonitrile To Dimethyl Carbonate And Benzamide Catalyzed By CeO2. *ChemCatChem* **2011,** *3*(2), 365.

[14] Honda, M.,Tamura, M.,Nakagawa, Y.,Sonehara, S.,Suzuki, K.,Fujimoto, K. I.,Tomishige, K. Ceria-Catalyzed Conversion Of Carbon Dioxide Into Dimethyl Carbonate With 2-Cyanopyridine. *ChemSusChem* **2013,** *6*(8), 1341.

[15] Ginder, W. F. Method For Removing Water From Ethanol. US 4407662 **1983**.

[16] Carton, A.,Gonzalez, G.,Iniguez de la Torre, A.,Cabezas, J. L. Separation Of Ethanol-Water Mixtures Using 3A Molecular Sieve. *Journal of Chemical Technology and Biotechnology* **1987,** *39*(2), 125.

[17] Einicke, W.,Heuchel, M.,Szombathely, M. V.,Bräuer, P.,Schöllner, R.,Rademacher, O. Liquid-Phase Adsorption Of Binary Ethanol-Water Mixtures On NaZSM-5 Zeolites With Different Silicon/Aluminium Ratios. *Journal of the Chemical Society, Faraday Transactions 1: Physical Chemistry in Condensed Phases* **1989,** *85*(12), 4277.

[18] Al-Rub, F. A. A.,Banat, F. A.,Jumah, R. Vapor-Liquid Equilibrium Of Ethanol-Water System In The Presence Of Molecular Sieves. *Separation Science and Technology* **1999,** *34*(12), 2355.

[19] Beery, K. E.,Ladisch, M. R. Adsorption Of Water From Liquid-Phase Ethanol - Water Mixtures At Room Temperature Using Starch-Based Adsorbents. *Industrial and Engineering Chemistry Research* **2001,** *40*(9), 2112.

[20] Al-Asheh, S.,Banat, F.,Al-Lagtah, N. Separation Of Ethanol–Water Mixtures Using Molecular Sieves And Biobased Adsorbents. *Chemical Engineering Research and Design* **2004,** *82*(7), 855.

[21] Al-Asheh, S.,Banat, F.,Fara, A. A. Dehydration Of Ethanol-Water Azeotropic Mixture By Adsorption Through Phillipsite Packed-Column. *Separation Science and Technology* **2009,** *44*(13), 3170.

[22] Quintero, J. A.,Cardona, C. A. Ethanol Dehydration By Adsorption With Starchy And Cellulosic Materials. *Industrial and Engineering Chemistry Research* **2009,** *48*(14), 6783.

[23] E. Ivanova, D. D., M. Kostova. Adsorption Separation Of Ethanol-Water Liquid Mixtures By Natural Clinoptilolite. *Journal of the University of Chemical Technology and Metallurgy* **2009,** *44*(3).

[24] Wang, K. S.,Liao, C. C.,Chu, R. Q.,Chung, T. W. Equilibrium Isotherms Of Water And Ethanol Vapors On Starch Sorbents And Zeolite 3A. *Journal of Chemical and Engineering Data* **2010,** *55*(9), 3334.

[25] Kim, Y.,Hendrickson, R.,Mosier, N.,Hilaly, A.,Ladisch, M. R. Cassava Starch Pearls As A Desiccant For Drying Ethanol. *Industrial and Engineering Chemistry Research* **2011,** *50*(14), 8678.

[26] Okewale, A. O.,Etuk, B. R.,Igbokwe, P. K. Adsorption And Kinetic Modelling Of The Uptake Of Water From Ethanol – Water Systems Using Starchy Adsorbents. *International Journal of Engineering & Technology* **2011,** *11*(6), 81.

[27] Baylak, T.,Kumar, P.,Niu, C. H.,Dalai, A. Ethanol Dehydration In A Fixed Bed Using Canola Meal. *Energy and Fuels* **2012,** *26*(8), 5226.

[28] Yamamoto, T.,Kim, Y.,Kim, B.,Endo, A.,Thongprachan, N.,Ohmori, T. Adsorption Characteristics Of Zeolites For Dehydration Of Ethanol: Evaluation Of Diffusivity Of Water In Porous Structure. *Chemical Engineering Journal* **2012,** *181-182*, 443.

[29] Tajallipour, M.,Niu, C.,Dalai, A. Ethanol Dehydration In A Pressure Swing Adsorption Process Using Canola Meal. *Energy & Fuels* **2013,** *27*, 6655.

[30] Jain, L. K.,Gehrhardt, H. M.,Kyle, B. G. Liquid Phase Adsorption Equilibria With Molecular Sieve Adsorbent. *Journal of Chemical & Engineering Data* **1965,** *10*(2), 202.

[31] Mjalli, F.,Al-Asheh, S.,Banat, F.,Al-Lagtah, N. Representation Of Adsorption Data For The Isopropanol-Water System Using Neural Network Techniques. *Chemical Engineering and Technology* **2005,** *28*(12).

[32] Sircar, S.,Myers, A. L.,Molstad, M. C. Adsorption Of Dilute Solutes From Liquid Mixtures. *Transactions of the Faraday Society* **1970,** *66*.

[33] Burdett, N. A. Thermogravimetric Determinations Of The Water Sorption Characteristics Of Molecular Sieve In High-Pressure CO2 And N2. *Thermochimica Acta* **1985,** *87*(C), 1.

[34] Mohammad, S. A.,Gasem, K. A. M. Modeling The Competitive Adsorption Of CO2 And Water At High Pressures On Wet Coals. *Energy & Fuels* **2011,** *26*(1), 557.

[35] Mohammad, S. A.,Gasem, K. A. M. Multiphase Analysis For High-Pressure Adsorption Of CO2/Water Mixtures On Wet Coals. *Energy & Fuels* **2012,** *26*(6), 3470.

[36] Gruszkiewicz, M. S.,Simonson, J. M.,Burchell, T. D.,Cole, D. R. Water Adsorption And Desorption On Microporous Solids At Elevated Temperature. *Journal of Thermal Analysis and Calorimetry* **2005,** *81*(3), 609.

[37] Simo, M.,Sivashanmugam, S.,Brown, C. J.,Hlavacek, V. Adsorption/Desorption of Water and Ethanol on 3A Zeolite in Near-Adiabatic Fixed Bed. *Industrial & Engineering Chemistry Research* **2009,** *48*(20), 9247.

[38] Lalik, E.,Mirek, R.,Rakoczy, J.,Groszek, A. Microcalorimetric Study Of Sorption Of Water And Ethanol In Zeolites 3A And 5A. *Catalysis Today* **2006,** *114*(2–3), 242.

[39] Stephan, K.,Lucas, K. *Viscosity Of Dense Fluids*; Plenum Press: **1979**.

[40] Dean, D.,Stiel, L. The Viscosity Of Nonpolar Gas Mixtures At Moderate And High Pressures. *AIChE Journal* **1965,** *11*(3), 526.

[41] Stiel, L.,Thodos, G. The Thermal Conductivity Of Nonpolar Substances In The Dense Gaseous And Liquid Regions. *AIChE Journal* **1964,** *10*(1), 26.

[42] Chung, T.,Ajlan, M.,Lee, L.,Starling, K. Generalized Multiparameter Correlation for Nonpolar and Polar Fluid Transport properties. *Industrial and Engineering Chemistry Research* **1988,** *27*(4), 671.

[43] Glueckauf, E. Theory Of Chromatography. Part 10.-Formulae For Diffusion Into Spheres And Their Application To Chromatography. *Transactions of the Faraday Society* **1955,** *51*(0), 1540.

[44] Da Silva, F.,Rodrigues, A. Adsorption Equilibria and Kinetics for Propylene and Propane over 13X and 4A Zeolite Pellets. *Industrial & Engineering Chemistry Research* **1999,** *38*(5), 2051.

[45] Wilke, C.,Chang, P. Correlation Of Diffusion Coefficients In Dilute Solutions. *AIChE Journal* **1955,** *1*(2), 264.

[46] Kaczmarski, K.,Poe, D.,Tarafder, A.,Guiochon, G. Efficiency Of Supercritical Fluid Chromatography Columns In Different Thermal Environments. *Journal of Chromatography A* **2013,** *1291*, 155.

[47] Sassiat, P. R.,Mourier, P.,Caude, M. H.,Rosset, R. H. Measurement of diffusion coefficients in supercritical carbon dioxide and correlation with the equation of Wilke and Chang. *Analytical Chemistry* **1987,** *59*(8).

[48] He, C.-H.,Yu, Y.-S. New Equation For Infinite-Dilution Diffusion Coefficients In Supercritical And High-Temperature Liquid Solvents. *Industrial & Engineering Chemistry Research* **1998,** *37*(9), 3793.

[49] Schoenmakers, P. J.,Uunk, L. G. Supercritical Fluid Chromatography-Recent And Future Developments. *European Chromatography News* **1987,** *1*(3), 14.

[50] Wilson, E.,Geankoplis, C. Liquid Mass Transfer At Very Low Reynolds Numbers In Packed Beds. *Industrial & Engineering Chemistry Fundamentals* **1966,** *5*(1), 9.

[51] Kataoka, T.,Yoshida, H.,Ueyama, K. Mass Transfer In Laminar Region Between Liquid And Packing Material Surface In The Packed Bed. *Journal of Chemical Engineering of Japan* **1972,** *5*(2), 132.

[52] Sherwood, T. K.,Pigford, R. L.,Wilke, C. R. *Mass Transfer*; McGraw-Hill: **1975**.

[53] Ruthven, D. M. *Principles Of Adsorption And Adsorption Processes*; John Wiley & Sons: New York, **1984**.

[54] Wakao, N.,Funazkri, T. Effect Of Fluid Dispersion Coefficients On Particle-To-Fluid Mass Transfer Coefficients In Packed Beds: Correlation Of Sherwood Numbers. *Chemical Engineering Science* **1978,** *33*(10), 1375.

[55] Petrovic, L. J.,Thodos, G. Mass Transfer In Flow Of Gases Through Packed Beds. Low Reynolds Number Region. *Industrial & Engineering Chemistry Fundamentals* **1968,** *7*(2), 274.

[56] Tan, C.-S.,Liou, D.-C. Modeling Of Desorption At Supercritical Conditions. *AIChE Journal* **1989,** *35*(6), 1029.

[57] Tan, C.,Liou, D. Axial Dispersion of Supercritical Carbon Dioxide in Packed Beds. *Industrial and Engineering Chemistry Research* **1989,** *28*(8), 1246.

[58] Catchpole, O.,Bernig, R.,King, M. Measurement And Correlation Of Packed-Bed Axial Dispersion Coefficients In Supercritical Carbon Dioxide. *Industrial and Engineering Chemistry Research* **1996,** *35*(3), 824.

[59] Chung, S.,Wen, C. Longitudinal Dispersion of Liquid Flowing Through Fixed and Fluidized Beds. *AIChE Journal* **1968,** *14*(6), 857.

[60] Hsu, L.,Haynes, H. Effective Diffusivity By The Gas Chromatography Technique: Analysis And Application To Measurements Of Diffusion Of Various Hydrocarbons In Zeolite NaY. *AIChE Journal* **1981,** *27*(1), 81.

[61] Edwards, M.,Richardson, J. Gas Dispersion In Packed Beds. *Chemical Engineering Science* **1968,** *23*(2), 109.

[62] Yu, D.,Jackson, K.,Harmon, T. C. Dispersion And Diffusion In Porous Media Under Supercritical Conditions. *Chemical Engineering Science* **1999,** *54*(3), 357.

Chapter 6. Process Intensification for the Direct Synthesis of DMC

"Success consists of going from failure to failure without loss of enthusiasm." – Winston Churchill

This chapter is based on the following article: Santos, B., Pereira, C., Silva, V., Loureiro, J., Rodrigues, A. Design Of A True Moving Bed Reactor For The Direct Synthesis Of Dimethyl Carbonate. *Chemical Engineering Science*, Accepted.

6.1. Introduction

In several chemical processes, the reaction is reversible and its conversion is limited by thermodynamic properties (Gibbs free energy of reaction). In most of the industrial processes, this drawback is overcome by using excess of one reactant or/and by recycling the non reacted species [1]. Other approach is the use of reactive separation technologies [2, 3]. They are an excellent example of process intensification and consist in the integration of reaction and separation in the same unit, where one or more products are continuously separated during the reaction to shift the equilibrium towards product(s) formation. These technologies aim to reduce the process units, wastes production and energy consumption, contributing in a sustainable way for the so called "green chemistry" [4].

There are several reactive separation technologies (also known as multifunctional reactors) [5], such as reactive distillation [6], membrane reactors, reactive extraction, or reactive chromatography. This chapter is focused on the simulated moving bed chromatographic reactor (SMBR, subtype of reactive chromatography). Detailed information of these and other technologies is available elsewhere [5]: concepts, models, applications, etc.

In order to understand the concept of SMBR, the moving bed countercurrent chromatography is introduced, also called True Moving Bed (TMB). Let us take the example of the separation of a mixture of compounds "A" and "B" by TMB, where "A" is more strongly adsorbed compound on the adsorbent surface. In Figure 6.1a is depicted a sketch of a TMB with four zones. First, the Feed stream (F), containing both compounds, is fed to the unit; then, in Zone II, compound "A" (more strongly adsorbed) follows the adsorbent towards the Extract stream (X). In Zone III, compound "B" is transported by convection to the Raffinate stream (R), which allows the separation of the compounds in two different streams diluted in the Eluent (stream E). Zones I and IV are designed in order to avoid the accumulation of either "A" or "B" in the unit. In Zone I the flow rate should be high enough to regenerate the adsorbent avoiding the contamination of Zone IV by compound "A"; while in Zone IV the flow rate should be low enough to force the adsorption of "B", pushing it backwards.

Some operating restrictions should be obeyed in order to achieve this performance. Let us define γ_i as the ratio between liquid and solid flow rates in each zone:

$$\gamma_i = \frac{Q_{liq,i}}{Q_{sol.}}, \qquad i = Zone\ I, II, III, or\ IV \tag{6.1}$$

Considering the equilibrium theory [7, 8] (no mass transfer resistance) for linear isotherms ($q = K_{ads} \cdot C$), over an adsorbent with a certain particle porosity (ε_p), the following restrictions are imposed:

Zone I: $$\varepsilon_p + (1 - \varepsilon_p) K_{ads,A} \leq \gamma_I \tag{6.2}$$

Zone II: $$\varepsilon_p + (1 - \varepsilon_p) K_{ads,B} \leq \gamma_{II} \leq \varepsilon_p + (1 - \varepsilon_p) K_{ads,A} \tag{6.3}$$

Zone III: $$\varepsilon_p + (1-\varepsilon_p)K_{ads,B} \leq \gamma_{III} \leq \varepsilon_p + (1-\varepsilon_p)K_{ads,A} \quad (6.4)$$

Zone IV: $$0 \leq \gamma_{IV} \leq \varepsilon_p + (1-\varepsilon_p)K_{ads,B} \quad (6.5)$$

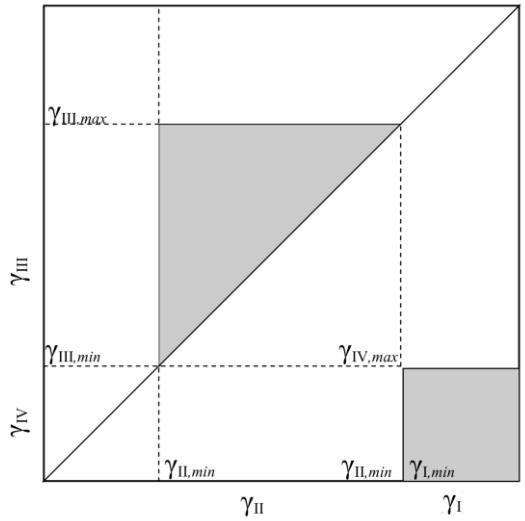

Scheme 6.1: Separation and regeneration regions for TMB based on equilibrium theory and linear isotherms.

These restrictions are commonly represented in the so-called separation and regeneration regions (Scheme 6.1), which are the feasible regions of operating flow rate ratios (γ_I, γ_{II}, γ_{III}, and γ_{IV}) that allow a complete separation between compounds "A" and "B". Other separation regions were proposed, based on the same principles, for non-linear isotherms, such as Langmuir [9-11] or Toth isotherms [12].

The introduction of the mass transfer resistance [13] in the separation regions determination is much more complicated, because mass transfer depends on the physical properties of the compounds (viscosity, diffusivities, etc), velocity, and particles size. In order to obtain more precise separation regions (taking into account mass transfer resistances), successive simulations should be performed using realistic mathematical models.

The concept of separation volume was also proposed [14-16] to predict the effect of mass transfer resistances, not only on the restrictions of Zones II and III, but also on the restrictions of Zones I and IV, giving more information but also requiring more effort. In spite of the more accurate results obtained when realistic models are used, the equilibrium theory is a very useful tool for a first guess in TMB design.

In Figure 6.1a the TMB is represented, while in Figure 6.1b is presented the concept of countercurrent chromatographic reactor, or true moving bed reactor (TMBR). In this figure, is depicted a generic (non-catalytic) reversible reaction: A ⇌ B + C; where "B" is the more strongly adsorbed followed by "A" and "C", respectively. The main principles are equal to the TMB, with the difference that compound "A" is completely converted into "B" and "C" in the reactive zone (Zones II and III). The complete conversion of "A" is caused by the continuous separation of the products (Le Chatelier's principle).

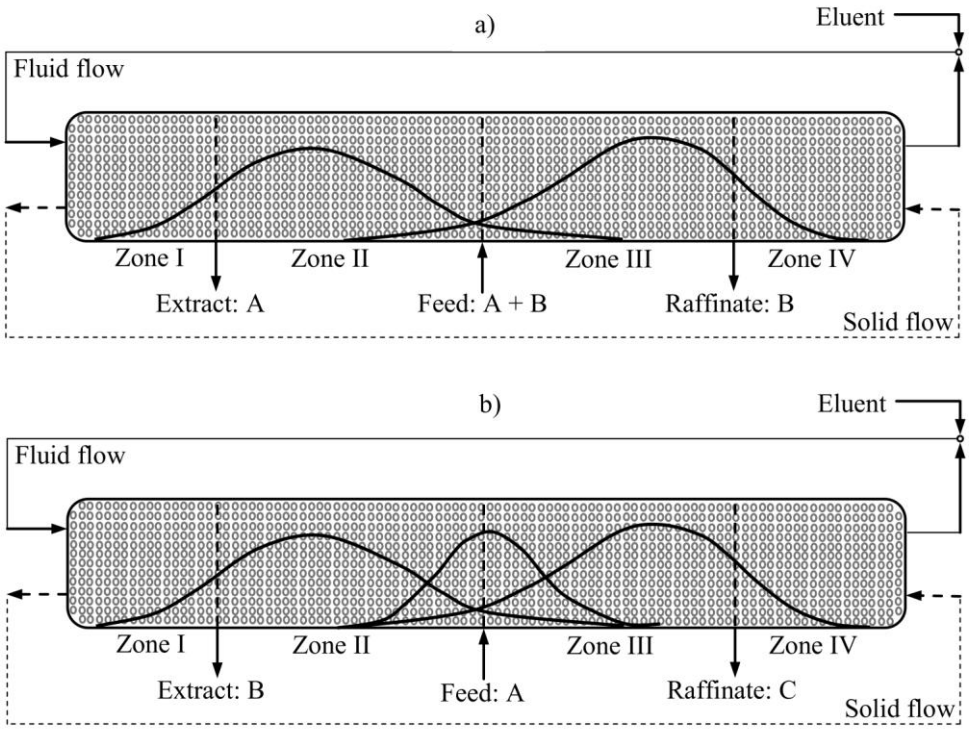

Figure 6.1: Countercurrent chromatography: a) TMB for separation of A and B. b) TMBR for the reaction A ⇌ B + C.

In spite of the simple description presented above, this process is not successfully applied for all reaction systems. For instance, Fricke et al. [17] reported some parameters range, such as kinetic and equilibrium parameters, in which this technology could be applied.

The major drawback of the TMBR is the difficulty of operating the solid stream: high energy demand, and challenging to ensure plug flow. Moreover, the movement of the particles can cause abrasion, which leads to a drop in the TMB efficiency. In order to overcome this drawback, a novel technology emerged: the Simulated Moving Bed (SMB). Patented in 1961 by Broughton and Gerhold [18], the SMB simulates the movement of the solid by changing the positions of the inlet and outlet streams. The first SMB design is shown in Figure 6.2. The column was divided into 12 sections connected to a multichannel valve, where the inlet (F, E) and outlet streams (X, R) are selected. In the end of each switching time (t_{switch}^{SMBR}), each stream moves one column ahead in direction of fluid flow. The SMB is similar to a TMB if the following equivalences are respected:

$$Q_{solid,TMB} = (1 - \varepsilon_b) V_{section} / t_{switch}^{SMBR} \tag{6.6}$$

$$Q_{fluid,SMB} = Q_{fluid,TMB} + Q_{solid,SMB} \tag{6.7}$$

where Q is the flow rate, ε_b is the bed porosity, and $V_{section}$ is the volume of the section between each pair of inlet and outlet streams.

Besides the similarities, it is worth to notice that the main difference is that the SMB does not reach a static steady state, but a dynamic cyclic steady state. However, Ruthven and Ching [7] claim that for a SMB with 2-4 columns per section the oscillation on Raffinate and Extract concentrations are smooth.

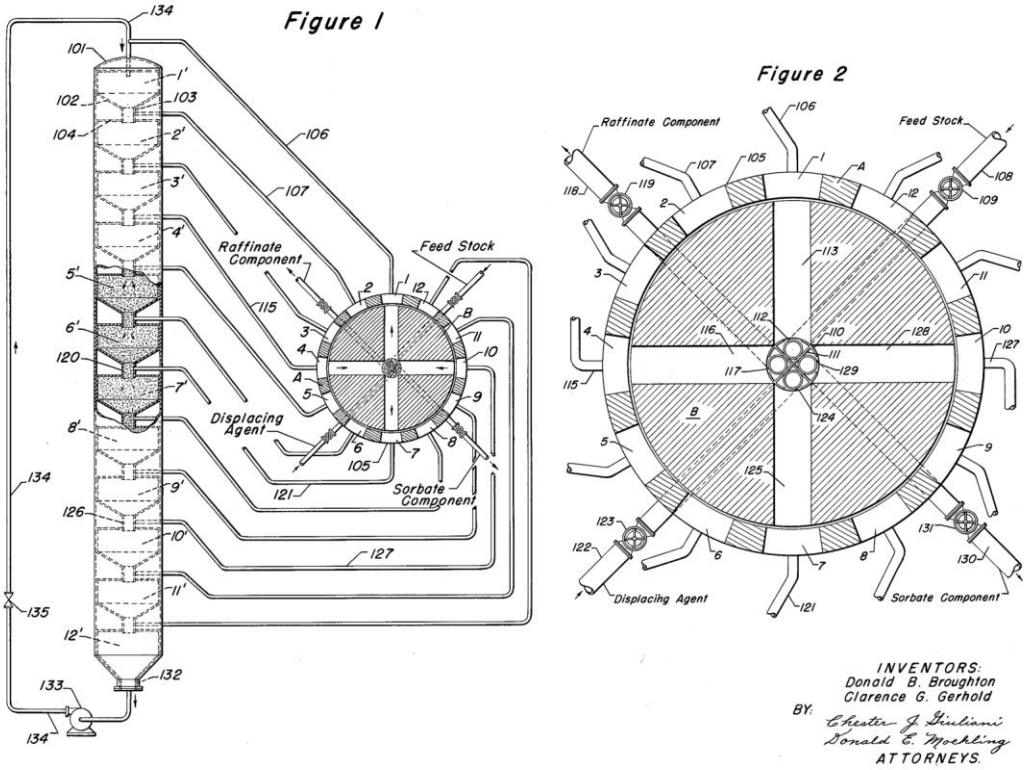

Figure 6.2: First SMB unit designed and patented by Broughton and Gerhold [18].

Nowadays, SMB technology has a large number of applications for the separation of several systems [19-26]. For example, the Sorbex^{TM} process developed by UOP Inc. is well widespread in different applications: separation of *p*-xylene (Parex^{TM}) [27] or *m*-xylene and ethylbenzene (Ebex^{TM}) from C_8 isomers [28], or the separation of fructose from corn syrup (Sarex^{TM}) [29].

After the dissemination of SMB, the concept of simulated moving bed reactor (SMBR) rapidly rose up as an interesting intensification process [30-37]. In 1983, Hashimoto et al. [38] proposed a system combining the SMB and the enzymatic reaction for high-pure fructose (45-65%), which was the first non-conventional SMBR. In this non-conventional configuration there is only one outlet stream (Raffinate) and the reaction is carried out in an alternating configuration of reactor and adsorption units. Afterwards, more configurations emerged and several applications for the SMBR were found: the synthesis of bisphenol A [39], production of acetals [40-47], sugar isomerisations [48-50], among others [51-59]. In our group, Rodrigues et al. have successfully conducted several works for SMB and SMBR applications [34, 40-45, 47-50, 60-70].

In this chapter, a SMBR unit will be designed to enhance the direct synthesis of DMC. In addition, it will be proposed a SMBR design approach starting from the equilibrium theory, and then refined based on

simulations. These simulations will be based on the experimental data collected so far: mass transfer, adsorption over zeolite 3A, reaction kinetics over cerium oxide, and reaction equilibrium. Then, a simple optimization is proposed to maximize the ratio between conversion, purity and adsorbent consumption. This approach attempts to obtain a quick assessment of the potentials and weaknesses of an SMBR process for the DMC production. However, before the SMBR design, simpler configurations to enhance the DMC equilibrium yield will be explored: simultaneous reaction and adsorption in batch (Scenario 1); batch reactor with external adsorption (Scenario 2); alternating reaction and adsorption in fixed bed columns (Scenario 3). This work also aims to better understand and quantify the potential of zeolite 3A in process intensification.

6.2. Methodology and Numerical Approach

In this chapter is studied the intensification process for the direct synthesis of DMC. As mentioned in the previous chapters, the idea is to partially remove water from the reacting mixture by adsorption on the surface of zeolite 3A.

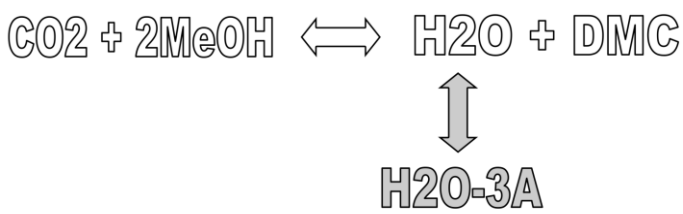

Scheme 6.2: Water removal by adsorption on zeolite 3A.

Based on the Le Chatelier's principle, with the removal of one of the products (from the reaction medium) by adsorption, the reaction will progress in the right direction to establish a new equilibrium condition, imposed by Thermodynamics. Mathematically, the reaction equilibrium constant (assuming ideal gas behaviour) can be expressed as [71]:

$$K_{eq}(T) = \frac{x_{DMC} \cdot x_{Water}}{x_{CO_2} \cdot (x_{MeOH})^2} \frac{P^o}{P} \tag{6.8}$$

where, K_{eq} is the equilibrium constant (function of temperature, T), x_i is the molar fraction of component i, P and P^o are respectively the absolute actual and standard pressures. Thus, if water is removed from the reaction mixture, the DMC fraction would increase in order to satisfy the value of the equilibrium constant imposed by the thermodynamic restrictions.

The goal of this work is to study several configurations, between reaction and adsorption, to improve the DMC yield and to quantify this improvement. In addition, this study will be helpful to identify the weaknesses of the proposed models and define the directions to take for a novel intensification process.

The strategy applied to reach these goals consists in the simulation of the different scenarios using the experimental data collected until now. First, the design of each process is specified and the mathematical

model is developed: adsorption and reaction equilibrium, mass transfer, and reaction kinetics. Then, each design is assessed by solving its mathematical model. Since no experimental data are available to validate the models, the simulations are preferably carried out within the range of conditions studied in the previous chapter; increasing then the confidence on the results. However, due either to some restrictions of the model or to the objective of improving the performance, some simulations were carried "out of the range of confidence".

The simulations were performed using either MatLab® (version R2010a) or gPROMS ModelBuilder® (version 3.6.0). MatLab® was used in Section 6.3 to solve algebraic and ordinary differential equations systems (*ode45* routine with a relative tolerance of 10^{-5}). The gPROMS software was especially helpful in section 6.4, 6.5, and 6.6 for solving iterative cycle problems with partial differential equations. The axial direction was discretized in 50 points, using the finite difference subroutine *CFDM*. The remaining differential-algebraic problem was solved with the aid of the *DASOLV* routine, using the *BDNLSOL* program to tackle the nonlinear algebraic equations. An absolute and a relative tolerance of 10^{-5} were used throughout.

6.3. Scenario 1: Batch Reaction with Adsorption

As mentioned above, this chapter aims to evaluate different process designs to attempt the improvement of the DMC yield, promoted by the selective adsorption of water on zeolite 3A surface. The first scenario studied is a batch process where reaction and adsorption take place at the same conditions. The goal of these simulations is to quantify the adsorbent capacity to improve the equilibrium conversion. Some water is transferred from the reaction mixture towards zeolite 3A surface, since it is more selective to water. The model of reaction with adsorption, neglecting mass transfer, is given by the following ordinary differential equation:

$$\frac{dC_i}{dt} = \frac{\vartheta_i \cdot r \cdot m_{cat}}{V_r \cdot \left[\varepsilon_b + (1-\varepsilon_b)\cdot \varepsilon_p + K_{ads,i} \cdot (1-\varepsilon_p)\right]}; C_i(t=0) = C_0 \qquad (6.9)$$

where C_i is the concentration of compound i in the bulk, t is the time, ϑ_i is the stoichiometric coefficient of compound i, r is the reaction rate, V_r is the reaction volume, ε_b is the bulk porosity, ε_p is the zeolite 3A particle porosity, and $K_{ads,i}$ is the slope of the adsorption isotherm of each compound on the zeolite surface. The reaction rate and the adsorption equilibrium were experimentally determined in Chapters 4 and 5, respectively. To ensure a proper evaluation of the effect of the adsorbent, the results were compared to simulation with no adsorption ($K_{ads} = 0$). In addition, the simulations were carried out using standard conditions (equal to the ones used on the kinetic experiments section): pressure of 20 MPa; temperature range between 383 K and 403 K; reactor volume fixed at 0.5 L; and a carbon dioxide to methanol initial ratio of 2.5. In addition, the estimation of the carbon dioxide concentration in solution was based on its pure concentration, calculated by Soave-Redlich-Kwong equation of state: 8.48 mol·L^{-1} at 373 K, 7.88 mol·L^{-1} at 383 K, 7.38 mol·L^{-1} at 393 K, and 6.93 mol·L^{-1} at 403 K, multiplied by its volume fraction in the solution. All these parameters are within the range studied in the kinetic experiments.

The amount of adsorbent should be maximized in order to increase the DMC yield. For a fixed bed, packed with homogeneous spheres, the value of bulk porosity is approximately 0.4. Herein, it is proposed a stirred reactor and therefore the bulk porosity should be higher in order to be able to promote agitation. A bulk porosity (ε_b) of 0.55 (225 mL of zeolite 3A) was considered.

The amount of catalyst was specified in order to reach the equilibrium in 24 hours; for each temperature, the amounts considered were: 35 g for 373 K, 12 g for 383 K, 5 g for 393 K, and 2 g for 403 K. Low temperatures benefits the DMC yield; however, the decrease of temperature leads to an exponential increase of the amount of catalyst required to have equal reaction rate.

With these parameters, the evolution of DMC along the time was simulated, by solving Equation 6.9. These results are shown in Figure 6.3 at different temperatures. As can be observed, the increase of temperature has a negative effect on the equilibrium yield (without adsorption) and on the adsorbent performance, which was already expected because both reaction and adsorption are exothermic processes. Even though, the benefits of coupling adsorption with reaction in the same unit are clear; the removal of water from the reaction mixture improves the DMC yield at equilibrium in: 24% at 373 K, 20% at 383 K, 17% at 393 K, and 14% at 403 K.

In the previous simulations, the mass transfer resistances were neglected. Herein, the internal mass transfer coefficient (k_{int}) is introduced in order to check this assumption. Thus, Equation 6.9 is replaced by the following equations:

$$\frac{dC_i}{dt} = \frac{\vartheta_i \cdot r \cdot m_{cat}}{V_r \cdot \varepsilon_b} - \frac{3}{r_p} \cdot k_{int,i} \cdot \left(C_i - \overline{C_{p,i}}\right) \cdot \frac{(1-\varepsilon_b)}{\varepsilon_b} \tag{6.10}$$

$$\frac{3}{r_p} \cdot k_{int,i} \cdot \left(C_i - \overline{C_{p,i}}\right) = \frac{d\overline{C_{p,i}}}{dt} \cdot \left[\varepsilon_p + K_{ads,i} \cdot \left(1-\varepsilon_p\right)\right] \tag{6.11}$$

$$t = 0 \Rightarrow C_i = \overline{C_{p,i}} = C_0 \tag{6.12}$$

where, r_p is the zeolite particle radius (1 mm), and $\overline{C_{p,i}}$ is the average concentration inside the particle. The internal mass transfer was estimated by the Wilke-Chang correlation (Eq. 5.33).

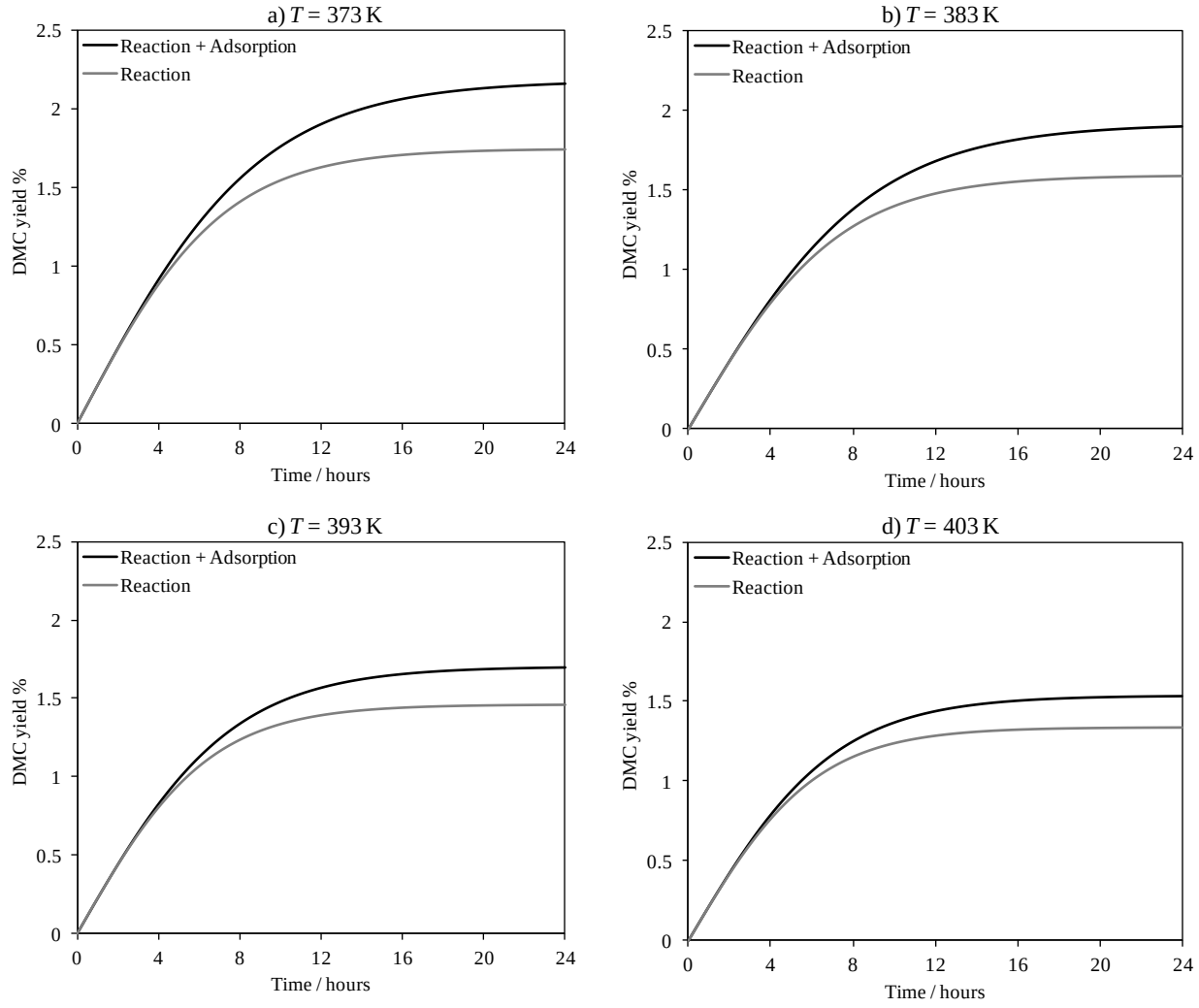

Figure 6.3: Simulation of DMC yield along time in a batch reactor at different temperatures. Conditions: 500 ml, 20 MPa, 225 mL of adsorbent, n_{CO_2}/n_{MeOH} = 2.5/1.

In Figure 6.4 are depicted the bulk and the average particle molar fraction of water and DMC as function of time. For both, DMC and water, the bulk and particle curves are coincident, which means that mass transfer resistance can be neglected. Due to the higher adsorption capacity for water, its concentration in the fluid (bulk and particle pores) is lower than the DMC concentration. This phenomenon is the explanation of the higher DMC yield previously observed; the DMC molar fraction increases to compensate the decrease of water concentration.

These simulations showed that the *in situ* adsorption of water can increase the DMC yield. In spite of the relative high increase of DMC yield (24% at 373 K and 20 MPa), the DMC yield is still very low (<2.5%). This is not enough, given the fact that, at these conditions, the DMC molar fraction is lower than 0.9% (CO_2 free basis), and also that DMC-methanol form an azeotropic mixture between 2.6 mol% (1.519 MPa) and 13.2 mol% (0.101 MPa) of DMC [72, 73]. Thus, a DMC molar fraction above the azeotropic composition is required for further purifications *via* simple distillation. In conclusion, reaction and adsorption should be carried out separately because of the high difference of operating temperature.

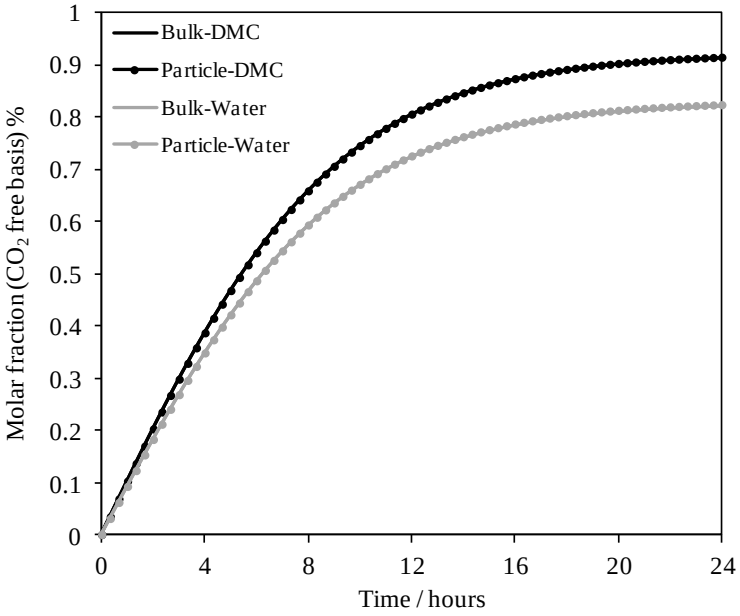

Figure 6.4: DMC and water molar fraction (bulk and particle) along time. Conditions: 500 ml, 20 MPa, 373 K, 225 mL of adsorbent, $R_{CO_2/MeOH}$ = 2.5.

6.4. Scenario 2: Batch Reaction with External Adsorption in Fixed Bed Column

Herein is proposed the direct synthesis of DMC by a semi-continuous process involving a continuous stirred tank reactor and two fixed bed columns (filled with zeolite 3A) with the objective of trapping the water produced by working in two alternating operating modes: adsorption and regeneration. Two heat exchangers are needed due to the temperature difference between reaction and adsorption. In Figure 6.5 is shown the flow diagram where column 1 is operating in adsorption mode and column 2 in regeneration mode. The circulating pump is merely figurative since no pressure drop is considered; and the reactor and adsorption models are the ones used in the previous Chapters 4 and 5, respectively. The simulations to evaluate this concept were carried out considering the following assumptions:

- ❖ No pressure drop was considered.
- ❖ There is a set of separation units able to purify DMC and water, and recover the unreacted carbon dioxide and MeOH.
- ❖ The flow rate change in the heat exchangers is mainly caused by the expansion/compression of CO_2 with the change of temperature.
- ❖ No dead volume was considered for the heat exchangers.

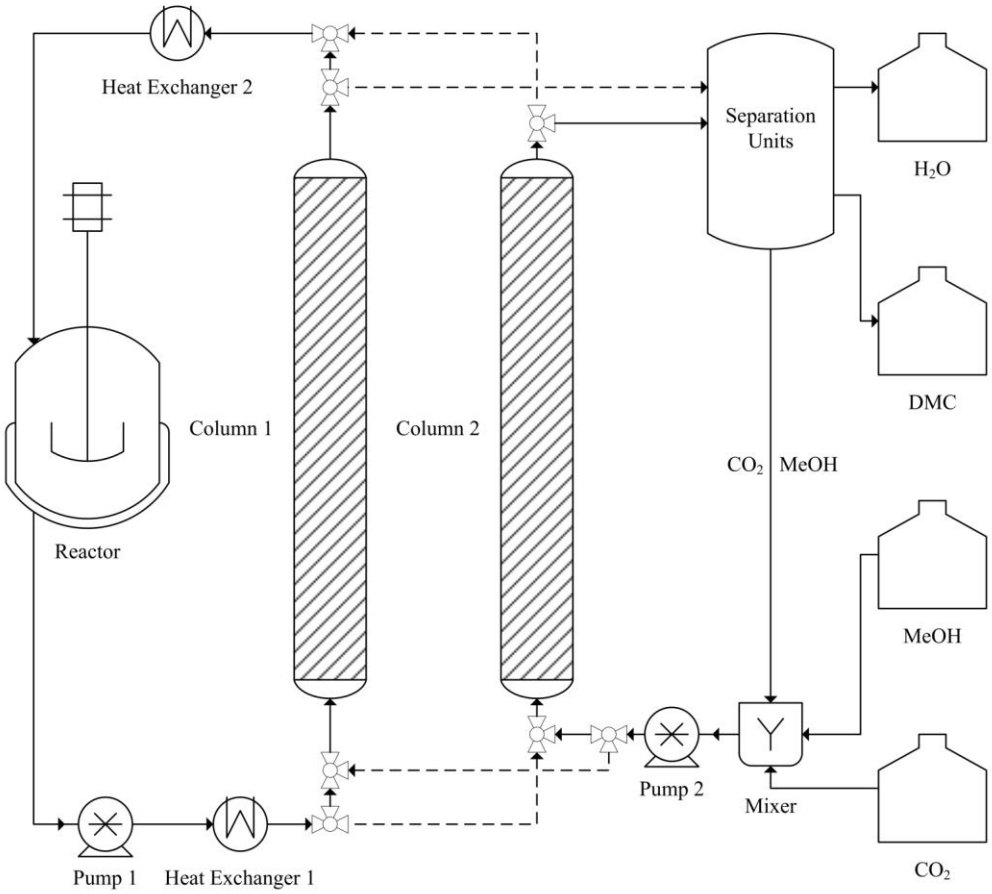

Figure 6.5: Flow diagram of a semi continuous process for direct synthesis of DMC.

The energy balance was not considered, and therefore, the heat exchangers units were modelled as simple expansion/compression units:

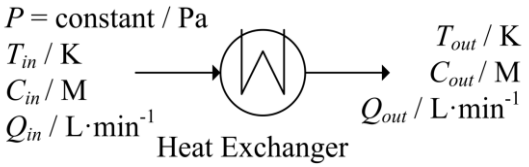

Scheme 6.3: Heat exchanger

$$C_{out} = \beta \cdot C_{in}\text{, where } \beta = \frac{C_{CO_2}(P, T_{out}, \text{pure}) + R_{CO_2/MeOH} \cdot C_{MeOH}(P^o, T^o, \text{pure})}{C_{CO_2}(P, T_{in}, \text{pure}) + R_{CO_2/MeOH} \cdot C_{MeOH}(P^o, T^o, \text{pure})} \tag{6.13}$$

$$Q_{in} \sum C_{in} = Q_{out} \sum C_{out} \tag{6.14}$$

As mentioned above, each column operates in alternating cycles of adsorption and regeneration; the total amount of DMC produced ($n_{DMC,T}$) is the sum of the DMC amount trapped in the column operating in adsorption cycle mode ($n_{DMC,cycle}$), plus the total DMC amount recovered in the regeneration mode ($n_{DMC,recov}$).

$$n_{DMC,T} = n_{DMC,cycle} + n_{DMC,recov} \tag{6.15}$$

The amount of DMC trapped in the cycle can be calculated by the following equations:

$$n_{cycle} = C_r \cdot V_r + \overline{C_b} \cdot V_{ads} \cdot \varepsilon_b + \overline{C_p} \cdot V_{ads}(1-\varepsilon_b)\varepsilon_p + \bar{q} \cdot V_{ads}(1-\varepsilon_b)\left(1-\varepsilon_p\right) \tag{6.16}$$

$$\bar{X} = \int_0^1 X\,(z) \cdot dz \;\; \left(X = \; C_b\,, C_p\,, q\right) \tag{6.17}$$

where C_r is the concentration in the reactor; V_r is the reactor volume; $\overline{C_b}$, $\overline{C_p}$, and $\bar{q}$ are the average concentrations in the bulk, pores and solid phase of the fixed bed column, respectively; V_{ads}, ε_b, and ε_p are the volume, bulk and particle porosities for the fixed bed columns.

The total amount of DMC, or other component, recovered in the regeneration step is calculated by the integral of the molar flux at the outlet stream of the column that is operating in regeneration mode:

$$n_{recov} = \int_0^{t_{final}} Q \cdot C_b\left(t_{(z=1)}\right) \cdot dt \tag{6.18}$$

The total amount of the limiting reactant ($n_{lim,T}$) is equal to its initial amount ($n_{lim,i}$) plus the total amount added to compensate the amount consumed by the reaction ($n_{lim,added}$).

$$n_{lim,T} = n_{lim,i} + n_{lim,added} \tag{6.19}$$

where the initial amount is calculated by the balance to the reactor and the adsorption columns:

$$n_i = C_{r,i} \cdot V_r + V_{ads} \cdot \left[\overline{C_{b,i}} \cdot \varepsilon_b + \overline{C_{p,i}}(1-\varepsilon_b) \cdot \varepsilon_p + \overline{C_{p,i}} \cdot K_{ads,i}(1-\varepsilon_b)\left(1-\varepsilon_p\right)\right] \tag{6.20}$$

While the amount of limiting reactant to be added is calculated by the difference between the amounts fed and recovered in the outlet stream of the column in regeneration mode:

$$n_{added} = \int_0^{t_{final}} Q_{feed} \cdot C_{feed}(t) - \left[Q \cdot C_b(t)\right]_{z=1} dt \tag{6.21}$$

Then, with the total amount of DMC produced and the total amount of the limiting reagent it is possible to calculate the reaction conversion (X_c) by the following relation:

$$X_c = \frac{|\vartheta_{lim}| \cdot n_{DMC,t}}{n_{lim(t=0)}} \tag{6.22}$$

6.4.1. Single column without regeneration

In order to define the model parameters for the cyclic configuration (flow rate and switching time) it is necessary to know the dynamic behaviour without regeneration. The set of parameters and variables defined is presented in Table 6.1. The pressure, reaction temperature and reactants ratio were set within the range studied in the kinetics section (Chapter 4). The highest pressure studied (20 MPa), and the lowest temperature (383 K) were considered for the simulation in order to relax the thermodynamic limitations. For the adsorption columns, a temperature of 298 K (near but out of the range previously studied, 313-353 K) was assumed, and then, the mass transfer coefficients of water and DMC were estimated by the Dean and Stiel correlation [74] for the viscosity, and Wilke and Change for the diffusion coefficient (Eq. 5.33), assuming only internal resistances to mass transfer. Other variables, such as the mass of catalyst, and the volume of the reactor and adsorption columns were assumed without further studies; the flow rate was the only variable assessed.

Table 6.1: Parameters and variables defined for the simulations of Scenario 2.

General		Heat Exchanger	
P / MPa	20	β	1.62
$R_{CO2/MeOH}$	1		
Reactor		**Fixed bed column**	
V_r / L	0.5	V_{ads} / L	5
T_r / K	383	T_{ads} / K	298
$C_{init.}$ / mol·L^{-1}	[11.55, 2.31, 0, 0]	Pe	100
Q / mL·min^{-1}	10, 100, 1000	k_L / mm·min^{-1}	[∞,∞, 0.52, 1.3]
m_{Cat} / g	250	ε_b	0.4

The simulation results are depicted in Figure 6.6, where it can be seen the evolution of the DMC and water concentrations inside the reactor and in the feed stream to the reactor. The effect of the flow rate in the dynamic behaviour is clear: at 1000 mL·min^{-1} the inside and feed concentration curves are almost overlapping. As the flow rate decreases, the delay between water and DMC curves increases which open some possibilities for the efficient DMC production by the proposed cyclic adsorption/regeneration system. At 100 mL·min^{-1}, it is observed a delay over 3 hours for the water coming from the outlet stream of the adsorption column, which leads to the oscillating behaviour observed in the graph. For a flow rate of 10 mL·min^{-1}, some water content in the reactor feed just appears after about 25 hours. In all cases, the difference between DMC and water concentration in the equilibrium is noticed, which is caused by the higher adsorption of water in zeolite 3A column.

In conclusion, the continuous decrease of the flow rate increases the delay, but it should be mentioned that, for a certain flow rate value, the external mass transfer resistance (that was considered constant) will become significant and will drastically increase the dispersion within the column affecting by this way its performance.

Nevertheless, due to the better results obtained, the flow rate of 10 mL·min^{-1} will be the one considered for the following study, where two parallel columns with regeneration are considered.

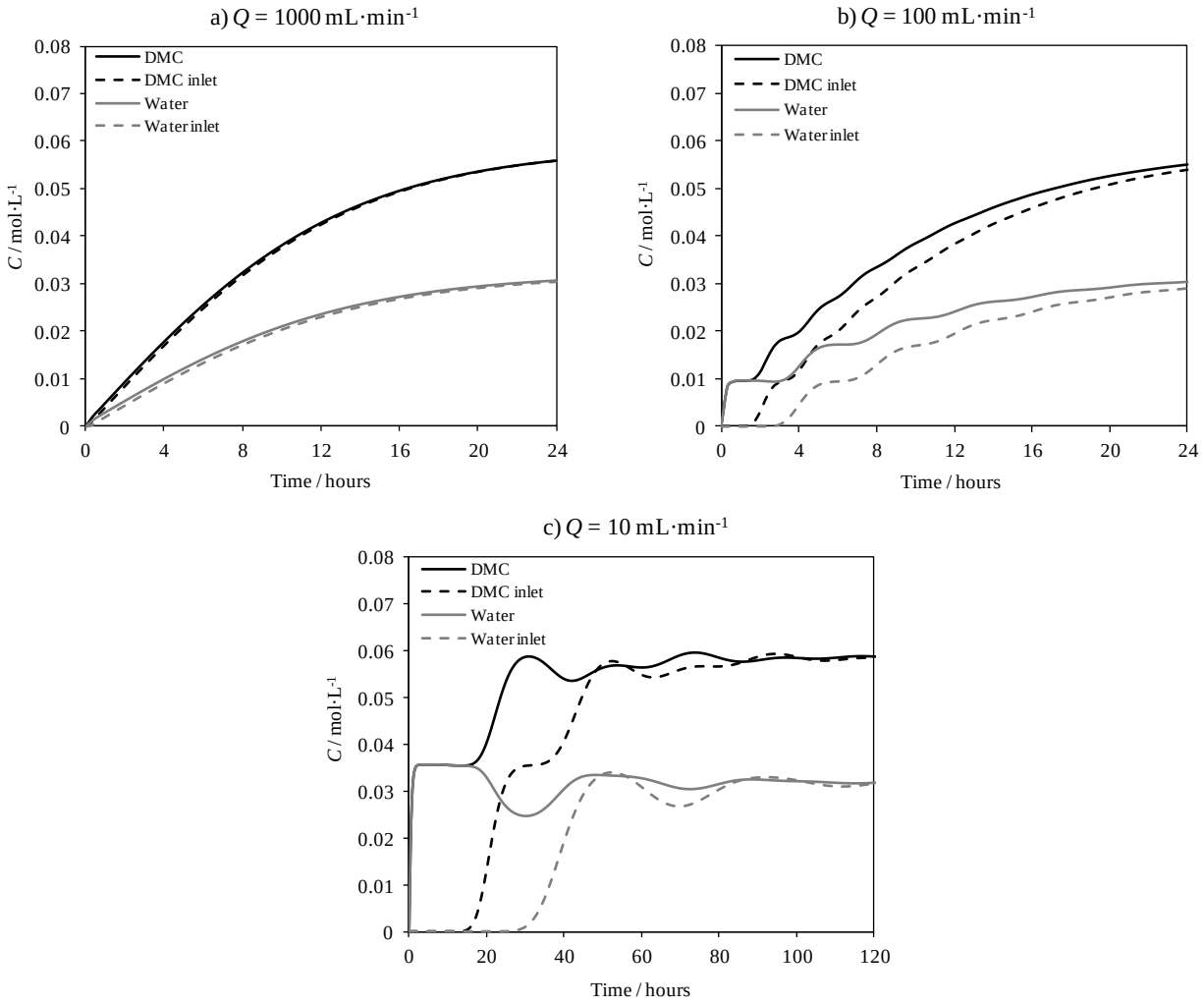

Figure 6.6: Inlet and inside concentration of DMC and H_2O in the reactor along time. The operating parameters are presented in Table 6.1.

6.4.2. Two parallel columns with regeneration

In this section, the concept of two columns working in different modes is explored: one column (column 1) is connected to the reactor in order to remove water from the reaction mixture; while the other column (column 2), in regeneration mode (by feeding carbon dioxide and methanol), avoids the "contamination" with water of the reactor feed stream by sending its outlet stream to a set of separation units. After the complete regeneration of column 2 and before the complete saturation of column 1, a new cycle starts, where the columns are switched: column 1 is now in regeneration mode, while column 2 is connected to the reactor. The simulations were performed using the same parameters as in the *single column without regeneration* simulations (see Table 6.1). As mentioned before, the flow rate was set at 10 mL·min^{-1}, and therefore a switching time of 25 h was considered since after this time water starts to elute. Furthermore, a new variable

was introduced, the regeneration flow rate, which was set at 100 $mL \cdot min^{-1}$ with concentration equal to the initial in the column to guarantee that the column will be completely regenerated before the next switch. The optimization of the flow rate is out of the scope of this work. Herein, we considered a value that could guarantee the complete regeneration in 25 h (before the next switch), but in a real situation this variable should and must be optimized to reduce pumping costs.

In Figure 6.7, the DMC yield is represented as function of time, during the first 10 cycles, with and without adsorption in the fixed bed columns. The vertical lines separate periods between switching times. It can be seen that the DMC yield increases along the time, showing an instantaneously decrease in the beginning of each cycle. This decrease is explained by the introduction of more limiting reactant, which leads to a decrease of its conversion (Equation 6.8): semi-continuous process. As can be observed, the concept without any adsorption, where part of the reaction product is separated from the reaction mixture and replaced by fresh reactants, would be possible to implement. However, the DMC would be lower in that case since some water – that is not retained in the column – would be fed to the reactor limiting the equilibrium conversion. It is clear that, with adsorption, the DMC and water amounts retained are higher which leads to a more sustainable separation: around 12.5% of DMC yield is reached with adsorption after 10 cycles, while only around 5% (2.5 times lower) is expected with no adsorption.

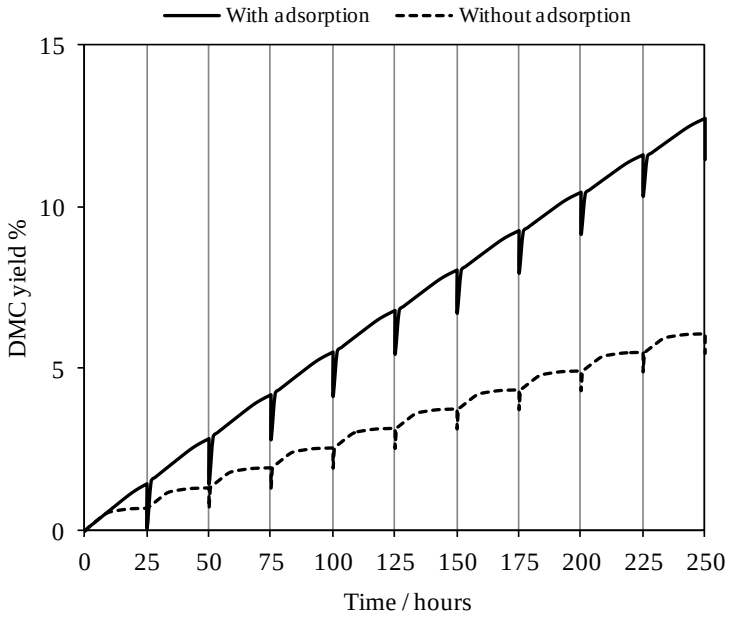

Figure 6.7: Evolution of DMC yield with the time.

In Figures 6.8 and 6.9, the water and DMC concentrations in the outlet stream of each column are represented along time. In the first cycle of the simulation, column 1 is connected to the reactor. As can be seen, water is mainly removed in the regeneration step, only water traces are fed to the reactor. DMC is in recirculation since it is not completely retained in the fixed bed column. After the second cycle the system reaches the cyclic steady state.

Additional information is shown in Figure 6.10, where the concentrations of DMC and water inside the reactor and at the inlet stream are plotted as function of time. It can be observed a delay of DMC in the inlet stream equal to the average residence time, and only traces of water content fed to the reactor.

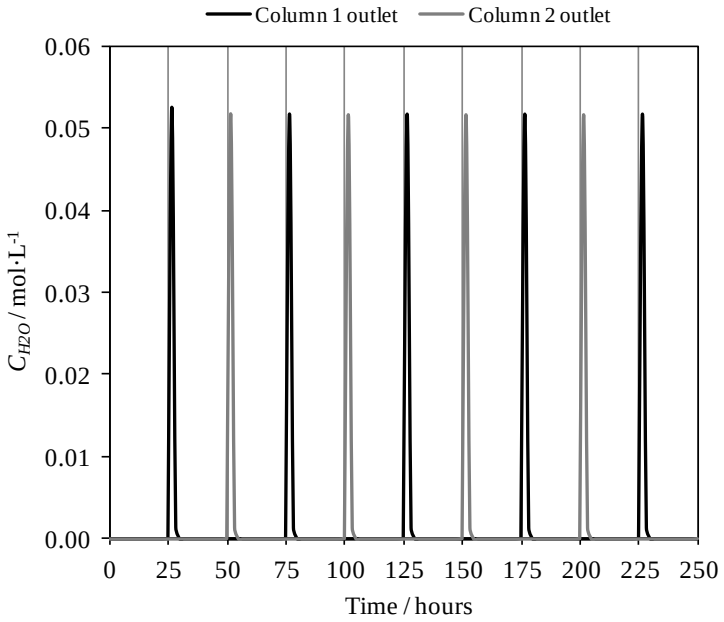

Figure 6.8: Evolution of H_2O concentration at the outlet stream of each column.

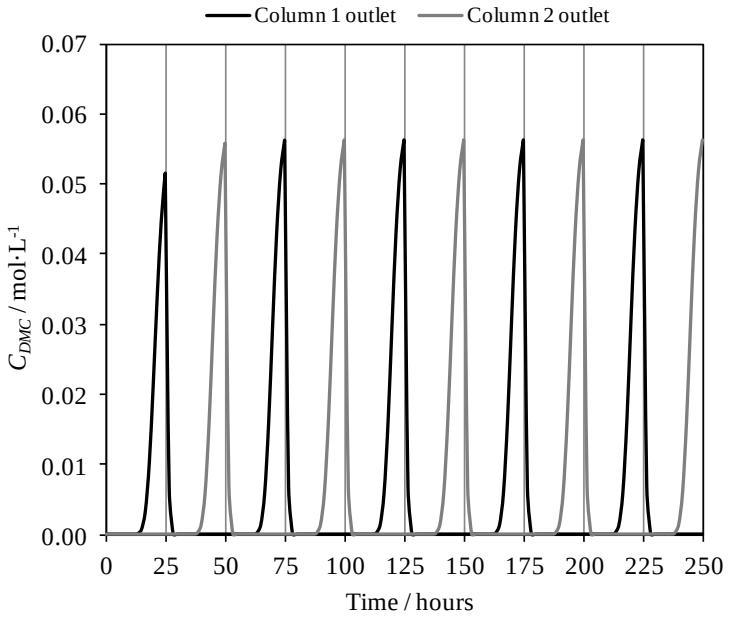

Figure 6.9: Evolution of DMC concentration at the outlet stream of each column.

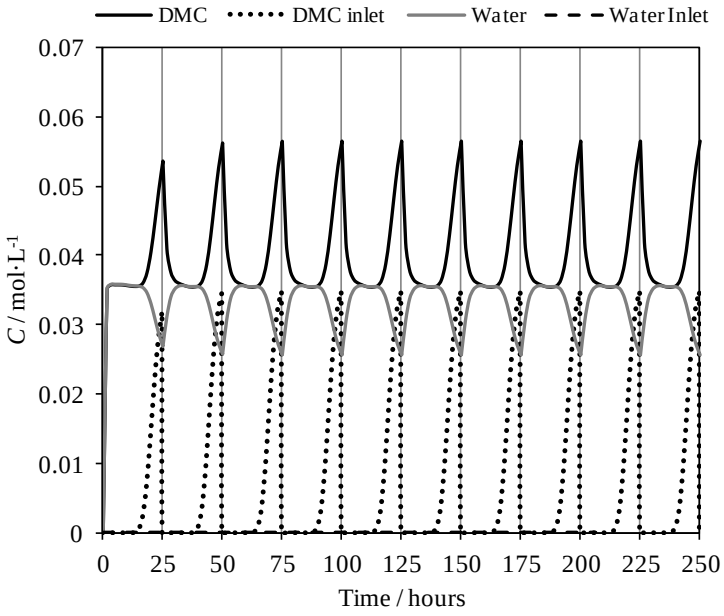

Figure 6.10: Inlet and inside reactor concentrations of DMC and H_2O along time.

6.4.3. Scenario 2 overview

The main goals of this section were to theoretically evaluate if it is possible to improve the DMC yield by coupling adsorption and reaction, and to understand if the implementation of such a process is feasible from a practical point of view. By running successive simulations, it was shown that the constant removal of water leads to an increase of the equilibrium yield, as it is predicted by the Le Chatelier's principle. Indeed, Figure 6.11 shows that a DMC yield up to 90% would be reached after 1000 cycles (~3 years) with the proposed process. Previously, it was observed that it is possible to shift the DMC yield from 2% up to 12.5% within 10 cycles. In summary, the simulations showed that combining adsorption and reaction would enhance the DMC yield, which is strongly conditioned by thermodynamic limitations; however, the very low productivity of this scenario turns it unfeasible.

Besides the low productivity, this process has two main drawbacks that might difficult its industrial applicability:

- Although part of the energy would be able to be recovered by heat integration, a huge supply of energy would still be needed because of the temperature difference between adsorption (298 K) and reaction (383 K) steps in heating and pumping equipments.
- The DMC and water recovery from the regeneration column outlet stream, due to the very low DMC and water concentrations (~0.3 $mol \cdot L^{-1}$), would also require an excessive amount of energy with probably low efficiency.

Therefore, novel configurations are required in order to have similar conversions but producing DMC and water at higher concentrations.

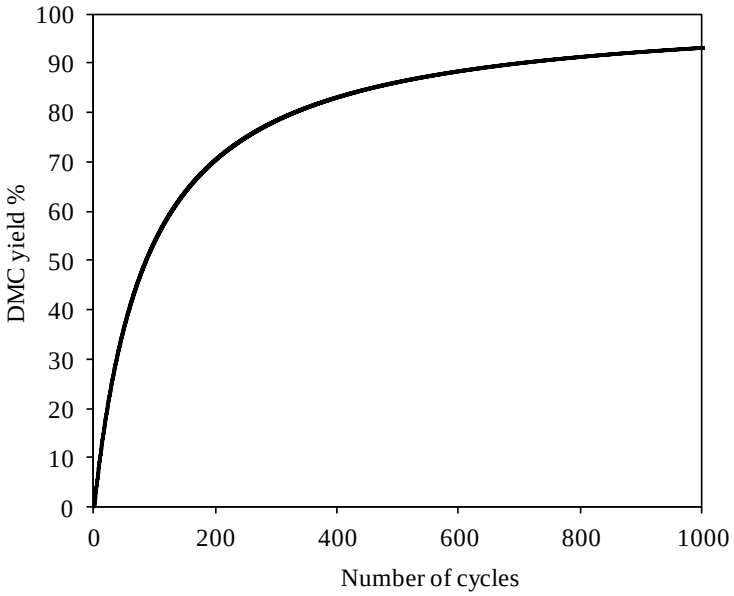

Figure 6.11: Effect of the number of cycles in the DMC yield.

6.5. Scenario 3: Series of Alternating Reaction and Adsorption Columns

The main goal of this work is to develop a SMBR to improve the reaction yield. Before that, a simpler configuration is proposed: a series of alternating reaction and adsorption columns. This configuration, depicted in Figure 6.12, may be seen as a representation of the reactive zone of a TMBR, although there is no countercurrent flow of the solid. In Figure 6.12a is shown the ideal scenario multilayer reactor; however, since the reaction and adsorption should be carried at different temperatures a heat exchanger between each column is needed (Figure 6.12b). This configuration is far from being sustainable due to the large number of heat exchangers and to the low efficiency of heating/cooling after each column. However, this theoretical study might point out if in a hypothetical scenario where adsorption and reaction were carried out at the same conditions, the sorption enhanced reaction would considerably improve the direct synthesis of DMC.

The mathematical model for the fixed bed reactors is detailed in Table 6.2; a typical one dimension model with axial dispersion is proposed. Besides, neither pressure drop nor mass transfer resistance were considered, based on the low reaction rates reported in Chapter 4.

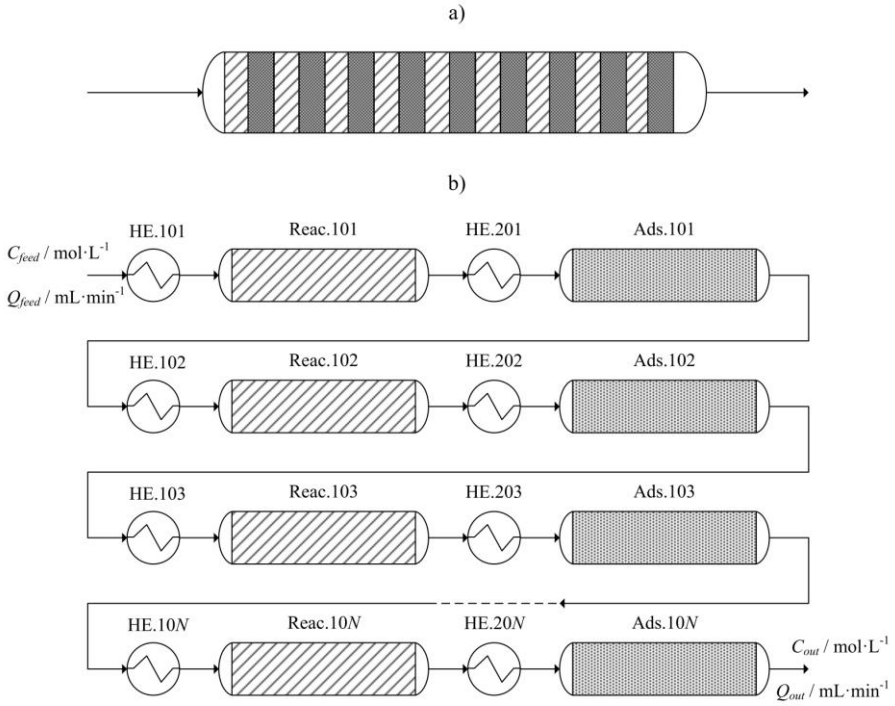

Figure 6.12: Alternating reaction and adsorption columns in series: a) ideal design; b) actual design.

In order to achieve more reliable results, the simulations were carried out at similar conditions of the pulse response experiments: flow rate (298 K) of 10 mL·min^{-1}, and a fixed superficial velocity of 0.2 cm·s^{-1}; the adsorption and reaction temperatures were fixed at 298 K and 383 K, and the respective axial dispersion coefficients were estimated and are equal to 0.55 cm^2·s^{-1} and 0.11 cm^2·s^{-1}, based on the results reported in Chapter 5. Furthermore, a pressure of 20 MPa and a methanol to carbon dioxide ratio equal to one were assumed. The total volume of reaction was estimated so the reaction equilibrium was able to be reached. In Figure 6.13, the simulation of a fixed bed reactor at the mentioned conditions is presented. It is worth noting that a flow rate of 16.16 mL·min^{-1} was used, which corresponds to the final volume after the expansion predicted for a flow rate of 10 mL·min^{-1} from 298 K to 383 K. It can be observed from the graph that with a volume of 500 mL the equilibrium is almost reached.

Afterwards, 10 sections were considered, which may be a reasonable representation of the reactive zone of a SMBR; this leads to a reactor volume of 50 mL. In order to have a similar diameter to length ratio as the used in Chapter 5 (1/25) a velocity of 0.135 cm·s^{-1} was computed. At this velocity the diffusion still controls the overall mass transfer resistance. In Table 6.3 are summarized the main parameters values used in the simulations.

In Figure 6.14a is shown the concentration history of DMC at the outlet for different volume ratios between reaction and adsorption. In all cases, it can be seen a roll-up on DMC curve which is caused by the delayed water wave inside the columns. As supplementary information, the relative enhancement of DMC concentrations, in comparison with the steady state, is shown in Figure 6.14b. As the adsorption column volume increases, the roll-up also increases (6% for 5 mL, 11% for 10 mL, 17% for 20 mL, 20% for 30 mL,

and 22% for 40 mL); however, this increase is not linear, it shows a smooth tendency till a maximum value. This phenomenon is explained by both axial and mass transfer dispersive effects, which decrease the efficiency of the unit.

In fact, in order to obtain the best performance of an integrated unit, this unit should have similar rate of water production, by the catalyst, and adsorption, by the adsorbent. In order to have a better understanding of the proposed configuration, the average rate of water production and the average rate of water adsorption were calculated by the following equations:

$$\overline{rate}_{reaction} = (1-\varepsilon_b)(1-\varepsilon_p)\rho_{cat} \cdot V_r \cdot \int_0^1 r_{H_2O}(z)\, dz \tag{6.23}$$

$$\overline{rate}_{adsorption} = (1-\varepsilon_b)(1-\varepsilon_p) \cdot V_{ads} \cdot \int_0^1 \frac{\partial q_{H_2O}}{\partial t}(z)\, dz \tag{6.24}$$

Table 6.2: Mathematical model of a fixed bed reactor with axial dispersion.

	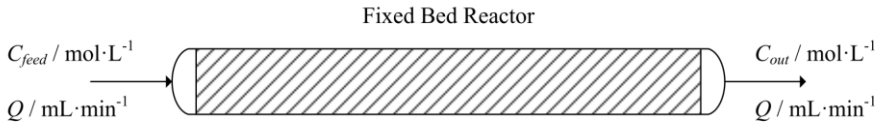	
Molar balance:	$\frac{\partial C_i}{\partial t}\frac{V}{Q}\left[\varepsilon_b + \varepsilon_p(1-\varepsilon_b)\right] + \frac{\partial C_i}{\partial z} - \vartheta_i \cdot r(1-\varepsilon_p)(1-\varepsilon_b)\frac{V}{Q}\rho_{solid} = \frac{1}{Pe}\frac{\partial^2 C_i}{\partial z^2}$	(6.25)
Initial conditions:	$C_i(t=0, \forall z) = C_i^{Eluent}$	(6.26)
Boundary conditions:	$C_i(\forall t, z=0) = C_i^{Feed}(t) + \frac{1}{Pe}\frac{\partial C_i}{\partial z}\Big\vert_{\forall t, z=0}$	(6.27)
	$\frac{\partial C_i}{\partial z}\Big\vert_{\forall t, z=1} = 0$	(6.28)
Reaction rate:	$r = \frac{k\left[x_{CO_2} \cdot x_{MeOH}^2 \cdot P^3 - \frac{x_{DMC} \cdot x_{H_2O} \cdot P^2 \cdot P^o}{K_{eq}}\right]}{\left(1 + \sum K_{ads,i}^{CeO_2} \cdot x_i \cdot P/P^o\right)^3}$	(6.29)
	$k = k_0 \cdot exp\left[-\frac{E_a}{R \cdot T}\right] \cdot exp\left[-\frac{\Delta v^{\#}(P - P_{ref})}{R \cdot T}\right]$	(6.30)
Chemical Equilibrium:	$K_{eq} = exp\left[-\frac{\Delta H_r}{R \cdot T} + \frac{\Delta S_r}{R}\right]$	(6.31)

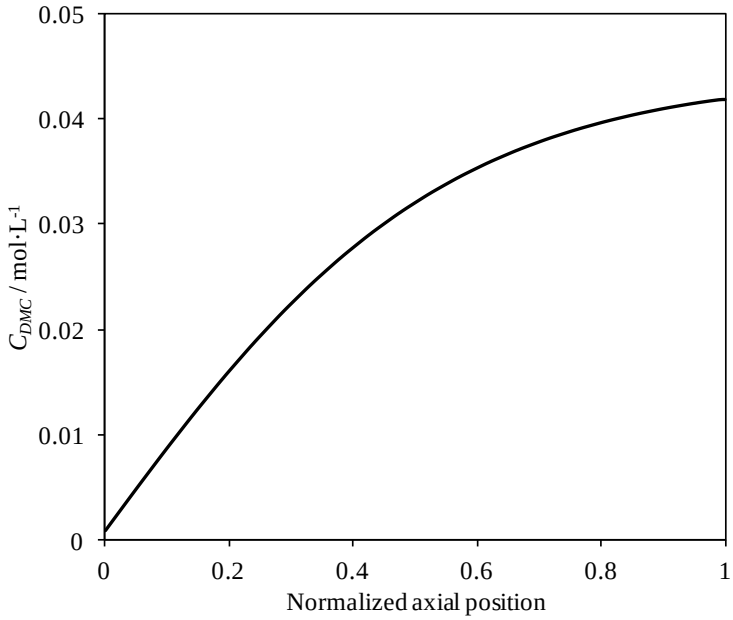

Figure 6.13: Concentration profile inside a fixed bed reactor (steady state). Conditions: 16.16 mL·min^{-1}, 383 K, 20 MPa, n_{CO_2}/n_{MeOH} = 1/1.

Table 6.3: Parameters and variables defined for the simulations of Model 3.

Number of columns (reac/ads)	10/10	P / MPa	20
$V_{Total\ reac.}$ / mL	500	β	1.616
V_r/V_{ads} / mL·mL^{-1}	50/5-50/40	Q / mL·min^{-1}	10 at 298 K (16.16 at 383 K)
D_{ads} / cm	1.03	Compounds	[CO_2 MeOH DMC H_2O]
D_r / cm	1.31	C_{feed} / M	[10.68 10.68 0 0]
T_r / K	383	k_L / mm·min^{-1}	[∞ ∞ 0.52 1.3]
T_{ads} / K	298	K_{ads}	[0 0 2.4 6.0]

In Figure 6.15 is illustrated the average rate of adsorption and production of water for the last columns. Moreover, the results for the simulation with reaction to adsorption volumes of 50 to 5 (Figure 6.15a) and 50 to 40 (Figure 6.15b) are compared. In the second graph, the peaks of rates are coincident, which means that the adsorption and reaction have similar rates leading to higher roll-up of DMC concentration as observed in the previous results. Contrarily to the $V_{r.}$ to V_{ads} ratio of 50 to 5, where there is a lag between the two curves.

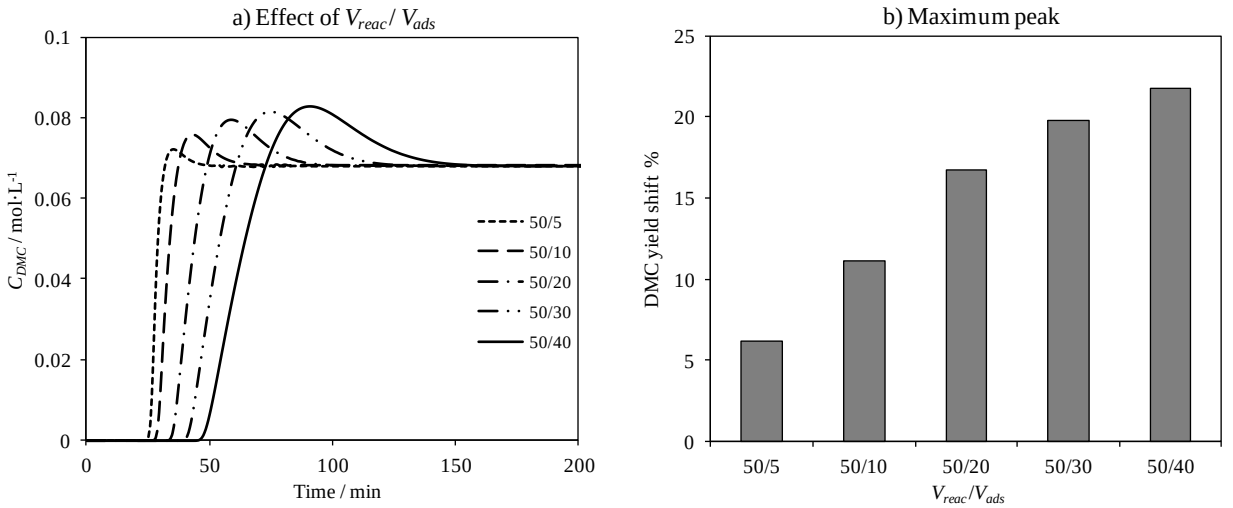

Figure 6.14: Simulation of the outlet DMC concentration along time for Scenario 3: 20 MPa, 10 mL·min^{-1} (298K), T_r = 383 K, T_{ads}= 298 K, n_{CO_2}/n_{MeOH}= 1/1. Other parameters in Table 6.3.

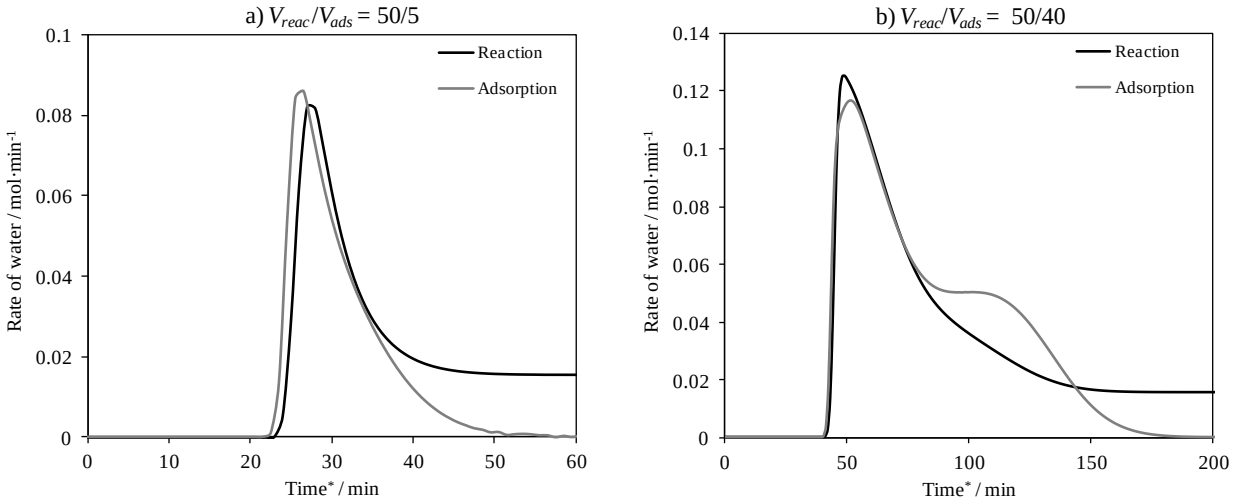

*for the adsorption curve it was considered a delay equal to the average residence time in the reactor.

Figure 6.15: Evolution of the average rate of water adsorption (on zeolite 3A) and production (on cerium oxide) at the last columns along the time.

6.6. Design of a SMBR

Several works are available elsewhere for the design of an SMB unit [12, 75-79]; however, few works have been reported on the design of an SMBR [48, 80] so far. Most of the works focus on the optimization of an existing unit, using single [81-83] or multiple [84-87] objective functions. Optimization with multiple objective functions is an interesting, but also complex methodology, handling with an infinite set of optimum solutions: the Pareto set [88]. Nevertheless, when a balance between several objective functions is desired this might be the best option. For simpler cases, and when it is possible, single optimization is encouraged because it is a simpler approach and gives a unique solution.

In this section the design of a TMBR is presented, based on the assessment of a corresponding TMBR. In addition, a unique objective function is proposed for the optimization of the unit. In Figure 6.16 is shown a sketch of the SMBR proposed for the direct synthesis of DMC. In this configuration, similar to the proposed by Hashimoto et al. [38], the reaction and adsorption occur in separate vessels; furthermore, the reactors are shifted as well as the stream positions, simulating only the movement of the adsorbent.

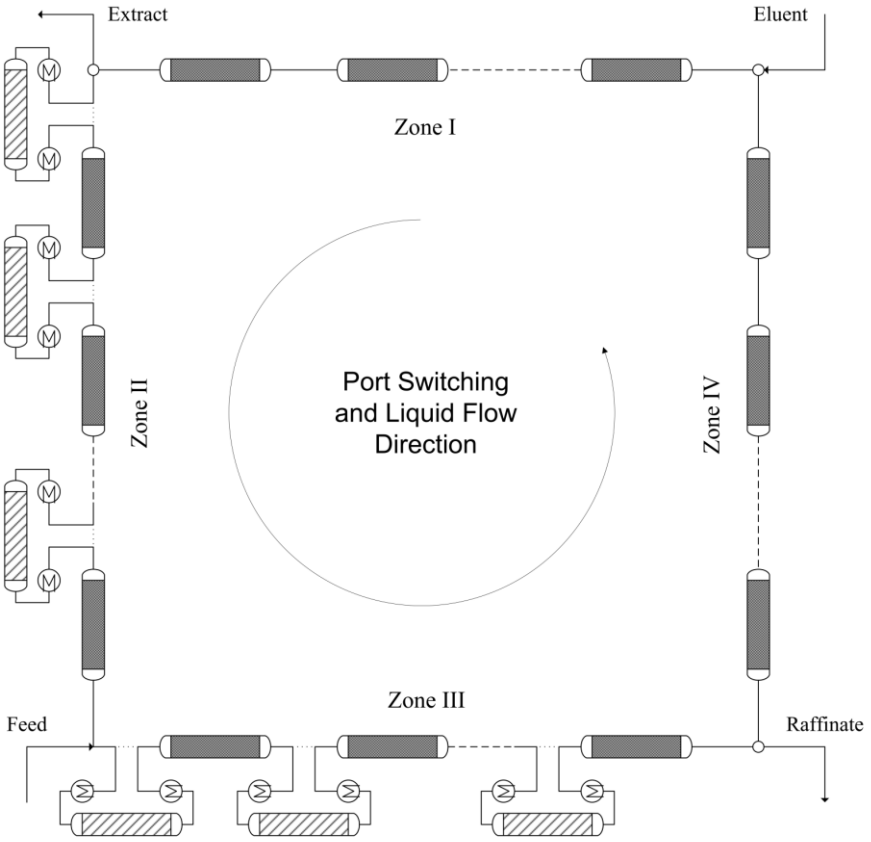

Figure 6.16: Sketch of the SMBR (Hashimoto type [38]) proposed for the direct synthesis of DMC.

6.6.1. Model

As previously mentioned, the evaluation of the proposed SMBR system was performed by the simulation of the equivalent TMBR, which made the assessment much easier and still reliable. The reactor model was the proposed in the previous section. The nodes were modelled imposing conservation of molar amounts and volumetric flows rate (for ideal mixtures - excess volumes equal to zero):

$$\sum Q_{in} \cdot C_{in} = \sum Q_{out} \cdot C_{out} \tag{6.32}$$

$$\sum Q_{in} = \sum Q_{out} \tag{6.33}$$

The mathematical model for the moving bed columns is detailed in Table 6.4; the following considerations were assumed:

- ❖ One dimension model with plug flow for the solid and axial dispersed plug flow model for the liquid.
- ❖ Linear driving force to model the global mass transfer resistance.
- ❖ Velocity, temperature and pressure changes are neglected.
- ❖ Instantaneous adsorption equilibrium.
- ❖ Linear adsorption equilibrium isotherms.
- ❖ Danckwerts boundary conditions.

Table 6.4: Mathematical model for the adsorption over Zeolite 3A in a moving bed column, with linear driving force and axial dispersion.

	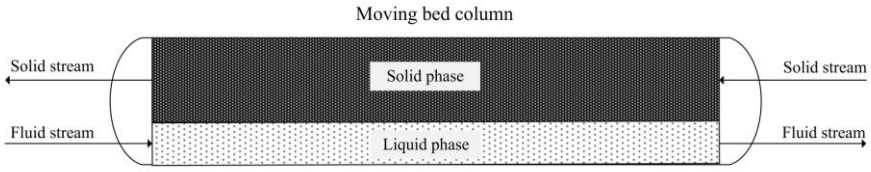	
Molar balance (liquid phase):	$\frac{V}{Q_{liquid}}\left[\frac{\partial C_i}{\partial t}\varepsilon_b + (1-\varepsilon_b)\frac{3k_L}{r_p}\left(C_i - \bar{C}_{p,i}\right)\right] + \frac{\partial C_i}{\partial z} = \frac{1}{Pe}\frac{\partial^2 C_i}{\partial z^2}$	(6.34)
Molar balance (solid phase):	$\frac{Q_{solid}}{V\cdot(1-\varepsilon_b)}\left[\varepsilon_p\frac{\partial \bar{C}_{p,i}}{\partial z} + \left(1-\varepsilon_p\right)\frac{\partial \bar{q}_i}{\partial z}\right] + \frac{3k_L}{r_p}\left(C_i - \bar{C}_{p,i}\right) = \varepsilon_p\frac{\partial \bar{C}_{p,i}}{\partial t} + \left(1-\varepsilon_p\right)\frac{\partial \bar{q}_i}{\partial t}$	(6.35)
Initial conditions:	$C_i(t=0,\forall z) = \bar{C}_{p,i}(t=0,\forall z) = C_i^{Eluent}$	(6.36)
Boundary conditions:	$C_i(\forall t, z=0) = C_i^{Feed}(t) + \frac{1}{Pe}\frac{\partial C_i}{\partial z}\Big\vert_{\forall t, z=0}$	(6.37)
	$\frac{\partial C_i}{\partial z}\Big\vert_{\forall t, z=1} = 0$	(6.38)
	$\bar{C}_{p,i}(\forall t, z=1) = \bar{C}_{p,i}^{\ Feed}(t)$	(6.39)
Adsorption isotherm:	$\bar{q}_i = K_{ads,i}^{zeolite\ 3A}\cdot\bar{C}_{p,i}$	(6.40)
	$K_{ads}^{zeolite\ 3A} = exp\left[-\frac{\Delta H_{ads}}{R\cdot T} + \frac{\Delta S_{ads}}{R}\right]$	(6.41)

In order to evaluate the performance of the TMBR, the following parameters were assessed: overall conversion (X_c); purity of water and DMC in the extract and raffinate streams (PUR – carbon dioxide free

basis); the purity of water and DMC in respect to each other ($PUR.II$); recovery of water and DMC; desorbent consumption (DC), and productivity ($PROD$). The parameters were calculated using equations 6.42 to 6.47:

$$X_c = 1 - \frac{C_X^{Lim.} \cdot Q_X + C_R^{Lim.} \cdot Q_R}{C_F^{Lim.} \cdot Q_F + C_E^{Lim.} \cdot Q_E} \tag{6.42}$$

$$PUR_{i,j} = \frac{C_j^i}{C_j^{MeOH} + C_j^{DMC} + C_j^{H_2O}};\ i = \text{DMC} \cup \text{H}_2\text{O};\ j = R \cup X \tag{6.43}$$

$$PUR.II_{i,j} = \frac{C_j^i}{C_j^{DMC} + C_j^{H_2O}};\ i = \text{DMC} \cup \text{H}_2\text{O};\ j = R \cup X \tag{6.44}$$

$$REC_{i,j} = \frac{C_j^i \cdot Q_j}{C_X^i \cdot Q_X + C_R^i \cdot Q_R};\ i = \text{DMC} \cup \text{H}_2\text{O};\ j = R \cup X \tag{6.45}$$

$$DC = \frac{V_{M,lim}\left[C_F^{lim} \cdot Q_F + C_E^{lim} \cdot Q_E - |\vartheta_{lim}|\left(C_R^{DMC} \cdot Q_R + C_X^{DMC} \cdot Q_X\right)\right]}{C_R^{DMC} \cdot Q_R} \tag{6.46}$$

$$PROD = \frac{C_R^{DMC} \cdot Q_R}{V_{adsorbent,total}} \tag{6.47}$$

6.6.2. First guess design

In order to design the TMBR unit it is necessary to define the flow rates, although they depend on the unit dimensions, column diameter (D), column length (L), particle diameter, number of columns per zone, etc. Indeed, the geometrical parameters have a considerable effect on the mass transfer resitance, which lead to smaller separation regions in comparison with the ones determined by the equilibrium theory (Scheme 6.1). Therefore, this bilateral dependence between the TMBR design and flow rates leads to an iterative problem.

In order to shortcut this problem, a different approach is proposed: first, an initial guess for the operating conditions is made; then, based on this guess, the TMBR unit is designed; finally, using simulation as a validation tool it can be verified if the initial guess fits the separation requirements. This topic will be deeply discussed in the end of this section.

The first guess for the operating conditions is represented in Figure 6.17 together with the ideal separation region based on equilibrium theory, at 298 K. The following criteria were assumed:

- $\gamma_{III}^{guess} = 0.5\times\left(\gamma_{III,max}^{ideal} + \gamma_{III,min}^{ideal}\right)$
- $\gamma_{II}^{guess} = 0.5\times\left(\gamma_{II,min}^{ideal} + \gamma_{III}^{guess}\right)$
- $\gamma_{IV}^{guess} = 0.25\times\gamma_{IV,max}^{ideal}$
- $\gamma_{I}^{guess} = \gamma_{I,min}^{ideal} + 0.25\times\gamma_{IV,max}^{ideal}$

A higher reduction was considered for sections II and III, because besides the typical mass transfer phenomena, reaction also takes place, which leads to a further decrease of the separation region.

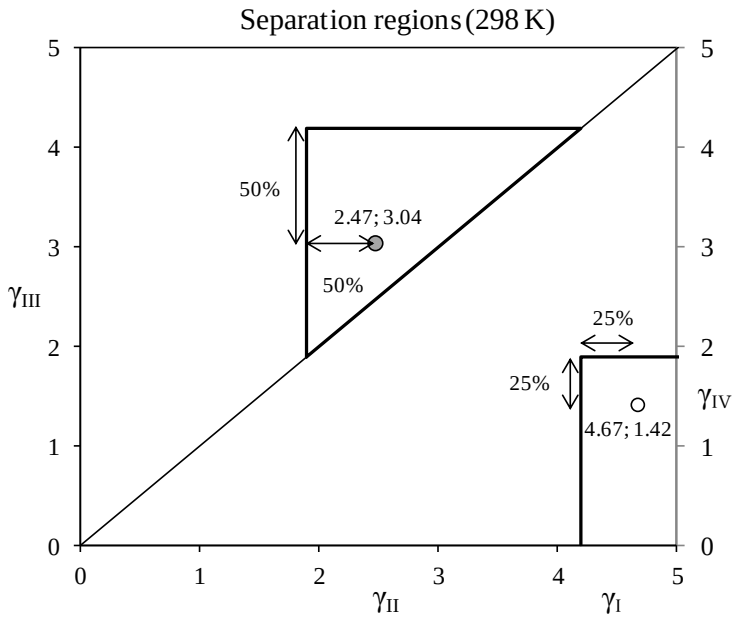

Figure 6.17: Separation region at 298 K and first operating conditions guess.

After defining the operating conditions, a feed flow rate of 20 mL·min^{-1} was considered as basis of calculation, for a small scale TMBR. Table 6.5 contains all defined and calculated flow rates from the first guess of liquid to solid flow rates.

Table 6.5: First guess of TMBR flow rates for Q_{Feed} = 20 mL·min^{-1} (γ_{Feed} = 0.58).

γ_I	γ_{II}	γ_{III}	γ_{IV}
4.67	2.47	3.04	1.42
Q_I / mL·min^{-1}	Q_{II} / mL·min^{-1}	Q_{III} / mL·min^{-1}	Q_{IV} / mL·min^{-1}
161.02	85.17	104.82	48.96
Q_X / mL·min^{-1}	Q_R / mL·min^{-1}	Q_E / mL·min^{-1}	Q_{Solid} / mL·min^{-1}
75.85	55.86	111.71	34.48

A TMBR composed by 24 columns was considered; this large number of columns attempts to increase the number of reaction units, since they are alternately connected with the adsorption columns. A large number of columns for a SMB was already used for the purification of *p*-xylene (24 columns) [63]. Furthermore, it was considered that both reactants, methanol and carbon dioxide, are present in the feed and in the eluent stream at the molar ratio of one.

In order to calculate the dimensions of the columns it is important to account for the superficial velocity (u_0), which affects both mass transfer and pressure drop. A superficial velocity value of 0.3 cm·s^{-1} is a reference for liquid velocity in a fixed bed column [89]. The effect of superficial velocity on the global mass transfer coefficient, for water and DMC, is shown in Figure 6.18a. A particle diameter of 0.1 mm – a tenth of the used on the experimental section of Chapter 5 – was considered in order to decrease the internal mass transfer resistance. The mass transfer coefficients were estimated using the Dean and Stiel correlation [74] for viscosity, the Kataoka correlation [90] for the external mass transfer coefficient, and the Wilke and Chang correlation [91] for molecular diffusivity (Chapter 5). In addition, it can be observed that above 0.1 cm·s^{-1} the mass transfer coefficient becomes independent of the fluid velocity, which indicates that the internal mass transfer resistance controls the global mass transfer resistance. Hence, 0.1 cm·s^{-1} was defined as the minimum velocity (in Zone IV, since it has the low fluid flow rate) and, since diffusion dominates the mass transfer phenomena, it was the only one considered for further simulations.

Furthermore, a length to diameter ratio of 1 to 5 was assumed, and based on this information a column diameter of 3.2 cm and a column length of 16 cm were calculated. In industrial applications, a diameter to length ratio between 1 to 1 and 5 to 1 is recommended [92] as a trade-off between axial dispersion and pressure drop. However, flow distributors are used to prevent radial dispersion, which is not considered here.

Figure 6.18b shows the total pressure drop as a function of the particle diameter for different velocities. The total pressure drop drastically decreases with the increase of the particle size, but within the range studied (0.1 to 1 mm) these values are insignificant, when compared to the 20 MPa. So, the particle diameter assumed (0.1 mm) is well acceptable for the operating conditions defined.

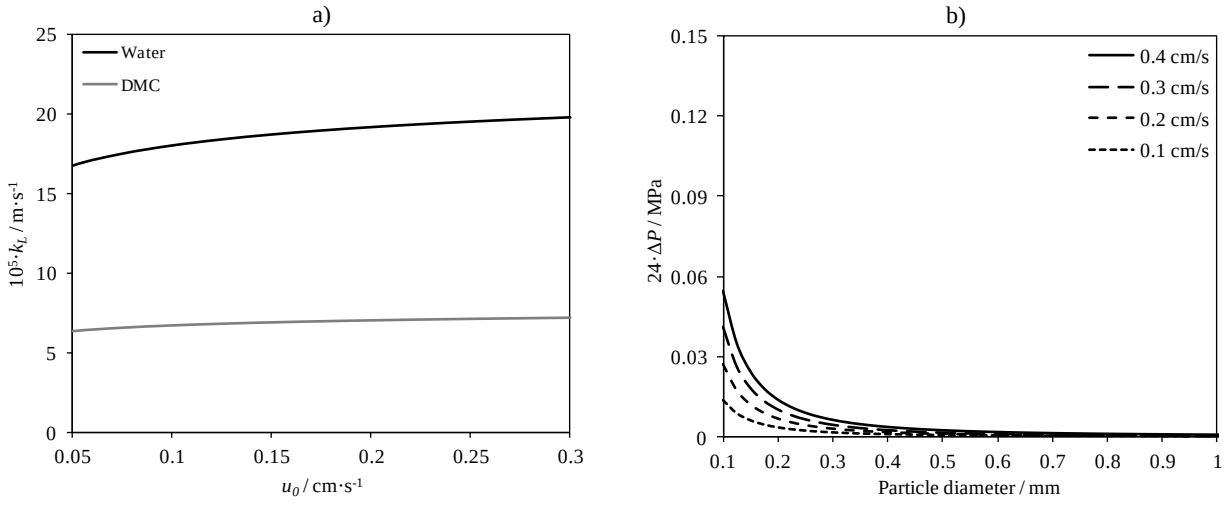

Figure 6.18: a) Estimation of global mass transfer as function of superficial velocity for a binary mixture of CO_2 and MeOH for dp = 0.1 mm. b) Simulation of total pressure drop (Ergun equation) inside the TMBR (24 columns, 16 cm per column) as a function of the particle diameter. Conditions: 20 MPa, 298 K, x_{MeOH} = 0.5.

With the dimensions of the adsorption columns defined, we can set the reactor dimensions. First, the configuration of the TMBR was set: 3-9-9-3, which means 3 columns in Zone I, 9 columns in Zones II and III, and 3 columns in Zone IV. With this configuration, 17 reactors are coupled to the unit; the sum of all reactor volumes was uniformly distributed (300 mL) so the total volume was equal to approximately 5000 mL. This volume (5000 mL) would be the volume necessary to reach the equilibrium in a fixed bed reactor at the same conditions of the TMBR and for a flow rate equal to the average between Zones II and III. The reactor was dimensioned considering a diameter to length ratio of 1/5 ($L \times D$ = 21.22 cm × 4.24 cm), which gives an acceptable superficial velocity of 0.1 cm·s^{-1}.

Finally, in Table 6.6 are displayed the geometrical features and the operating conditions for the first TMBR unit considered. In addition, the Péclet number was estimated based on the average velocity in all the four zones, and assuming the same axial dispersion coefficient of section 6.5.

Table 6.6: Summary of simulation parameters for the first design.

Adsorption column		Reactor	
V / mL	128	V / mL	300
L/D	5/1	L/D	5/1
D / cm	3.2	D	4.24
L / cm	16	L / cm	21.22
D_{ax} / cm^2·s^{-1}	0.55	D_{ax} / cm^2·s^{-1}	0.11
Pe	20	Pe	50
T / K	298	T / K	383
Compounds	[CO_2 MeOH DMC H_2O]	P / MPa	20
k_L / mm·min^{-1}	[∞ ∞ 5.2 13]	Heat exchanger	
K_{ads}	[0 0 2.4 6.0]	β	1.616
General			
C_{Feed}	[10.68 10.68 0 0]	Q_{Feed} / mL·min^{-1}	20
C_{Eluent}	[10.68 10.68 0 0]	Configuration	3-9-9-3
γ_I	γ_{II}	γ_{III}	γ_{IV}
4.67	2.47	3.04	1.42

The TMBR unit proposed was assessed by simulation; the concentration profiles obtained for a stationary state are depicted in Figure 6.19. In Figure 6.19a is shown the concentration profile along the adsorption column and it can be seen that the wave of DMC concentration is shifted towards the raffinate stream (end of column 21), while the water is shifted for the extract stream (end of column 3). The concentrations of methanol and carbon dioxide barely change, so they are not described in the graph. The similarity of the curves to a stair in Zones II and III is caused by the alternation between adsorption and reaction units.

The concentration profiles along the reactor units are shown in Figure 6.19b, where it can be observed a slightly increase of water and DMC concentrations in the direction of the fluid (from 0 to 17). In addition, the

overall concentration was quite low (0.33%), indicating that at these conditions the TMBR was not able to improve the DMC yield. The only advantage of the use of the TMBR is the separation of water from DMC into two different outlet streams, extract and raffinate, respectively. In Table 6.7 are summarized the main results obtained from the simulation studies: conversion and purities. Indeed, the TMBR as a separation unit is very efficient leading to a separation higher than 99% between water and DMC. Even though, this positive feature is not enough to compensate the high complexity of the TMBR equipment, especially for industrial application. Moreover, purity in carbon dioxide free basis is lower than 1%, which would require a large energy intensive separation process.

Table 6.7: Main results for the simulation of the first guess design.

X_c	$PUR_{DMC,R}$	$PUR_{H_2O,X}$	$PUR.II_{DMC,R}$	$PUR.II_{H_2O,X}$
0.33%	0.78%	0.57%	99.30%	99.42%

Since the results obtained are not attractive, before further studies/optimizations (as the determination of the separation regions using the volume separation method), a new approach will be done attempting to find a more suitable TMBR process.

6.6.3. Second guess design

In the previous subsection it was concluded that, at the conditions proposed, the TMBR designed was far from being sustainable to improve the reaction system. Therefore, a new approach is necessary, which leads to a new start in the design procedure: define new general conditions (temperatures, pressure and inlet concentrations) that may lead to better results. In other words, it is essential to enhance the DMC equilibrium yield in order to improve the performance of the TMBR unit.

Define new conditions

The direct synthesis of DMC (CO_2 + 2MeOH ⇌ DMC + H_2O) is an exothermic and a volume decreasing reaction, which means that low temperature and high pressure favour the formation of DMC. However, there should be sustainable temperature and pressure ranges, addressing the kinetics limitation, energy demand, and equipment costs.

In Figure 6.20 is displayed the DMC yield at equilibrium as between 363 K and 403 K, (Eq. 4.1 and Eq. 4.2); in addition, the effect of pressure (15, 20, 25, and 30 MPa) and carbon dioxide to methanol ratio (1/1, 1/2, 10/1, and 1/10) are also explored. As predicted, DMC yield increases with the increase of pressure and the decrease of temperature (Figure 6.20a), passing from 0.97% at 403 K and 15 MPa to 1.97% at 363 K and 30 MPa; which represents an improving around 100%.

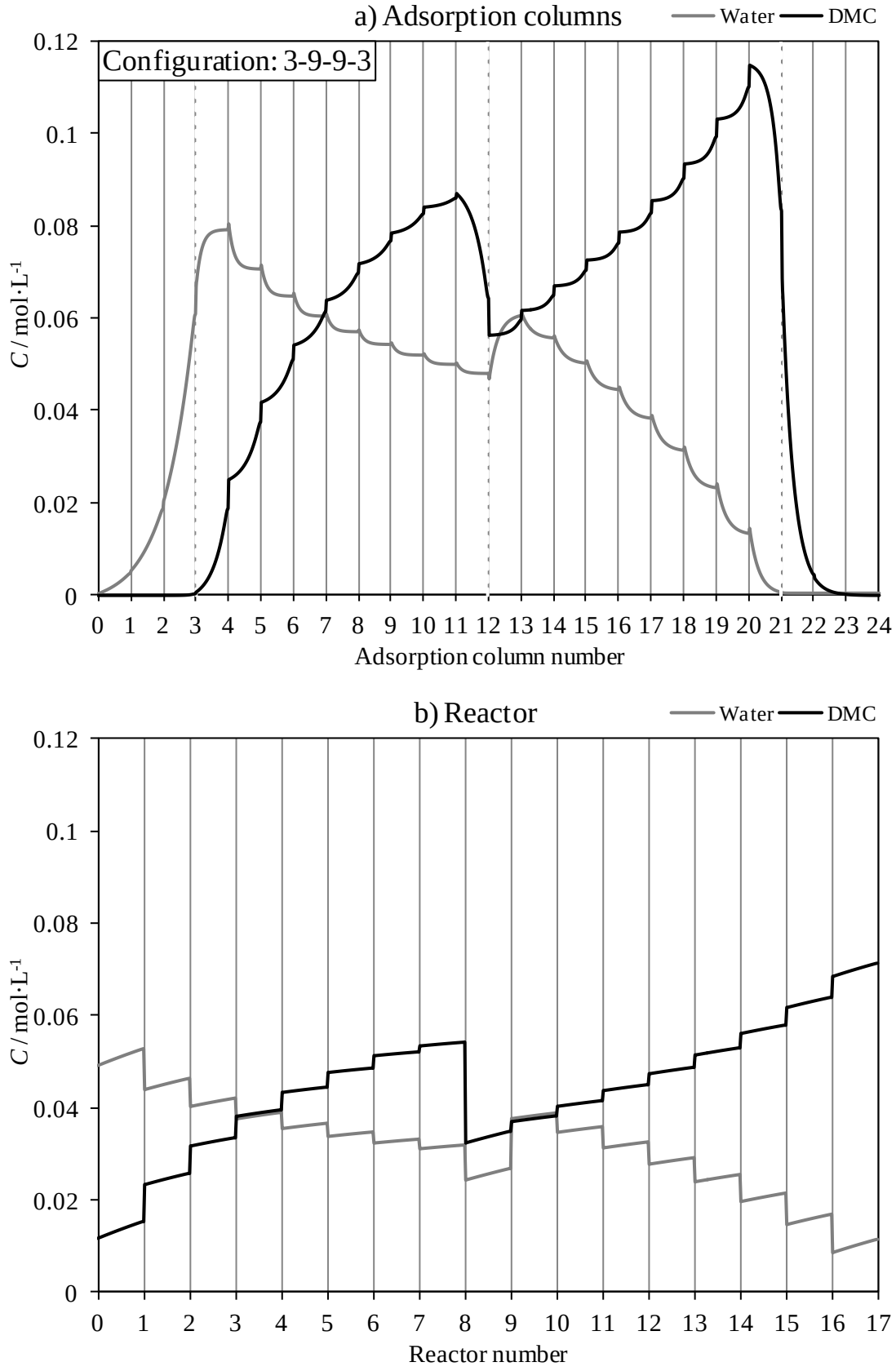

Figure 6.19: TMBR profile concentrations of water and DMC along the: a) adsorption columns; b) fixed bed reactors. Simulation parameters described in Table 6.6.

More remarkable is the effect of excess of one reactant, especially for methanol due to its higher stoichiometric coefficient number. Indeed, a DMC yield of 4.18% is predicted with a carbon dioxide to methanol ratio of 1 to 10, which represents an improvement around 150% in comparison to the stoichiometric ratio (1.61%) at 363 K and 30 MPa.

In conclusion, more harsh conditions are needed to improve the DMC yield at equilibrium state. Hence, for this new design attempt, the following conditions will be set:

- The adsorption temperature will be the same (298 K) which is already low enough to promote a reasonable separation region.
- The pressure will be set at 30 MPa.
- The carbon dioxide to methanol ratio in the feed stream will remain equal (1/1).
- However, the eluent stream will be set as pure methanol in order to operate with excess of methanol.

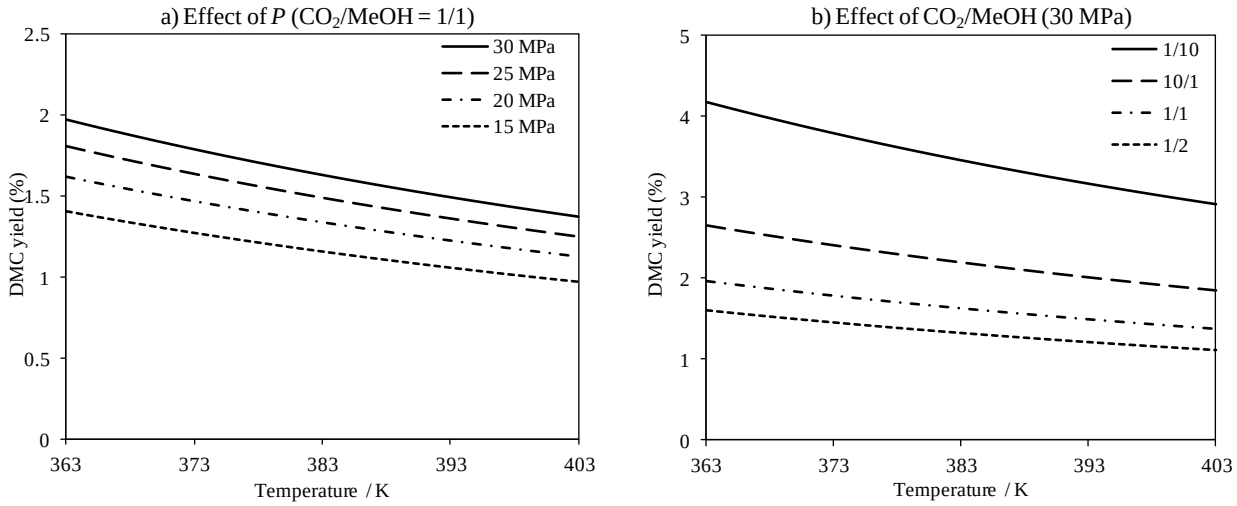

Figure 6.20: DMC equilibrium yields as function of temperature at different: a) pressures; b) reactant ratios.

Design of adsorption columns

Let us now reassign the effect of velocity on the global mass transfer coefficient. First of all, the same feed flow rate (20 mL·min^{-1}) and γ_i ([4.67 2.47 3.04 1.42]) were considered as a starting point for this new attempt; and, the same particle diameter (d_p = 0.1 mm) was also assumed.

Based on these conditions, together with the new feed and eluent concentrations, the global average of methanol molar fraction is equal to 93%, although this value varies in the different sections of the TMBR. In addition, methanol to carbon dioxide ratio is also dependent of the feed to eluent ratio, which will be studied in order to optimize the unit. Hence, for further calculations, a methanol molar fraction of 90% will be used, that will then be corrected for the final design.

In Figure 6.21a is displayed the effect of superficial velocity on the global mass transfer for the new conditions: 30 MPa, 298 K, and a methanol molar fraction of 0.9. As concluded before, above 0.1 cm·s^{-1} the

mass transfer phenomena are mainly controlled by diffusion. Nevertheless, the values are lower due to the higher density at 30 MPa (compared to 20 MPA) and the higher amount of methanol (x_{MeOH} = 0.9 *vs.* x_{MeOH} =0.5).

Therefore, 0.1 cm·s^{-1} was set as the minimum velocity (Zone IV), which leads to equal geometry for the adsorption columns (D = 3.2 cm and L = 16 cm), assuming the same length to diameter ratio of 5 to 1. Moreover, the global mass transfer coefficient for water and DMC were set equal to the average values between 0.1 cm·s^{-1} and 0.4 cm·s^{-1}: 7.66·10^5 m·s^{-1} and 3.20·10^5 m·s^{-1}, respectively.

In addition to this, Figure 6.21b demonstrates that the total pressure drop can be neglected; since its value is residual (ΔP < 0.12 MPa) even at a superficial velocity of 0.4 cm·s^{-1}, when compared to the total pressure of 30 MPa ($\Delta P/P$ < 0.4%).

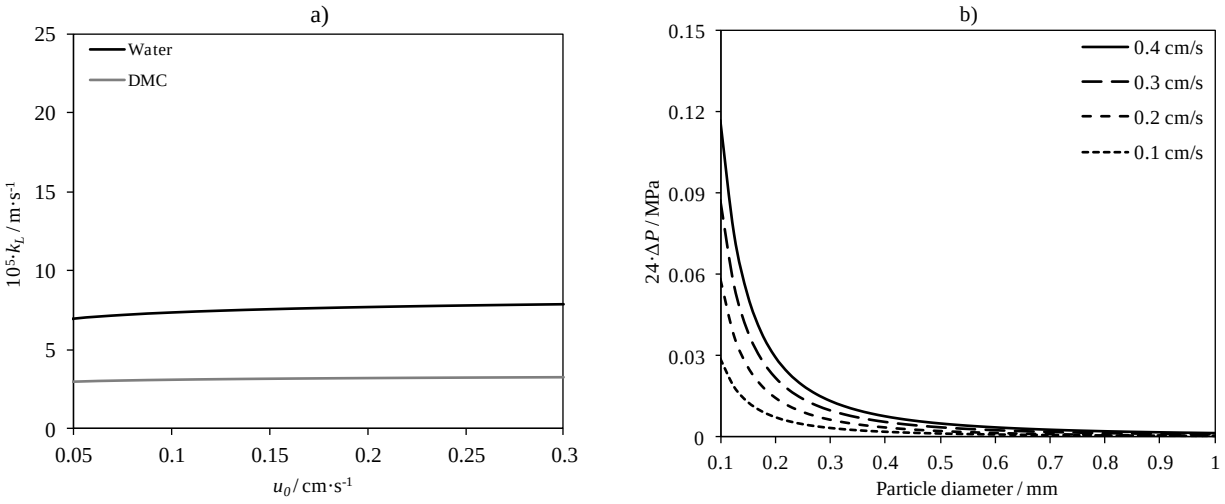

Figure 6.21: a) Estimation of global mass transfer as function of superficial velocity for a binary mixture of CO_2 and MeOH for dp = 0.1 mm; b) Simulation of total pressure drop (Ergun equation) inside the TMBR (24 columns, 16 cm per column) as a function of the particle diameter. Conditions: 30 MPa, 298 K, x_{MeOH} = 0.9.

Design of the reactors

The reactor configuration for this new design of a SMBR unit (based on TMBR) needs to be changed. Since now the carbon dioxide is only fed in the feed stream, the reaction should only occur in Zone III; otherwise, it would be an excessive and unnecessary effort in Zone II. This New configuration is depicted in Figure 6.22.

The reactor design is based on the guess operating conditions: Q_{III}= 105 mL·min^{-1} (at 298 K), 30 MPa, 363 K, x_{MeOH} = 0.9, β = 1.04. At these conditions, a total volume of 53 L would be required, to reach the equilibrium, if the reactor were carried out in a fixed bed reactor filled with cerium oxide particles. This volume was uniformly distributed (3300 mL) by the total number of reactors (equal to the number of adsorption columns in Zone III).

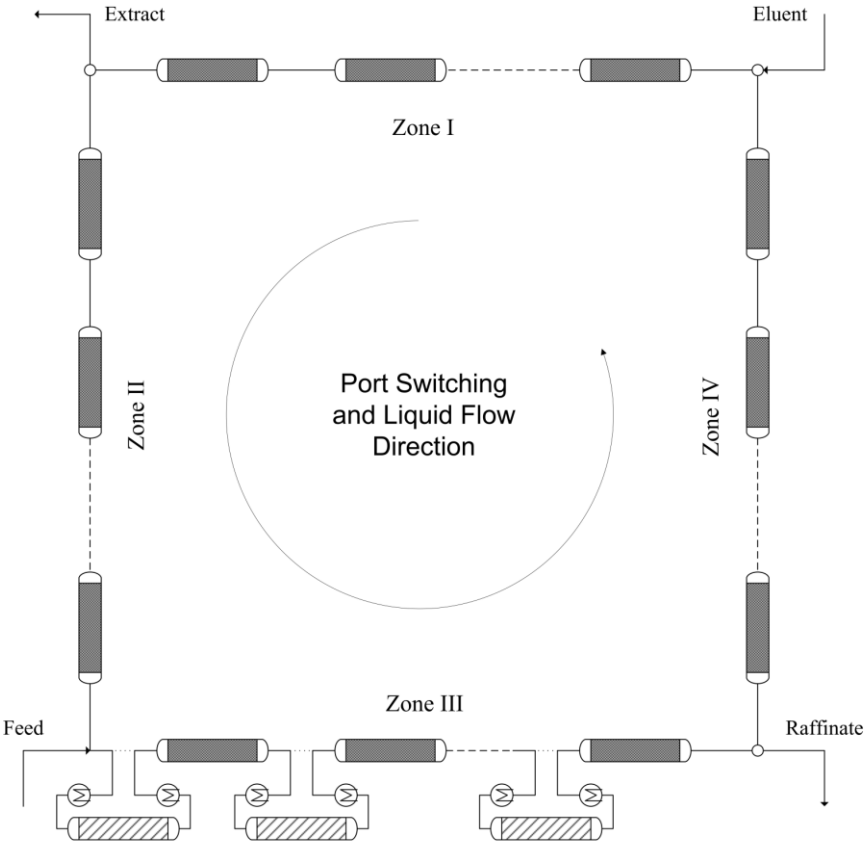

Figure 6.22: Sketch of the new SMBR (Hashimoto type [38]) proposed for the direct synthesis of DMC: reaction only in Zone III.

Preliminary tests

After defining new conditions, configuration and design, it is important to evaluate the performance of the proposed TMBR unit. Hence, a sensitivity analysis was carried out to assess the effect of some parameters (adsorption column volume, configuration, and flow rate ratios) on the overall performance (conversion, purity, and recovery).

In Table 6.8 are displayed the main results obtained in the simulations of the steady state TMBR, as well as the respective changed parameters; the other parameters were set as specified above. Furthermore, since the mixture is mainly composed by methanol, it is expected a behaviour more similar to high performance liquid chromatography (Péclet of a particle tends to 2), and therefore a larger Péclet value of 1000 was assumed.

The first simulation was carried out assuming the previous conditions and a configuration of 3-11-7-3, in order to guarantee a complete recovery of DMC in the raffinate stream. Indeed, an almost complete recovery was accomplished (99.98%) but a purity of DMC (MeOH and cerium oxide free basis) of 97.70% was observed; which means that 2.30% of water is contained in the raffinate. The respective concentration profiles are displayed in Annex C.

Hence, the adsorption volume was doubled (Design 2.2) in order to enhance the separation; and a DMC purity of 99.80% (MeOH and carbon dioxide free basis) was reached. Afterwards, different configurations were tested (Design 3: 3-7-11-3 and Design 4: 3-1-17-3) and it was concluded that one column in Zone II would be enough to achieve higher conversion (3.96%) and a DMC purity of 99.89% (MeOH and carbon dioxide free basis).

Besides the great separation between DMC and water, the DMC purity (carbon dioxide free basis) is still very low: 0.67% for Design 2.4. This is an important performance parameter because it is related to the separation energy demand for further purification. In Design 2.5 and 2.6 were studied the effects of raffinate and extract flow rates, by changing γ_{II} and γ_{III}, but fixing γ_{feed}. It was observed a significant increase from 0.67% (Design 2.4) to 0.98% (Design 2.6).

Afterwards, it was simulated at the same conditions but using a slightly different configuration: 3-2-16-3; 2 columns in Zone II was set as a safety parameter in order to guarantee a separation higher than 99% between water and DMC in hardest conditions; or, in other words: to improve the separation region without compromising the reaction conversion.

Table 6.8: Main results of the preliminary tests for the TMBR.

Design	V_{ads} / mL	Configuration	γ_i	X_c	$PUR_{DMC,R}$	$PUR.II_{DMC,R}$	$REC_{DMC,R}$
2.1	128	3-11-7-3	[4.67 2.47 3.04 1.42]	3.73%	0.63%	97.70%	99.98%
2.2	**260**	3-11-7-3	[4.67 2.47 3.04 1.42]	3.77%	0.63%	99.80%	99.99%
2.3	260	**3-7-11-3**	[4.67 2.47 3.04 1.42]	3.86%	0.65%	99.81%	99.99%
2.4	260	**3-1-17-3**	[4.67 2.47 3.04 1.42]	3.96%	0.67%	99.82%	99.73%
2.5	260	3-1-17-3	**[4.67 2.18 2.76 1.42]**	3.94%	0.82%	99.89%	98.95%
2.6	260	3-1-17-3	**[4.67 1.89 2.47 1.42]**	3.68%	0.98%	99.93%	95.71%
2.7	260	**3-2-16-3**	[4.67 1.89 2.47 1.42]	3.87%	1.06%	99.93%	97.70%

Finally, the overall design is specified in Table 6.9, together with the general operating conditions. The reactors were designed assuming a large length to diameter ratio of 25 to 1. This ratio is 1.5 higher than the ratio for the adsorption columns, although considering a laboratory scale this ratio is acceptable, since an equal ratio was used in the experimental section of Chapter 5. With this restriction, the diameter and length of each reactor are respectively 5.52 cm and 138 cm; which leads to an acceptable superficial velocity of 0.07 cm·s^{-1}, according to the reference value (0.3 cm·s^{-1}).

Separation volume method

The previous operating conditions were a starting point for the optimization of the proposed TMBR unit. Herein, is proposed the separation volume method in order to evaluate the effect of the flow rate ratios on the separation regions. Furthermore, the contour maps within the separation region are also studied: conversions, purities and desorbent consumption.

Table 6.9: Summary of simulation parameters for the final design.

Adsorption column		Reactor	
V / mL	260	V / mL	3300
L/D	~10/1	L/D	25/1
D / cm	3.2	D	5.52
L / cm	32.3	L / cm	138
Pe	1000	Pe	1000
T / K	298	T / K	363
Compounds	[CO2 MeOH DMC H2O]	P / MPa	30
k_L / mm·min^{-1}	[∞ ∞ 1.92 4.6]	Heat exchanger	
K_{ads}	[0 0 2.4 6.0]	β	1.04
General			
C_{Feed}	[11.15 11.15 0 0]	Configuration	3-2-16-3
C_{Eluent}	[0 24.7 0 0]	Reactor configuration	0-0-16-0

In Figure 6.23 is displayed the algorithm used for building the separation regions. The algorithm is divided in two: the first one (Figure 6.23a) for the separation region of Zones II and III; and the second for the regeneration region of Zones I and IV. Summarizing, the algorithm consists in simulating the TMBR model by changing the flow rate ratios (γ) consistently; the values of flow rate ratios studied are inside the separation region predicted by the equilibrium theory. Then, if the desired purities (MeOH and carbon dioxide free basis) are reached the results are saved and plotted.

It is worth to remember, that the TMBR was designed based on the guess for the flow rate ratios (γ_I = 4.67, γ_{II} = 2.47, γ_{III} = 3.04, γ_{IV} = 1.42). Therefore, any large change on the operating conditions may lead to undesirable velocities, which will affect the mass transfer phenomena or affect the compressibility factor and the reactor size. None of these variables were adapted to the operating conditions because this would considerably increase the complexity of the problem; and the uncertainties related to the estimation of several variables might be within the same order of magnitude of the uncertainties of the first hypothesis. However, after achieving the so called optimum conditions, the unit will be redesigned in order to fit the previous requirements.

Moving forward, in Figure 6.24 is represented the separation volume for a purity of 99% for both water and DMC, in the extract and raffinate streams, respectively. The simulations were carried out assuming the same solid flow rate obtained from the first guess (34.7 mL·min^{-1}).

In addition, in Figures 6.24a and 6.24b are shown the effects of γ_I and γ_{IV} on the separation regions. The decrease of γ_I or the increase of γ_{IV} leads to a reduction of the separation region; ideally, γ_I should be the lowest value possible and γ_{IV} the highest in order to minimize the eluent consumption, but without reducing the separation region. Thus, the values of 4.67 and 1.70 were found, for γ_I and γ_{IV}, so that eluent consumption is minimum, but without affecting the separation region of Zones II and III.

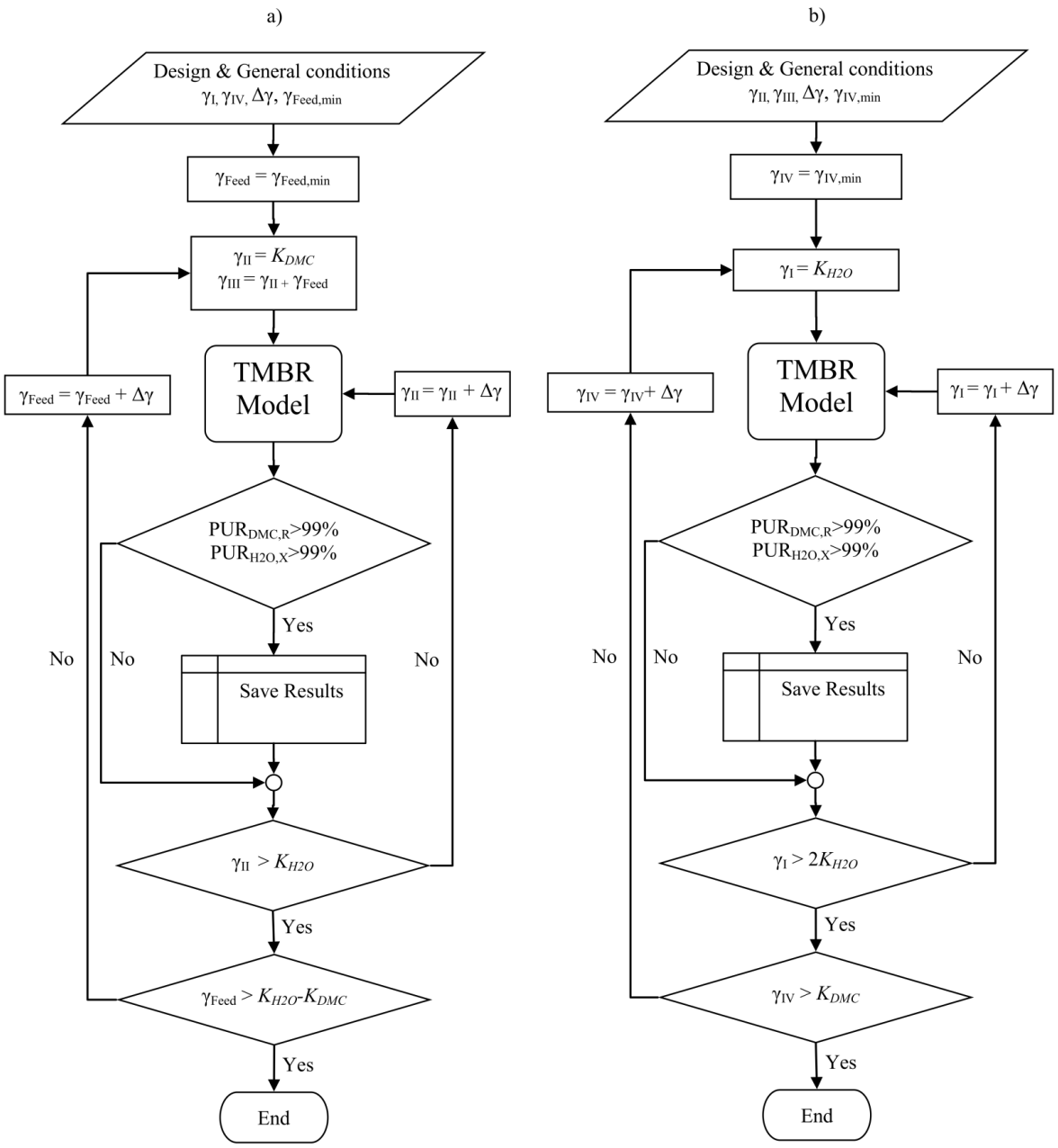

Figure 6.23: Algorithm for the numerical determination of the separation region: a) Zones II-III; b) Zones I-IV.

In addition to these results, the separation regions together with the contour maps of some important performance parameters (conversion, purities, and desorbent consumption) are now depicted in Figure 6.25. First of all, in Figure 6.25a is represented the contour map for the DMC purity (MeOH and carbon dioxide free basis), where it can be seen the patterns of DMC purity increasing with the decrease of γ_{II} and γ_{feed} ($\gamma_{feed} = \gamma_{III} - \gamma_{II}$); moreover, in the figure are displayed two white stars that represent the first guess for flow rate ratios.

Then, in Figure 6.25b is observed an almost linear increase of the reaction conversion with the decrease of γ_{feed}. In fact, decreasing the γ_{feed} leads to an increase of methanol to carbon dioxide ratio; this consequently raises the conversion of the limiting reactant (imposed by the thermodynamic limitations).

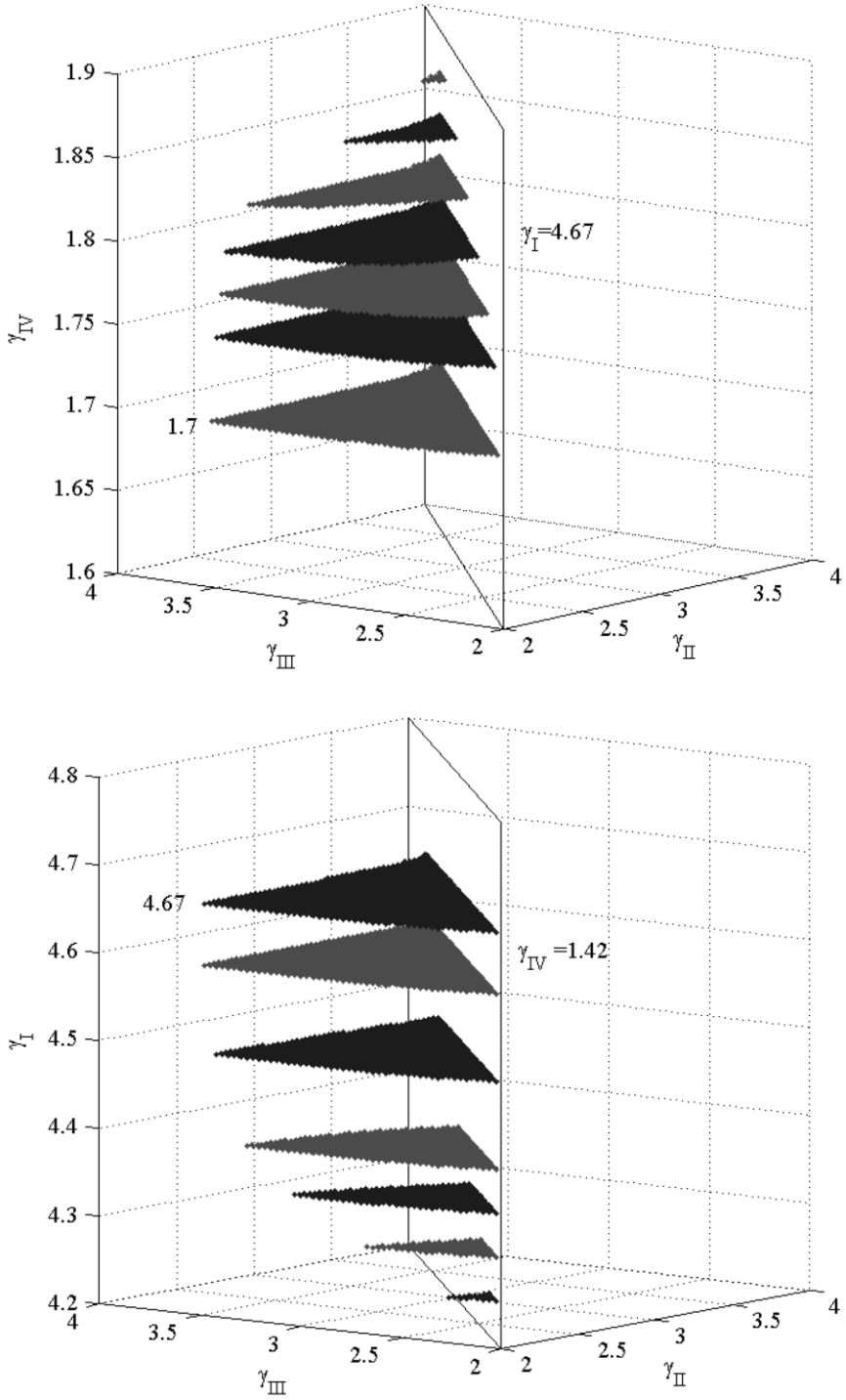

Figure 6.24: Volume separation above 99%: a) effect of γ_I ($\gamma_{II} \times \gamma_{III} \times \gamma_{IV}$); b) effect of γ_{IV} ($\gamma_{II} \times \gamma_{III} \times \gamma_I$). General condition/design is described in Table 6.9; Q_{Solid} = 34.7 mL·min^{-1}.

Another important parameter, already discussed before, is the purity of DMC in a carbon dioxide free basis. Carbon dioxide is easily separated by evaporation due to its very low boiling point, although the separation of methanol and DMC is much more energy intensive, even because these two compounds originate an azeotropic mixture. Thus, the DMC purity is represented in Figure 6.25c, where can be seen a variation between 0.3% and 1.1% in a major part of the graph. The DMC purity increases inversely with γ_{II};

nevertheless, the increment of DMC purity leads to a reduction of water purity on the extract stream, because the eluent (MeOH) is divided between these two streams.

Finally, in Figure 6.25d is visible the contour map of the desorbent consumption, inside the separation region. The DC increases with γ_{feed}, but, unlike the eluent consumption, it appears to tend to a maximum value at a γ_{feed} different of the triangle peak. This phenomenon is explained by the fact that the eluent (MeOH) is also a reactant and its conversion benefits the desorbent consumption.

In order to optimize a TMBR unit it is of great relevance to define which parameter is more crucial. It could be the maximization of the productivity, or the reaction conversion, or even the minimization of desorbent consumption. I believe that in a TMBR/SMBR unit the purity also plays an essential role. Therefore, in order to optimize the unit, a simple objective function was proposed (F_{Obj}):

$$F_{Obj} = max\left\{\frac{X_c \cdot PUR_{DMC,R}}{DC}\right\} \tag{6.48}$$

Along these lines, the contour map for the objective function is laid out in Figure 6.26. It can be observed from the graph that there is a maximum near the border of the triangle.

Finally, the best operating conditions established based on these results are collected in Table 6.10. As mentioned before, the difference between the first guess and the optimum estimation for the operating condition might lead to inappropriate design of the TMBR. Below this subject is discussed in more detail.

Table 6.10: Optimum flow rates for the TMBR (Q_{Solid} = 34.72 mL·min^{-1}).

γ_I	γ_{II}	γ_{III}	γ_{IV}
4.67	2.25	2.50	1.70
Q_I / mL·min^{-1}	Q_{II} / mL·min^{-1}	Q_{III} / mL·min^{-1}	Q_{IV} / mL·min^{-1}
162.14	78.12	86.80	59.02
Q_{Feed} / mL·min^{-1}	Q_E / mL·min^{-1}	Q_X / mL·min^{-1}	Q_R / mL·min^{-1}
8.7	103.1	84.0	27.8

Best Design

Since the flow rates obtained after the optimization are considerable different from the first guess, it is necessary to redesign the unit in order to have adequate velocities that enhance the mass transfer. Furthermore, the reactor volumes might also need to be recalculated based on the new flow rates and concentration profiles.

First of all, a pre-simulation without altering any parameters was carried out to have an estimation of the concentration profiles, which is essential to estimate the mass transfer coefficients. After the simulation, an average molar fraction around 0.95 of methanol, and 0.05 of carbon dioxide (neglecting DMC and water) was found; these values are not far from the previous estimation: 0.9 and 0.1, for the methanol and carbon dioxide, respectively.

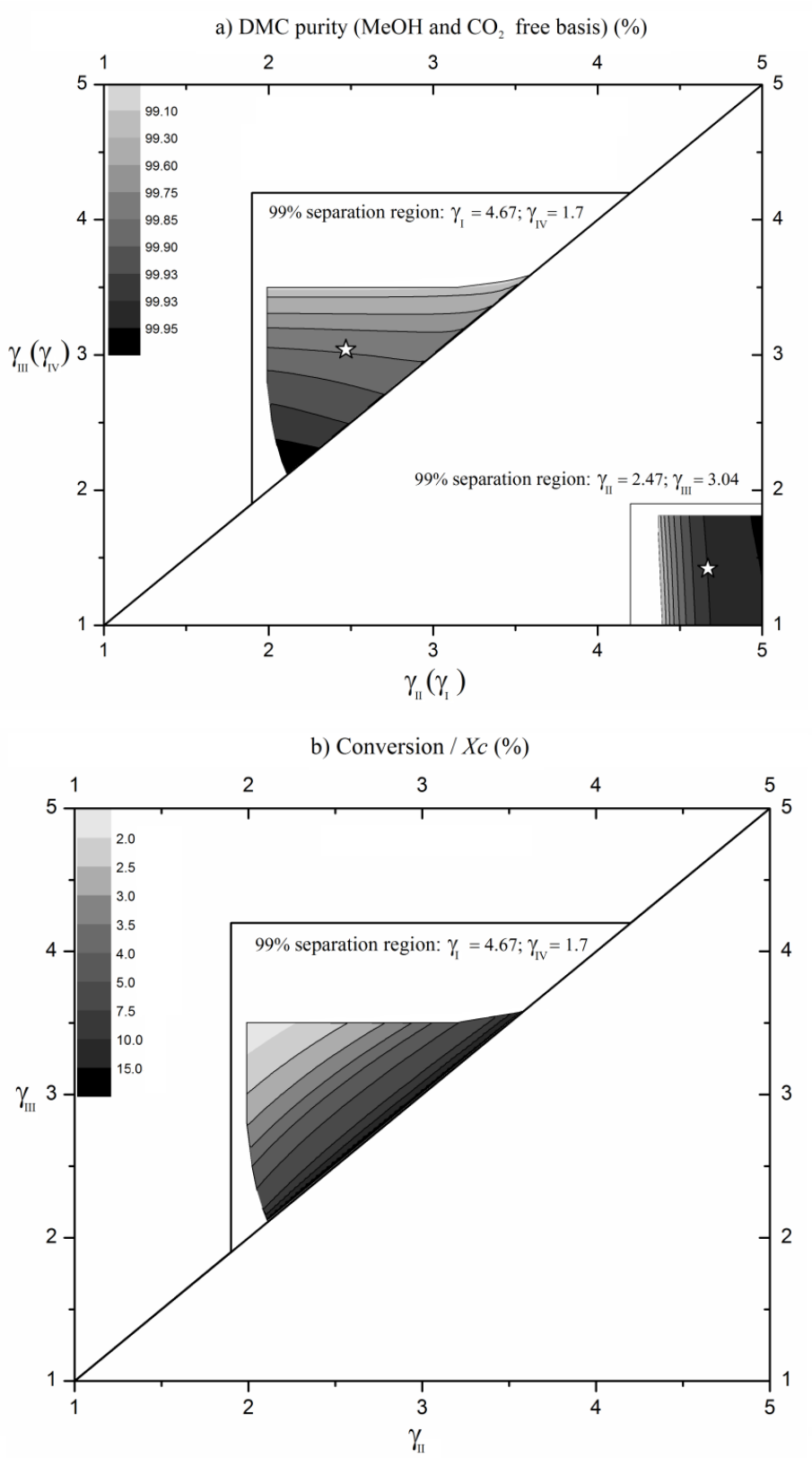

Figure 6.25: Separation regions (above 99%) and contour maps for the proposed TMBR (Stars = first guess): a) DMC purity (MeOH and CO_2 free basis); b) conversion; c) DMC purity (CO_2 free basis); d) desorbent consumption ($L_{MeOH} \cdot mol_{DMC}^{-1}$). General condition/design is described in Table 6.9; Q_{Solid} = 34.7 $mL \cdot min^{-1}$.

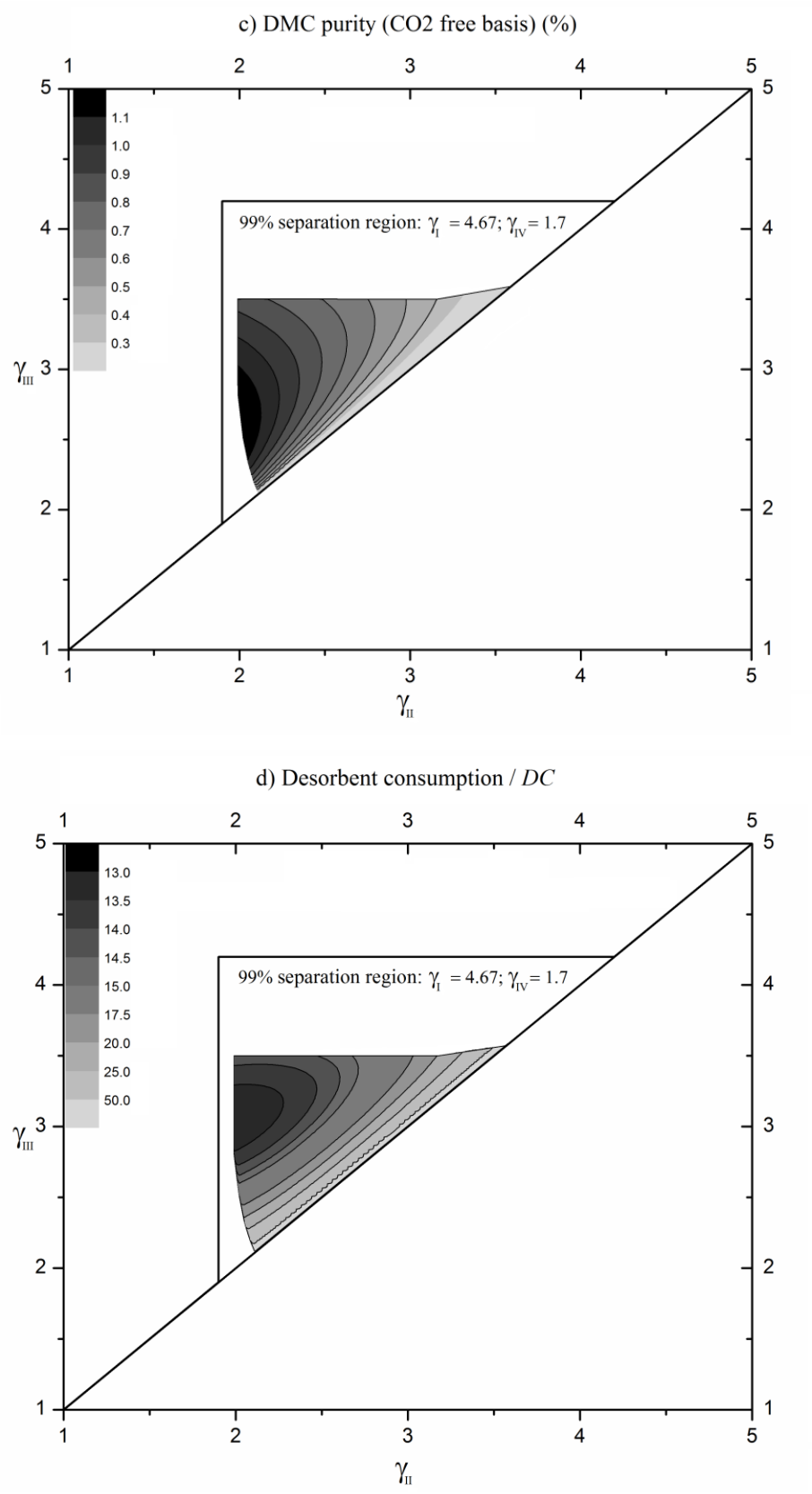

Figure 6.25: Separation regions (above 99%) and contour maps for the proposed TMBR (Stars = first guess): a) DMC purity (MeOH and CO_2 free basis); b) conversion; c) DMC purity (CO_2 free basis); d) desorbent consumption ($L_{MeOH} \cdot mol_{DMC}^{-1}$). General condition/design is described in Table 6.9; Q_{Solid} = 34.7 $mL \cdot min^{-1}$.

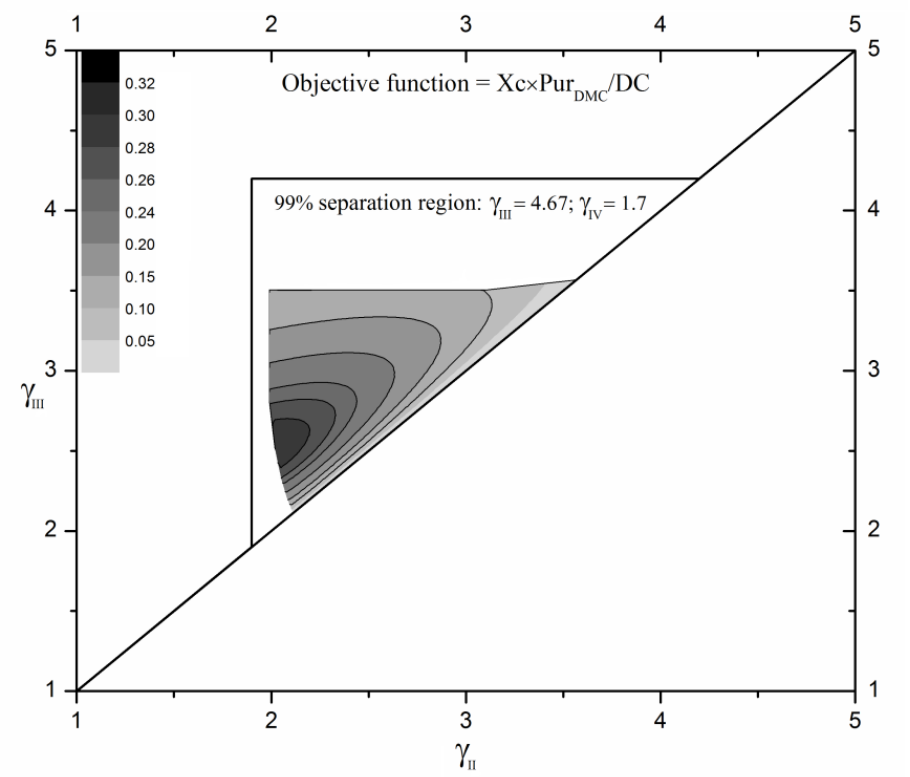

Figure 6.26: Separation region together with the contour map for the objective function, for the proposed TMBR. General condition/design is described in Table 6.9; Q_{Solid} = 34.7 mL·min^{-1}.

Hence, it is acceptable to assume the same global mass transfer coefficients, since the estimation of the mass transfer coefficient, based on the correlations used, might have considerable uncertainties, as discussed in Chapter 5. The same Péclet number was then assumed. Furthermore, the compressibility factor was also estimated again: 1.03 against the 1.04 previously assumed.

Assuming the same global mass transfer coefficients at these new conditions, a velocity of 0.1 cm·s^{-1} along Zone IV is required (as concluded before). Thus for a flow rate of 59.02 ml·min^{-1} a diameter of 3.5 cm was calculated, together with a column length of 26.4 cm in order to have a column volume of 260 mL. These dimensions give a reasonable length to diameter ratio around 7.5.

Finally, the reactor was readjusted to be adapted to the new flow rate in Zone III (86.80 mL·min^{-1}) and concentration inlet in the first reactor. Therefore, these conditions were used to simulate a steady-state fixed bed reactor; and it was concluded that a volume of 60 L is needed to reach the equilibrium. This volume was again uniformly distributed by the 16 reactors (3750 mL each), and by assuming a length to diameter ration of 25 it was computed a length and diameter of 132.8 cm and 5.3 cm, respectively. In addition, a velocity of 0.05 cm·s^{-1} is expected along the reactors. In Table 6.11 is detailed the overall design of the final TMBR, after optimization and redesign.

Table 6.11: Summary of simulation parameters for the final design.

Adsorption column		Reactor	
V / mL	260	V / mL	3750
L/D	~7.5/1	L/D	25/1
D / cm	3.5	D	5.3
L / cm	26.4	L / cm	132.8
Pe	1000	Pe	1000
T / K	298	T / K	363
Compounds	[CO_2 MeOH DMC H_2O]	P / MPa	30
k_L / mm·min^{-1}	[∞ ∞ 1.92 4.6]	Heat exchanger	
K_{ads}	[0 0 2.4 6.0]	β	1.03
General (Q_{Solid} = 34.72 mL·min^{-1})			
C_{Feed}	[11.15 11.15 0 0]	Configuration	3-2-16-3
C_{Eluent}	[0 24.7 0 0]	Reactor configuration	0-0-16-0
t_{switch}^{SMBR} / min	4.5	γ_i	[4.67 2.25 2.50 1.70]

In Table 6.12 are presented the main results to assess the performance of the TMBR unit. As imposed, the purity of water and DMC (MeOH and carbon dioxide free basis) were over 99%: 99.93% for DMC in the Raffinate, and 99.69% for water in the extract. Although the separation between water and DMC is high, both compounds are much diluted in methanol in the outlet streams. This represents a big drawback of the unit even if the reaction and adsorption were carried at the same temperature, because it would demand an energy intensive separation afterwards. Nevertheless, a reaction conversion near 6% was observed, which would be six times higher than for a fixed bed reactor if it were performed in the conditions and with the same feed concentration as the first reactor unit (1.65 $mol_{CO2}·L^{-1}$, 21.84 $mol_{MeOH}·L^{-1}$, 0.049 $mol_{DMC}·L^{-1}$, 0.084 $mol_{H2O}·L^{-1}$).

Table 6.12: Main results for the simulation of the final design.

$PUR_{DMC,R}$	$PUR_{H_2O,X}$	$PUR.II_{DMC,R}$	$PUR.II_{H_2O,X}$
0.87%	0.27%	99.93%	99.69%
Inlet n_{MeOH}/n_{CO2}	X_c	$PROD$/ mol·min^{-1}·L^{-1}	DC/L·kg^{-1}
27.31	5.95%	1.45	20.14

Finally, in Figure 6.27 are displayed the concentration profiles along the adsorption columns (Figure 6.27a) and along the fixed bed reactor (Figure 6.27b). From Figure 6.27a is clear the good separation of DMC and water, forming two well defined waves in opposite directions. In addition, it can be observed that the DMC peak is higher than for water due to the lower raffinate flow rate in comparison with the extract flow rate.

Figure 6.27b shows the concentration profiles of DMC, water and carbon dioxide. Methanol profile was not depicted in order to be easily observed the variation of carbon dioxide along the reactors; nevertheless, the methanol profile has the same tendency as carbon dioxide but at higher concentration (between 22.6 and 24 $mol \cdot L^{-1}$). Moreover, the carbon dioxide curve smoothes, unlike the water and DMC curves, because it is assumed that it is not adsorbed in the adsorption columns that are placed between each two reactor columns.

Further, it was observed a slight increase of DMC and water along the reactor column. This is caused by the high thermodynamic restrictions that limit the reaction conversion in each reactor. Unfortunately, this leads to low conversion (~6%) even though harsh conditions are applied: high pressure (30 MPa) and high methanol to carbon dioxide ratio (around 27 to 1 in the reaction section).

Design algorithm

In Figure 6.28 is summarized a pseudo-algorithm used for the design and optimization of the TMBR unit. This algorithm may be used as a guide to develop new units for other separation and separation/reaction systems. The energy demand for the further separations (solvent recycle) were not considered; however, it would be of great interest since one of the weaknesses of the TMB and TMBR technology is the fact that the products are usually much diluted in the eluent at the outlet streams, which consequently will require more energy for their purification.

Therefore, instead of the typical maximization of productivity or minimization of desorbent consumption, it could be evaluated the total energy amount necessary on these separation processes. Thus, contour maps inside of the separation region for this energy demand might be a powerful tool to optimize / design TMBR units.

Comparison with a fixed bed reactor

Finally, the performance of the TMBR is compared with a fixed bed reactor in order to evaluate the improvements achieved. Hence, the same reaction conditions were assumed to simulate the fixed bed reactor. Moreover, the feed stream of the fixed bed reactor is equal to the sum of the feed and eluent streams of the optimized TMBR unit.

After simulating, it was observed that the fixed bed reactor reaches higher DMC conversion (~8%) than the TMBR (~6%); this is explained by the fact that the extract (rich in methanol) is removed, and is not effectively used for the reaction. Therefore, the fixed bed reactor is operated at higher methanol to carbon dioxide ratio than the reactive section of the TMBR.

Nevertheless, the major advantage of the TMBR is the separation of water and DMC into two different streams. Besides, the purities of DMC and water are higher than for the fixed bed reactor outlet, which is an important feature to reduce the energy consumption on further purifications. For instance, the DMC purity (carbon dioxide free basis) in the Raffinate is around 3 times higher for the TMBR (~0.9%) than for the fixed bed (~0.3%). Another important feature of the TMBR/SMBR is its great capacity to handle high contents of water in the feed stream, without reducing the overall performance.

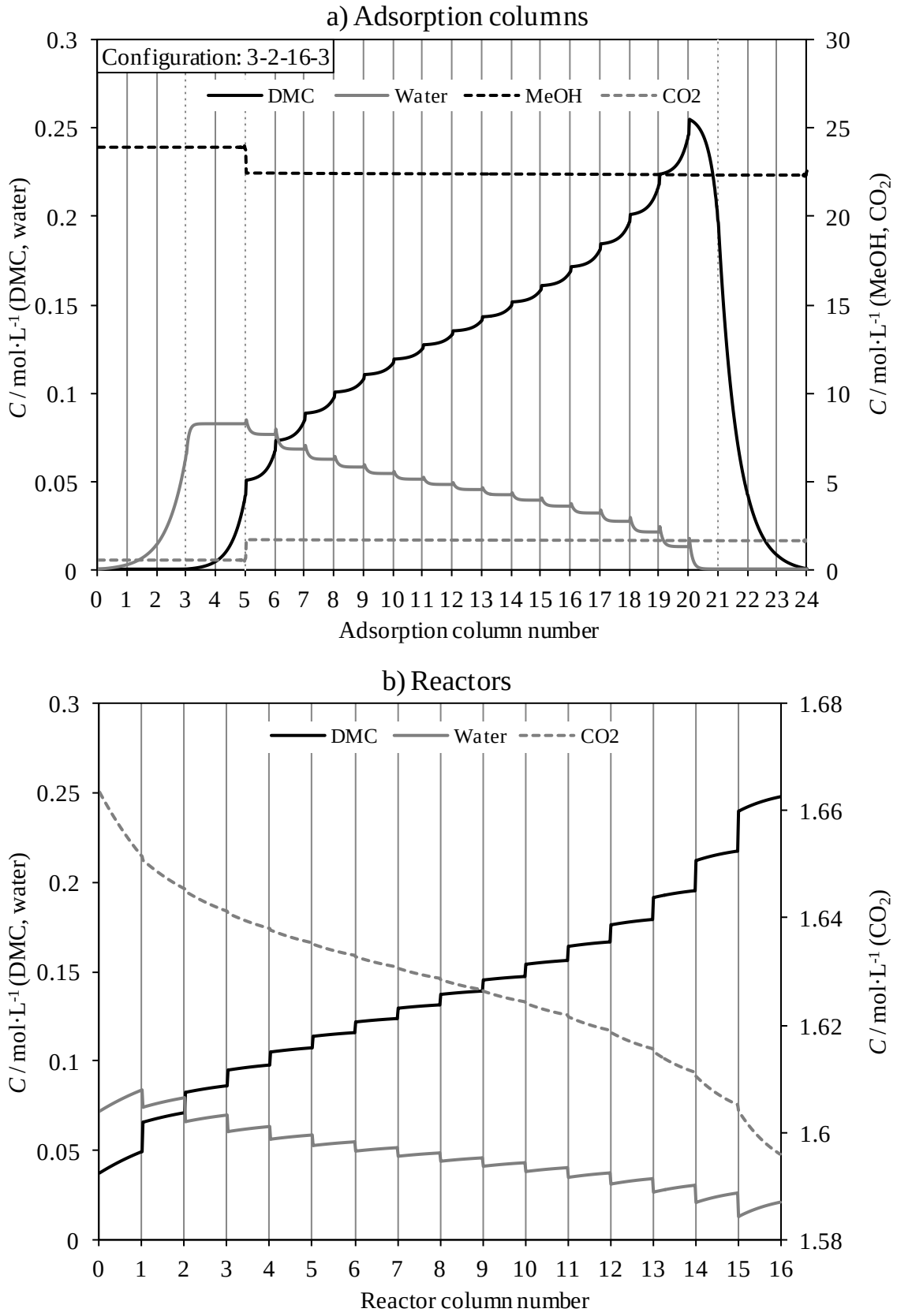

Figure 6.27: TMBR profile concentrations of water and DMC along the: a) adsorption columns; b) fixed bed reactors (C_{MeOH} = 22.6-24 mol·L^{-1}). Simulation parameters described in Table 6.11.

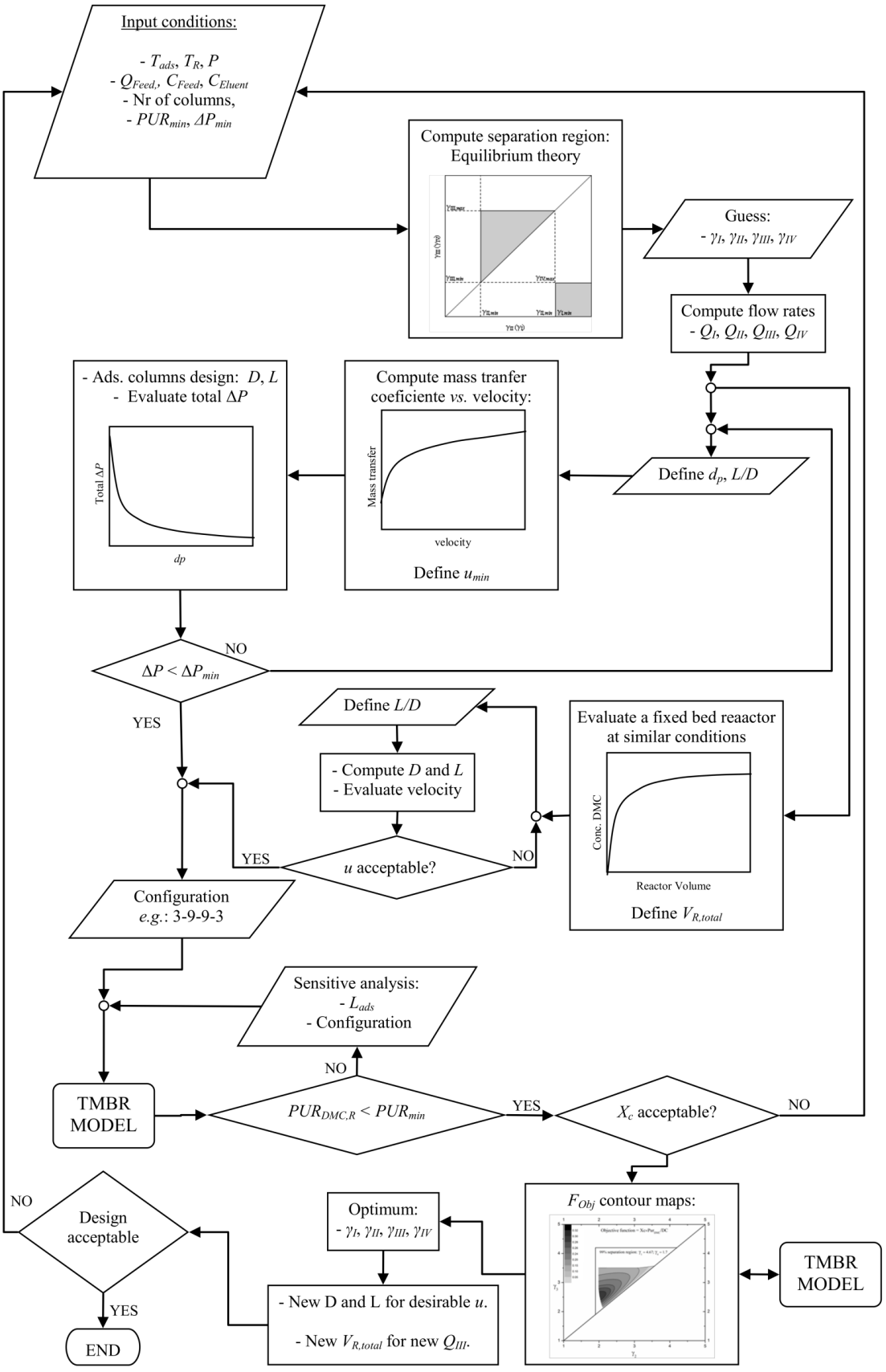

Figure 6.28: Flow diagram algorithm used for the design and optimization of the TMBR unit.

In Figure 6.29b are depicted the effects of the total water content in the inlet streams on the DMC yield and on the DMC purity (carbon dioxide free basis) at the outlet stream. For the fixed bed reactor, the graphs show a drastic decrease of DMC yield and purity with the presence of water traces. For instance, with 3% of water the DMC yield is lower than 1% and the DMC purity is lower than 0.05%. For the TMBR simulation, the DMC yield and purity are almost not sensitive to the water content, as long as it is in the feed stream. Otherwise, if the eluent had a similar amount of water, it would "contaminate" the reaction section affecting then remarkably the DMC yield.

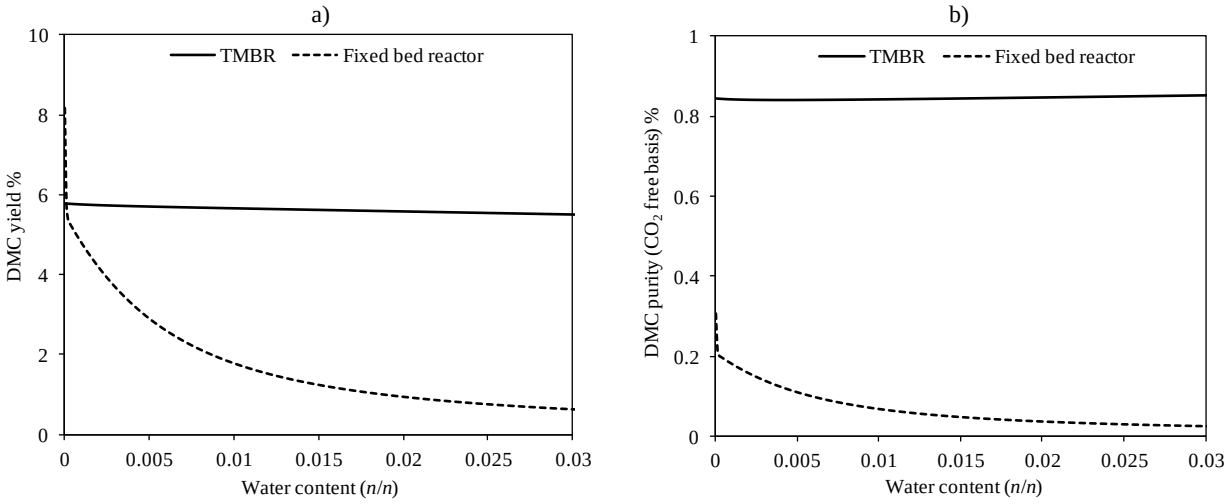

Figure 6.29: Effect of the water content (feed stream) on: a) DMC yield; b) DMC purity (CO_2 free basis) for a TMBR and a fixed bed reactor.

The effect of water content in the feed stream of the TMBR is now discussed in more detail. In Figure 6.30 are displayed the TMBR profiles for 0% and 90% of water (carbon dioxide free basis) in the feed stream, where it can be observed that water is effectively removed from the reaction section of the TMBR, and after the column 7 the profile of water is similar for both situations. Nevertheless, it still has an effect on the DMC profile, which leads to slightly lower yield as reported before.

In conclusion, this capacity to handle high amount of water in the feed stream is of great interest for industrial application. Not only a small amount of water is commonly present in industrial streams, but also it might decrease the energy consumption and/or the distillation column size for the further separation of water and methanol.

In spite of these advantages, it is important to measure the real benefits of the proposed TMBR. Would it be profitable? To answer this question it would be necessary to study the overall process from the raw materials to the final product. However, it seems clear that the low DMC purity (carbon dioxide free basis) of 0.9% is the major limitation, especially because methanol and DMC form an azeotropic mixture. Hence the separation of DMC from methanol would be too expensive and might compromise the process. Using an excess of carbon dioxide instead of methanol would lead to lower DMC yield but it might be cheaper to purify.

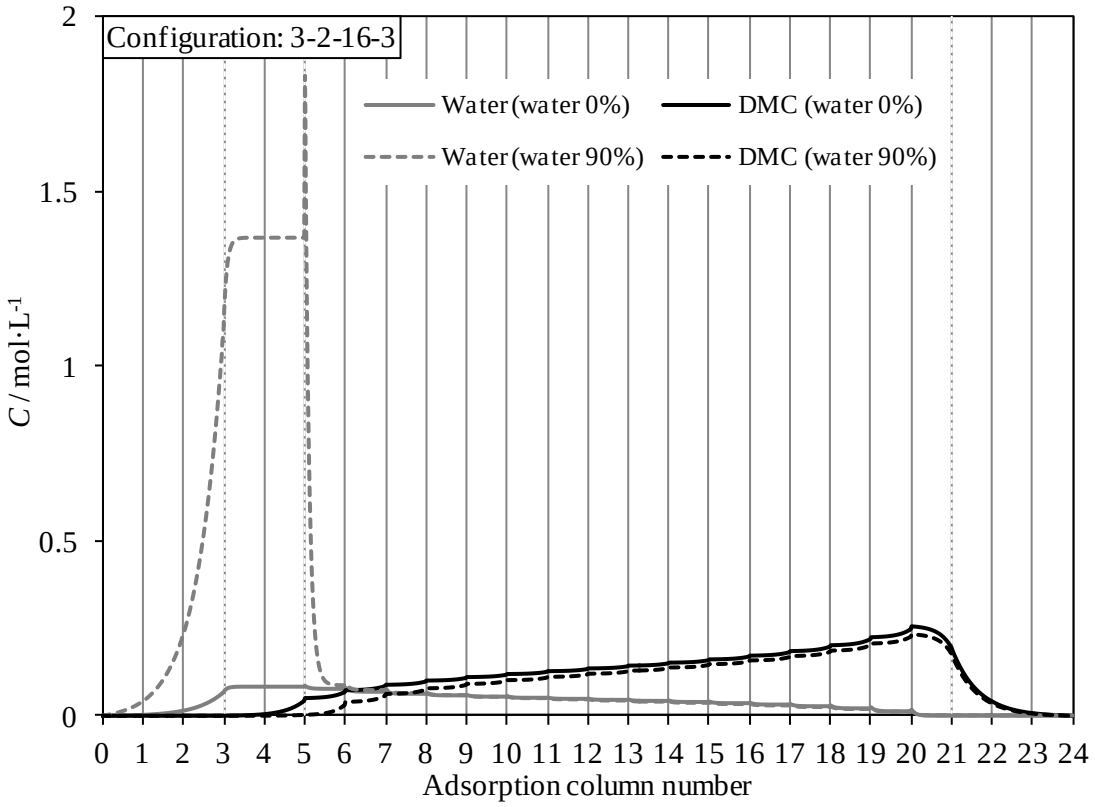

Figure 6.30: TMBR profile concentrations of water and DMC along the adsorption columns for 0% and 90% water content (CO_2 free basis) on the feed stream.

6.7. Conclusions

In this chapter different scenarios were studied, coupling adsorption and reaction technologies to enhance the DMC yield from the direct synthesis from methanol and carbon dioxide: $CO_2 + 2MeOH \rightleftharpoons DMC + H_2O$. The major drawbacks presented in all the scenarios were the different temperatures for the adsorption and reaction, which leads to an intensive energy process. Nevertheless, this study aimed to quantify the potentiality of combining reaction and adsorption, in order to know if it would be a possible alternative if adsorption and reaction could be carried out in same conditions. Finally the following main conclusions were withdrawn:

❖ The first scenario, single batch reactor, demonstrated the impossibility to perform the reaction plus adsorption at the same conditions. It was concluded that besides the relative high improvement (~24%) the DMC yield would still be low (~2.2%).

❖ In the second scenario it was studied the performance of a reactor connected to a fixed bed column by an external loop. In order to transform the process into a semi-continuous one, two columns were considered, alternating between adsorption and regeneration modes. With this theoretical study it was concluded that it would be possible to achieve near 100% of conversion if it would be possible to recover the DMC and water from a much diluted mixture (~0.3 $mol \cdot L^{-1}$). However, the process is far to be feasible due to this problem.

❖ Then, it was simulated a set of alternating fixed bed reactors and adsorption columns, to enhance the DMC yield in a transient state. This study was conducted in order to evaluate the potential of a TMBR using a Hashimoto type configuration. In fact, it was observed a shift of the DMC yield over 20%, at 20 MPa, 10 mL·min^{-1} (298K), T_{reac} = 363 K, T_{ads}= 298 K, and n_{CO_2}/n_{MeOH}= 1/1.

❖ Next, it was proposed an algorithm for the design and optimization of a TMBR/SMBR unit for the synthesis of DMC. With the optimum design and optimum conditions proposed (30 MPa, T_r = 383 K, T_{ads}= 298 K, and n_{CO_2}/n_{MeOH} ~ 1/27) it were obtained the following main results: $PUR_{DMC,R}$ = 0.87%, $PUR_{H_2O,X}$ = 0.27, $PUR.II_{DMC,R}$ = 99.93%, $PUR.II_{H_2O,X}$ = 99.69%; X_c=5.95%.

❖ Finally, it were compared the performances of the TMBR and of a fixed bed reactor; and it was concluded that the TMBR not only separates the water and DMC in two streams, but it also has a large capacity to handle large contents of water in the feed stream. In fact, with a feed stream with 0.9 molar fraction of water (carbon dioxide free basis) the performance remained almost the same.

In spite of these remarkable results, the low concentration of DMC in the Raffinate stream remains an issue that should be overcome. A possibility would be operating with excess of carbon dioxide instead of methanol. Although the excess of carbon dioxide leads to lower conversion, it is easily separated by evaporation and the products would definitely be more concentrated in the outlet streams.

Nomenclature

Symbols

β	Compressibility factor
C_i	Bulk concentration of each compound *i* (mol·m$_{bulk}^{-3}$)
$\bar{C}_{p,i}$	Average pores concentration of each compound (mol·m$_{porous}^{-3}$)
γ	Liquid to solid flow rate ratio
D	Column diameter (m)
DC	Desorbent consumption (m$_{eluent}^{3}$·mol$_{DMC}^{-1}$)
d_p	Particle diameter (m)
E_a	Activation energy (J·mol^{-1})
ε_b	Bulk porosity (m$_{bulk}^{-3}$·m$_{total}^{-3}$)
ε_p	Particle porosity (m$_{porous}^{-3}$·m$_{particle}^{-3}$)
F_{Obj}	Objective Function
$\Delta H_{ads}, \Delta H_r$	Enthalpy change of adsorption and reaction (J·mol^{-1})

ϑ	Stoichiometric coefficient
k_{int}, k_L	Internal and global mass transfer coefficient ($m \cdot s^{-1}$)
k, k_0	Kinetic constant, respective pre-exponential factor ($mol \cdot Pa^{-3} \cdot s^{-1} \cdot g_{cat}^{-1}$)
K_{eq}	Reaction equilibrium constant
K_{ads}	Adsorption equilibrium constant ($m_{porous}^{-3} \cdot m_{solid}^{-3}$)
L	Column length (m)
m_{cat}	Catalyst weight (g)
n	Molar amount (mol)
P, P_{ref}	Pressure, reference pressure (Pa)
Pe	Péclet number
$PROD$	TMBR productivity ($mol_{DMC} \cdot s^{-1} \cdot m^{-3}$)
PUR	Molar purity (CO_2 free basis)
$PUR.II$	Molar purity (CO_2 and MeOH free basis)
q_i	Adsorbed amount of compound *i* ($mol \cdot m_{solid}^{-3}$)
Q	Volumetric flow rate ($m^3 \cdot s^{-1}$)
r	Reaction rate ($mol \cdot s^{-1} \cdot g_{cat}^{-1}$)
r_p	Particle radius (m)
R	Ideal gas constant ($J \cdot K^{-1} \cdot mol^{-1}$)
$R_{CO_2/MeOH}$	Carbon dioxide to methanol molar ratio
REC	Recovery of water or DMC
ρ	Density ($kg \cdot m^{-3}$)
$\Delta S_{ads}, \Delta S_r$	Entropy change of adsorption and reaction ($J \cdot K^{-1} \cdot mol^{-1}$)
t	Time (s)
T	Temperature (K)
u_0	Superficial velocity ($m \cdot s^{-1}$)
V	Volume (m^3)
V_M	Molar volume ($m^3 \cdot mol^{-1}$)
x	Molar fraction
X_C	Reaction conversion of limiting reactant

z	Dimensionless axial position

Sub- and superscripts

ads	Adsorption / Adsorption column
b	Bulk
cat	Catalyst
lim	Limiting reactant
^{o}	Standard
reac	Reaction / Reactor
0	Initial

Abbreviations

DMC	Dimethyl carbonate
E	Extract
F	Feed
HE	Heat exchanger
MeOH	Methanol
R	Raffinate
SMB(R)	Simulated Moving Bed (Reactor)
TMB(R)	True Moving Bed (Reactor)
X	Extract

References

[1] Seider, W. D.,Seader, J. D.,Lewin, D. R. *Product And Process Design Principles: Synthesis, Analysis And Design*; 3rd ed.; Wiley Global Education: **2008**.

[2] Lutze, P.,Gani, R.,Woodley, J. M. Process Intensification: A Perspective On Process Synthesis. *Chemical Engineering and Processing: Process Intensification* **2010,** *49*(6), 547.

[3] Stankiewicz, A. I.,Moulijn, J. A. Process Intensification: Transforming Chemical Engineering. *Chemical Engineering Progress* **2000,** *96*(1), 22.

[4] Anastas, P.,Warner, J. *Green Chemistry: Theory And Practice*; 1st ed.; Oxford University Press: New York, **1998**.

[5] Kulprathipanja, S. *Reactive Separation Processes*; Taylor & Francis: **2001**.

[6] Sundmacher, K.,Kienle, A. *Reactive Distillation: Status And Future Directions*; Wiley: **2006**.

[7] Ruthven, D. M.,Ching, C. B. Counter-Current And Simulated Counter-Current Adsorption Separation Processes. *Chemical Engineering Science* **1989,** *44*(5), 1011.

[8] Zhong, G.,Guiochon, G. Analytical Solution For The Linear Ideal Model Of Simulated Moving Bed Chromatography. *Chemical Engineering Science* **1996,** *51*(18), 4307.

[9] Chiang, A. S. T. Equilibrium Theory For Simulated Moving Bed Adsorption Processes. *AIChE Journal* **1998,** *44*(11), 2431.

[10] Mazzotti, M.,Storti, G.,Morbidelli, M. Robust Design Of Countercurrent Adsorption Separation Processes: 2. Multicomponent Systems. *AIChE Journal* **1994,** *40*(11), 1825.

[11] Migliorini, C.,Mazzotti, M.,Morbidelli, M. Design Of Simulated Moving Bed Multicomponent Separations: Langmuir Systems. *Separation and Purification Technology* **2000,** *20*(1), 79.

[12] Sá Gomes, P.,Lamia, N.,Rodrigues, A. E. Design of a gas phase simulated moving bed for propane/propylene separation. *Chemical Engineering Science* **2009,** *64*(6).

[13] Zhong, G.,Guiochon, G. Simulated Moving Bed Chromatography. Effects Of Axial Dispersion And Mass Transfer Under Linear Conditions. *Chemical Engineering Science* **1997,** *52*(18), 3117.

[14] Rodrigues, A. E.,Minceva, M. Modelling And Simulation In Chemical Engineering: Tools For Process Innovation. *Computers and Chemical Engineering* **2005,** *29*(6 SPEC. ISS.), 1167.

[15] Rodrigues, A. E.,Pais, L. S. Design Of SMB Chiral Separations Using The Concept Of Separation Volume. *Separation Science and Technology* **2004,** *39*(2), 245.

[16] Azevedo, D. C. S.,Rodrigues, A. E. Design Of A Simulated Moving Bed In The Presence Of Mass-Transfer Resistances. *AIChE Journal* **1999,** *45*(5), 956.

[17] Fricke, J.,Meurer, M.,Dreisörner, J.,Schmidt-Traub, H. Effect Of Process Parameters On The Performance Of A Simulated Moving Bed Chromatographic Reactor. *Chemical Engineering Science* **1999,** *54*(10), 1487.

[18] Broughton, D. B.,Gerhold, C. G. Continuous Sorption Process Employing Fixed Bed Of Sorbent And Moving Inlets And Outlets. US 2985589, **1961**.

[19] Adachi, S. Simulated Moving-Bed Chromatography For Continuous Separation Of Two Components And Its Application To Bioreactors. *Journal of Chromatography A* **1994,** *658*(2), 271.

[20] Juza, M.,Mazzotti, M.,Morbidelli, M. Simulated Moving-Bed Chromatography And Its Application To Chirotechnology. *Trends in Biotechnology* **2000,** *18*(3), 108.

[21] Imamoglu, S. Simulated Moving Bed Chromatography (SMB) For Application In Bioseparation. *Advances in biochemical engineering/biotechnology* **2002,** *76*, 211.

[22] Cai, Y.,Ding, Y.,Zhang, D.,Dai, J.,Shi, G.,Xu, W. Simulated Moving Bed Technology And Its Applications. *Se pu = Chinese journal of chromatography / Zhongguo hua xue hui* **2004,** *22*(2), 111.

[23] Seidel-Morgenstern, A.,Keßler, L. C.,Kaspereit, M. New Developments In Simulated Moving Bed Chromatography. *Chemical Engineering and Technology* **2008,** *31*(6), 826.

[24] Rajendran, A.,Paredes, G.,Mazzotti, M. Simulated Moving Bed Chromatography For The Separation Of Enantiomers. *Journal of Chromatography A* **2009,** *1216*(4), 709.

[25] Šunjić, V.,Franić, D.,Kontrec, D.,Rojeb, M. Recent Achievements In Simulated Moving Bed (SMB) Technology. Part II. *Kemija u industriji/Journal of Chemists and Chemical Engineers* **2010,** *59*(9), 439.

[26] Sá Gomes, P.,Rodrigues, A. E. Simulated Moving Bed Chromatography: From Concept To Proof-Of-Concept. *Chemical Engineering and Technology* **2012,** *35*(1), 17.

[27] Broughton, D. B.,Neuzil, R. W.,Pharis, J. M.,Brearley, C. S. Parex Process For Recovering Paraxylene. *Chemical Engineering Progress* **1970,** *66*(9), 70.

[28] Broughton, D. B. Production Of Pure M-Xylene And Pure Ethyl Benzene From A Mixture Of C8 Aromatic Isomers. US 4306107, **1981**.

[29] Broughton, D. B. Sucrose Extraction From Aqueous Solutions Featuring Simulated Moving Bed. US 4404037, **1983**.

[30] Haynes, T. N.,Caram, H. S. The Simulated Moving Bed Chemical Reactor. *Chemical Engineering Science* **1994,** *49*(24), 5465.

[31] Ray, A. K.,Carr, R. W.,Aris, R. The Simulated Countercurrent Moving Bed Chromatographic Reactor: A Novel Reactor-Separator. *Chemical Engineering Science* **1994,** *49*(4), 469.

[32] Migliorini, C.,Fillinger, M.,Mazzotti, M.,Morbidelli, M. Analysis of simulated moving-bed reactors. *Chemical Engineering Science* **1999,** *54*(13-14).

[33] Lode, F.,Mazzotti, M.,Morbidelli, M. A New Reaction-Separation Unit: The Simulated Moving Bed Reactor. *Chimia* **2001,** *55*(10), 883.

[34] Minceva, M.,Rodrigues, A. E. Simulated Moving-Bed Reactor: Reactive-Separation Regions. *AIChE Journal* **2005,** *51*(10), 2737.

[35] Zondervan, E.,Nikacevic, N.,Khajuria, H.,Pistikopoulos, E. N.,de Haan, A. B. Integrated Operation And Design Of A Simulated Moving Bed Reactor. *Computer Aided Chemical Engineering* **2012,** *30*, 642.

[36] Xu, J.,Liu, Y.,Xu, G.,Yu, W.,Ray, A. K. Analysis Of A Nonisothermal Simulated Moving-Bed Reactor. *AIChE Journal* **2013,** *59*(12), 4705.

[37] Migliorini, C.,Fillinger, M.,Mazzotti, M.,Morbidelli, M. Analysis Of Simulated Moving-Bed Reactors. *Chemical Engineering Science* **1999,** *54*(13–14), 2475.

[38] Hashimoto, K.,Adachi, S.,Noujima, H.,Ueda, Y. A New Process Combining Adsorption And Enzyme Reaction For Producing Higher-Fructose Syrup. *Biotechnology and Bioengineering* **1983,** *25*(10), 2371.

[39] Kawase, M.,Inoue, Y.,Araki, T.,Hashimoto, K. The Simulated Moving-Bed Reactor For Production Of Bisphenol A. *Catalysis Today* **1999,** *48*(1-4), 199.

[40] Silva, V. M. T. M.,Rodrigues, A. E. Novel Process For Diethylacetal Synthesis. *AIChE Journal* **2005,** *51*(10), 2752.

[41] Pereira, C. S. M.,Gomes, P. S.,Gandi, G. K.,Silva, V. M. T. M.,Rodrigues, A. E. Multifunctional Reactor For The Synthesis Of Dimethylacetal. *Industrial and Engineering Chemistry Research* **2008,** *47*(10), 3515.

[42] Rodrigues, A. E.,Silva, V. M. T. In *Simulated Moving Bed Adsorptive Reactor For The Synthesis Of Green Diesel Additives (Acetals)*, CAMURE 7 & ISMR 6, **2009**.

[43] Silva, V. T.,Silva, R.,Rodrigues, A. E. In *Green Diesel Additive Synthesis: Elimination Of Azeotropic Distillation By Coupling Simulated Moving Bed Reactor With Solvent Recovery Units*, AIChE meeting, **2009**.

[44] Graça, N. S.,Pais, L. S.,Silva, V. M. T. M.,Rodrigues, A. E. Analysis Of The Synthesis Of 1,1-Dibutoxyethane In A Simulated Moving-Bed Adsorptive Reactor. *Chemical Engineering and Processing: Process Intensification* **2011,** *50*(11-12), 1214.

[45] Graça, N. S.,Pais, L. S.,Silva, V. M. T. M.,Rodrigues, A. E. Thermal Effects On The Synthesis Of Acetals In A Simulated Moving Bed Adsorptive Reactor. *Chemical Engineering Journal* **2012,** *207-208*, 504.

[46] Rodrigues, A. E.,Pereira, C. S. M.,Santos, J. C. Chromatographic Reactors. *Chemical Engineering and Technology* **2012,** *35*(7), 1171.

[47] Pereira, C. S. M.,Rodrigues, A. E. Process Intensification: New Technologies (SMBR And PermSMBR) For The Synthesis Of Acetals. *Catalysis Today* **2013,** *218-219*, 148.

[48] Azevedo, D. C. S.,Rodrigues, A. E. Design Methodology And Operation Of A Simulated Moving Bed Reactor For The Inversion Of Sucrose And Glucose-Fructose Separation. *Chemical Engineering Journal* **2001,** *82*(1-3), 95.

[49] Da Silva, E. A. B.,Souza, D. P.,De Souza, A. A. U.,Souza, S. M. A. G. U.,Rodrigues, A. E. Analysis Of The Behavior Of The Simulated Moving Bed Reactor In The Sucrose Inversion Process. *Separation Science and Technology* **2005,** *40*(12), 2373.

[50] Da Silva, E. A. B.,De Souza, A. A. U.,Rodrigues, A. E.,De Souza, S. M. A. G. U. Glucose Isomerization In Simulated Moving Bed Reactor By Glucose Isomerase. *Brazilian Archives of Biology and Technology* **2006,** *49*(3), 491.

[51] Kruglov, A. V. Methanol Synthesis In A Simulated Countercurrent Moving-Bed Adsorptive Catalytic Reactor. *Chemical Engineering Science* **1994,** *49*(24 PART A), 4699.

[52] Tonkovich, A. L. Y.,Carr, R. W. A Simulated Countercurrent Moving-Bed Chromatographic Reactor For The Oxidative Coupling Of Methane: Experimental Results. *Chemical Engineering Science* **1994,** *49*(24 PART A), 4647.

[53] Kawase, M.,Suzuki, T. B.,Inoue, K.,Yoshimoto, K.,Hashimoto, K. Increased Esterification Conversion By Application Of The Simulated Moving-Bed Reactor. *Chemical Engineering Science* **1996,** *51*(11), 2971.

[54] Kruglov, A. V.,Bjorklund, M. C.,Carr, R. W. Optimization Of The Simulated Countercurrent Moving-Bed Chromatographic Reactor For The Oxidative Coupling Of Methane. *Chemical Engineering Science* **1996,** *51*(11), 2945.

[55] Kawase, M.,Pilgrim, A.,Araki, T.,Hashimoto, K. Lactosucrose Production Using A Simulated Moving Bed Reactor. *Chemical Engineering Science* **2001,** *56*(2), 453.

[56] Lode, F.,Francesconi, G.,Mazzotti, M.,Morbidelli, M. Synthesis Of Methylacetate In A Simulated Moving-Bed Reactor: Experiments And Modeling. *AIChE Journal* **2003,** *49*(6), 1516.

[57] Yu, W.,Hidajat, K.,Ray, A. K. Modeling, Simulation, And Experimental Study Of A Simulated Moving Bed Reactor For The Synthesis Of Methyl Acetate Ester. *Industrial and Engineering Chemistry Research* **2003,** *42*(26), 6743.

[58] Fissore, D.,Tejedor, D. G.,Barresi, A. A. Experimental Investigation Of The SCR Of NOX In A Simulated Moving Bed Reactor. *AIChE Journal* **2006,** *52*(9), 3146.

[59] Pilgrim, A.,Kawase, M.,Matsuda, F.,Miura, K. Modeling Of The Simulated Moving-Bed Reactor For The Enzyme-Catalyzed Production Of Lactosucrose. *Chemical Engineering Science* **2006,** *61*(2), 353.

[60] Da Silva, E. A. B.,De Souza, A. A. U.,De Souza, S. G. U.,Rodrigues, A. E. Simulated Moving Bed Technology In The Reactive Process Of Glucose Isomerization. *Adsorption* **2005,** *11*(1 SUPPL.), 847.

[61] Minceva, M.,Silva, V. M. T.,Rodrigues, A. E. Analytical Solution For Reactive Simulated Moving Bed In The Presence Of Mass Transfer Resistance. *Industrial and Engineering Chemistry Research* **2005,** *44*(14), 5246.

[62] Borges da Silva, E. A.,Ulson de Souza, A. A.,de Souza, S. G. U.,Rodrigues, A. E. Analysis Of The High-Fructose Syrup Production Using Reactive Smb Technology. *Chemical Engineering Journal* **2006,** *118*(3), 167.

[63] Minceva, M.,Gomes, P. S.,Meshko, V.,Rodrigues, A. E. Simulated Moving Bed Reactor For Isomerization And Separation Of P-Xylene. *Chemical Engineering Journal* **2008,** *140*(1-3), 305.

[64] Pereira, C. S. M.,Silva, V. M. T. M.,Rodrigues, A. E. Fixed Bed Adsorptlve Reactor For Ethyl Lactate Synthesis: Experiments, Modelling, And Simulation. *Separation Science and Technology* **2009,** *44*(12), 2721.

[65] Pereira, C. S. M.,Zabka, M.,Silva, V. M. T. M.,Rodrigues, A. E. A Novel Process For The Ethyl Lactate Synthesis In A Simulated Moving Bed Reactor (SMBR). *Chemical Engineering Science* **2009,** *64*(14), 3301.

[66] Borges Da Silva, E. A.,Pedruzzi, I.,Rodrigues, A. E. Simulated Moving Bed Technology To Improve The Yield Of The Biotechnological Production Of Lactobionic Acid And Sorbitol. *Adsorption* **2011,** *17*(1), 145.

[67] Silva, V. M. T. M.,Pereira, C. S. M.,Rodrigues, A. E. PermSMBR-A New Hybrid Technology: Application On Green Solvent And Biofuel Production. *AIChE Journal* **2011,** *57*(7), 1840.

[68] Pereira, C. S. M.,Silva, V. M. T. M.,Rodrigues, A. E. Green Fuel Production Using The PermSMBR Technology. *Industrial and Engineering Chemistry Research* **2012,** *51*(26), 8928.

[69] Pereira, C. S. M.,Rodrigues, A. E. New Sorption Enhanced Reaction Technologies (SMBR And PermSMBR) For The Production Of Diesel Blends And Green Solvents. *Chimica Oggi/Chemistry Today* **2013,** *31*(3), 64.

[70] Pereira, C. S. M.,Silva, V. M. T. M.,Rodrigues, A. E. Coupled PermSMBR - Process Design And Development For 1,1-Dibutoxyethane Production. *Chemical Engineering Research and Design* **2013,** *xx*(xx).

[71] Smith, J. M.,Ness, H. C. V.,Abbott, M. M. *Introduction To Chemical Engineering Thermodynamics*; 6th ed.; McGraw-Hill: New York, **2005**.

[72] Luyben, W. L. *Distillation Design And Control Using Aspen Simulation*; Wiley: **2013**.

[73] Wei, H.-M.,Wang, F.,Zhang, J.-L.,Liao, B.,Zhao, N.,Xiao, F.-k.,Wei, W.,Sun, Y.-H. Design And Control Of Dimethyl Carbonate–Methanol Separation Via Pressure-Swing Distillation. *Industrial & Engineering Chemistry Research* **2013,** *52*(33), 11463.

[74] Dean, D.,Stiel, L. The Viscosity Of Nonpolar Gas Mixtures At Moderate And High Pressures. *AIChE Journal* **1965,** *11*(3), 526.

[75] Azevedo, D. C. S.,Rodrigues, A. E. Design And Optimization Of New Simulated Moving Bed Plants. *Brazilian Journal of Chemical Engineering* **2006,** *23*(2), 171.

[76] Mota, J. P. B.,Araújo, J. M. M.,Rodrigues, R. C. R. Optimal Design Of Simulated Moving-Bed Processes Under Flow Rate Uncertainty. *AIChE Journal* **2007,** *53*(10), 2630.

[77] Pais, L. S.,Rodrigues, A. E. Design Of Simulated Moving Bed And Varicol Processes For Preparative Separations With A Low Number Of Columns. *Journal of Chromatography A* **2003,** *1006*(1-2), 33.

[78] Charton, F.,Nicoud, R.-M. Complete Design Of A Simulated Moving Bed. *Journal of Chromatography A* **1995,** *702*(1–2), 97.

[79] Fricke, J.,Meurer, M.,Schmidt-Traub, H. Design And Layout Of Simulated-Moving-Bed Chromatographic Reactors. *Chemical Engineering and Technology* **1999,** *22*(10), 835.

[80] Fricke, J.,Schmidt-Traub, H. A New Method Supporting The Design Of Simulated Moving Bed Chromatographic Reactors. *Chemical Engineering and Processing: Process Intensification* **2003,** *42*(3), 237.

[81] Nilchan, S.,Pantelides, C. C. On The Optimisation Of Periodic Adsorption Processes. *Adsorption* **1998,** *4*(2), 113.

[82] Kloppenburg, E.,Gilles, E. D. A New Concept For Operating Simulated Moving-Bed Processes. *Chemical Engineering & Technology* **1999,** *22*(10), 813.

[83] Dünnebier, G.,Fricke, J.,Klatt, K.-U. Optimal Design And Operation Of Simulated Moving Bed Chromatographic Reactors. *Industrial & Engineering Chemistry Research* **2000,** *39*(7), 2290.

[84] Subramani, H. J.,Zhang, Z.,Hidajat, K.,Ray, A. K. Multiobjective Optimization Of Simulated Moving Bed Reactor And Its Modification — Varicol Process. *The Canadian Journal of Chemical Engineering* **2004,** *82*(3), 590.

[85] Zhang, Z.,Hidajat, K.,Ray, A. K.,Morbidelli, M. Multiobjective Optimization Of SMB And Varicol Process For Chiral Separation. *AIChE Journal* **2002,** *48*(12), 2800.

[86] Zhang, Z.,Mazzotti, M.,Morbidelli, M. Multiobjective Optimization Of Simulated Moving Bed And Varicol Processes Using A Genetic Algorithm. *Journal of Chromatography A* **2003,** *989*(1), 95.

[87] Ziyang, Z.,Hidajat, K.,Ray, A. K. Multiobjective Optimization Of Simulated Countercurrent Moving Bed Chromatographic Reactor (SCMCR) For MTBE Synthesis. *Industrial & Engineering Chemistry Research* **2002,** *41*(13), 3213.

[88] Censor, Y. Pareto Optimality In Multiobjective Problems. *Applied Mathematics & Optimization* **1976,** *4*(1), 41.

[89] McCabe, W. L.,Smith, J.,Harriott, P. *Unit Operations Of Chemical Engineering*; McGraw-Hill Education: **2005**.

[90] Kataoka, T.,Yoshida, H.,Ueyama, K. Mass Transfer In Laminar Region Between Liquid And Packing Material Surface In The Packed Bed. *Journal of Chemical Engineering of Japan* **1972,** *5*(2), 132.

[91] Wilke, C.,Chang, P. Correlation Of Diffusion Coefficients In Dilute Solutions. *AIChE Journal* **1955,** *1*(2), 264.

[92] Do Duong, D. *Adsorption Analysis: Equilibria And Kinetics*; Imperial College Press: **1998**.

Chapter 7. Conclusion and Suggestions for Future Work

"What we know is a drop, what we don't know is an ocean." – Isaac Newton

7.1. Main Conclusions

In this Thesis it was explored the direct synthesis of dimethyl carbonate from carbon dioxide and methanol ($CO_2 + CH_3OH \rightleftharpoons DMC + H_2O$) at high pressure conditions, combining reaction and adsorption technologies to enhance the DMC yield, which is strongly limited by thermodynamic restrictions. Hence, a Simulated Moving Bed Reactor was proposed to overcome this issue, where the water produced in the reaction is continuously separated from the reacting mixture to increase the overall conversion.

Initially an extensive state-of-the-art study was conducted, which allowed to choose cerium oxide and zeolite 3A (molecular sieve) as catalyst and adsorbent for this process. Although these materials are not the most efficient in terms of activity and capacity, respectively, they have high selectivity and are easy to obtain. Other materials are mentioned in the state-of the-art but their preparation or development was out of the scope of this work.

In order to achieve this goal the project was divided in four milestones: the development of a thermodynamic model, able to predict the physical equilibrium and other thermodynamic properties; the development of a kinetic model over cerium oxide, based on experiments conducted in a batch reactor; the determination the isotherm and mass transfer coefficients, for water and DMC (diluted in carbon dioxide and methanol) over the zeolite 3A surface, through the analysis of pulse injection in a supercritical fluid chromatograph; and finally, the design and optimization of the Simulated Moving Bed Reactor.

Thermodynamic model

In order to predict the thermodynamic properties of the reacting mixture, vapour-liquid data was fitted to the Soave-Redlich-Kwong cubic equation of state (Eq. 3.5) coupled with five different mixing rules: classic van der Waals one-fluid, modified first order Huron-Vidal, modified second order Huron-Vidal, linear combination of Vidal and Michelsen, and Wong and Sandler. With exception of the classic van der Waals mixing rule, the other mixing rules were based on the excess Gibbs free energy, which was estimated from the UNIQUAC model.

Among the five mixing rules, the modified second order Huron-Vidal mixing rule, with only two fitted parameters, was found to be the best model, showing high performance for the estimation of vapour liquid equilibrium for all the binary systems, as well as for the ternary mixture between carbon dioxide, methanol, and water.

Kinetic model

The kinetic experiments were carried out in a batch reactor, catalysed by cerium oxide, with high reproducibility and in the absence of external mass transfer resistances. Surprisingly, the kinetics and the chemical equilibrium were better modelled by considering an ideal gas than assuming real gas behaviour, predicted by the cubic equation of state fitted before. This indicates that the thermodynamic model has inconsistencies to predict the fugacity above the critical point. Nevertheless, considering the ideal gas, a

standard enthalpy, a Gibbs free energy, and an entropy change of reaction were adjusted from reaction equilibrium data: -20±2 $kJ \cdot mol^{-1}$, 31±1 $kJ \cdot mol^{-1}$, and -174±8 $J \cdot K^{-1} \cdot mol^{-1}$, respectively.

Then, two reaction rate expressions, based on the Langmuir-Hinshelwood and Eley-Rideal mechanisms, were fitted from the experimental data. Besides the similar high performance of these two expression, the one based on Langmuir-Hinshelwood mechanism showed an activation energy (106 $kJ \cdot mol^{-1}$) in accordance with the estimated by the slope of the Arrhenius plot between the initial reaction rate and the inverse of absolute temperature (107 $kJ \cdot mol^{-1}$). In addition, it was also studied the effect of pressure on the kinetic constant, which revealed an activation volume of 0.4±0.2 $dm^3 \cdot mol^{-1}$ by adjusting the experimental data.

Adsorption and mass transfer models

The adsorption of water and DMC over the surface of zeolite 3A was achieved through the analysis of the pulse injection responses in a fixed bed column filled with the zeolite 3A in the following conditions: 10-12 $ml \cdot min^{-1}$ of carbon dioxide and methanol (40% (*v*/*v*)) as eluent at 20 MPa between 313 K and 353 K. Similar experiments were conducted with an equal column, filled with glass particles with similar diameter, to study the hydrodynamics, which were well described by an axial dispersion model with Péclet values of 79±1 (353 K), 59±1 (333 K), and 31±1 (313 K), obtained from the fitting.

Since with this methodology the isotherms are not directly measured and it just comprises a small range of concentrations, linear isotherms were considered and the initial slope of the isotherm was computed from the average retention time of the peaks: 0.6±0.2 (333 K), 0.8±0.1 (333 K), and 1.4±0.2 (313K) for DMC; and 1.1±0.3 (353 K), 1.9±0.3 (333 K), and 3.3±0.4 (313 K) for water. In addition, the enthalpies of adsorption were computed from the Van't Hoff equation: -25±6 $kJ \cdot mol^{-1}$ for water and -20±6 $kJ \cdot mol^{-1}$ for DMC.

Furthermore, the experiments were also used to find reliable correlations to predict the mass transfer phenomena. A linear driving force model was used, considering a global mass transfer coefficient as the result of the combination of external and internal mass transfer resistances in series. Since the internal resistance represented around 90% of the overall resistance, all the correlations for the external mass transfer gave reasonable predictions; however, it does not mean that they are reliable. In summary, several correlations were tested, but the estimation of the internal mass transfer resistance was better achieved using the Dean and Stiel correlation for the viscosity of the mixture, and the Wilke and Chang equation for the molecular diffusivity.

Simulated Moving Bed Reactor design and optimizations

Finally, after collecting all the information and developing the mathematical models, it was possible to design and optimize the Simulated Moving Bed Reactor. The major challenge is the difference between reaction and adsorption temperatures, which represents an excessive need of energy. Nevertheless, this work aims to explore the potential of Simulated Moving Bed Reactor to enhance the DMC yield.

In order to design and optimize the unit, a theoretical True Moving Bed Reactor model was considered, and a design methodology supported by contour maps inside the separation region was proposed. Then, using methanol as eluent, optimum design and conditions (30 MPa, 383 K for reaction, and 298 K for adsorption) were reached, leading to the following main results: 0.87% (carbon dioxide free basis) and 99.93% (carbon

dioxide and methanol free basis) for the purity of DMC at the raffinate stream; 0.27% (carbon dioxide free basis) and 99.69% (carbon dioxide and methanol free basis) for the purity of water at the extract stream; and, 5.95% for the carbon dioxide conversion.

Finally, the performance of the optimum True Moving Bed Reactor was compared with a simple fixed bed reactor in the same conditions. From this assessment it was estimated that the True Moving Bed Reactor has the advantage of separating the water and DMC into two streams, and it also has a large capacity to handle large contents of water in the feed stream (up to a molar fraction of 0.9 without losing much performance).

General conclusions

The Simulated Moving Bed proposed enables the enhancement of the reaction performance by increasing the reaction conversion and allowing the separation of water and DMC in two different streams. Although the conversion is still low, considering the high pressure required, this process might still be feasible due to the low cost of the reactants, which allows a higher margin for energetic consumption costs. However, there still are two major drawbacks that should be addressed: the first one is the related to the low concentration of DMC at the outlet stream, which is difficult to separate from methanol due to the formation of an azeotropic mixture; the second issue is the difference of temperatures between reaction and adsorption, which requires a heat exchanger between the units and turns the process unfeasible.

The first issue might be overcome using excess of carbon dioxide, which is easily separated due to its low boiling point. Nevertheless, it leads to more energy required for the compression stage; therefore, it is a sensible case that needs to be optimized. The second issue is still far from being solved since it is strictly dependent on the advances in materials; it is necessary to find a catalyst to decrease the reaction temperature and an adsorbent with high capacity at higher temperatures.

7.2. Suggestions for Future Work

In spite of all the issues that still need to be addressed, this topic is of great importance since it is related to the valorisation of carbon dioxide as building block for organic carbonates; in addition, the methodologies developed can be also extended to other reaction systems. As it was discussed along this work, the use of carbon dioxide for organic synthesis might become in one of the sustainable solutions to mitigate its high emissions to the atmosphere. Furthermore, carbon dioxide represents a low cost feedstock with low harmful properties, either for the environment or for human beings. Of course, this still is a mirage for large industrial applications, because carbon dioxide is a very stable molecule, which leads (in most of the cases) to low conversions and low reaction rates.

As previously mentioned, in order to turn the direct synthesis of DMC into a feasible and sustainable process, there still is a lot of research to be done. Herein, are discussed some suggestions for future work related with this subject.

Dehydrating agents

The use of dehydrating agents, which remove the water in order to shift the reaction towards DMC formation, is pointed as a key solution to overcome the high thermodynamic limitations; and, indeed, the major improvements for this route were obtained thanks to this methodology. The first attempt was in 1998 with trimethyl orthoacetate (453 K, 30 MPa), but only in 2013 was it possible to reach 94% of conversion in moderate conditions (393 K, 5 MPa) with 2-cyanopyridine (see Chapter 2). In my opinion, the use of these dehydrating agents will be essential for a sustainable process; nevertheless, these compounds are not a commodity and, therefore, are expensive and if not fully recovered inside the process will represent a significant increase of the feedstock cost, which is the main competitive advantage of this alternative process. Therefore, it is important to find a very selective and also easy to recycle dehydrating agent.

Process simulation and economical analysis

Concerning the last topic a lot of progress has been done, but only in a very small scale. Hence, it would be important to measure how these achievements have improved the direct synthesis of DMC in terms of energy costs. Therefore, I believe that is important to design a process in order to measure these enhancements, which would give the idea of how far we are of a sustainable process. In particular, it would be interesting developing a process based on the use of 2-cyanopyridine as dehydrating agent. In addition, it could also give us the idea of values for catalyst activity and features of the dehydrating agents that are required to turn this process competitive comparing to the other alternative processes.

Annex A. Analytical Method

Herein is presented the analytical method developed for the quantification of water, DMC and methanol. This method was used for the quantification of the samples obtained during the reaction experiments (see Chapter 4).

A.1. Operating Conditions

All the samples were analyzed by GC chromatography (GC2010 plus, Shimadzu®) using a fused silica capillary column (polyethylene glycol as bound phase), Chrompack CP-Wax 52 CB (25 m × 0.25 mm × 1.2 µm) to separate the compounds coupled with thermal conductivity (TCD) and flame ionization (FID) detectors. Helium N50 was used as carrier gas at a constant linear velocity of 30 $cm \cdot s^{-1}$ with a split ratio equal to 30 for 2 µL of sample injected. The temperature of the injector and the detectors were set at 573 K, while the oven temperature was set at 348 K during 5 min of analyzing time. TCD was used to quantify the amount of each compound, since FID is not sensitive to water.

A typical chromatogram of a ternary mixture using the operating conditions mentioned is shown in Figure A.1, where it can be seen a complete separation of the components.

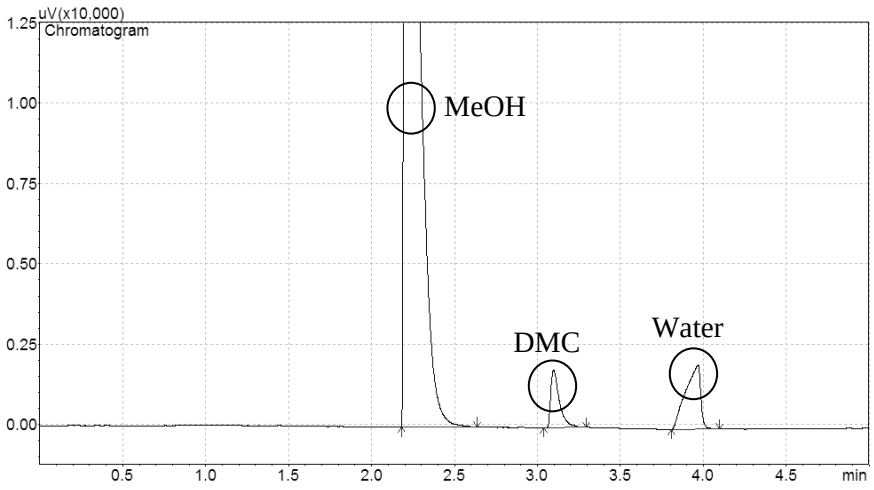

Figure A.1: Chromatogram of a ternary mixture**.**

A.2. Calibration

Some standard solutions (in this case three) with known mass fractions were prepared, and analyzed by gas chromatography (3 times per sample). In Table B.1 is described an example of three solutions used as standards for the calibration of the analytical method. Low concentrations of water and DMC were used, since the samples collected from the reaction experiments are also highly diluted in methanol.

Table A.1: Standard solution concentrations.

Sample	MeOH mass fraction	DMC mass fraction	Water mass fraction
1	99.32%	0.33%	0.35%
2	98.57%	0.77%	0.66%
3	96.14%	1.84%	2.02%

Then, in Figure A.2 are depicted the peak area ratios (DMC/methanol and water/methanol) as function of the respective mass ratios. In addition, a linear tendency can be observed, which allows the determination of the mass fraction (x) for DMC and water (where k_i is the slope of linear fitting, obtained by minimization of least squares):

$$x_i = \frac{k_i \frac{A_i}{A_{MeOH}}}{1 + k_{water}\frac{A_{water}}{A_{MeOH}} + k_{DMC}\frac{A_{DMC}}{A_{MeOH}}}, i = \text{DMC or water} \quad \text{(A.1)}$$

While the methanol mass fraction is computed by the following equation:

$$x_{MeOH} = 1 - x_{DMC} - x_{water} \quad \text{(A.2)}$$

With this approach, a maximum absolute error (for the more diluted solution) of 0.02% for DMC and 0.03% for water were achieved, which represent relative deviations lower than 5% and 9%, respectively.

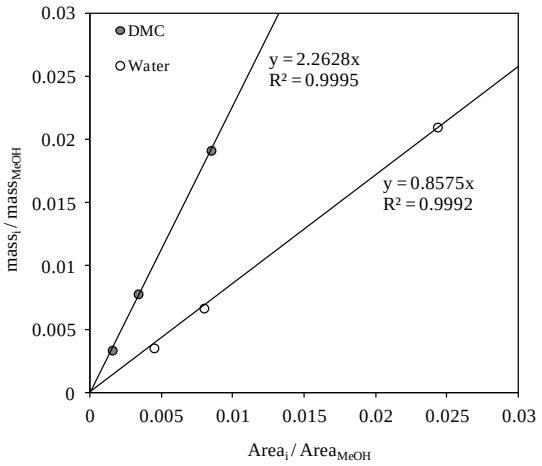

Figure A.2: Peaks area ratios (from TCD) *versus* mass ratios.

Annex B. Reactor Set-Up

This set up was designed for high pressure reactions in the presence of supercritical carbon dioxide with sampling along the time. However, it has also the versatility to be used at low pressure conditions and in the absence of carbon dioxide. In addition, the set-up can be divided in two parts:

❖ *Feed System*: A HPLC pump (K-1900 100mL head, Knauer®) is used to feed the reactor with carbon dioxide (liquid or supercritical). This pump is a pneumatic pump that delivers a carbon dioxide flow depending on the inlet air pressure and the head pressure. Furthermore, a cooling bath is used in order to keep cold the pump head avoiding the vaporization of carbon dioxide. Besides, other chemicals can be directly inserted in the reactor before closing or can be added from the feed cylinder through the carbon dioxide stream.

❖ *Reactor*: The set-up is mainly composed by an autoclave reactor (HP reactor 4575A, Parr®), a 500 mL stainless steel vessel designed to operate up to 34 MPa and 773 K. The temperature is controlled (±1K) by an external reactor controller module (4848 reactor controller, Parr®), which also controls the stirrer speed and measures the pressure inside the reactor. The set-up also allows taking samples from a precise metering valve (1/16”), which promotes a smooth depressurization. The depressurization of the system is easily done through other metering valve into a trap cylinder to expand the carbon dioxide; moreover, this valve is heated by an external resistance thereby avoiding freezing caused by the drastic vaporization of carbon dioxide.

In Figure B.1 and B.2 are depicted a detailed sketch and a photo of the reactor set-up, respectively. In addition to this, in Tables B.1 and B.2 are contained the some specifications for the main components and valves, respectively.

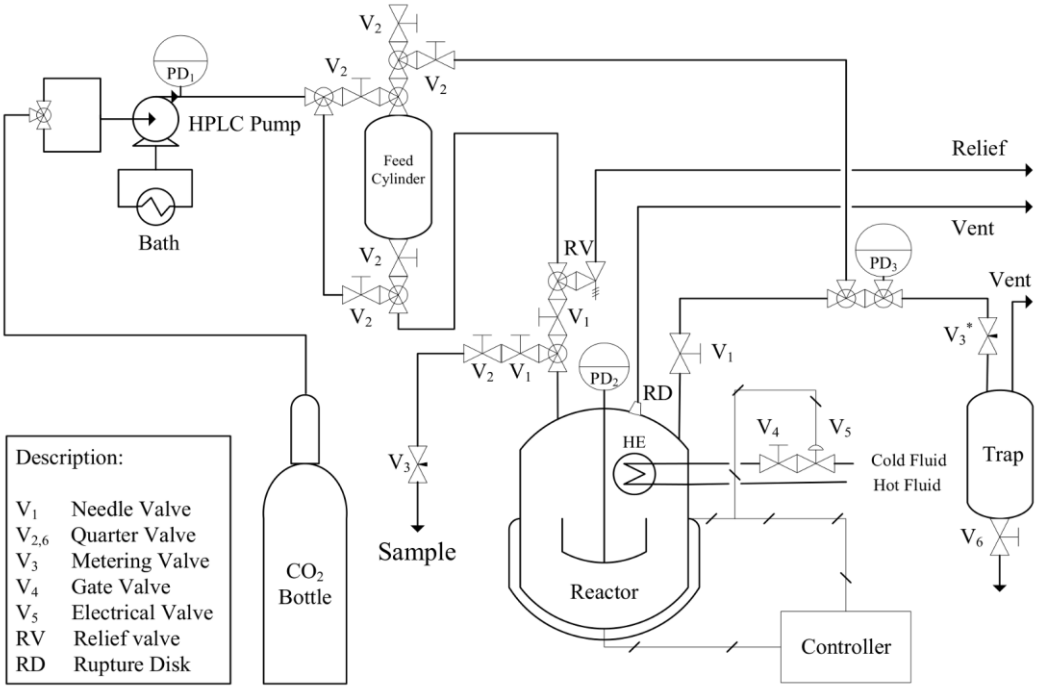

Figure B.1: Sketch of the experimental set-up for high pressure reactions.

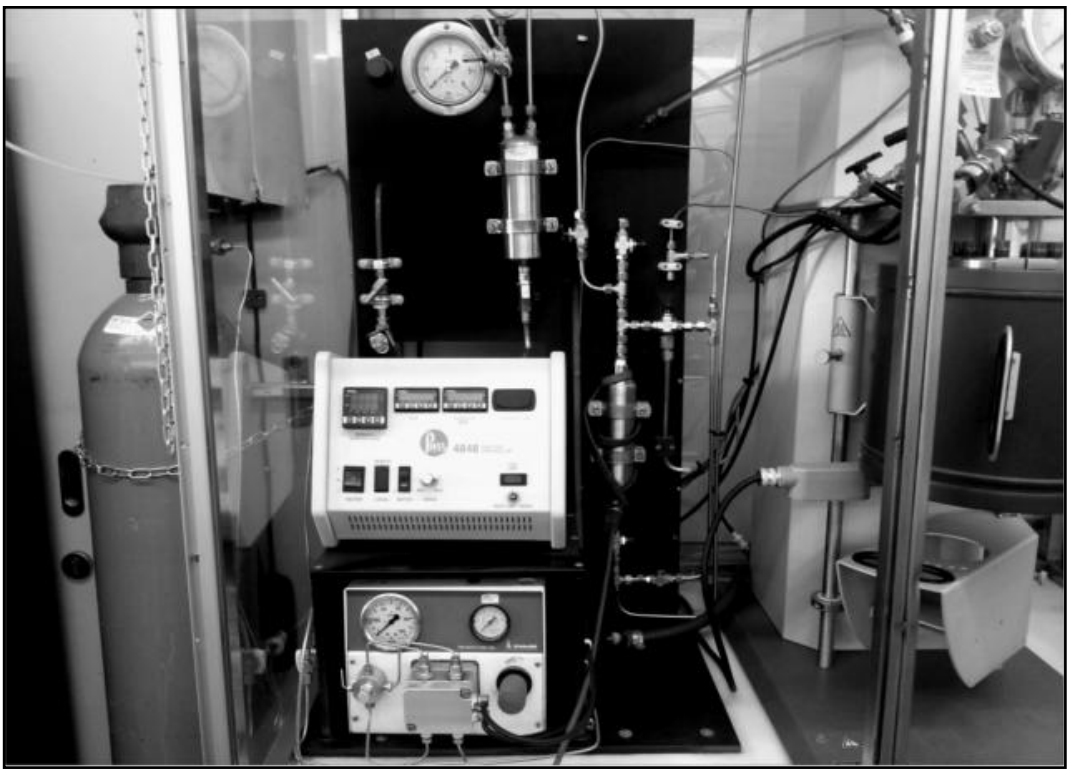

Figure B.2: Photo of the reactor set-up

Table B.1: Brief description of the main components.

Equipment	Description
HPLC Pump	Pneumatic-Pump
	Max. pressure: 100 MPa
	Pump head: 100 mL
Controller	Temperature and stirrer speed controller;
	Pressure gauge manometer
Reactor	Reactor vessel, 500 mL (fixed head)
	Max. pressure: 34 MPa
	Max. temperature: 773 K
HE	Heat Exchanger: U tube
RD	Rupture disc: 45 MPa (295 K) – Alloy 600
Carbon dioxide Bottle	Carbon dioxide 37.5 kg
	High purity: 0.99995 (Saturated liquid)
Bath	Temperature range: 253-373 K
	External recirculation; Capacity: 6 L
Trap cylinder	Cylindrical vessel: 500 mL
	Max. pressure: 50 bar
Feed cylinder	Cylindrical vessel: 150 mL
PD_1(Pressure Device)	Max. pressure: 100 MPa
PD_2	Max. pressure: 34 MPa
PD_3	Max. pressure: 20.6 MPa

Table B.2: Valves specifications

Valve	Description	Size	Seal Material	Supplier (reference)
RV	Relief valve	1/4"	Viton	Swagelook (SS-4R3A1 / 177-R3A-K1-F)
V_1	Needle valve	1/4"	Grafoil	Swagelok (SS-3HNRF4-G)
V_2	Quarter valve	1/4"	-	Paralab (SAHB1-H-4T)
V_3^*	Needle valve	1/8"(*1/4")	Buna	Swagelok (SS-SS2 (*SS-SS4))
V_4	Gate valve	1/4"	-	Paralab (NV-2-H-4T-R)
V_5	Electric valve	-	-	Paralab (SANV2-H-4T-R)
V_6	Quarter Valve	1/4"	-	-

In addition, other relevant photos of individual parts of the reactor set-up are displayed in Figure B.3.

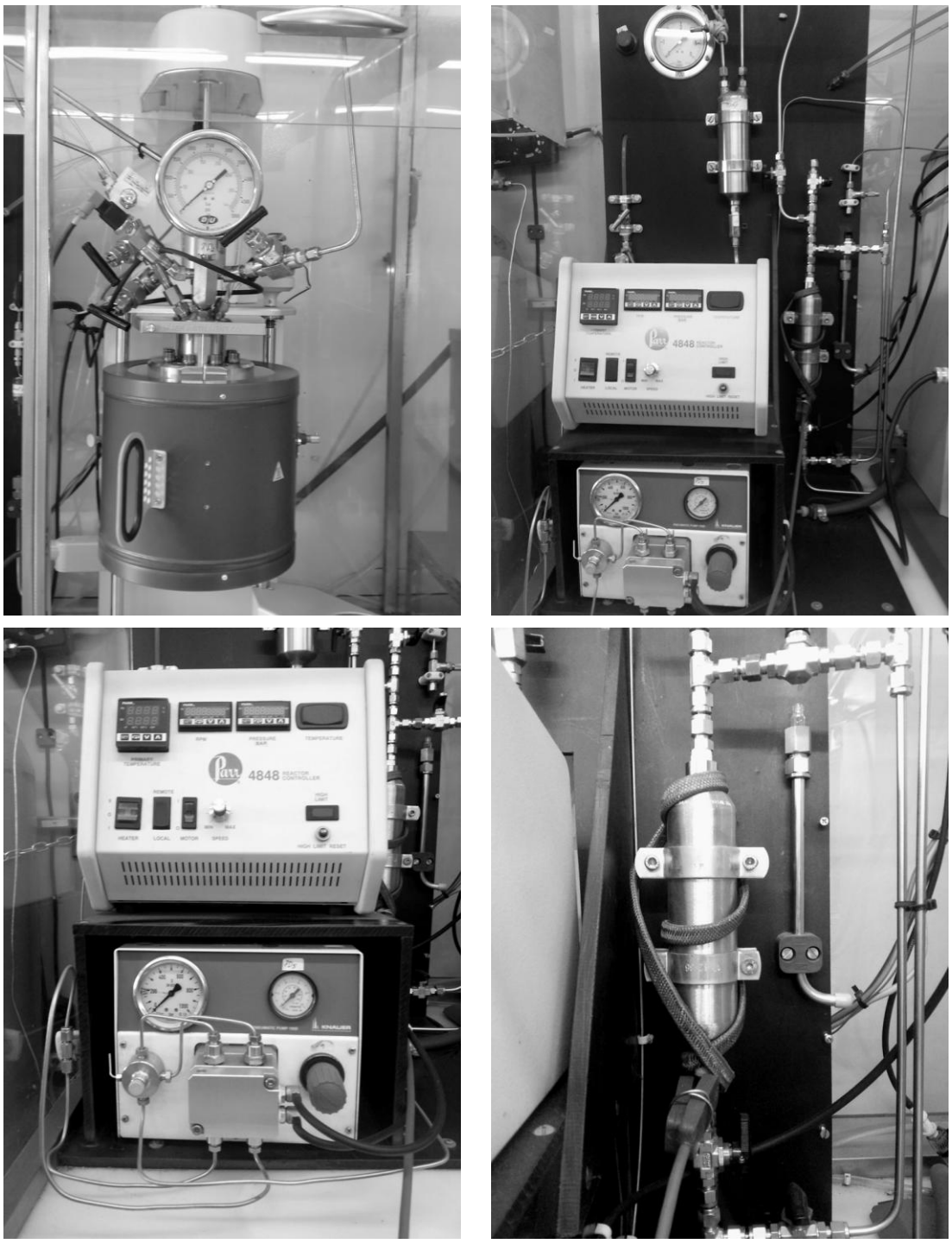

Figure B.3: Other photos of the reactor set-up.

Annex C. TMBR Concentration Profiles

Herein are depicted the simulated TMBR concentration profiles that were used to study the effect of several parameters in the overall performance of the TMBR. The main results were already depicted in Table 6.8 form Chapter 6 (Section 6.6.3). In Table C.1 are displayed the other parameters used in the simulation.

Table 6.8: Main results of the preliminary tests for the TMBR.

Design	V_{ads} / mL	Configuration	γ_i	X_c	$PUR_{DMC,R}$	$PUR.II_{DMC,R}$	$REC_{DMC,R}$
2.1	128	3-11-7-3	[4.67 2.47 3.04 1.42]	3.73%	0.63%	97.70%	99.98%
2.2	260	3-11-7-3	[4.67 2.47 3.04 1.42]	3.77%	0.63%	99.80%	99.99%
2.3	260	3-7-11-3	[4.67 2.47 3.04 1.42]	3.86%	0.65%	99.81%	99.99%
2.4	260	3-1-17-3	[4.67 2.47 3.04 1.42]	3.96%	0.67%	99.82%	99.73%
2.5	260	3-1-17-3	[4.67 2.18 2.76 1.42]	3.94%	0.82%	99.89%	98.95%
2.6	260	3-1-17-3	[4.67 1.89 2.47 1.42]	3.68%	0.98%	99.93%	95.71%
2.7	260	3-2-16-3	[4.67 1.89 2.47 1.42]	3.87%	1.06%	99.93%	97.70%

Table C.1: Summary of general parameters for TMBR simulation.

Adsorption column		Reactor	
V / mL	-	V / L	53/ (number of columns section III)
Pe	1000	Pe	1000
T / K	298	T / K	363
Compounds	[CO_2 MeOH DMC H_2O]	P / MPa	30
k_L / mm·min^{-1}	[∞ ∞ 1.9 4.6]	Heat exchanger	
K_{ads}	[0 0 2.4 6.0]	β	1.1
General			
C_{Feed}	[11.15 11.15 0 0]	Q_{Feed} / mL·min^{-1}	20
C_{Eluent}	[0 24.7 0 0]	Configuration	-

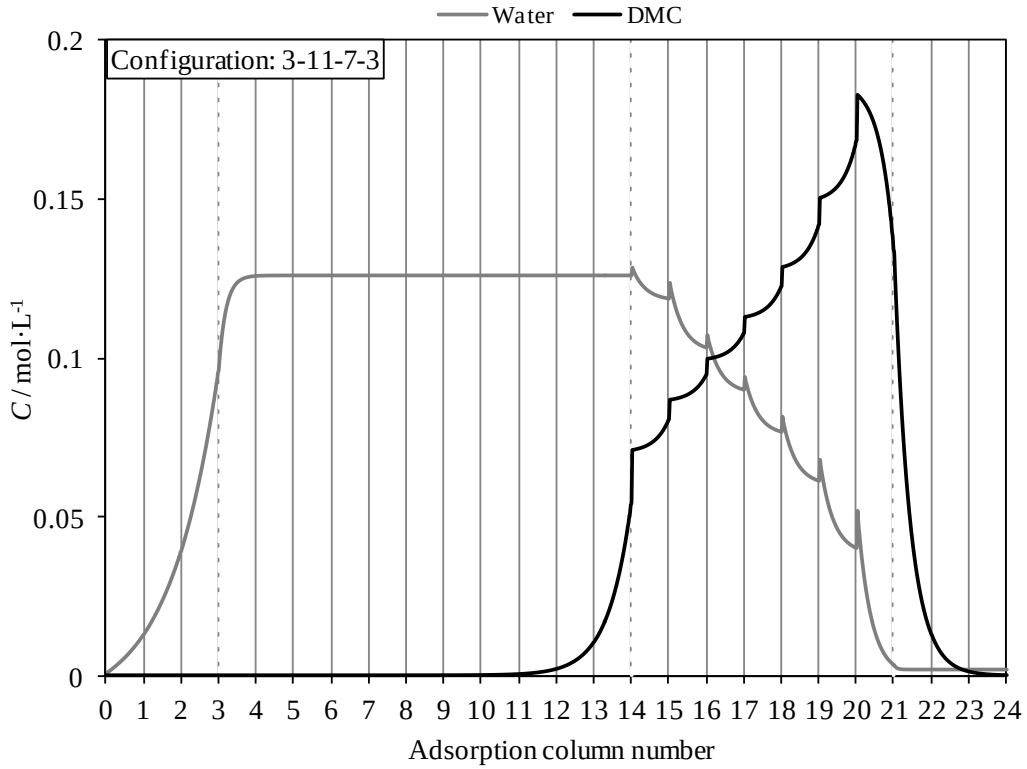

Figure C.1: TMBR profile concentrations of water and DMC along the adsorption columns (Design 2.1).

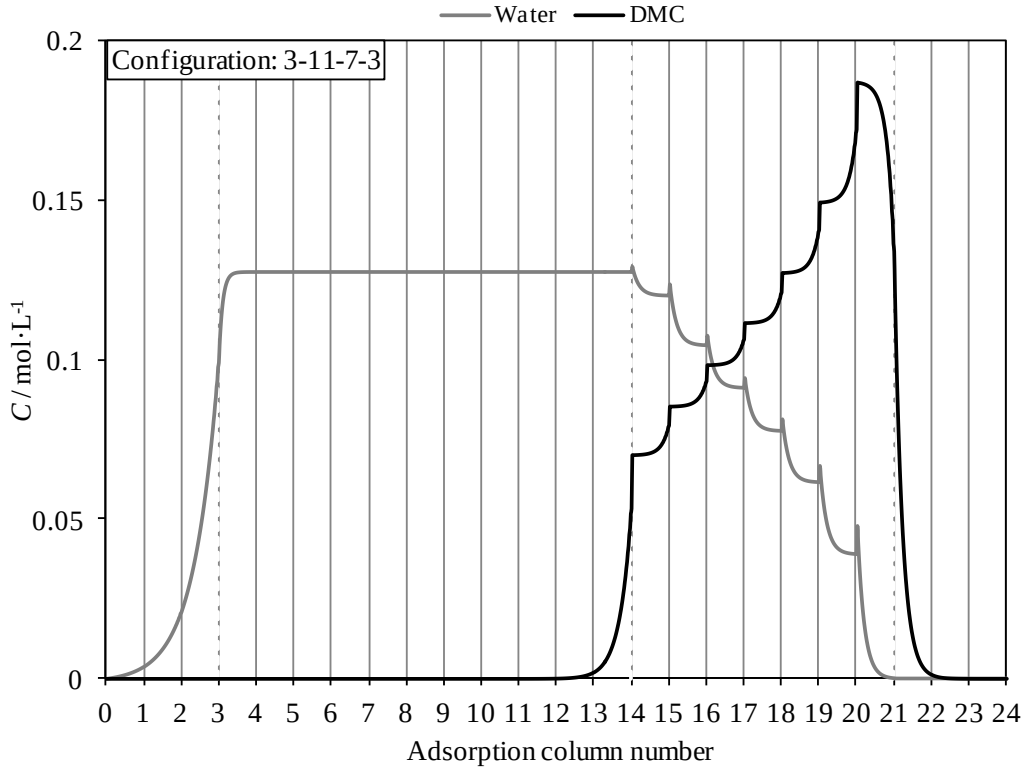

Figure C.2: TMBR profile concentrations of water and DMC along the adsorption columns (Design 2.2).

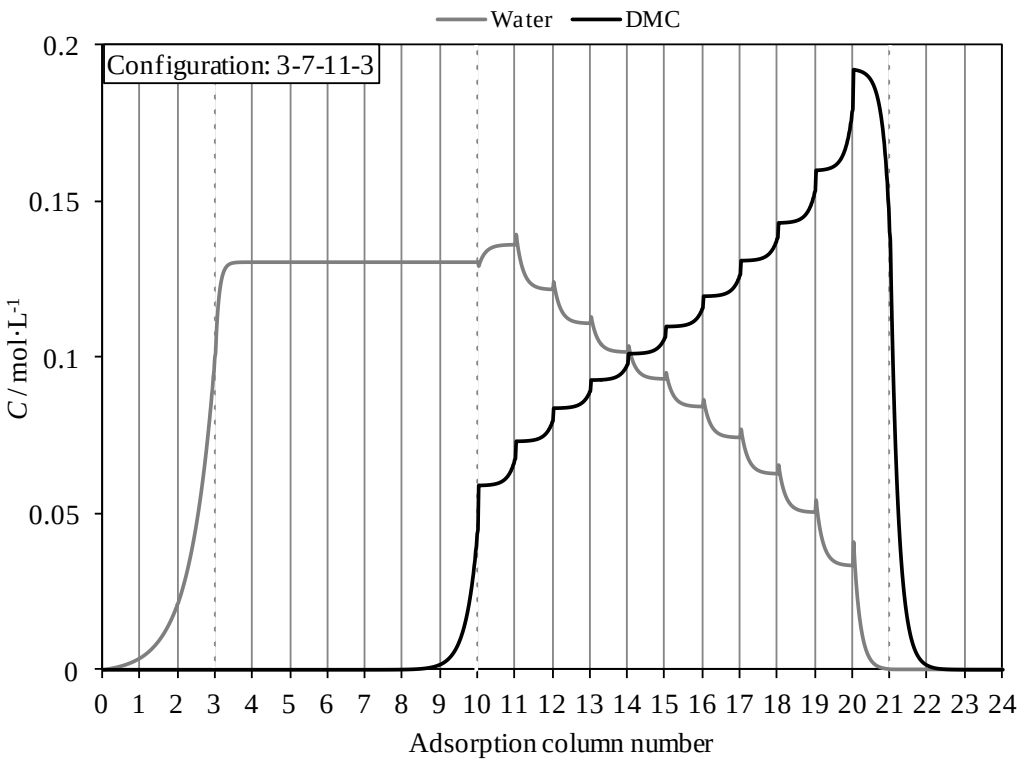

Figure C.3: TMBR profile concentrations of water and DMC along the adsorption columns (Design 2.3).

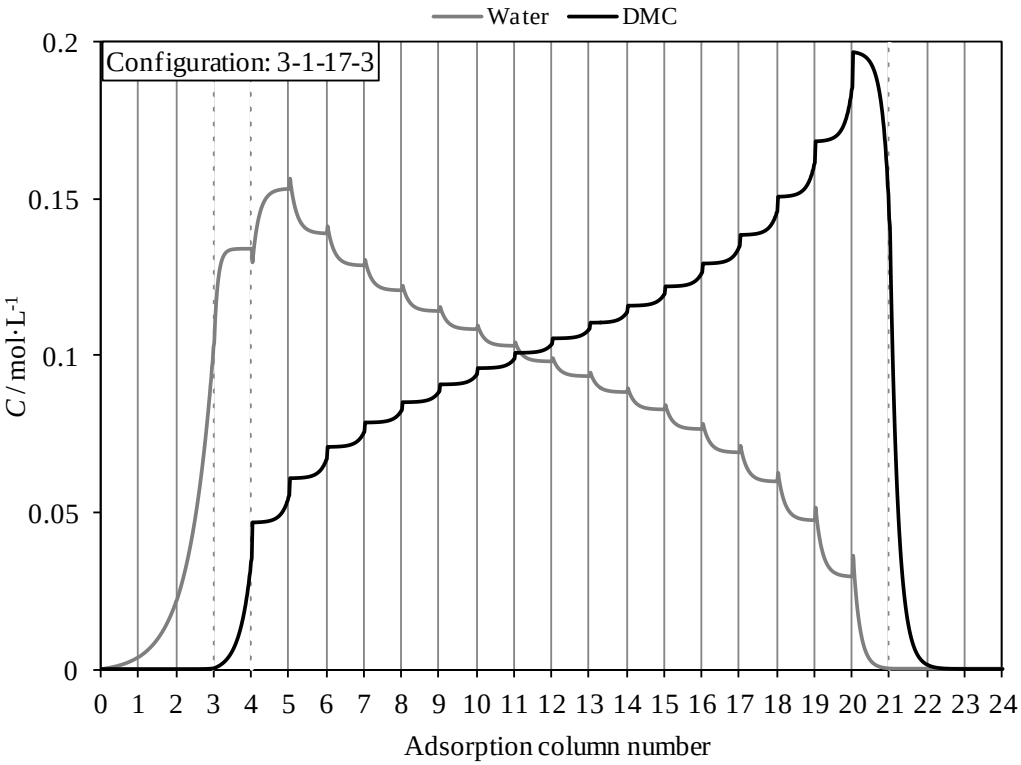

Figure C.4: TMBR profile concentrations of water and DMC along the adsorption columns (Design 2.4).

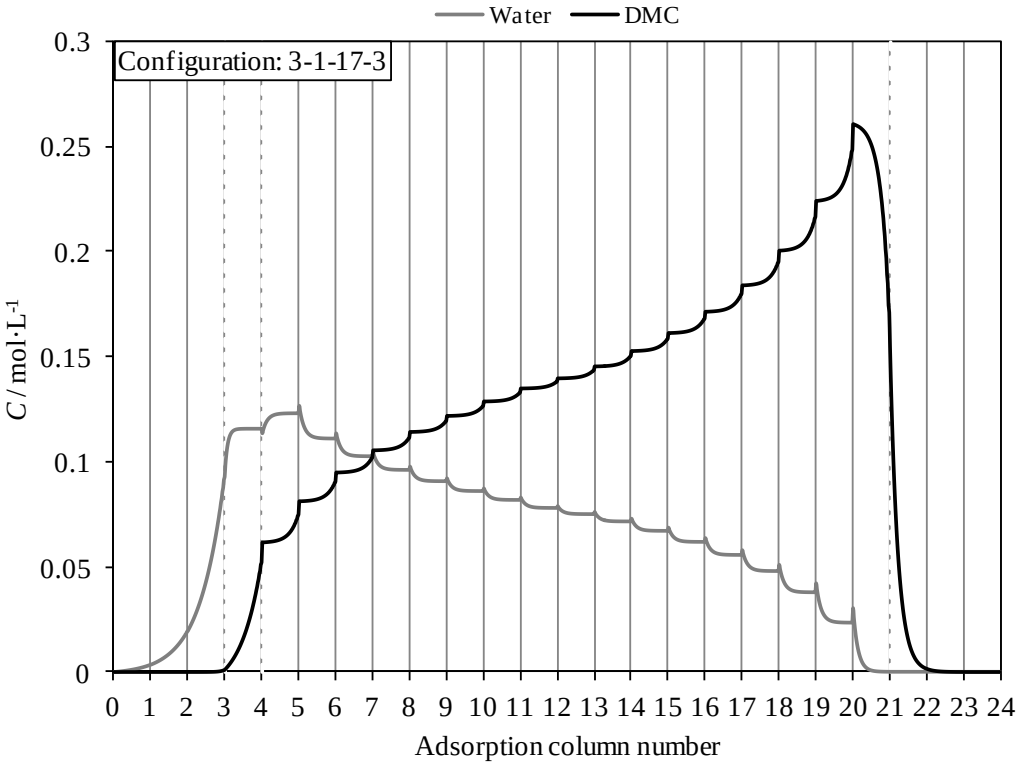

Figure C.5: TMBR profile concentrations of water and DMC along the adsorption columns (Design 2.5).

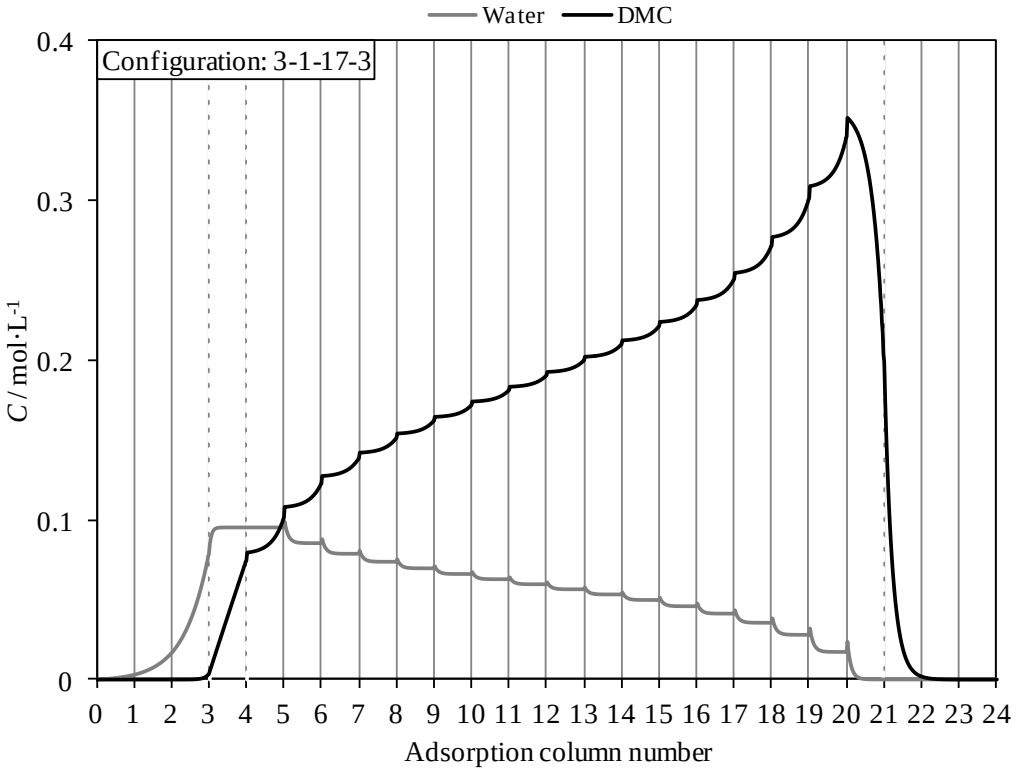

Figure C.6: TMBR profile concentrations of water and DMC along the adsorption columns (Design 2.6).

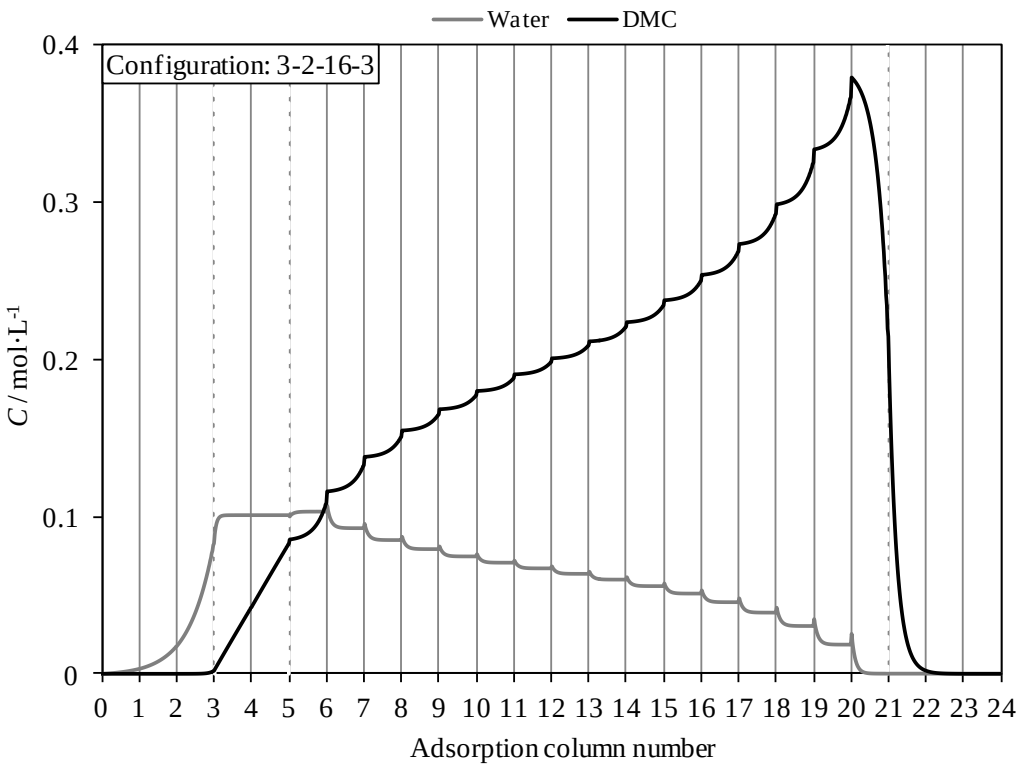

Figure C.7: TMBR profile concentrations of water and DMC along the adsorption columns (Design 2.7).